THE ROLE OF ELONGATED INCLUSIONS IN THE HYDROGEN ASSISTED CRACKING OF STEEL

By

T. V. Venkatasubramanian

A thesis submitted for the degree of
Doctor of Philosophy
of the University of London

Department of Metallurgy and Materials Science,
Royal School of Mines,
Imperial College of Science and Technology,
London, S.W.7.

January, 1981.

..... Metals which are beaten into Rods upon an Anvil, or drawn into Wire through a Wire-Iron, are very strong Length-ways, but Breadth-ways they are many times easier to break than Workmen would have them. And we observe Strings in them, as in the [1]Slip of an [2]Ozier.

These strings ought not to be in Metal that is cast and has not been forged: And so we find that cast Metal is as easy to break one Way as another.

Jacques Rohault
17th Century French Philosopher
in
Traité de physique
Paris, 1671

Quoted from "A History of Metallography"
by C.S. Smith, p.79, The University of Chicago Press (1960).

1. Long narrow strip of thin wood.
2. Species of willow used in basket work.

ABSTRACT

The effect of inclusion orientation and volume fraction on threshold stress intensity, K_{TH}, and crack growth rate has been studied as a function of matrix strength and hydrogen activity of the environment by employing a medium carbon hardenable steel having two different sulphur contents (0.04% and 0.15%). The presence of plate-like inclusions leads to enhanced crack growth rate and decreased K_{TH} in the short transverse orientations. In the longitudinal and transverse orientations, inclusions result in the elevation of K_{TH} and reduction of crack growth rate. The extent of anisotropy in crack growth rate and K_{TH}, caused by a given inclusion dispersion, is diminished by an increase in either matrix strength or hydrogen activity of the environment. In environments of high hydrogen activity, such as H_2S saturated NaCl solution, the short transverse orientations show discontinuous crack growth which is associated with the development of inclusion assisted subsidiary cracks ahead of the main crack. It is proposed that the failure criterion for crack growth in hydrogen involves the attainment of a critical tensile stress at a microstructurally significant distance ahead of the crack tip. The orientation dependence of K_{TH} is attributed to inclusion induced perturbations of the crack tip stress field. The results of the permeation experiments show that there is no significant directionality in the diffusivity of hydrogen and hence it is deduced that anisotropy of crack growth rate must also be caused primarily by the inclusions affecting the crack tip stress field. In environments of high hydrogen activity, besides causing matrix embrittlement, hydrogen accumulates at the inclusion-matrix interface in a molecular form and thereby assists crack growth by a pressurisation mechanism. The operation of the latter mechanism is responsible for the discontinuous crack growth.

ACKNOWLEDGEMENTS

I would like to thank Dr. T.J. Baker for his sustained encouragement, unflagging enthusiasm and valuable advice throughout this project. I am indebted to the Science Research Council Marine Technology Directorate who provided financial support for this project. Thanks are also due to Professors J.G. Ball and D.W. Pashley for the provision of research facilities at Imperial College. I am grateful to the following: Dr. B.A. Unvala for his advice in designing the AC potential drop system; Dr. N. Okumura with whom the slow crack growth experiments were carried out; Mr. I.C. Mayes for several useful discussions; Mr. K.M. Iyer for building the punch interface; and Mrs. G. Flower for typing this thesis.
I would also like to thank the members of the technical staff for their assistance and M/S Doncasters Blaenavon for forging the steel billets.

TABLE OF CONTENTS

		Page
Abstract		3
Acknowledgements		4
Chapter 1	Introduction	17
Chapter 2	Review of Hydrogen Assisted Cracking	20
2.1.	Introduction	20
2.2.	Early Observations and Theories	20
2.2.1.	Planar Pressure Theory	20
2.2.2.	Embrittlement Theories	21
2.3.	The Application of Fracture Mechanics to the Study of Hydrogen Embrittlement	23
2.3.1.	Stress Intensity Vs Crack Growth Rate	24
2.3.2.	Testing Methods	24
2.3.3.	Interpretation of K Vs Crack Growth Rate Behaviour	25
2.3.4.	Meaning of K_{TH}	25
2.3.5.	Interpretation of Stage I and Stage II Behaviour	27
2.4.	Effect of Hydrogen Activity on Crack Growth Rate and Threshold	27
2.5.	Effect of Metallurgical Variables	28
2.5.1.	Role of Matrix Strength	28
2.5.2.	Role of Composition and Microstructure	29
2.6.	Connection Between Temper Embrittlement and Hydrogen Embrittlement	30
2.7.	Mechanism of Cracking in 3½% NaCl Solution	30
2.8.	Conclusions	31
Chapter 3	The Role of Non-Metallic Inclusions in Hydrogen Assisted Cracking	32
3.1.	Introduction	32
3.2.	General Observations	32
3.3.	Experiences of the Steel Making Industry	33
3.4.	Experiences of the Welding Industry	33
3.5.	Anisotropy Effects in High Strength Steels	34
3.6.	Role of Inclusions in the Hydrogen Assisted Cracking of Low Strength Steels	35
3.7.	Conclusions	37

		Page
Chapter 4		38
4.1.	Introduction	38
4.2.	Material	38
	4.2.1. The Need for Using a Model System	38
	4.2.2. Requirements of a Model System	39
	4.2.3. Selection of the Model System	40
	4.2.4. Material Characteristics	40
4.3.	Testing Methods	41
	4.3.1. Time to Failure Tests	41
	4.3.2. Rising Load Testing and its Evaluation	42
	4.3.3. Crack Arrest Method and its Evaluation	43
	4.3.4. Details of the Crack Arrest Method	44
4.4.	Specimen Preparation	44
	4.4.1. Specimen Dimensions	44
	4.4.2. Extraction of Specimens	45
	4.4.3. Heat Treatment	46
4.5.	Test Environment	47
4.6.	Measurement of Crack Length and Stress Intensity	48
	4.6.1. Crack Shorting in Environment Induced Cracking	49
	4.6.2. Crack Length Measurement by a Compliance Technique	50
	4.6.3. Determination of Crack Length Using the Instrumented Loading Pin	52
	4.6.4. Errors Arising from the Crack Length Monitoring Technique	53
4.7.	Testing Procedure	54
	4.7.1. Fatigue Pre-cracking	54
	4.7.2. Testing in 3½% NaCl Solution	54
	4.7.3. Testing in H_2S Gas	55
	4.7.4. Testing in H_2S Saturated 3½% NaCl Solution	57
	4.7.5. Fractography	58
	4.7.6. Determination of K Vs Crack Growth Rate Behaviour	59
Chapter 5	Results of Crack Growth Behaviour	60
5.1.	Introduction	60
5.2.	Crack Growth Behaviour in 3½% NaCl Solution	60
	5.2.1. Behaviour of En16 at a σ_{ys} = 1250 MPa	60
	5.2.2. Behaviour of En16M at a σ_{ys} = 1300 MPa	60

		Page
5.2.3.	Effect of Inclusion Volume Fraction on Apparent Threshold and Crack Growth Rate	61
5.2.4.	Fractography of Short Transverse Orientations	62
5.2.5.	Fractography of Longitudinal and Transverse Orientations	63
5.2.6.	Effect of Increasing Matrix Strength to 1450 MPa	64
5.2.7.	Fractography of 1450 MPa Yield Strength Condition	65
5.2.8.	'Incubation Time' Behaviour in 3½% NaCl Solution	65
5.3.	Effect of Decreasing Matrix Strength to 800-900 MPa	65
5.3.1.	Behaviour of En16M	65
5.3.2.	Behaviour of En16	67
5.3.3.	Fractography of Specimens Tested in H_2S Saturated Salt Solution	67
5.4.	Behaviour of En16M in the 600 MPa Yield Strength Condition	68
5.5.	Effect of Increasing Hydrogen Activity on the Behaviour of En16M in the 1200-1300 MPa Yield Strength Condition	69
5.5.1.	Testing in H_2S Gas	69
5.5.2.	Fractography	69
5.5.3.	Testing in H_2S Saturated Salt Water	70
5.5.4.	Fractography	70
5.6.	Testing of Unstressed Specimens in H_2S Saturated NaCl Solution	71
5.7.	Comparison of Low Temperature Fracture Modes with the Fracture Modes in Hydrogen Embrittlement	73
5.8.	Location of Inclusions	73
Chapter 6	Orientation Dependence of Hydrogen Transport Behaviour	75
6.1.	Introduction	75
6.2.	Diffusion of Hydrogen in Steel	75
6.3.	Effect of Metallurgical Variables on the Transport Behaviour of Hydrogen	76
6.4.	Experimental Method	77
6.5.	Experimental Apparatus	79
6.6.	Preparation of Experimental Materials	80
6.7.	Experimental Procedure	80
6.8.	Analysis of Results	80
6.9.	Discussion	81

		Page
Chapter 7	Discussion	83
7.1.	Introduction	83
7.2.	Hydrogen Assisted Cracking in the Absence of Inclusions	84
7.2.1.	Carbide Initiated Cleavage Fracture in Steels	84
7.2.2.	Fracture Criterion in Hydrogen Embrittlement	87
7.2.3.	Effect of Hydrogen on σ_f	88
7.2.4.	Size of Crack Nuclei and Critical Distance	89
7.2.5.	Relating K_{TH} to Microstructural and Continuum Variables	90
7.2.6.	Variation of K_{TH} with Hydrogen Activity	91
7.2.7.	Variables Determining Crack Growth Rate	93
7.3.	Mechanisms by which Inclusions Influence Crack Growth Behaviour	95
7.4.	Effect of MnS Inclusions on Electrochemical Reactions at the Crack Tip	95
7.5.	Effect of Inclusions on the Crack Tip Stress and Strain Distribution	97
7.5.1.	Behaviour of the LT Orientation in the 1250-1300 MPa Yield Strength Condition in 3½% NaCl Solution	97
7.5.2.	Behaviour of TL Orientation in the 1250-1300 MPa Yield Strength Condition in 3½% NaCl Solution	100
7.5.3.	Behaviour of the Short Transverse Orientations in the 1250-1300 MPa Yield Strength Condition in 3½% NaCl Solution	101
7.6.	Anisotropy of Crack Growth Rate of the 1250-1300 MPa Yield Strength Condition in Salt Solution	104
7.7.	Effect of Increasing Matrix Strength	106
7.8.	Effect of Decreasing Matrix Strength	107
7.8.1.	Conditions for Crack Growth by a Pressurisation Mechanism	107
7.8.2.	Nature of Crack Growth in the Short Transverse Orientation by a Pressurisation Mechanism	108
7.8.3.	Nature of the Hydrogen Source Provided by H_2S Saturated Salt Solution and its Consequences	112
7.8.4.	The Applicability of Fracture Mechanics to the Characterisation of Macroscopic Crack Growth by a Pressurisation Mechanism	114

Page

7.8.5. Effect of Inclusion Volume Fraction on Crack Growth Behaviour of the 800-900 MPa Yield Strength Condition 115

7.9. Effect of Increasing Hydrogen Activity on the Crack Growth Behaviour of En16M in the High Strength Condition (σ_{ys} = 1200-1300 MPa) 115

7.9.1. Anisotropy of Crack Growth Rate 115

7.9.2. Threshold Behaviour 116

7.9.3. Crack Growth by a Pressurisation Mechanism 117

7.10. Fractographic Features 118

7.10.1. Fracture Modes 118

7.10.2. Inclusion Participation in the Short Transverse Orientation 120

7.11. The Consequences of the Association Between Inclusions and Interdendritic Segregation 120

Chapter 8 Conclusions 121

8.1. Summary of Results 121

8.2. Some Practical Implications of the Present Work 125

8.3. Suggestions for Further Work 127

Appendix 1 Development of an AC Potential Drop System for Monitoring Crack Length 128

A.1.1. Introduction 128

A.1.2. Sources of Error in the DCPD Technique 128

A.1.3. Distinguishing Features of the ACPD Technique 129

A.1.4. Development of an ACPD System 130

A.1.5. Circuit Details 130

A.1.6. Results and Discussion 132

A.1.6.1. Calibration Using Simulated Crack 132

A.1.6.2. Stability 133

A.1.6.3. Monitoring Fatigue Crack Growth 133

A.1.6.4. Application of ACPD to the Determination of R Curves 134

A.1.7. Conclusions 136

Appendix 2 Variation of Stress Intensity with Crack Length for a Griffith Crack Pressurised by a Constant Amount of an Ideal Gas 137

References 138

List of Tables

		Page
4.1.	Chemical Composition of En16 and En16M	143
5.1.	Details of Heat Treatment and Mechanical Properties	144
5.2.	Orientation Dependence of K_{IC} for En16M at a Yield Strength of 1300 MPa	145
5.3.	Comparison of Fracture Modes in Hydrogen Assisted Cracking with those in Air at Room and liquid Nitrogen Temperatures	146
6.1.	Orientation Dependence of Apparent Diffusivity of Hydrogen	147
A.1.1.	Comparison of COD Corresponding to the Minimum of the PD-CGOD Trace and Initiation COD Obtained by the Multispecimen Technique	148

LIST OF ILLUSTRATIONS

		Page
1.1.	Fracture appearance of a cracked pipe.	149
1.2.	Quasi-cleavage between MnS inclusions.	149
2.1.	Effect of hydrogen on the interatomic stress-distance curve.	150
2.2.	Schematic representation of the normally observed dependence of crack growth rate on stress intensity.	150
2.3.	Effect of H_2S pressure on K_{TH}.	151
2.4.	Effect of hydrogen pressure on K_{TH}.	153
2.5.	Relationship between hydrogen permeability and embrittlement susceptibility.	154
4.1.	Principle of the crack arrest technique using a modified self loaded WOL specimen.	155
4.2.	Sulphur print of a transverse section of En16.	157
4.3.	Sulphur print of a transverse section of En16M.	157
4.4.(a)	MnS inclusions in En16. Plane of view T.	158
(b)	MnS inclusions in En16. Plane of view L.	158
4.5.(a)	MnS inclusions in En16M. Plane of view T.	159
(b)	MnS inclusions in En16M. Plane of view L.	159
4.6.	Variation in lateral spread of MnS inclusions across the width and thickness of the billet.	160
4.7.	WOL specimen, bolt and loading pin.	161
4.8.	Crack plane orientation identification.	162
4.9.	Inclusion orientation in relation to the specimen orientation.	163
4.10.	Microstructure of En16 in the mid-section after quenching in normal oil and tempering at 400°C.	164
4.11.	Microstructure of En16M in the mid-section after quenching in fast oil and tempering at 300°C.	164
4.12.	Comparison of crack lengths measured by DCPD and compliance technique for a CKS specimen, under constant load.	165
4.13.	Strain gauge locations evaluated for monitoring load.	166
4.14.	Variation of load cell output with clip gauge output.	167
4.15.	WOL specimen with load cell and clip gauge.	168
4.16.	Testing in 3½% NaCl solution.	169
4.17.	Sectional view of the chamber used for testing in H_2S gas.	170
4.18.	External view of the chamber used for testing in H_2S gas.	171
4.19.	Variation of 'K' with crack growth under different testing conditions.	172

Page

5.1. Crack growth behaviour of En16 at a σ_{ys} of 1250 MPa in 3½% NaCl solution. 173

5.2. Crack growth behaviour of En16M at a σ_{ys} of 1300 MPa in 3½% NaCl solution. 174

5.3. Effect of inclusion volume fraction on K_{TH} in 3½% NaCl solution (σ_{ys} = 1250 - 1300 MPa). 175

5.4. Effect of inclusion volume fraction on stage II crack growth rate in 3½% NaCl solution (σ_{ys} = 1250 - 1300 MPa). 176

5.5. Fracture surface of En16M tested in 3.5% NaCl solution. Orientation ST. σ_{ys} = 1300 MPa. K ≃ 17 $MNm^{-3/2}$. 177

5.6. Fracture surface of En16M tested in 3.5% NaCl solution. Orientation ST. σ_{ys} = 1300 MPa. K ≃ 28 MN $m^{-3/2}$. 177

5.7. Fracture surface of En16M tested in 3.5% NaCl solution. Orientation ST. σ_{ys} = 1300 MPa. K ≃ 35 $MNm^{-3/2}$. 178

5.8. Fracture surface of En16M tested on 3.5% NaCl solution. Orientation SL. σ_{ys} = 1300 MPa. K ≃ 35 $MNm^{-3/2}$. 178

5.9. Fracture surface of En16M tested in 3.5% NaCl solution. Orientation SL. σ_{ys} = 1300 MPa. K ≃ 20 $MNm^{-3/2}$. 179

5.10. Fracture surface of En16 tested in 3.5% NaCl solution. Orientation SL. σ_{ys} = 1250 MPa. K ≃ 22 $MNm^{-3/2}$. 179

5.11. Nickel plated section of the fracture surface of En16M tested in 3.5% NaCl solution showing inclusion assisted intergranular cracking. Plane of view L. Orientation ST. σ_{ys} = 1300 MPa. 180

5.12. Fracture surface of En16M tested in 3.5% NaCl solution. Orientation LT. σ_{ys} = 1300 MPa. K ≃ 45 $MNm^{-3/2}$. 181

5.13. Fracture surface of En16M tested in 3.5% NaCl solution. Orientation LT. σ_{ys} = 1300 MPa. K ≃ 35 $MNm^{-3/2}$. 181

5.14. Section of the nickel plated fracture surface showing cracking along inclusions in En16M tested in 3.5% NaCl solution. Orientation LT. σ_{ys} = 1300 MPa. Plane of view T. 182

5.15. Section of the nickel plated fracture surface showing the opening of the inclusion-matrix interface and the retention of MnS inclusions exposed to the environment. All other details same as Figure 5.14. 182

5.16. Fracture surface of En16 tested in 3.5% NaCl solution. Orientation LT. σ_{ys} = 1250 MPa. K ≃ 32 $MNm^{-3/2}$. 183

5.17. Fracture surface of En16 tested in 3.5% NaCl solution. Orientation TL. σ_{ys} = 1250 MPa. K ≃ 33 $MNm^{-3/2}$. 183

Page

5.18. Nickel plated section of the fracture surface of En16 tested in 3.5% NaCl solution. Plane of view L. Orientation TL. σ_{ys} = 1250 MPa. 184

5.19. Cracking along the inclusions in TL orientation of En16. Other details same as Figure 5.18. 184

5.20. Crack growth behaviour of En16 at a yield strength of 1450 MPa in 3.5% NaCl solution. 185

5.21. Fracture surface of En16 tested in 3.5% NaCl solution. Orientation ST. σ_{ys} = 1450 MPa. $K \simeq 23\ MNm^{-3/2}$. 186

5.22. Fracture surface of En16 tested in 3.5% NaCl solution. Orientation ST. σ_{ys} = 1450 MPa. $K \simeq 17 MNm^{-3.2}$. 186

5.23. Discontinuous crack growth in En16M at a yield strength of 800 MPa in H_2S saturated 3.5% NaCl solution. 187

5.24. Discontinuous crack growth in En16M at a yield strength of 800 MPa in H_2S saturated 3.5% NaCl solution. 188

5.25. Discontinuous crack growth in En16M at a yield strength of 800 MPa in H_2S saturated 3.5% NaCl solution. 189

5.26. Continuous crack growth in En16 at a yield strength of 1250 MPa in 3.5% NaCl solution. 190

5.27. Crack growth behaviour of En16M at a yield strength of 800 MPa in H_2S saturated 3½% NaCl solution. 191

5.28. Crack growth behaviour of En16 at a yield strength of 900 MPa in H_2S saturated 3½% NaCl solution. 192

5.29(a and b) Fracture surface of En16M tested in H_2S saturated salt solution. Orientation: ST. σ_{ys} = 800 MPa. $K \simeq 40\ MNm^{-3/2}$. 193

5.30. Fracture surface of En16M tested in H_2S saturated 3.5% NaCl solution. Orientation SL. σ_{ys} = 800 MPa. $K \simeq 40\ MNm^{-3/2}$. 194

5.31. Fracture surface of En16M tested in H_2S saturated 3.5% NaCl solution. Orientation TL. σ_{ys} = 800 MPa. $K \simeq 40\ MNm^{-3/2}$. 194

5.32. Secondary cracks observed below the fracture surface in En16M. Orientation ST. σ_{ys} = 800 MPa. Plane of view L. Environment H_2S saturated 3.5% NaCl Solution. 195

5.33 Sub-surface cracks originating from inclusions in En16. Orientation ST. σ_{ys} = 900 MPa. Plane of view L. Environment H_2S saturated 3.5% NaCl solution. 195

Page

5.34. Sub-surface crack in En16M formed by the linkage of closely spaced inclusions. Orientation TL. σ_{ys} = 800 MPa. Plane of view L. Environment. H_2S saturated 3.5% NaCl solution. 196

5.35(a and b) Inclusion assisted secondary crack nucleation ahead of the main crack in En16. Orientation: ST. σ_{ys} = 900 MPa. Plane of view L. Environment H_2S saturated 3.5% NaCl solution. 197

5.36. Microstructure of En16M after hardening and tempering at 690°C. 198

5.37. Cracks in En16M tested in acidified 3.5% NaCl solution saturated with H_2S. Plane of view L. Orientation ST. $\sigma_{ys} \simeq 600$ MPa. 198

5.38. Modified procedure for testing in H_2S saturated 3.5% NaCl solution. 199

5.39. Crack growth behaviour of En16M at a yield strength of 1300 MPa in 0.1 MPa H_2S gas. 200

5.40. Fracture surface of En16M tested in 0.1 MPa H_2S gas. Orientation ST. σ_{ys} = 1300 MPa. $K \simeq 33$ MNm$^{-3/2}$. 201

5.41. Fracture surface of En16M tested in 0.1 MPa H_2S gas. Orientation ST. σ_{ys} = 1300 MPa. $K \simeq 20$ MNm$^{-3/2}$. 201

5.42. Discontinuous growth in En16M at a yield strength of 1200 MPa in H_2S saturated 3.5% NaCl solution. 202

5.43. Crack growth behaviour of En16M at a yield strength of 1200 MPa in H_2S saturated 3.5% NaCl solution. 203

5.44(a and b) Cracking ahead of the main crack as seen on the fracture surface of En16Mtested at a yield strength of 1200 MPa in H_2S saturated 3.5% NaCl solution. Orientation SL. 204

5.45. Cracking ahead of the main crack as seen on the fracture surface of En16Mtested at a yield strength of 1200 MPa in H_2S saturated 3.5% NaCl solution. Orientation SL. 205

5.46. Cracking ahead of the main crack as seen on a nickel plated section. Specimen details same as in Figure 5.44. 205

5.47. Cracking ahead of the main crack as seen on a nickel plated section. Specimen details same as in Figure 5.44. 206

5.48. Sub-surface crack in En16M. Specimen details same as in Figure 5.44. 206

		Page
5.49(a and b)	Inclusion assisted secondary cracks ahead of the main crack in En16M tested in H_2S saturated 3.5% NaCl solution. Orientation ST. σ_{ys} = 1200 MPa. Plane of view L.	207
5.50.	Inclusion induced cracking in En16M exposed to H_2S saturated 3.5% NaCl solution. Plane of view L. σ_{ys} = 800 MPa.	208
5.51.	Effect of interaction between inclusions on cracking in En16M exposed to H_2S saturated 3.5% NaCl solution. Plane of view L. σ_{ys} = 800 MPa.	208
5.52.	Cracks emanating from inclusions in En16 exposed to H_2S saturated 3.5% NaCl solution. Plane of view T. σ_{ys} = 800 MPa.	209
5.53.	Fracture surface associated with an internal crack in En16M exposed to H_2S saturated 3.5% NaCl solution. $\sigma_{ys} \simeq$ 600 MPa.	209
5.54.	Location of MnS inclusions in relation to the prior austenite grain boundaries in En16M. Plane of view L.	210
5.55.	Association of MnS inclusions with interdendritic segregation in En16M. Plane of view L.	210
6.1.	Electrical circuit for studying permeation behaviour.	211
6.2.	Permeation apparatus used for studying hydrogen transport behaviour.	212
6.3.	Permeation Cell (Schematic).	213
6.4.	Schematic rise and decay transients.	214
7.1.	Smith's model for cleavage fracture in mild steel.	215
7.2.	Variation of σ_{11} stress ahead of a stationary crack under monotonic loading.	215
7.3.	Variation of fracture stress, σ_f, with local intergranular concentration of Sb, Sn and P.	216
7.4.	Variation of σ_{11} stress ahead of a growing crack compared with that prevailing ahead of a stationary crack.	216
7.5.	Effect of hydrogen activity on K_{TH}.	217
7.6.	Effect of changing yield strength, critical distance and the inherent fracture strength of the matrix on the K_{TH} Vs. hydrogen activity relationship.	218
7.7.	Relative hydrogen concentration ahead of a growing crack as a function of V/D.	219
7.8.	Effect of inclusion orientation on hydrogen permeation.	220
7.9.	Energy-temperature curves for multiple laminates of the crack-divider type.	221

Page

7.10. Effect of Sulphur content on impact-transition temperature. 221
7.11. Ellipsoidal inclusion. 222
7.12. Thickness dependence of K_c (fracture toughness). 223
7.13. Cumulative hydrogen transmission through steel in aqueous hydrogen sulphide solution. 224
7.14. Effect of solution replacement on hydrogen transmission. 224
7.15. Effect of Sulphur content on time to failure. 224
7.16. Effect of plastic zone size and sulphur content on the apparent area fraction of inclusions on the fracture surfaces of the short transverse orientations. 225
A.1.1. Block diagram of the ACPD system. 226
A.1.2. Circuit for signal amplification and rectification. 227
A.1.3. Current and potential lead positions on the WOL specimen. 228
A.1.4. ACPD calibration for a WOL specimen with a simulated crack. 229
A.1.5. ACPD calibration for a WOL specimen with a fatigue crack. 230
A.1.6. Effect of load on the output from a fatigue cracked specimen. 231
A.1.7. Variation of PD and load with displacement during slow crack growth. 232
A.1.8. Comparison of a single specimen R curve obtained by ACPD and multispecimen R curve. 233
A.2.1. Mode I displacement of a Griffith crack under a uniform internal pressure 'p'. 234

CHAPTER 1

INTRODUCTION

Anisotropy of mechanical behaviour is manifested by several commonly used materials of which wood is a well known example. Even from early periods, the poor transverse properties of wood were well recognised and so it would not have come as a surprise to find wrought metals exhibiting similar behaviour. The absence of directional behaviour in cast metals led to the association of the working operation with the introduction of anisotropy. With the advent of the Industrial Revolution, problems caused by anisotropy in wrought steel were more acutely felt. There was a growing realisation that the cleanness of the steel determined the severity of anisotropy and so initial attempts were directed towards eliminating the problem at the source. But, even the cleanest steel of the day showed poor transverse and short transverse ductility and this was accepted as an unavoidable characteristic of the wrought condition as such. The problem, however, led to practices such as the specification of flow-line patterns in forgings and direction of bending in pressings and some of these practices have continued to this day.

Recent research on non-metallic inclusions in steel has been motivated primarily by the need to guard against the occurrence of low energy fibrous fracture. Hence, most work has centred around the deformation behaviour of inclusions during rolling and their role in fibrous fracture . It is now known that the adverse effect of inclusions on ductility and toughness is a consequence of the weak nature of the inclusion-matrix interface and the simultaneous deformation and alignment of non-metallic inclusions during hot working which provides low energy fracture paths in the short transverse plane. This leads to a pronounced deterioration of the through-thickness properties.

Compared to the study of non-metallic inclusions in steel, the subject of hydrogen embrittlement is of recent origin. The deleterious effect of hydrogen on ductility was first noted in high strength steels. It was soon realised that hydrogen assisted damage in steel could manifest itself at the different stages of production, processing, fabrication and use. The occurrence of hairline cracks, flakes and fish-eyes in ingots and forgings, blistering and embrittlement during electro-plating and pickling, heat affected zone (HAZ) cracking in welds and delayed failure in service were some of the problems caused by hydrogen.

It became regular practice to take special precautions to avoid the introduction of hydrogen at all stages, especially in the case of higher strength steels. This is also exemplified by the practice of matching welding consumables to process and material variables to minimise the risk of HAZ cracking in welds.

Although the adverse effect of hydrogen on the ductility of steel is now well appreciated, the reasons for the same are not well understood. Current opinion indicates two independent mechanisms by which hydrogen can cause damage at ambient temperature. First, as dissolved hydrogen it can cause embrittlement of the matrix. Secondly, by accumulating at weak interfaces in molecular form, it can assist cracking by a pressurisation mechanism. It is the embrittlement mechanism that has received by far the greater attention because the majority of problems caused by hydrogen occur in high strength steels where this mechanism predominates. The operation of the pressurisation mechanism was not considered to give rise to any serious problem as long as embrittlement was avoided. It was in this belief that low strength steels (<600 MPa yield strength) were specified for service in environments promoting the entry of large amounts of hydrogen. Recently, this long held notion had to be reviewed with the failure of a number of pipelines handling sour oil and gas, i.e. oil or gas containing hydrogen sulphide.

The pipeline material in all cases was controlled rolled steel. Failure was by stepwise cracking resulting from the linkage of a number of short cracks lying in the short transverse plane (Figure 1.1). On a finer scale, the short cracks were shown to be associated with elongated type II MnS inclusions, linked together by cleavage-like failure of the matrix (Figure 1.2). These failures were attributed to pressurisation of the inclusion-matrix interface by molecular hydrogen. This, combined with the unfavourable inclusion shape and distribution, resulted in the formation of numerous cracks in the short transverse plane which linked together to cause complete penetration of the pipe wall. The weak nature of the inclusion-matrix interface which permits the accumulation of molecular hydrogen, and the unfavourable shape and distribution of inclusions are once again seen to be the key factors in causing failure in the short transverse plane. The occurrence of a brittle mode of fracture in the matrix, at temperatures greatly in excess of the ductile/brittle transition temperature is indicative of the concurrent operation of the embrittlement mechanism.

The incidence of several failures over a short period resulted in a spate of investigations aimed at elucidating the role of inclusions in determining susceptibility to hydrogen assisted cracking. Most of these investigations were qualitative in nature and were limited to pipeline steels in wet H_2S environments. (An immediate and sure solution to the problem was to reduce the sulphur content to very low levels, typically less than 0.005%.) Although it has been claimed that the problem of hydrogen assisted cracking in pipeline steels has been solved, it appears that very little systematic work has been carried out. It is the aim of the present investigation to elucidate the role of non-metallic inclusions in hydrogen assisted cracking over a range of strength levels. By employing a fracture mechanics approach to the problem, it is hoped that more meaningful information will be obtained. The variables that are of interest include inclusion volume fraction, matrix strength, specimen orientation and hydrogen activity of the environment. Because crack growth rates are likely to be related to the rate of transport of hydrogen, the latter has been studied as a function of inclusion orientation.

CHAPTER 2

REVIEW OF HYDROGEN ASSISTED CRACKING

2.1. Introduction

Although the topic of hydrogen assisted cracking is of recent origin, there has been a rapid growth in the research effort, with the result that there is now a voluminous literature on hydrogen effects in ferrous materials alone. This chapter reviews the literature on important topics relevant to the present investigation. These will include the development of the theories of hydrogen embrittlement, the application of fracture mechanics to the characterisation of hydrogen assisted cracking, rationalisation of stress intensity effects and the effect of microstructural variables. A detailed discussion of the role of non-metallic inclusions, which is the theme of the present work, will form a separate chapter.

2.2. Early Observations and Theories

As in any other field, the evolution of theories of hydrogen embrittlement has been largely determined by observations and these are mostly macroscopic effects characteristic of hydrogen assisted cracking. The observation of blisters in pickled steel sheets, and fish-eyes and flakes in ingots and forgings showed that hydrogen can cause damage even in the absence of external stress. The detrimental effect of hydrogen on ductility was more marked in slow strain rate tests than under conditions of impact, and this indicated hydrogen transport to be an important step in the process of embrittlement. Baking at high temperatures (>200^{o}C) could be employed successfully to restore the properties, provided the hydrogen containing steel had not been kept at low temperatures for extended periods. This established embrittlement to be reversible under certain conditions. Compared to low strength steels, high strength steels were more susceptible and very small hydrogen concentrations typically 1-2 ppm, could cause severe embrittlement.

2.2.1. Planar pressure theory

The earliest theory proposed to account for hydrogen assisted cracking was the planar pressure theory of Zapffe (1941, 1947). According to this theory, hydrogen held in supersaturated solid solution precipitates at interfaces as molecular hydrogen. The pressure developed within the voids is determined by the extent of supersaturation.

For example, a dissolved hydrogen concentration of 2 ppm at ambient temperatures could lead to a pressure of 8000 bar (800 MPa) (Kazinczy, 1959). Such high internal pressures could cause cracking and premature failure with or without the application of external stress. The theory successfully explained the occurrence of flakes and fish-eyes in ingots and forgings. However, it ignored the embrittlement of the matrix by dissolved hydrogen and hence could not explain the loss of ductility.

The pressure theory suffered a major set-back when it was shown that hydrogen gas even at low pressures 1 bar (0.1 MPa) had a strong embrittling effect on high strength steels (Hancock and Johnson, 1966). It was argued that the pressure developed at internal defects could not exceed the external hydrogen pressure for thermodynamic reasons. This would therefore be too insignificant to contribute to the growth of internal cracks.

2.2.2. Embrittlement theories

The embrittlement theories invoked the effect of hydrogen on the interatomic stress-separation curve of the material to explain the deleterious influence of hydrogen (Figure 2.1).

Petch (1952, 1956) proposed that hydrogen atoms by being adsorbed on crack surfaces, effectively reduced the surface energy γ_s and hence decreased the fracture stress (the area under the stress-distance curve of Figure 2.1 represents 2 γ_s).

A similar embrittlement theory was proposed by Troiano (1960) who suggested that hydrogen atoms dissolved in the metal reduced the cohesive strength, σ_{max}, of the lattice (Figure 2.1). To explain the existence of an incubation period preceding crack initiation, and embrittlement by a small bulk concentration of hydrogen, Troiano invoked an interaction between stress state and hydrogen solubility. The introduction of hydrogen atoms into the interstitial sites of the iron lattice is accompanied by a positive volume change of the lattice. Therefore, to maintain a position independent chemical potential, hydrogen would tend to concentrate in regions of dilatational elastic strain, and would become depleted in regions of compressive strain. Thus, the triaxial stress state prevailing ahead of cracks and notches aids the concentration of the embrittling agent to a region that is most susceptible to fracture. It was suggested that at a certain combination of stress and hydrogen concentration fracture initiation took place.

Although there was no experimental proof at the time the model was proposed for hydrogen concentrating in regions of triaxiality, there was ample evidence to suggest that the region of maximum triaxial stress was the site of crack initiation. In tests carried out on notched tensile specimens pre-charged with hydrogen, it was found that the site of crack nucleation shifted towards the surface with decreasing notch root radius (Johnson et al, 1958). The effect of stress on hydrogen solubility has been confirmed by subsequent work (Wriedt and Oriani, 1970; Bockris et al, 1971).

Apart from the influence of stress triaxiality on hydrogen solubility, there is no real difference between the decohesion theory of Troiano and the surface adsorption theory of Petch. While the former emphasises the effect of dissolved hydrogen in lowering cohesive strength, the latter stresses the influence of adsorbed hydrogen in decreasing surface energy. This is merely a conceptual difference and reduction in surface energy or cohesive strength is looking at the same embrittling effect from two different points of view. However, it has been argued by Oriani (1977) that species which decrease the area under the stress-distance curve (Figure 2.1) need not necessarily reduce the cohesive strength σ_{max} (Figure 2.1) and it is only the latter effect that can cause embrittlement. Even if this argument were to be accepted, the method of incorporating the embrittling effect of hydrogen in any fracture criterion is through a decrease in the area under the stress-distance curve and hence mathematically there is little to choose between the two approaches.

An often quoted objection to the adsorption theory is that oxygen which adsorbs strongly on steel does not cause embrittlement. On the contrary, it actually reduces it markedly when present in a hydrogen environment, even in very small amounts.

It follows from the above theories that hydrogen may contribute to cracking by two independent mechanisms, namely matrix embrittlement and pressurisation. Embrittlement is the dominant mechanism in high strength steels (σ_{ys} > 1250 MPa), but in the absence of external stress pressurisation effects can be manifested. In the case of lower strength steels, which can tolerate much higher hydrogen activities, pressurisation effects dominate cracking behaviour but this is invariably accompanied by matrix embrittlement. There is considerable fractographic evidence to suggest that the pressurisation mechanism operates hand in hand with

embrittlement. For example, fish-eyes observed in forgings, weldments and hydrogen charged tensile specimens, normally show a zone of cleavage fracture around plate-like inclusions (Baker and Watkinson, 1961; Farrell and Quarrell, 1964). Following these observations, simple superposition models unifying the two effects have been proposed (Tetelman, 1973).

The term 'hydrogen embrittlement' is normally used in those cases where embrittlement effects dominate. More generally all hydrogen associated fracture phenomena can be referred to as 'hydrogen assisted cracking'.

2.3. The Application of Fracture Mechanics to the Study of Hydrogen Embrittlement

The traditional method of assessing susceptibility to hydrogen embrittlement consisted of testing smooth or notched tensile specimens pre-charged with hydrogen, at different stress levels and plotting stress against time to failure. Such comparative tests yielded information that was not amenable to quantitative interpretation and hence was of limited value.

The science of fracture mechanics was developed primarily for designing against unstable fracture in components containing cracks. Essentially, it employs the stress intensity factor 'K' to characterise the stress field at the crack tip. For an infinite plate containing a crack of length 2a under a remote stress σ normal to the crack plane, the stress intensity factor $K = \sigma\sqrt{\pi a}$. In the case of geometries with finite boundaries

$$K = \sigma Y\sqrt{\pi a}$$

where Y is a factor which takes into account the effect of the presence of finite boundaries. In materials which satisfy the requirements of linear elastic fracture mechanics (LEFM), the resistance to unstable crack propagation can be characterised by K_{IC}, the plane strain fracture toughness. The application of K to the study of sub-critical crack growth followed as a logical extension.

Brown (1968) was the first to apply fracture mechanics concepts extensively to the study of environment assisted sub-critical crack growth. His tests were similar to traditional environmental test methods except that notched specimens were replaced by pre-cracked specimens and stress was replaced by stress intensity factor 'K'. These tests demonstrated the existence of a threshold stress intensity, K_{TH}, below which there was

negligible crack growth. For a specific material environment combination, K_{TH} was found to be geometry independent, demonstrating the validity of the fracture mechanics approach.

In the early stages, interest was primarily on K_{TH}. Most subsequent studies have also aimed at studying crack growth behaviour over a range of stress intensities. It is important to recognise that unlike the traditional approach where time to failure includes the time required for both nucleation and growth of a crack, only the sub-critical growth of a pre-existing defect is considered with a pre-cracked specimen. This is one of the main reasons why the response to changes in metallurgical and environmental variables is not always similar in the two cases.

2.3.1. Stress intensity Vs crack growth rate

Typical K vs crack growth rate behaviour is shown in Figure 2.2. It is customary to separate this into three regions. In stage I, K has a strong influence on crack growth rate. In stage II, velocity is either independent of K or weakly dependent on it. The upper limit of stage II is set by the onset of instability when K tends to K_{IC}. This transition from stage II to K_{IC} represents stage III. In most high strength steels the transition from stage II to stage I behaviour is abrupt with the crack velocity dropping steeply to very low values ($<10^{-5}$ mm/sec). In those cases where the stage I shows a more gradual drop in crack growth rate, the existence of a genuine K_{TH} is difficult to establish. In such cases, the K corresponding to the smallest detectable crack growth rate (10^{-5} - 10^{-6} mm/sec) represents only an apparent K_{TH}.

2.3.2. Testing methods

Before discussing the K vs crack growth rate behaviour, it is appropriate to mention the testing methods employed to determine K_{TH}. Broadly they can be classified into two categories, namely rising load techniques and crack arrest techniques.

In the rising load test, a pre-cracked specimen is subjected to successively increasing load in the environment using small load increments until crack growth is detected. The load is maintained constant from this point and the crack length is monitored continuously. The minimum K necessary to cause detectable crack growth corresponds to K_{TH}.

In the crack arrest technique, crack growth is initiated in the environment at a stress intensity well above the expected K_{TH}. If the crack is allowed to grow under constant displacement conditions, K decreases with crack growth and the crack arrests at K_{TH}.

A detailed evaluation of the two techniques is made in section 4.3.

2.3.3. Interpretation of K vs crack growth rate behaviour

It is convenient to consider K_{TH} as a critical stress intensity factor very similar to K_{IC} (i.e. K_{TH} is the K_{IC} of the material in a hydrogen inducing environment). On reaching K_{IC} the crack grows in an unstable fashion. However, on exceeding K_{TH} the crack does not grow in an unstable manner because hydrogen transport is necessary for continued propagation. This leads to stable growth between K_{TH} and K_{IC}. With an understanding of the factors determining K_{TH} and the transport behaviour of hydrogen it should be possible to characterise K vs crack growth rate behaviour. Except for minor details, most models rely on the above approach to explain crack growth behaviour. Thus it is appropriate to examine the meaning of K_{TH} and attempt to relate it to microstructural and environmental variables.

2.3.4. Meaning of K_{TH}

The true K_{TH} in theory represents an equilibrium condition. At K_{TH}, a small increase of hydrogen pressure or stress intensity should result in crack advance. Conversely a small reduction in pressure or K should arrest a slowly moving crack. That this is so has been shown by Oriani (1977), who could arrest and restart a crack by varying hydrogen pressure slightly at various K values. From this a relationship could be obtained between hydrogen pressure and K, under conditions of crack arrest. These results provide convincing evidence for the existence of a genuine K_{TH} in steels of the type employed by Oriani (σ_{ys} = 1700 MPa).

McIntyre and Priest (1972) correlated K_{TH} with the formation of a stretch zone. The K_{TH} determined by the rising load technique was found to be similar in 3½% NaCl solution, 1 bar (0.1 MPa) hydrogen and H_2S gas of the same pressure. Pre-cracked specimens were loaded in air to K levels slightly above and below K_{TH}. It was claimed that no stretch zone formed at stress intensities below K_{TH}, but above K_{TH} a stretch zone could be detected. It was concluded that stretch zone formation led to the exposure of fresh metal surface facilitating

hydrogen adsorption from the environment. Hence stretch zone formation constituted the critical step in the embrittlement process. In other words, K_{TH} was determined mechanically and not environmentally.

There are various objections to this argument. Stretch zone formation is simply a manifestation of crack tip blunting prior to the onset of crack growth. With fatigue pre-cracks, stretch zone formation must commence as soon as the maximum stress intensity used in pre-cracking is exceeded and from then onwards it is likely to be continuous. It is difficult to visualise how it could be abrupt as suggested by McIntyre and Priest.

As pointed out earlier, K_{TH} can also be determined by arresting a growing crack and such a crack has no stretch zone associated with it.

The width of the stretch zone at a given K is inversely related to the yield stress. Therefore, high strength steels are likely to be more resistant to stretch zone formation than low strength steels. If the proposed arguments are valid, it follows that K_{TH} should increase with increasing yield strength. However, it is well known that high strength steels are more susceptible to hydrogen embrittlement than low strength steels.

As a corollary to McIntyre and Priest's interpretation of K_{TH}, it follows that K_{TH} is independent of hydrogen activity. While their results support such a view, there is now considerable evidence which indicates that K_{TH} depends on hydrogen activity. This aspect is discussed in detail in section 2.4.

Steels pre-charged with hydrogen show K vs crack growth rate behaviour very similar to that of steels tested under a gaseous hydrogen environment. In the case of pre-charged specimens, stretch zone formation has little relevance in determining K_{TH}. Any interpretation of K_{TH} should be applicable to both external and internal hydrogen embrittlement.

Since crack growth is extremely rapid in H_2S gas, it has been suggested by McIntyre and Priest that K_{TH} determination in H_2S gas can be used as an accelerated test technique to characterise the K_{TH} of a steel in any other hydrogen inducing environment. Clark and Landes (1976) carried out an extensive test programme to verify this and found that it had serious limitations. Even under a rising load test it was possible to detect a significant dependence of K_{TH} on H_2S gas pressure

and this dependence became more pronounced with decrease in strength (Figure 2.3). It may be concluded that it is only in high strength steels that K_{TH} can be relatively insensitive to hydrogen activity in the range of hydrogen activities normally encountered.

2.3.5. Interpretation of stage I and stage II behaviour

In stage I, crack growth rate strongly depends on K (Figure 2.2). Whether stage I represents a separate stage of crack growth or not is controversial. Most of the available evidence indicates that stage I merely represents a transition from threshold to the steady state growth conditions normally encountered in stage II. That it does not always show a steep slope may be attributed to K_{TH} being a narrow band for a given material rather than a unique value as is assumed normally. The microstructural inhomogeneity of the material and the statistical nature of cracking could be the cause of this behaviour. It is also of note that the transition from stage I to stage II is not accompanied by specific changes in fractographic features.

It is widely believed that stage II velocity is controlled by the rate of transport of hydrogen to the region of cracking. The weak dependence of crack growth rate on K is normally attributed to surface adsorption being the rate determining step in the transport of hydrogen. However, similar stage II behaviour is observed with pre-charged specimens (Lessar and Gerberich, 1976) and in this case only bulk diffusion can be rate controlling. Also it seems unlikely that surface adsorption would be rate controlling in such widely differing environments as H_2S gas, H_2 gas, sea water and distilled water.

2.4. Effect of Hydrogen Activity on Crack Growth Rate and Threshold

A considerable amount of data is available in the literature on the effect of different environments on crack growth rates. There is general agreement on the effect of increasing hydrogen activity on stage II growth rate. To quote one example, the stage II velocities for a high strength steel (σ_{ys} = 1350 MPa) in 3½% NaCl solution, 1 bar (0.1 MPa) hydrogen gas and H_2S gas of the same pressure were 0.001 mm/sec, 0.02 mm/sec and 10 mm/sec respectively (McIntyre, 1973). The extremely rapid growth rate observed in H_2S gas is explained by its ability to develop a high effective hydrogen activity. However, it is surprising to observe a slower growth rate in 3½% NaCl solution compared to 1 bar (0.1 MPa) hydrogen gas. If it is assumed that velocity is proportional

to the square root of the partial pressure of hydrogen, then the hydrogen pressure necessary to produce the same growth rate as in 3½% NaCl solution is 2.5 x 10^{-3} MPa. (This argument assumes that hydrogen embrittlement is the dominant mechanism of crack growth in 3½%NaCl solution. This point is discussed in section 2.7). The pH at the tip of a crack is ≈3.5 and the potential is - 0.4 (NHE) (Smith et al, 1970). The equivalent hydrogen pressure $P(H_2)$ calculated using the relationship

$$E_{H/H^+} = - 0.059\ pH - 0.029\ P(H_2)$$

turns out to be 4.5 x 10^4 MPa. This discrepancy leads to the conclusion that kinetic barriers at the surface control hydrogen ingress and lower the effective hydrogen activity of the environment.

The effect of hydrogen activity of the environment on K_{TH} depends on the embrittlement susceptibility of the steel. A compilation (Akhurst, 1979) of the results obtained from various sources on the effect of hydrogen pressure on K_{TH} is presented in Figure 2.4. The results tend to follow a relationship of the form

$$K_{TH} \alpha [P(H_2)]^{-m}$$

where $P(H_2)$ = pressure of hydrogen

m = exponent which varies between 0.1 and 0.5.

Clark and Landes (1976) found that K_{TH} became more sensitive to H_2S pressure as the strength level decreased (Figure 2.3). The results of McIntyre and Priest (1972) indicate that K_{TH} is independent of the hydrogen activity of the environment. The picture that emerges from the above observations is that K_{TH} depends on hydrogen activity. However, the range of hydrogen pressures over which K_{TH} is highly sensitive to hydrogen pressure depends on strength level. It occurs at lower hydrogen pressures over a narrow range in high strength steels. At increased hydrogen pressures because of saturation effects, the sensitivity to hydrogen activity is reduced. (The origins of the saturation effect are discussed in section 7.2.6.) As strength decreases pressure sensitivity is manifested over a wider, as well as a higher range of hydrogen activity.

2.5. Effect of Metallurgical Variables

2.5.1. Role of matrix strength

This is perhaps the most important variable that determines susceptibility to embrittlement. In aqueous and other hydrogen inducing

environments of low hydrogen activity, steels with σ_{ys} > 1250 MPa are found to be highly susceptible to embrittlement. This strength level is normally taken as the dividing line above which hydrogen embrittlement is a serious problem even in environments of low hydrogen activity. In environments promoting high hydrogen activity, the strength level below which there is relative freedom from cracking drops to about 600 MPa. This is the basis of the well known NACE (National Association of Corrosion Engineers) criterion which specifies a maximum hardness of HRc22 for steels used in an H_2S bearing wet environment. These observations bring out the strong interplay between matrix strength and hydrogen activity in determining susceptibility to cracking.

2.5.2. Role of composition and microstructure

In an extensive study of the effect of composition on susceptibility to cracking in quenched and tempered steels, Sandoz (1972) showed carbon and manganese to be detrimental. Other common alloying elements like Cr, Mo, S, P and Co appeared to have no significant effect on cracking susceptibility. Carter (1969) investigating the effect of Si additions on cracking resistance of AISI 4340 in aqueous environments, obtained significantly reduced stage II velocity but with very little improvement in K_{TH}. The beneficial effect of Si is normally attributed to its effect in postponing the transformation of ε carbide to cementite to higher temperatures, thus providing an increased number of hydrogen trapping sites.

In pure iron the addition of titanium has been found to reduce the amount of intergranular cracking in electrolytically charged specimens. Again this is attributed to its role as an effective hydrogen trap (Bernstein and Thompson, 1976).

The matrix microstructure has been found to exert a pronounced influence on resistance to embrittlement. For example, twinned martensite is found to have a greater susceptibility to embrittlement as compared to lath martensite (Boniszewski and Baker, 1965). Also in lower strength steels ($\sigma_{ys} \simeq 550$ MPa) quenched and tempered structures are found to be superior to normalised structures (Snape, 1968).

Intergranular fracture along prior austenite grain boundaries is the most common mode of cracking observed in hydrogen embrittlement. Hence it might be expected that prior austenite grain size could influence susceptibility to cracking. The reported results of the effect of

an increase in grain size on K_{TH} are conflicting and range from a favourable effect (Gerberich et al, 1976), no effect (Proctor and Paxton, 1969) to an unfavourable effect (Webster, 1969).

2.6. Connection Between Temper Embrittlement and Hydrogen Embrittlement

There is now increasing evidence for the existence of a strong connection between temper embrittlement and susceptibility to hydrogen embrittlement (Briant and Banerji, 1978). It is of course well known that temper embrittled steels fail along prior austenite grain boundaries which is identical to the fracture mode normally encountered in hydrogen embrittlement. Also noteworthy is the fact that tramp elements like As, Sb, Bi, Pb and P whose accumulation at the prior austenite grain boundaries results in reduced grain boundary cohesion, also happen to be hydrogen recombination poisons which promote hydrogen entry into the steel. There is some similarity in the role of alloying elements in affecting hydrogen embrittlement and temper embrittlement. Manganese is detrimental and titanium is beneficial in temper embrittlement (Briant and Banerji, 1978) and this is similar to their effect on hydrogen embrittlement (Sandoz, 1972; Bernstein and Thompson, 1976). The similarity is by no means complete. Silicon, which is beneficial in hydrogen embrittlement, is a temper embrittlement promoter.

It has been found that HY130 in the temper embrittled condition shows reduced K_{TH} and increased crack growth rate compared with the unembrittled condition (Yoshino and McMahon, 1974; Briant et al, 1978). It was also found that the fracture mode in hydrogen changed from intergranular separation in the embrittled condition to transgranular cleavage in the unembrittled steel. On this basis, it would appear that the fracture mode in hydrogen should be related to the low temperature fracture mode. However, it has been found that in commercial ultra-high-strength steels (σ_{ys} > 1400 MPa), the fracture mode in hydrogen is intergranular irrespective of whether or not the steel is in the temper embrittled condition (Briant and Banerji, 1978). It is regrettable that steels which have been tested for hydrogen embrittlement susceptibility have not usually had their low temperature fracture modes characterised. A simple test such as this would have yielded useful information about the existence of a correlation between the two fracture modes.

2.7. Mechanism of Cracking in 3½% NaCl Solution

To this day, there has been no direct evidence for hydrogen being the cause of cracking in aqueous environments like 3½% NaCl solution.

In such environments hydrogen is produced by corrosion reactions. However, this must necessarily involve simultaneous anodic dissolution. Hence, the identification of the dominant mechanism assisting crack growth becomes difficult. Several observations are often invoked as indirect evidence for the operation of a hydrogen embrittlement mechanism.

(i) The similarity in the responses of cracking susceptibility and hydrogen permeability to changes in applied potential as shown in Figure 2.5 is considered to support a hydrogen embrittlement mechanism (Barth et al, 1969).

(ii) The potential at the crack tip is - 0.4 (NHE) and the pH is ≈3.5. Both of these favour hydrogen discharge (Smith et al, 1970).

(iii) The activation energy of stage II crack growth rate in salt water and distilled water has been found to be around 34 kJ/mole (McIntyre, 1973; Landes and Wei, 1973). This value is similar to the activation energy of hydrogen permeation in steel.

(iv) Fracture modes obtained in hydrogen gas are similar to those in 3½% NaCl solution.

(v) For high strength steels, K_{TH} in 3½% NaCl solution, hydrogen gas and H_2S gas are similar (McIntyre and Priest, 1972).

All these observations are consistent with a hydrogen embrittlement mechanism operating in aqueous environments like 3½% NaCl solution.

2.8. Conclusions

The deleterious effect of hydrogen on the fracture behaviour of steel has been discussed in terms of the material and environmental variables. It has been shown that there is a complex interaction between embrittlement susceptibility, hydrogen activity, strength and microstructure, the last being the least understood. Fracture mechanics has found wide application mainly because of its ability to characterise cracking behaviour. However, very little progress has been made towards the more important aspect of relating microstructural features to stress intensity effects and this perhaps will be the most important and fruitful avenue of future research.

CHAPTER 3

THE ROLE OF NON-METALLIC INCLUSIONS IN HYDROGEN ASSISTED CRACKING

3.1. Introduction

In this chapter the literature on the role of non-metallic inclusions in hydrogen assisted cracking of steel will be reviewed. This will include the experiences of the welding and steel making industries where important observations on inclusion-hydrogen interactions have been made. The role of inclusions in hydrogen assisted cracking is discussed with emphasis on the behaviour of pipeline steels in sour oil environments. The effect of non-metallic inclusions on hydrogen transport is discussed in Chapter 6.

3.2. General Observations

Perhaps the most widely noted example of hydrogen-inclusion interaction is the occurrence of blisters in pickled steel sheets. These are invariably associated with plate-like inclusions or lamination defects. The shape and orientation of the inclusions, coupled with the low strength of the steel, favoured the formation of blisters in environments promoting the entry of large amounts of hydrogen.

Blister formation in steel sheets represents one extreme where pressure effects are dominant. More interesting cases of inclusion-hydrogen interaction show both embrittlement and pressurisation effects simultaneously. Fish-eyes observed on the fracture surfaces of ingots, forgings and weldments are often associated with inclusion features. Baker and Watkinson (1961) found that large plate-like inclusions formed the "pupil" of the fish-eye in fractured weld metal containing hydrogen. This was surrounded by a region which had failed by a cleavage mode, followed by a region of microvoid coalescence. Farrell and Quarrell (1964) observed very similar fish-eyes on fracture surfaces of hydrogen charged high strength steel. Ohnishi (1971) while studying directionality aspects of hydrogen embrittlement in a 800 MPa yield strength steel plate, observed fish-eyes in hydrogen charged specimens of different orientations. In all cases the fish-eyes were parallel to the plate surface and they became larger as the time of exposure to the hydrogen inducing environment was increased. Colangelo and Heiser (1974) observed that fish-eyes in forgings always ran parallel to the forging direction.

These observations suggest that hydrogen accumulates at the inclusion-matrix interface in molecular form. Because of the unfavourable shape of the inclusion, the resultant pressurisation leads to crack growth in the adjoining embrittled matrix.

3.3. Experiences in the Steel Making Industry

The possibility that hydrogen could be trapped in a harmless form by inclusions has been evaluated to reduce the incidence of hairline cracking. Barraclough (1961a) carried out experiments to determine the connection between the incidence of hairline cracking and the inclusion content of the steel. Additions of Ti, Al and Zr were tried and on subsequent processing of the ingots it was found that Ti treated steel was more resistant to hairline cracking. However, the steel was found to be too dirty and the technique could not be exploited. This beneficial role of Ti was rediscovered by Bernstein and Thompson (1976) as mentioned earlier. Barraclough (1961b) also reported that ultra-clean steels were more prone to hairline cracking compared with normal steels. Similarly the problem was rarely encountered in leaded steels. Hewitt (1961a) obtained results which were in agreement with Barraclough's. The occurrence of hairline cracking in blooms was found to be related to the sulphur content, higher sulphur contents having a beneficial effect. However, when the same approach was tried to overcome problems of hydrogen induced delayed failure in service, higher sulphur contents proved to be detrimental (Hewitt, 1961b). The unfavourable effect of sulphur on susceptibility to cracking under service conditions was confirmed by the findings of Haynes (1961). It was found that the time to failure of a high strength steel (σ_{UTS} = 1700 MPa) in 0.1 N HCl decreased with increasing sulphur and phosphorus contents. The large differences in time to failure are likely to be due to the poisoning effect of S and P on the hydrogen recombination reaction.

3.4. Experiences in the Welding Industry

In the welding industry, it is a widely held view that a steel of low sulphur content is more prone to HAZ cracking compared to a steel of normal sulphur content. This is normally attributed to the inclusions acting as innocuous traps for hydrogen. Investigations by Smith and Bagnall (1968) and Hewitt and Murray (1968) tended to confirm the beneficial role of sulphur in reducing HAZ cracking. However, the

mechanisms responsible for this behaviour were not determined. In view of the conflicting results obtained from later work, a detailed investigation was undertaken at the Welding Institute to study the reasons for the beneficial role of sulphur (Hart and Brooks, 1977). The results suggested that the favourable effect of sulphur on susceptibility to HAZ cracking was through a reduction in hardenability leading to decreased hardness of the HAZ. Because there was no correlation between sulphur content and diffusivity of hydrogen, the beneficial role of sulphur was not considered to arise from a hydrogen trapping mechanism.

Unlike the effect on HAZ cracking, the interaction of inclusions and hydrogen was shown to result in increased susceptibility to lamellar tearing. In another investigation at the Welding Institute (Farrar, 1977), it was found that in cases where lamellar tearing was a potential problem, high hydrogen contents in the weld metal tended to promote its incidence. No definite conclusions were reached about the mechanism by which hydrogen assists lamellar tearing. It is likely that hydrogen pressurisation of the inclusion-matrix interface, coupled with embrittlement of the matrix, assists the initiation of a lamellar tear. The examination of the fracture mode in relation to the presence of hydrogen could give useful information on the mechanism of hydrogen assisted lamellar tearing.

3.5. Anisotropy Effects in High Strength Steels

Hughes et al (1965) found that the time to failure of unnotched bend specimens of a high strength steel (σ_{UTS} = 1700 MPa) in 3% NaCl solution was strongly dependent on orientation. The short transverse orientation showed the shortest times compared to the longitudinal orientation which recorded much longer times. Very similar results were obtained by Davis (1963) on a similar high strength steel using unnotched specimens. In both these investigations the fracture surfaces did not reveal any inclusion features. For smooth specimens tested in aqueous environments, the time to failure is determined mostly by the time taken for the initiation of a defect, this being the slowest step. Also, as observed by Davis (1963) and Hughes et al (1965), the initiation site was always associated with sulphide inclusions. As inclusions are elongated in the rolling direction, the effective crevice depth and the number of corrosion sites will be sensitive to

orientation and this possibly explains the dependence of time to failure on specimen orientation.

3.6. Role of Inclusions in the Hydrogen Assisted Cracking of Low Strength Steels

As pointed out in the introductory chapter, the revival of interest in the role of inclusions in hydrogen assisted cracking, has been primarily brought about by a number of service failures in pipelines handling sour gas or oil. Most of the investigations in this field have been by the Japanese steel manufacturers who were the suppliers of the pipeline material. Almost all of them have employed the BP (British Petroleum) test method for the evaluation of susceptibility to hydrogen assisted cracking in sour environments (British Petroleum, 1973). In this test, ground blanks of the susceptible steel are immersed for 96 hours in a synthetic sea-water solution (ASTM D1141-75, 1975) saturated with H_2S gas. Transverse sections of the blanks are examined for the presence of stepwise cracks. The susceptibility is characterised in terms of the total length of the stepwise cracks over a given area. Although the test is qualitative in nature, useful information, in the form of trends, has been obtained.

Using the above method, Moore and Warga (1976) found that the most important factor affecting susceptibility to cracking was the sulphide inclusion morphology. Compared to type I inclusions, type II inclusions were found to be extremely detrimental. In a more detailed investigation at the Sumito Metal Industries (Miyoshi et al, 1976), the role of inclusion variables on cracking susceptibility was evaluated. Besides confirming the overwhelming influence of inclusions in determining susceptibility, it was found that cracking was favoured by the presence of low temperature transformation products which showed high hardness (HV 450). These hard regions were associated with the microsegregation of substitutional solute elements such as Mn and P. As would be expected, the regions of segregation were associated with sulphide inclusions which further aggravated the situation.

Miyoshi et al found that compared to controlled rolled steels, seamless tubes which were finished around 1000°C showed much less susceptibility to cracking, the extent of cracking being largely independent of sulphur content. Even in controlled rolled steels, low finishing temperatures had an adverse effect only when the sulphur content was high (0.016%) and not when the sulphur was low (0.007%).

The presence of crystallographic texture in controlled rolled steels was not considered to be a significant factor in determining resistance to cracking.

Miyoshi et al tried many approaches to eliminate the problem. Reducing the sulphur content to very low levels (<0.005%) largely solved the problem. Shape control of inclusions by rare earth additions was beneficial but did not eliminate the problem. Although the inclusions were spheroidised by the treatment, their clustering and realignment on rolling encouraged cracking. The addition of Cu(0.5%) eliminated cracking susceptibility by reducing the amount of hydrogen absorbed by the steel. This beneficial role of Cu has been confirmed by others (Inagaki et al, 1978) and is mainly attributed to the formation of a copper rich sulphide film which not only reduces corrosion but also prevents hydrogen ingress. The results of subsequent investigations are broadly in agreement with the above observations.

Results obtained in well casing steels of 700 MPa yield strength, in H_2S saturated acidified 3½%NaCl solution, show that the time to failure for the longitudinal orientation decreases with increasing sulphur content (Ohki et al, 1976). In this case the adverse effect of sulphur could be largely eliminated by shape control of inclusions using rare earth additions.

There have been very few investigations of the role of inclusions in hydrogen assisted cracking using the fracture mechanics approach. Cold worked C-Mn steel (σ_{ys} = 700-820 MPa) tested in sulphate solutions containing H_2S, was found to display pronounced anisotropy in crack growth rate and K_{TH} (Lees, 1977). The transverse orientation showed a stage II growth rate five times faster than the longitudinal orientation. The K_{TH} in the longitudinal orientation was approximately 50 $MNm^{-3/2}$ compared to 30 $MNm^{-3/2}$ in the transverse orientation. More significantly, crack growth was found to be discontinuous and this was taken as evidence that pressurisation of the inclusion-matrix interface was assisting crack growth.

A similar orientation dependence of K_{TH} has been reported by McIntyre and Banks (1978) in controlled rolled steels. The K_{TH} value of the TL orientation was lower than that of the LT orientation (Refer Figure 4.8 for orientations), the difference tending to increase with increasing sulphur content. Surprisingly, on cerium treatment

the orientation dependence of K_{TH} was reversed. This was attributed to the presence of cracks in the rare earth inclusions perpendicular to the rolling direction, caused by the low finishing temperatures. Anisotropy effects were also found in quenched and tempered steels, the LT orientation displaying superior resistance to cracking as compared to the ST orientation (Figure 4.8).

3.7. Conclusions

The role of non-metallic inclusions in hydrogen assisted cracking has been reviewed. From this it is apparent that under conditions of limited hydrogen availability and when inclusions are present in more innocuous shapes, the trapping of hydrogen at the inclusion-matrix interface can be beneficial. However, inclusions invariably have an unfavourable role when there is an unlimited supply of hydrogen, since this allows the development of high pressures at the inclusion-matrix interface. Increased volume fraction of inclusions, high aspect ratios and unfavourable inclusion types lead to rapid deterioration of resistance to cracking. .Also, in aqueous environments sulphide inclusions are found to have a deleterious effect in accelerating crack nucleation.

CHAPTER 4

CHOICE OF MATERIAL AND EXPERIMENTAL TECHNIQUES

4.1. Introduction

The primary aim of the work to be described in the following chapters is to determine the role of elongated inclusions in hydrogen assisted cracking as a function of matrix strength, hydrogen activity of the environment and inclusion orientation and volume fraction. This chapter concentrates on the selection of a suitable steel for this purpose and problems associated with it. The choice of the test techniques and the measurement of variables, especially crack length, are also discussed in detail.

4.2. Material

4.2.1. The need for using a model system

The bursting of pipelines handling sour gas or oil was primarily attributed to the presence of unfavourable MnS inclusion dispersions. With MnS inclusions, the inclusion characteristics can be controlled relatively simply and therefore it is convenient and appropriate to employ a steel containing MnS in the present investigation. It may appear from these arguments that controlled rolled steels similar to those from which the failed pipelines were manufactured, should be considered as the first candidate material. However, a number of reasons effectively eliminate this possibility as listed below.

(i) The inclusion content is maintained very low in pipeline steels and by the nature of the deoxidation practice followed, the inclusions are likely to be type II MnS unless the steel is rare earth treated. Type II MnS inclusions are not readily detected even in the as-cast condition and by the time the steel has been hot worked, the inclusions are usually less than 1μm in thickness and hence beyond the resolution of the optical microscope. If rare earth treated there is very little anisotropy and the inclusions tend to segregate heavily. It follows that the inclusion dispersions obtained in pipeline steels are uncontrollable and unquantifiable.

(ii) The range of strength levels that can be obtained with controlled rolled steels is limited and with the same steel it is not possible to change the strength level significantly by simple heat treatment.

(iii) Controlled rolled steels often show a pronounced crystallographic texture which is either inherited from the austenite or induced by the deformation of ferrite. This can introduce additional anisotropy effects and it will be difficult to isolate this from inclusion effects.

The nature of the material variables to be studied precludes the possibility of using commercial pipeline steels. Hence, it becomes necessary to use an alternative steel as a model system and the desirable features of such a system are discussed below.

4.2.2. Requirements of a model system

Ideally a model system selected for the present investigation should possess the following characteristics.

(i) It should have an inclusion population which can be controlled and characterised.

(ii) It should be possible to vary the matrix properties without altering the nature of the inclusion dispersion.

(iii) The dimensions of the specimen employed to determine K_{TH} and crack growth rate are dictated by the need to maintain plane strain conditions. The K measurement capacity of the specimen is strongly influenced by height 'H' (Figure 4.1). This means, ideally the material should be at least 62.5 mm (2½") thick. The selected material should be available in a size such that it is possible to extract specimens in all orientations of interest, satisfying the above requirements.

(iv) To study the effect of inclusion volume fraction on crack growth behaviour, the material should be available with two different inclusion volume fractions, with the matrix composition remaining constant. All the other inclusion characteristics, other than volume fraction, should be identical.

(v) The required range of strength levels (σ_{ys} = 1500 - 600 MPa) should be readily achieved in 25 mm thick sections by simple heat treatment, with the microstructure across the section remaining uniform.

(vi) While meeting requirement (iii) on size, the inclusions should be plate-like and show significantly different aspect ratios in the three planes, so that anisotropy effects will be substantial.

4.2.3. Selection of the model system

The necessity for obtaining a range of strength levels by simple heat treatment narrowed the choice to medium carbon low alloy constructional steels. Such a steel had to be available in two different sulphur contents. There were two possible means of achieving this. One way would have been to make two matched heats specially for the purpose of this investigation. By this means it would have been possible to keep the matrix conditions identical by adjusting the composition. Against this advantage, the ingot size would have been small (200 kg maximum) and when this had been worked to the required size, the reduction would not have been sufficient to introduce strong anisotropy. The other alternative was to use a commercial low alloy steel available in the resulphurised and in the unresulphurised versions. The steels En16 and En16M (presently known as 605/M/36 and 606/M/36 respectively) were selected because, besides being available with two different sulphur contents, they also appeared to satisfy the hardenability requirements. However, these steels are rarely produced in plate form and are normally used as rounds. Using either squares or rounds means that little difference in properties can be expected between the transverse and short transverse orientation. As a compromise solution, 110 mm square billets of En16 and En16M were obtained from Duport Steel and were subsequently hot forged to 62.5 mm x 150 mm section. The forging temperature was kept lower than normal (less than 1050°C) in order to increase the relative plasticity of the sulphide inclusions.

4.2.4. Material characteristics

The chemical compositions of the two steels are shown in Table 4.1 along with the specification requirements. The alloying elements Mn and Mo seem to have been kept intentionally on the lower limit. The carbon content of En16 is on the top side of the specification, while for En16M the reverse is true. It was found that while En16 responded to hardening quite well in conventional quenching oil, En16M had borderline hardenability and 25.4 mm (1") thick sections hardened in accelerated quenching oil showed transformation products besides martensite. The higher sulphur content of En16M meant that the Mn available for hardenability improvement was decreased by about 0.2% compared to that in En16. Also, the presence of MnS inclusions could have affected hardenability adversely through the following mechanisms.

(i) Inclusion-matrix interfaces by virtue of their high energy are preferred sites for ferrite nucleation.

(ii) Local depletion of Mn around MnS inclusions also promotes ferrite nucleation.

(iii) By inhibiting grain growth, inclusions lead to finer austenite grain sizes which also decreases hardenability.

Sulphur prints of transverse sections of the two steels are shown in Figures 4.2 and 4.3. Besides indicating the difference in sulphur content, they also show that compared to En16, there is noticeable segregation of sulphur in En16M. Typical MnS inclusions as observed on the longitudinal and transverse sections of specimens extracted from the core region of the billet are shown in Figures 4.4 (a,b) and 4.5 (a,b) for the two steels. The appearance of the deformed MnS inclusions suggest that in the as-cast condition they must have been of type I morphology

Metallographic examination revealed a variation in the lateral spread of the inclusions across both the thickness and the width of the billet section. The inclusions in the core region of the billet had suffered maximum lateral spread, whilst towards the peripheral region of the billet there was a gradual decrease in lateral spread. This variation in lateral deformation of inclusions was confirmed by the results of the quantitative metallography (Figure 4.6).

The mean apparent lengths of the inclusions were 25 μm and 28 μm in En16 and En16M respectively. The number of inclusions having greater than 2 μm width on the transverse section was 140/mm^2 and 630/mm^2 in En16 and En16M respectively. The ratio of the numbers of inclusions observed on the transverse section is similar to the ratio of the sulphur contents of the two steels. Hence, it is concluded that the characteristics of the inclusion dispersions other than volume fraction are comparable for the two steels.

4.3. Testing Methods

4.3.1. Time to failure tests

This method was originally employed for studying environment induced cracking using fracture mechanics concepts. Pre-cracked cantilever beam specimens are subjected to varying initial stress intensities under dead loading conditions and the time to failure is

recorded. The latter increases with decreasing initial K and tends to ∞ at K_{TH}.

Between the moment of load application and the onset of crack growth there is a finite time during which the fatigue pre-crack appears to be dormant. The failure time includes this incubation time and hence time to failure tests can be used only for K_{TH} determination and not for crack growth rate studies.

4.3.2. Rising load testing and its evaluation

In the rising load technique a pre-cracked specimen is subjected to successively increasing load in the environment until crack growth is detected. The load is maintained constant from this point and the crack extension is measured continuously. The lowest stress intensity necessary to cause detectable crack growth corresponds to K_{TH}.

The rising load technique is susceptible to a number of errors which can lead to the overestimation of K_{TH}. These are discussed below.

The incubation time mentioned earlier has been found to be sensitive to both the applied K and the maximum K used for fatigue pre-cracking. The incubation time will tend to 0 when K approaches K_{IC}, and when K approaches K_{TH} the incubation time will tend to ∞. A general trend of this nature has been found by Wei et al (1972). The incubation time is also sensitive to the environment. Aqueous environments in general show much larger periods (100 - 1000 hrs) compared to H_2S gas. The existence of the incubation period implies that the K_{TH} determined using a rising load test will be affected by the loading rate. This sensitivity to loading rate has in fact been found to exist. In general, the sensitivity of K_{TH} to strain rate is inversely related to the crack growth rate associated with the material/environment system. Therefore, the K_{TH} determined using a rising load test in aqueous environments is much more sensitive to strain rate than in gaseous H_2S environments (Clark and Landes, 1976). For the same reason the sensitivity to strain rate will be more marked in low strength steels than in high strength steels.

Incubation time has also been found to be related to the maximum stress intensity used for pre-cracking. Gilbreath and Adamson (1976) found that the incubation period reached very high values when the ratio of applied stress intensity to the maximum stress intensity used for

pre-cracking approached unity. This implies that a rising load test by its very nature is susceptible to history effects. It has been found by Jonas (1977) that prior overloading in air to a K above K_{TH} can result in an apparent increase of K_{TH} when measured by a rising load technique. Very similar effects have also been reported by Oriani and Josephic (1974). In their experiments it was found that when a given K was approached by a decrease in applied load, the hydrogen pressure necessary to cause crack growth was higher than when the same K was approached by an increase in load. These observations can be explained at least qualitatively in terms of overload effects. It can also be concluded from these observations that the maximum stress intensity to which a specimen is subjected outside the environment must be well below the anticipated K_{TH}, if valid K_{TH} values are to be obtained using a rising load test. For this reason, the maximum stress intensity used for pre-cracking must be kept low. This may not be a serious problem in low strength steels where K_{TH} is high. But in high strength steels where K_{TH} is around 7-20 $MNm^{-3/2}$, K_{TH} can be influenced by the pre-cracking procedure.

Besides being susceptible to stress history effects, there is evidence to show that the value of K_{TH} obtained in a rising load test, can also be influenced by the fracture mode obtained during fatigue pre-cracking. McIntyre and Walker (1977) found a K_{TH} of 17±1 $MNm^{-3/2}$ for a high strength steel (σ_{ys} = 1500 MPa) when the pre-crack had grown in a transgranular mode but K_{TH} decreased to 10.5±1 $MNm^{-3/2}$ when the pre-crack was grown with a 50% intergranular mode of fracture. In both cases the cracking mode in the environment was intergranular. While it is difficult to rationalise these effects, it shows the existence of another possible source of error.

In conclusion it can be stated that the K_{TH} determined using a rising load test is inherently susceptible to errors caused by sensitivity to loading rate, pre-cracking procedure and overload effects. However, if sufficient care is exercised to avoid these errors, it is possible to determine a true K_{TH} using the rising load technique.

4.3.3. Crack arrest method and its evaluation

In this method a pre-cracked specimen is subjected to an initial K considerably greater than the anticipated K_{TH}. The crack is then allowed to grow in the environment. If constant displacement of the loading point is maintained, K decreases continuously with crack growth

in most geometries and the crack arrests when $K = K_{TH}$. Normally the bolt loaded WOL (wedge opening loaded) specimen developed by Novak and Rolfe (1969) is employed to achieve constant displacement condition (Figure 4.1).

The crack arrest method does not suffer from any of the shortcomings of the rising load technique. Because the initial stress intensity is considerably higher than K_{TH}, the incubation times involved are necessarily small. Once the crack starts growing, steady state conditions are established at the crack tip and this continues until crack arrest. The region of crack arrest is then far removed from the pre-crack. This is an important difference and for this reason the crack arrest region where K_{TH} is determined is not prone to any of the history effects mentioned earlier. For these reasons it was decided to employ a crack arrest method to determine K_{TH} and crack growth behaviour in this investigation.

4.3.4. Details of the crack arrest method

Essentially, there are two possible ways of achieving decreasing K conditions with crack growth. One is to use a bolt loaded WOL specimen as mentioned earlier. The other alternative is to use a loading frame and maintain constant displacement conditions. Because of the relaxation of the loading frame with crack growth, the drop in load is not as fast as with an infinitely stiff loading frame. Hence, K does not drop rapidly with crack growth. This, of course, does not constitute a serious problem if a DCB (double cantilever beam) specimen with a long W (Figure 4.1) can be used. To achieve the same stiffness as obtained in a self loaded WOL specimen the loading frame would have to be extremely bulky. For this reason it was decided to take advantage of the inherent stiffness of the WOL specimen. However, it must be admitted that the measurement of load is more easily accomplished with a loading frame compared with the WOL specimen.

4.4. Specimen Preparation

4.4.1. Specimen dimensions

The dimensions of the bolt loaded WOL specimen are shown in Figure 4.7. Because the thickness of the forged stock was only 60 mm it was necessary to slightly scale down the dimensions of the modified 1T WOL specimen developed by Novak and Rolfe (1969). The specimens

were side grooved such that $B_n/B = 0.75$, where

B = unnotched specimen thickness

B_n = thickness measured between the roots of the side grooves. (Figure 4.7).

The stress intensity for the specimen with the side grooves is given by

$$K_I \text{ (Side grooved)} = K_I \text{ (plain)} \left(\frac{B}{B_n}\right)^{\frac{1}{2}}$$

Hydrogen embrittlement cracks and environment induced cracks in general have a tendency to deflect and this tendency is particularly pronounced in bend geometries like the WOL specimen. Also, the presence of strong anisotropy can accentuate this effect. By using side-grooved specimens, crack deflection can be avoided. Side grooves also suppress the formation of shear lips because of the increased constraint and thus increase the K measurement capacity of the specimen. This is an important consideration in testing low strength steels.

4.4.2. Extraction of specimens

The specimen orientations of interest are shown in Figure 4.8 and the configuration of inclusions in relation to the crack plane in the different orientations is shown in Figure 4.9. Each orientation is designated by two letters, the first representing the fracture plane by its normal and the second being the crack propagation direction. It would have been ideal to have studied inclusion orientation effects in all the six principal orientations. However, the dimensions of the forged stock were such that it was not possible to extract standard size specimens from the TS and LS orientations. Therefore, this investigation had to be confined to the study of LT, TL, SL and ST orientations.

As noted earlier in Section 4.2.4. a variation in lateral deformation of inclusions across both the width and thickness of the billet could be observed (Figure 4.6). In some cases inclusion rotation could also be seen near the periphery. For these reasons, it was considered necessary to avoid the sampling of the peripheral regions whenever feasible. Notches in the LT and the ST orientations were always cut from the side face and the fracture plane of the SL orientation always lay in the core of the forged stock. Ideally, all the specimens should have been extracted from the core of the billet.

However, this would have meant extensive machining and unacceptable wastage of material.

Heat treatment of an initial batch of machined specimens revealed the existence of a latent defect in the En16 billet. Subsequent non-destructive inspection revealed a lamination about 50 mm wide, located at the centre and running right through the forged stock. Therefore, the specimens in this case had to be positioned so as to avoid the defect. This necessarily meant that the crack plane of specimens in the SL and ST orientations could not be positioned at the ideal locations.

4.4.3. Heat treatment

The strength levels to be studied required a σ_{ys} ranging from 1500 MPa to 600 MPa. Machining a complicated geometry like the WOL specimen at high hardness levels proved to be difficult and hence it was decided to heat treat the specimens after finish machining. On austenitising at 840°C for 1 hour and quenching in conventional oil, En16 hardened right through the section (Figure 4.10) whereas En16M showed significant amounts of intermediate transformation products and gave a maximum hardness of 400 HV on the surface, dropping to 300 HV at the centre. This was clearly unacceptable. Quenching in accelerated quenching oil from 860°C was tried and this gave a more uniform hardness ranging from 470 to 500 HV. However, the structure still showed a small amount of ferrite and bainite (Figure 4.11). The as-quenched hardness of En16 was between 550 and 600 HV. This difference in hardness between the two steels was due to the higher hardenability and higher carbon content of En16 compared to En16M. To achieve similar strength levels in the steels it was therefore necessary to employ different tempering temperatures, especially for the high strength condition ($\sigma_{ys} \simeq 1300$ MPa). This difference in response to heat treatment was a serious drawback. Later, it was found that En16M specimens hardened quite well on quenching in water and there were no cracking or serious distortion problems. However, it was felt that at the low tempering temperatures employed complete removal of residual stresses might not be achieved. Hence it was decided to use oil quenched specimens for studying crack growth behaviour in the high strength condition.

The hardening problem could have been solved more easily by reducing the section thickness to about 12.7 mm (½"). In the high strength condition, this would have been more than adequate to maintain plane strain conditions. However, this approach meant the preparation of a separate series of specimens, bolt, loading pin, etc. and would have caused considerable inconvenience.

4.5. Test Environment

At first sight the obvious test environment to employ for studying hydrogen assisted cracking is H_2 gas. However, H_2 gas was not considered to be the ideal test environment for the present study for the following reasons.

Hydrogen purity, especially the presence of O_2 has been found to have a pronounced influence on crack growth behaviour (Hancock and Johnson, 1966; McIntyre, 1977). This means that extensive purification is necessary if H_2 is to be used as the test environment. Also, hydrogen at high pressures would have to be used to obtain the high hydrogen activity which is necessary to cause cracking in medium and low strength steels. This would have posed serious problems in constructing apparatus for handling high pressure hydrogen. The explosion hazard associated with the use of hydrogen is also a serious disadvantage. Against these disadvantages, the use of hydrogen would have facilitated the easy characterisation and control of hydrogen activity and more accurate estimation of the pressures developed at the inclusion-matrix interface. Moreover, the fracture surfaces would have remained clean, permitting detailed study.

The other possible environments included 3½%NaCl solution, H_2S gas, H_2S saturated 3½% NaCl solution and continuous cathodic charging. In the case of high strength steels, all the above environments cause significant sub-critical crack growth. H_2S gas can provide one extreme of hydrogen activity and low hydrogen activities can be obtained using 3½% NaCl solution. With low strength steels neither of these environments can cause significant crack growth. In this case it is necessary to employ H_2S saturated 3½% NaCl solution.

The use of aqueous environments, especially those not containing H_2S, to study hydrogen assisted cracking has serious disadvantages. It is not possible to prove that anodic dissolution is not directly assisting crack growth and it is equally difficult to have direct evidence in favour of a hydrogen embrittlement mechanism.

The use of H_2S bearing environments poses serious practical problems. For the continuous use of H_2S, efficient fume extraction systems are essential. There is increasing resistance to its presence in laboratory environments and many commonly used materials are attacked by H_2S. This is especially true of steel fracture surfaces exposed to H_2S bearing environments for long periods. Also PVC covered cables and exposed solder joints are affected adversely.

Dynamic cathodic charging as a means of inducing hydrogen appears to have attractive possibilities because of the ease with which hydrogen activity can be controlled. The ability to characterise hydrogen activity using the Nernst equation also seems to be a factor favouring its use. These advantages may be relevant to the testing of smooth or blunt notched specimens. However, in the case of pre-cracked specimens, the changes obtained in stage II growth rate and K_{TH} by varying applied potential are much smaller than that indicated by the Nernst equation (Van der Sluys, 1969; McIntyre and Walker, 1977). This relative insensitivity to changes in applied potential is normally attributed to the large resistive drop within the crack which leaves the electrochemical conditons at the crack tip unaffected (Doig and Flewitt, 1978). Because of these reasons, cathodic polarisation of pre-cracked specimens does not in any way provide an ideal method of inducing hydrogen at the crack tip.

On the basis of the above considerations it was decided to employ H_2S gas, 3½% NaCl solution and H_2S saturated salt solution as test environments.

4.6. Measurement of Crack Length and Stress Intensity.

To determine K vs crack growth rate behaviour it is necessary to monitor continuously K and crack length. This can be achieved by measuring any two of three parameters, namely crack length, load and mouth opening displacement (MOD). This is made possible because the three parameters are related to the compliance of the specimen which is known as a function of crack length for most of the commonly employed specimen geometries.

A widely used method for monitoring crack length during sub-critical crack growth is the potential drop technique. The principle behind this is that the resistance of a cracked body is a function of crack length. The potential drop obtained across the crack, by passing a constant current through the specimen, is used to determine crack length.

Both DCPD (direct current potential drop) and ACPD (alternating current potential drop) systems have been developed, although the latter has not been widely used. The DCPD technique has been claimed to be highly successful in monitoring crack growth during fatigue crack propagation (Ritchie, 1972). However, its use to measure crack length in environment induced cracking is beset with serious problems caused by shorting of the crack surfaces.

In this work, it was intended to employ two independent methods of measuring crack length, namely the potential drop technique and the compliance technique. By these means it was hoped to obtain more reliable measurements of crack length. Initially it was planned to employ the conventional DCPD system. However, because of a delay in the delivery of the current source, it was considered expedient to investigate the possibility of using an ACPD system. Among other things an ACPD system was expected to show better stability compared to DCPD and this was clearly desirable since most of the testing involved monitoring of crack length over long periods of time.

A simple ACPD system was developed, the details of which are discussed in Appendix 1. In this section, it is appropriate to discuss the problems associated with the application of PD systems for monitoring crack length during environment induced cracking.

4.6.1. Crack shorting in environment induced cracking

It has been widely reported that the DCPD technique markedly underestimates crack length when used to study environment induced cracking. (McIntyre and Priest 1971; Landes and Wei, 1973; Akhurst 1979). The variation of crack length as measured by a compliance technique with that indicated by PD is shown schematically in Figure 4.12. This behaviour is observed for a CKS specimen tested under constant load. The underestimation of crack length has been normally attributed to the crack faces shorting behind the crack front.

The reasons for crack shorting are not well understood. The rough fracture surface and the small crack openings normally encountered in environment induced cracking have been considered to be responsible for crack shorting. However, it is somewhat surprising that crack shorting is not a serious problem in monitoring fatigue crack growth where considerably lower stress intensities are encountered. This may be associated with the fact that a growing hydrogen embrittlement crack has very little COD (crack opening displacement) and in this it

differs significantly from a growing fatigue crack. It may appear that the problem of crack shorting should exist only in hydrogen and not in those cases where the environment can form insulating reaction products on the fracture surface. However, crack shorting has been observed with cracks grown in widely different environments like H_2 gas, NaCl solution, and distilled water (McIntyre and Priest 1971; Landes and Wei 1973; Akhurst, 1979).

McIntyre and Priest (1971) employed a linear correction technique by which the underestimated crack length determined by DCPD is matched to the final crack length. Although crack length is predicted correctly at initial and final crack lengths, intermediate values are still likely to be underestimated. A more rational correction scheme based on crack face separation has been used by Landes and Wei (1973) and convincing supporting evidence for its effectiveness has been provided. However, it is unlikely to be successful in those cases that show pronounced variation of fracture surface roughness and fracture mode with stress intensity.

Crack shorting has been found to be a serious problem even with cracks grown under increasing K conditions. Hence, it is likely to be more severe with cracks grown under constant displacement conditions where the angle subtended by the crack faces at the crack tip decreases continuously.

There is little published information on the behaviour of ACPD, in particular on its performance in monitoring environment induced crack growth. First trials with the present ACPD equipment when employed for monitoring crack growth in H_2S gas gave extremely disappointing results. Even with significant crack growth, there was very little change in apparent crack length, indicating that ACPD was much more susceptible to crack shorting than DCPD. Its use in this investigation to monitor crack length was therefore abandoned. More fruitful applications of ACPD, to characterise other crack growth phenomena, are discussed in Appendix 1 .

4.6.2. Crack length measurement by a compliance technique

The failure of the PD technique meant total reliance on the compliance technique, this being the only other feasible method of monitoring crack length. There are two approaches to the compliance technique, when applied to a self loaded WOL specimen. One is the

measurement of the load at the loading point by instrumenting the bolt or the loading pin. The other alternative is to use the more recent method of back face strain measurement (BFS), developed by Deans and Richards (1979) and successfully applied to monitor crack growth in hydrogen by Akhurst (1979). In this method the strain on the back face of the specimen is monitored continuously. Using prior calibration relating back face strain, crack length and load or MOD, the crack length can be determined from the back face strain if one of the above parameters is known.

The BFS technique is ideally suited for measuring crack length with cracks grown under increasing K conditions, because the back face strain per unit load increases significantly with crack growth. For example, with a CKS specimen the BFS increases by a factor of 10 as the relative crack length a/W (Figure 4.1) changes from 0.3 to 0.7. However, when the BFS technique is employed under constant displacement conditions, the sensitivity is decreased to a large extent. This is because the increase in BFS caused by crack growth is offset by the drop in load. For example with an initial K of 40 $MNm^{-3/2}$, the back face strain of a 25.4 mm thick WOL specimen varies from 400 μstrain to 800 μstrain when a/W changes from 0.3 to 0.7. Corresponding strains at the end of the loading bolt are approximately 1600 μstrain and 240 μstrain. Relaxation of the bolt and the pin would have an adverse effect on the strain changes at the loading bolt and a favourable effect on BFS change for a given amount of crack growth. The BFS technique requires the use of at least one strain gauge for each specimen. Also, the strain gauges have to be protected from the environment and this is likely to be a serious problem when testing in wet environments. With the strain gauges located on the end of the loading bolt, the problem is not so severe because this position can be relatively easily isolated from the environment.

In the light of the above considerations, it was decided to instrument either the loading pin or the bolt. The bolt experiences very large strain changes and hence this location was tried first. The strain gauges were positioned on two flats machined on the bolt end as shown in Figure 4.13, Trial 1. A half bridge consisting of a compression gauge and a Poisson gauge, each of 350 Ω resistance was used. The leads were taken out through two grooves machined along the length of the bolt. The bridge was energised by 3 Volts, the voltage being maintained constant to better than 0.1% using a circuit developed

by Unvala and Green (1974). Although the output signal from the strain gauges was adequate, the relationship between MOD and strain gauge output was highly non-linear. This is attributed to the loading bolt being subjected to torsional strains as well as compressive strain. Friction between the bolt and the loading pin, which persisted despite extensive lubrication, was considered to be the main cause of the torsional strain. It was also difficult to fix the small size strain gauges on to the bolt. For these reasons it was decided to attach the strain gauges to the faces of the loading pin (Figure 4.13` Trial 2). As before a compression gauge and a Poisson gauge were tried. Although the problem of non-linearity was not as severe as with the previous arrangement, the sensitivity was poor. Also, the output from the strain gauges in some cases passed through a minimum, during the initial stages of loading. This was possibly caused by bending of the pin resulting from its significant aspect ratio, the poor surface finish of the recess and distortion accompanying heat treatment.

A logical solution to overcome both of the above problems was to halve the width of the pin and to use a full bridge (Figure 4.13, Trial 3). On either face of the pin a composite gauge consisting of two orthogonal gauges, each of 350Ω resistance was placed. This full bridge arrangement was energised with a 6 Volts power supply. With this arrangement sufficiently large outputs could be obtained. Typically a load of 20 kN produced an output of 8-10 mV. The output of the strain gauges was fed into a differential amplifier of a gain of 50. A typical plot of MOD (clip gauge output) against output from the strain gauges (load cell output) is shown in Figure 4.14.

4.6.3. Determination of crack length using the instrumented loading pin

The compliance of the specimen as a function of crack length is known for a WOL specimen (Novak and Rolfe, 1969). The relationship connecting loading point displacement and load can be converted to one relating MOD (V) and load for various crack lengths (Figure 4.1). This modified form of the compliance relationship is more useful because in practice it is MOD rather than loading point displacement that is measured. The compliance relationship can be expressed in a form with crack length as the subject using curve fitting procedures. Such a form facilitates the calculation of crack length if MOD and load are known.

The following procedure was adopted for measuring crack length using the instrumented loading pin (also referred to as the load cell). The pre-cracked specimen was loaded to the required stress intensity in steps. Simultaneously the MOD was also measured using a clip gauge. Thus a plot between load cell output and MOD was obtained. The initial crack length was measured accurately on the broken halves of the specimen at the completion of testing and the modified compliance of the specimen for the initial crack length was calculated. Using this, the load cell output vs MOD relationship was converted to load cell output vs load relationship.

During a test, both the decay of the load cell output and MOD were measured. The load cell output was converted to load using the calibration established from initial loading. From this the modified compliance V/P was calculated. Using the relationship between ($\bar{a}$/W) and *EBV/P, the crack length was evaluated.

It might be felt that a better way of estimating load from the load cell output would be by calibrating the load cell separately using a testing machine. However, there are drawbacks to this method. First, the type of loading experienced by the load cell when used in the WOL specimen is not the same as that obtained when the bolt and the pin in the recess are loaded together in simple compression. Secondly, the load cell output vs load relationship was found to be dependent on the nature of the profile and surface finish of the recess and these conditions could not be kept identical for all specimens. Hence, it would have been necessary to calibrate the load cell along with the recess of every specimen. Because of these inconveniences and uncertainties, the direct method of calibration was not used.

4.6.4. Errors arising from the crack length measuring technique

The final crack lengths obtained from the compliance technique differed by ±2mm from the actual crack lengths measured on specimens broken open at the completion of testing. The error in K arising from this discrepancy was about ±3% and the error in crack growth rate was about ±15%. There was an additional source of error in crack growth rate measurements arising from the drifting of the crack length monitoring system. This contribution will depend on crack growth rate and the time over which it is measured. However, the drift behaviour of the crack monitoring system could not be characterised and

*E = Young's Modulus.

hence the error caused by this could not be estimated.

In those cases that show anisotropic crack growth behaviour, the crack growth rates of the extreme orientations differed by a factor of between 5 and 10 and the apparent K_{TH} (corresponding to a crack growth rate of 10^{-5} mm/sec) differed by a factor of 1.3 - 2. These differences are much greater than the expected errors in either crack growth rate or K_{TH}.

4.7. Testing Procedure

4.7.1. Fatigue pre-cracking

All the specimens were fatigue pre-cracked in air after final heat treatment. The pre-cracking was carried out in a servo hydraulic fatigue testing machine at a frequency of 10 Hz. The maximum stress intensity in all cases was less than 20 $MNm^{-3/2}$ and the R ratio was less than 0.1. The maximum stress intensity may appear to be high. However, as pointed out earlier (Section 4.3.3.), this is permissible when using a crack arrest technique for measuring crack growth behaviour and K_{TH}. The crack length after pre-cracking was approximately 23 mm, this corresponding to 3-4 mm of crack extension by fatigue.

4.7.2. Testing in 3½% NaCl solution

A 3½wt% NaCl solution was prepared using AR grade NaCl and distilled water. The solution was not deoxygenated.

The bolt and the loading pin were well coated with grease. A pair of knife edges were mounted on the front face of the specimen using a cyanoacrylate adhesive. The specimen was then assembled with the loading pin and bolt, and the clip gauge was mounted between the knife edges. An assembled specimen, ready for testing is shown in Figure 4.15. The load cell and the clip gauge outputs were allowed to stabilise and this was normally achieved after 2-4 hours. The specimen was then loaded in steps to the required MOD depending on the initial stress intensity desired. The loaded specimen was then placed vertically inside a flat bottomed glass dish (Figure 4.16). The dish was then filled with the 3½% NaCl solution to a level just above the notch, so that the load cell was clear of the solution. This level was maintained throughout the test by adding distilled water when necessary.

The load cell output was monitored continuously on a Honeywell x-t recorder. The clip gauge output was also recorded at regular intervals.

Crack growth in all cases was found to occur after an incubation period which was dependent on the strength level, initial stress intensity and orientation. The tests were terminated when the change in the load cell output over 12 hours was of the order of 0.5-2% of the initial reading (the lower limit corresponded to those cases where crack arrest took place farthest from the initial crack, around an a/W of 0.7 - 0.8). The crack growth rate corresponding to this change in load cell output was of the order of 10^{-5} mm/sec. Most of the tests lasted for a period of 2-6 days. The specimen was unloaded at the completion of a test and the zero of the load cell was checked. This was the primary indication of the state of the load cell. The unloading displacement obtained at the loading point at the end of the test was found to be always less (by up to 30%) than the initial V_y to which the specimen was loaded. Only an increase in V_y is possible during crack growth and this is due to the relaxation of the bolt and the pin. Therefore, the smaller displacement obtained on unloading was considered to arise from the rough fracture surfaces causing crack closure.

4.7.3. Testing in H_2S gas

For testing in H_2S gas a stainless steel chamber was fabricated. A sectional view of the same is shown in Figure 4.17 and an outside view is shown in Figure 4.18. The specimen is located between the two blocks fixed to the bottom plate, the usual loading bolt being replaced by a shaft with a threaded end. The shaft runs through the top plate and on the top end it is fitted with a worm gear attachment. With this simple loading system a large mechanical advantage is achieved. Other facilities like viewing port, electrical lead-throughs (not shown in Figure 4.17) were also incorporated. Because crack growth rates in H_2S are high, it was decided to record the outputs on punched tape. A high speed punch with a suitable interface was employed for this purpose.

To carry out a test, the top plate with the worm gear/shaft assembly was first removed and the pre-cracked specimen was threaded onto the shaft, and the load cell and the clip gauge assembled. The ACPD system built during the course of this investigation was first used to monitor crack growth in H_2S gas. To ensure that there were no parallel paths for current flow across the crack, a 1 mm thick Tufnul strip was placed between the load cell and the end of the loading shaft (Figure 4.17). For the same reason insulating strips were placed

where the specimen came into contact with the locating blocks and the bottom plate.

After the outputs from the load cell and the clip gauge had stabilised the chamber was evacuated to $<10^{-4}$ torr (1.3×10^{-8} MPa) using an oil diffusion pump backed by a rotary pump. The specimen was then loaded gradually and the output of the load cell and the clip gauge was recorded. The chamber was then isolated from the evacuating system and H_2S gas of commercial purity (99.5%) admitted into the chamber. The outlet valve on the chamber was opened and a continuous flow of H_2S (3-5 cc/minute) was maintained. Crack growth could not be initiated at stress intensities around 25 $MNm^{-3/2}$ even after waiting for a period of 3-4 hours. Therefore, the specimen was loaded further until crack growth could be detected and this occurred around 38 MN $m^{-3/2}$. Once cracking was initiated, it propagated rapidly.

Initial results showed that K dropped very little, even when the crack had grown from an a/W of 0.35 to an a/W greater than 0.9. This behaviour was somewhat unexpected from a WOL specimen. However, it was soon realised that the insertion of the 1 mm thick Tufnul strip was the major cause of the problem. The modulus of Tufnul being 6700 MPa (Harrison, 1978) it had suffered an elastic displacement equivalent to that of a 30 mm thick piece of steel of the same cross section. The use of Tufnul also gave rise to another problem. Because it was visco-elastic, at high stress intensities (hence at high loads), the load started decaying with time and this relaxation in load made crack initiation even more unlikely.

Because the results from the ACPD system were disappointing, its use was discontinued and subsequent tests did not require the insertion of a Tufnul strip.

With the removal of the Tufnul strip, there was a significant drop in K with crack growth. Also crack growth could be initiated at a lower stress intensity ($\simeq$33 MN $m^{-3/2}$). In spite of these improvements, the drop in K was not sufficiently rapid and in all cases, the crack arrested beyond an a/W of 0.8. This made it impossible to calculate K_{TH}.

An analysis of the variation of K with crack growth is shown for a number of cases in Figure 4.19. Besides showing the effect of the Tufnul strip in causing relaxation, it also shows that compared to the

behaviour of a WOL specimen externally tested in 3½% NaCl solution, K drops less rapidly for specimens tested in H_2S gas in the chamber. It is concluded that the elastic relaxation is significantly more for the specimen tested in the chamber. The retention of the applied torque through a flexible loading train was considered to be the cause of the increased relaxation.

Several attempts were made to initiate crack growth at a sufficiently low K, that crack arrest would take place within the valid region. Instead of loading in vacuum followed by exposure to H_2S gas, the specimen was gradually loaded after filling the chamber with H_2S. However, this modified procedure did not lead to a significant drop in the K required for initiating crack growth. Reduction of load on a growing crack was also tried. However, even a small decrease in load (5-10%) led to immediate crack arrest and hence this technique also could not be used. Therefore, from the tests carried out in H_2S gas only an upper limit for K_{TH} could be established.

4.7.4. Testing in H_2S saturated 3½% NaCl solution

A 3½% NaCl solution was kept in a glass dish and saturated with H_2S gas. A gas disperser was used to obtain effective mixing and the H_2S flow rate was maintained between 15-20 cc per minute for 4 hours. The bolt and the load cell were well greased before assembly. The assembled specimen was loaded and placed inside the glass dish containing the H_2S saturated salt solution. The level of the solution was kept just above the notch. The volume of the solution was around 500 cc. The dish with the specimen was kept inside an empty desiccator during the test to prevent rapid evaporation of the solution. The flow rate of H_2S was reduced to 5-10 cc per minute after a few hours of specimen immersion and was maintained at that level till the end of the test. Periodic (daily) additions of distilled water were made to the solution to make up for losses. After a few hours of specimen immersion, the solution started turning black on the precipitation of FeS. The pH of the solution remained around 4.5 throughout the test. Most of the tests lasted for a period of 300 hours. On the completion of testing, the specimens were unloaded and as before the zeroing of the load cell was checked. Because the load cell had been exposed to a very aggressive environment for a long period, it was considered desirable to use a new load cell with each specimen to obtain reliable results.

4.7.5. Fractography

At the completion of testing, most of the specimens were broken open in air. Specimens exposed to H_2S gas and H_2S saturated salt water were left outside the environment for 2-3 days before they were broken open. Some of the specimens were sectioned on a plane parallel to the crack growth direction and perpendicular to the crack plane at the middle section. This was done mostly with specimens tested in the ST and SL orientations. Such sections provided useful information on the role of inclusions in crack propagation. The formation of cracks ahead of the main crack could also be studied.

10 mm square specimens were extracted from the fracture surface for examination in the SEM. The fracture surfaces of specimens tested in 3½% NaCl solution were cleaned in a solution of 6N HCl containing 1.5 grams/litre of hexamethylenetetramine using an ultrasonic cleaner. The cleaning resulted in the removal of all the MnS inclusions exposed to the fracture surface. The results from cleaning in inhibited HCl were satisfactory with most specimens although a few specimens showed pitting damage.

On fracture surfaces exposed to H_2S gas or H_2S saturated 3½% NaCl solution, a black film of FeS had formed. The severity of attack decreased as the crack arrest region was approached. Most of the examination had to be restricted to these regions of crack arrest. It has been claimed that reduction in H_2 gas at high temperatures effectively reduces FeS to Fe which can be removed by ultrasonic cleaning (Interrante and Hicho, 1976). However, exposure to flowing H_2 gas at 650°C for 10 hours, followed by ultrasonic cleaning did not lead to a significant improvement in fracture surface appearance. Therefore all the specimens exposed to H_2S were also cleaned in 6N HCl with inhibitor added. This was effective only in those cases which had not suffered excessive attack by H_2S. These were mostly around the region of crack arrest. Even in such cases examination at high magnifications (> x 1000) did not yield meaningful information and hence most of the observations on the SEM were carried out at low magnification (≃ X 300).

To supplement the information provided by SEM observations, nickel plated sections of the fracture surfaces were examined. In such cases the fracture surfaces were not cleaned in the derusting solution, so

that inclusions, if any, were retained on the fracture surface. Plating of specimens tested in 3½% NaCl solution did not pose any serious problem. However, with specimens exposed to H_2S gas or H_2S saturated salt solution it was very difficult to get an adherent deposit and hence in these cases only a limited number of specimens were examined.

Most of the useful observations from optical metallography were made on sections transverse to the rolling direction. This is mainly attributed to the fact that the number of inclusions sampled by a plane section is maximum on this plane.

4.7.6. Determination of K vs crack growth rate behaviour

As mentioned in section 4.6.3., crack length and load at various instants were calculated from the load cell output and MOD. Using the relationship given by Novak and Rolfe (1969), corresponding K values were evaluated. All these calculations were carried out on a programmable pocket calculator.

Crack length values were plotted against time and a smooth curve was drawn through the points. The gradients of the tangents to the curve were determined at a number of points. The data points shown on the crack growth rate vs K plots correspond to some of the points at which the slopes were measured.

CHAPTER 5

RESULTS OF CRACK GROWTH BEHAVIOUR

5.1. Introduction

In this section measurements of crack growth behaviour of En16 and En16M tested in 3½%NaCl solution, H_2S saturated 3½%NaCl solution and 0.1 MPa H_2S gas are presented together with fractographic observations. Also reported are the results of exposure tests on unstressed specimens in H_2S saturated 3½%NaCl solution, and a comparison is made between the fracture modes in air at liquid nitrogen temperature and the modes of fracture obtained during hydrogen assisted crack growth.

5.2. Crack Growth Behaviour in 3.5%NaCl Solution

5.2.1. Behaviour of En16 at a σ_{ys} = 1250 MPa

The heat treatment details and mechanical properties for the steel in this condition are given in set A of Table 5.1. The crack growth behaviour for this set of specimens is summarised in Figure 5.1. All the crack growth rate vs stress intensity curves show the characteristic two stage behaviour consisting of a nearly K independent stage II followed by a steeply falling stage I leading to an apparent threshold stress intensity K_{TH}. It is seen that specimen orientation exerts a pronounced influence both on crack growth rate and on K_{TH}. The LT orientation shows the highest threshold and the lowest crack growth rate. This is followed by the TL orientation with the short transverse orientation, SL, showing the highest crack growth rate and the lowest threshold.

5.2.2. Behaviour of En16M at a σ_{ys} = 1300 MPa

The mechanical properties and heat treatment details for this condition are given in set B of Table 5.1. The crack growth behaviour of this set of specimens is shown in Figure 5.2. The orientation dependence of crack growth behaviour is very similar to the previous case. However, it is of note that the differences in stage II crack growth rate and K_{TH} between the longitudinal and the short transverse orientations have increased. This suggests that inclusion volume fraction has a pronounced effect on the anisotropy of crack growth behaviour. Two curves, corresponding to two specimens, are shown for the LT orientation. This indicates the extent to which the results are reproducible.

5.2.3. Effect of inclusion volume fraction on apparent threshold and crack growth rate

From the results of the tests on sets A and B, the effect of inclusion volume fraction on K_{TH} can be determined and this is illustrated in Figure 5.3. Here the apparent K_{TH} is taken to be the K that will result in a crack growth rate of 10^{-5} mm/sec. It is seen from Figure 5.3. that elongated inclusions increase the K_{TH} of the LT and TL orientations, while the reverse is true for the ST and SL orientations.

In arriving at the above conclusions, it has been assumed that inclusion characteristics other than volume fraction, such as size and aspect ratio, are identical for both the steels. More importantly an implicit requirement for plotting Figure 5.3. is that the response of the matrix to embrittlement is the same for the two steels. Although the strengths of the En16 and En16M are similar, the matrix characteristics of the two materials show differences in composition and microstructure and this can result in an overall shift of K_{TH} in all the orientations. The matrix microstructure of En16M shows a significant amount of bainite besides tempered martensite (Figure 4.11), whereas En16 consists wholly of tempered martensite (Figure 4.10). Results obtained by McIntyre and Priest (1972) indicate that K_{TH} in 3.5%NaCl solution is not significantly different for martensitic and bainitic microstructures at comparable strength levels. The free Mn content of En16 is 0.2% higher than that of En16M and the carbon content is similarly higher by 0.05%. Both carbon and manganese have been found to enhance susceptibility to cracking in 3.5%NaCl solution (Sandoz, 1972), but it is not possible to predict the magnitude of any downward shift in K_{TH} of En16 caused by the difference in composition. Such a shift, if present, should be small and it would be manifested in all orientations. It is therefore not likely to alter the trends shown in Figure 5.3. substantially.

The K_{IC} values of En16M in the 1300 MPa yield strength condition were determined for the different orientations using 25.4 mm thick CKS specimens. In all cases the micromechanism of fracture was fibrous. The results of the fracture toughness tests are presented in Table 5.2. At a yield strength of 1300 MPa the K_{IC} for a material with a low volume fraction of inclusions is expected to be about 100 MN $m^{-3/2}$ (Birkle et al , 1966). From the data given in Table 5.2.

inclusions are seen to have a detrimental effect on K_{IC} in all the orientations, although the effect is most pronounced with SL, ST and TL orientations. If this behaviour is compared with the effect of inclusions on K_{TH} (Figure 5.3.), important differences emerge. An increase in inclusion volume fraction has a strong beneficial effect on K_{TH} in the LT orientation and a less pronounced, although still favourable effect in the TL orientation. The decrease in K_{TH} in the short transverse orientation is not as pronounced as with K_{IC}.

The effect of inclusion volume fraction on stage II crack growth rate is shown in Figure 5.4. and it is seen that the introduction of inclusions increases the stage II crack growth rate in the short transverse orientations and decreases it in the longitudinal orientation. The effect of inclusions on the crack growth rate of the TL orientation is not very pronounced. Comparing Figure 5.3. and 5.4. it is seen that in those orientations where the presence of inclusions increases K_{TH}, the stage II crack growth rates are decreased and vice versa.

5.2.4. Fractography of short transverse orientations

On the macroscopic scale, the texture of the fracture surface showed a gradual variation with stress intensity. Regions corresponding to the initial stages of crack growth (regions of high stress intensity) had a rough, woody fracture surface. The roughness progressively decreased with crack growth and at the region of crack arrest the fracture surface was relatively smooth.

Specimens for examination in the SEM were cleaned in inhibited HCl. This dissolved all the MnS inclusions and hence their presence on the fracture surface could not be directly detected during observations in the SEM. However, this could be inferred from the appearance of the matrix associated with the inclusion. In all the ensuing discussions of SEM observations, any reference to the appearance of inclusions on the fracture surface really refers to the impressions left behind in the matrix which are indicative of their presence.

The fracture surface appearance of the ST orientation of En16M (for the 1300 MPa yield strength condition) in the region of crack arrest is shown in Figure 5.5. The matrix has failed in an intergranular mode, with a relatively small area fraction of inclusions appearing on the fracture surface. At slightly increased stress intensities, corresponding to the transition from stage I to stage II

there is no significant change in fracture mode (Figure 5.6). However, the extent of inclusion participation as indicated by the area fraction of inclusions on the fracture surface has increased. At still higher stress intensities there is a progressive decrease in the amount of intergranular fracture (Figure 5.7). This is largely replaced by fibrous fracture and some isolated regions of quasi-cleavage. Also, the area fraction of inclusions appearing on the fracture surface has increased.

The fracture surface of the SL orientation of En16M at a stress intensity corresponding to stage II, is shown in Figure 5.8. The features are very similar to those of the ST orientation shown in the previous figure. The arrest region in the SL orientation is shown in Figure 5.9. Again this is very similar to the arrest region of the ST orientation shown in Figure 5.5. and the decrease in inclusion participation is clearly apparent.

The fracture surface appearance of the arrest region of the SL orientation in En16, is shown in Figure 5.10. The level of inclusion participation is very similar to that of En16M in the arrest region.

It can be concluded from the fractographic observations that the ST and SL orientations have very similar fracture surface features. Examination of the region of crack arrest in the short transverse orientations indicated that the crack front had not assumed any preferred configuration with respect to the inclusions.

The extent of inclusion participation is seen to be related to the stress intensity. This dependence is manifested macroscopically as a change in fracture surface roughness with crack growth. Also, the appearance of a large area fraction of inclusions on the fracture surface is indicative of preferential crack propagation via inclusions. To confirm this possibility, nickel plated sections of the fracture surface were examined. This revealed a number of subsidiary cracks linking with the fracture surface, and these cracks were invariably associated with inclusion clusters. An example of this is shown in Figure 5.11.

5.2.5. Fractography of longitudinal and transverse orientations

On a macroscopic scale, the fracture surfaces of both the LT and TL orientations showed delaminations oriented normal to the fracture plane and parallel to the direction of crack growth. These were more

numerous with the LT orientation and at higher inclusion volume fractions. The appearance of the splits was similar to that obtained when this orientation undergoes fibrous fracture.

The fracture mode in the LT orientation was a mixture of quasi-cleavage and intergranular cracking (Figure 5.12). This was true even at the region of crack arrest. A number of holes can be seen on the fracture surface corresponding to the previous location of MnS inclusions. It is clearly seen from Figure 5.13 that there is a strong tendency for the holes to lie at the prior austenite grain boundaries. Also, the holes are all parallel to each other and are aligned to the direction of crack growth, adding further evidence that they correspond to MnS inclusions. However, it is not possible to conclude from the SEM observations whether there was any opening of the inclusion-matrix interface. To verify this, nickel plated sections of the uncleaned fracture surface were examined. It is seen from Figure 5.14 that the crack has branched in several regions along the inclusions which effectively act as crack dividers. The opening of the inclusion-matrix interface is also apparent (Figure 5.15). In cases where the inclusions lie close to each other, the matrix between them tends to fail in shear. Another important observation is that the inclusions have been retained on the fracture surface. This implies that there was no significant chemical attack of the inclusions exposed to the environment. Fracture surface features for the same orientation in En16 are similar to those of En16M (Figure 5.16).

The TL orientation also showed splits associated with inclusions. These had resulted in significant amounts of fibrous fracture in shear (Figure 5.17). The similarity in fracture surface profiles between TL (Figure 5.18) and the LT orientation (Figure 5.14) should be noted. The opening of the inclusion-matrix interface and the crack branching along the inclusions into the short transverse plane (Figure 5.19) also bore a strong resemblance to similar features observed in the case of LT orientation.

As with the short transverse orientation, the arrested crack front profile did not bear any specific relationship to the inclusions.

5.2.6. Effect of increasing matrix strength to 1450 MPa

A set of En16 specimens were quenched and tempered to a yield strength of 1450 MPa (Set C of Table 5.1). Their crack growth behaviour

in 3.5% NaCl solution is shown in Figure 5.20. It can be seen that there is very little orientation dependence of either K_{TH} or stage II crack growth rate. Also the growth rates are much higher and the thresholds considerably lower than in the case of the 1250 MPa yield strength condition. The presence of stage III behaviour and its persistence to low stress intensities in some cases should also be noted.

5.2.7. Fractography of 1450 MPa yield strength condition

The fracture surfaces from the 1450 MPa yield strength condition were very much smoother than in the previous cases. SEM observations showed that in the short transverse orientation there was little inclusion participation in the fracture process even at regions corresponding to stage III (Figure 5.21). Also the amount of tearing was negligible. Although the inclusion participation was small there was a progressive drop in inclusion participation with crack growth. At crack arrest there were no inclusion features on the fracture surface and cracking was almost entirely intergranular (Figure 5.22).

5.2.8. 'Incubation Time' behaviour in 3½% NaCl solution

The time elapsed between the immersion of the loaded specimen in the environment and the onset of crack growth is normally termed the incubation time. In the case of En16 in the 1450 MPa yield strength condition, this was only a few minutes. However, with En16M and En16 in the 1300/1250 MPa yield strength condition the incubation time was between 30 minutes and 2 hours depending on the orientation and initial stress intensity. The longitudinal and transverse orientations showed longer periods compared to the short transverse orientations.

5.3. Effect of Decreasing Matrix Strength to 800-900 MPa

5.3.1. Behaviour of En16M

A set of En16M specimens were tempered to a yield strength of 800 MPa (heat treatment details are those of set D Table 5.1). To obtain significant crack growth at this strength level, the environment had to be H_2S saturated 3.5% NaCl solution. It also required the use of high initial stress intensities (55 $MNm^{-3/2}$) even in the short transverse orientations. Most of the tests lasted for a period of 300 hours.

A distinguishing feature of the cracking behaviour of this set of specimens was the discontinuous nature of crack extension. This is illustrated in Figures 5.23 - 5.25. This behaviour was in contrast to that of the high strength steels ($\sigma_{ys} \geq 1250$ MPa) in 3.5% NaCl solution where crack growth was continuous (Figure 5.26). The latter resulted in a smooth transition to near zero growth rate at crack arrest. Similar behaviour was seen in the medium strength steels ($\sigma_{ys} = 800$ MPa) during the initial stages of crack growth. However, in this case crack arrest was only apparent and it was followed by periods of rapid crack growth, each of which was preceded by an interval over which there was very little crack advance. Several cycles of discontinuous growth were observed before final arrest. The increment of rapid crack extension varied between 0.5 mm and 2 mm. The period of arrest preceding each burst of fast growth ranged from 4 - 12 hours.

In order to characterise the crack growth rate vs K behaviour, the discontinuous curve was averaged to a smooth curve and the slope of this curve was measured at various points as before. The results thus obtained are shown in Figure 5.27, for the three orientations ST, SL and TL. The LT orientation did not show significant crack growth even at a stress intensity of 80 $MNm^{-3/2}$. This was close to the maximum permissible stress intensity dictated by the need to maintain plane strain conditions.

It is seen from Figure 5.27 that the maximum crack growth rate encountered in the short transverse orientation is greater than that for the same orientation, in the high strength condition (1300 MPa) in 3½% NaCl solution. However, it should be noted that the latter occurs at a lower range of K. Also, the difference in growth rate between the short transverse and the transverse orientations is greater than in the higher strength condition (1300 MPa). While the TL orientation exhibited a definite stage II regime, there was no clear indication of similar behaviour with the ST and SL orientations. The existence of discontinuous growth following an apparent arrest invariably led to a gradually decreasing stage I behaviour. This was rarely the case with the higher strength conditions.

5.3.2. Behaviour of En16

A set of En16 specimens, tempered to a yield strength of 900 MPa were also tested in H_2S saturated 3½% NaCl solution (heat treatment details and mechanical properties are given in Table 5.1, set E). This set of specimens showed intermittent growth characteristics similar to En16M in the 800 MPa yield strength condition. The results are shown in Figure 5.28. It is seen that the difference in stage II crack growth rate between the transverse and the short transverse orientations is less than that observed with En16M. Also, the crack growth rates are significantly lower compared to the previous case although they persist to lower stress intensities. Again, a gradually decreasing stage I behaviour is seen in the short transverse orientations. It is somewhat surprising that the apparent thresholds (corresponding to a crack growth rate of 10^{-5} mm/sec) of the short transverse and the transverse orientations are less than those of En16M in the 800 MPa yield strength condition.

5.3.3. Fractography of specimens tested in H_2S saturated salt solution

In all the specimens exposed to H_2S saturated salt solution, most of the fracture surface and the specimen faces were covered with a black film of FeS. On visual observation the specimens did not show evidence of blistering on the surface.

The typical fracture surface appearance of the ST orientation is shown in Figure 5.29 a and b. The extent of inclusion participation has increased compared to the high strength condition and the intervening matrix has failed in a quasi-cleavage mode. The fracture surface resembles the pipeline fracture shown in Figure 1.2. The fracture surfaces of SL and TL are shown in Figures 5.30 and 5.31, and the fracture modes are broadly similar to those of the ST orientation. (The cleaning process in this case has not been very effective.) Fracture surfaces in the case of En16 were very similar in appearance to those of En16M. However, in this case a significant amount of intergranular cracking could also be seen.

Examination of nickel plated sections of the fracture surface revealed a small number of secondary cracks below the fracture surface. These were mostly associated with closely spaced inclusions (Figures 5.32 and 5.33). However, there was no significant opening of the inclusion-matrix interface that could be taken as direct evidence for hydrogen pressurisation. Although sub-surface cracks were more

common in the SL and ST orientations, they were also seen in the TL orientation. An example of this is shown in Figure 5.34. Again the cracks are seen to emanate from closely spaced large inclusions. Specimens sectioned at the mid-thickness as mentioned in 4.7.5. showed the formation of secondary cracks ahead of the main crack and apparently not connected to it. An example of this can be seen in Figure 5.35 a and b. The secondary crack has formed at a distance of about 0.15 mm ahead of the main crack and it is clearly associated with inclusions. This indicates that its formation is inclusion assisted.

5.4. Behaviour of En16M in the 600 MPa Yield Strength Condition

A set of En16M specimens were tempered to a yield strength of 600 MPa for testing in H_2S saturated salt water. The heat treatment details and mechanical properties are given in Table 5.1, set F. The matrix microstructure consists of spheroidised carbides in a ferrite matrix (Figure 5.36). The maximum permissible stress intensity dictated by the need to maintain plane strain conditions was 67 $MNm^{-3/2}$. At a stress intensity of 60 $MNm^{-3/2}$ even the short transverse orientations did not show significant amounts of crack growth. This implies that the hydrogen activity at the crack tip was insufficient to cause crack growth.

It has long been known that H_2S saturated salt water is one of the severe environments that is capable of inducing large amounts of hydrogen and can cause extensive blister formation. Results obtained by Skei et al (1953) showed that the hydrogen input induced by such an environment was high in the initial stages of exposure, but then decreased rapidly because of FeS film formation. It was also shown that continuous replacement of the solution resulted in high hydrogen inputs being maintained over long periods. (A detailed discussion of this phenomenon and its relevance to the present work will be postponed to Section 7.8.3.) In an attempt to obtain cracking in the 600 MPa yield strength condition of En16M at sufficiently low stress intensities, it was decided to feed the notch tip continuously with H_2S saturated NaCl solution. The solution was also acidified with ½% acetic acid to promote greater hydrogen input. Figure 5.38 shows the arrangement used for continuously feeding the notch tip with fresh solution. With this arrangement crack growth could be obtained at a stress intensity of 40 $MNm^{-3/2}$ and it was found to be

discontinuous . However, after 6 - 7 mm of growth, the crack arrested. Subsequent examination of the specimen revealed evidence of blistering near the notch tip implying that a high hydrogen activity had been maintained for long periods at the notch tip. A sectional view of the arrested crack is shown in Figure 5.37. The formation of a number of disconnected subsidiary cracks ahead of the main crack can be seen and it is of note that these are associated with inclusion arrays.

5.5. Effect of Increasing Hydrogen Activity on the Behaviour of En16M in the 1200-1300 MPa Yield Strength Condition.

5.5.1. Testing in H_2S gas

To determine the effect of hydrogen activity on the anisotropy of crack growth behaviour, a set of En16M specimens was tested in 0.1 MPa (1 atmosphere) H_2S gas. The heat treatment details and the mechanical properties correspond to those of set B in Table 5.1.

As discussed in detail in section 4.7.3. valid K_{TH} values could not be obtained because of the difficulty of initiating crack growth at a sufficiently low K such that crack arrest took place within an a/W = 0.8. However, information on crack growth rate was obtained and this is presented in Figure 5.39. For all the orientations the stage II crack growth rate is higher than that in 3½% NaCl solution for the same condition. Also, there is very little orientation dependence of crack growth rate. For all the orientations the K_{TH} is less than 22 $MNm^{-3/2}$, implying that the LT and the TL orientations have much lower K_{TH} in H_2S gas than in 3½% NaCl solution.

5.5.2. Fractography

Only a limited number of specimens could be examined successfully because of the difficulty in removing the FeS film. The fracture surface appearance at high stress intensities is shown in Figure 5.40. The extent of inclusion participation is similar to that in 3½% NaCl solution for the same condition (Figure 5.7). However, cracking in H_2S gas is predominantly by a mixture of quasi-cleavage and intergranular fracture with a small amount of fibrous fracture. In 3½% NaCl solution, the predominant fracture mode at similar stress intensities was fibrous. This difference indicates that the severity of embrittlement in H_2S gas is greater than in 3½% NaCl solution.

Towards the region of arrest the mode of fracture in all orientations is predominantly intergranular with little evidence of tearing (Figure 5.41). This is also in contrast to the behaviour in 3½% NaCl solution where a significant amount of tearing could be observed even under arrest condition (Figures 5.5 and 5.9).

5.5.3. Testing in H_2S saturated salt water

Because valid K_{TH} values could not be obtained in H_2S gas, it was decided to use H_2S saturated salt water to study the effect of hydrogen activity on K_{TH}. This being a wet environment, crack growth could be initiated at sufficiently low stress intensities. The heat treatment details and the mechanical properties are given in Table 5.1 set G.

The crack growth behaviour of the SL orientation which was tested for a period of 6 days, is shown in Figure 5.42. After showing an apparent arrest, there is a burst of crack extension and this behaviour is similar to that obtained while testing the 800/900 MPa yield strength condition. In the case of the ST and LT orientations tested for similar periods, no discontinuous growth was observed. The crack growth rate vs K behaviour for the three orientations is shown in Figure 5.43. Although there is a pronounced orientation dependence of crack growth rate, the thresholds are relatively insensitive to orientation. The gradual fall in crack growth rate in the stage I regime of the SL orientation is a consequence of the discontinuous growth.

5.5.4. Fractography

The predominant fracture mode in all of the testing orientations was intergranular cracking. Most SEM observations were made at the region of crack arrest and the specimens in this case were not cleaned. In Figure 5.44a is shown a view of the arrested crack front observed on a specimen broken open in air 3 days after the completion of testing. An enlarged view of the region ≈1 mm ahead of the crack front is shown in Figure 5.44b. Zones of intergranular cracking often associated with inclusions can be seen together with areas that have failed in a fibrous mode. The latter were produced when the specimen was deliberately broken open in air. This strongly suggests that the intergranular cracking must have occurred ahead of the main crack during exposure to the environment. Another example of an isolated

region of intergranular cracking ahead of the main crack is shown in Figure 5.45. Examination of nickel plated sections of the fracture surface also revealed the presence of cracks ahead of the main crack (Figure 5.46 and 47). A small number of cracks could also be seen below the hydrogen induced fracture surface (Figure 5.48) and these were invariably associated with inclusions. It is also of note that these inclusions are present within the light etching regions. A sectional view of the arrested crack in the ST orientation is shown in Figure 5.49a. At the region of arrest a number of subsidiary cracks lying on different planes could be seen ahead of the main crack. An enlarged view of one of these subsidiary cracks shows it to be associated with an inclusion cluster (Figure 5.49b).

5.6. Testing of Unstressed Specimens in H_2S Saturated NaCl Solution

Blisters and internal cracks have frequently been observed in specimens of pipeline steels exposed to H_2S saturated synthetic sea water for 96 hours (British Petroleum Test, 1973). It was somewhat surprising therefore that similar features were not observed in 25 mm thick WOL test specimens exposed to the environment for more than 12 days. This apparent discrepancy is considered to arise for the following reasons. First, H_2S saturated NaCl solution does not constitute an unlimited source of hydrogen at the steel surface. Secondly, the concentration of hydrogen (dissolved and trapped) in the steel is influenced by the ratio of surface area to volume of the test piece. Finally, the extent to which blistering and internal cracking occurs is obviously related to the hydrogen concentration in the steel. However, it is also dependent on the volume fraction, shape, size and distribution of the inclusions, which act as sites for the accumulation of hydrogen. Hence, in the case of pipeline steel where section thickness is usually less than 10 mm and inclusions are low in volume fraction but have high aspect ratios, conditions are conducive to blistering and cracking. By comparison, the 25 mm thick WOL specimens containing a large volume fraction of inclusions when exposed to a limited supply of hydrogen do not show blisters or internal cracks.

To confirm the above ideas, as well as to study the role of inclusions in cracking of unstressed specimens, a number of plain specimens in various thicknesses were exposed to H_2S saturated 3½% NaCl solution. The specimens were 50 mm long, 25 mm wide and the thickness

was varied between 2 mm and 5 mm. The test piece orientations were such that either the T plane or the S plane formed the 25 mm x 50 mm surface of the specimen. It was reassuring to see blisters even after 96 hours of exposure. The extent of blistering appeared to be greater in the thinner specimens. Subsequent metallographic examination of polished and etched sections revealed inclusions assisting both initiation and propagation of cracks. Most of these cracks were observed on transverse sections (L plane) and they were seen to be associated with inclusions that had large dimensions in the transverse direction (Figure 5.50 and 5.51). A crack initiating from an inclusion normally propagated in the plane of the maximum tensile stress. However, when it approached a nearby inclusion which was not lying in the same plane, it deviated to join up with it. This effect of crack path being dictated by the presence of neighbouring inclusions is also seen from Figure 5.50 and 5.51. These observations clearly demonstrate the existence and the significance of inclusion-inclusion interaction in both the initiation and propagation of cracks caused by hydrogen pressurisation at the inclusion-matrix interface. This interaction is also seen to depend on the dimensions and the relative positions of the inclusions.

It was somewhat puzzling that in the same specimen, very few cracks could be observed on the T plane (Figure 5.52) when large numbers of them could be seen on the L plane. In those cases where cracking was observed the cracks initiated and propagated in the light etching regions of the banded structure. Another significant aspect of cracking from inclusions was the absence of any significant crack opening displacement at the tip of inclusions. This implies that in addition to providing a source of stress by pressurisation of the inclusion-matrix interface, the hydrogen embrittles the steel and permits a brittle mode of crack propagation.

Some specimens in which the T plane formed the 25 mm x 50 mm surface, were fractured in the short transverse plane, a few days after the completion of testing. Examination of the fracture surface (uncleaned) in the SEM revealed zones that had failed by inclusion induced hydrogen assisted cracking (Figure 5.53). The mode of failure in the matrix was quasi-cleavage. The significance of the role of closely spaced inclusions in causing cracking is again apparent.

5.7. Comparison of Low Temperature Fracture Modes with the Fracture Modes in Hydrogen Embrittlement

It was argued in section 2.6 that the fracture mode in hydrogen assisted cracking may be related to the low temperature fracture mode. To verify the existence of such a correlation, Charpy size specimens were fractured at liquid nitrogen temperature and then examined in the SEM. The fracture modes obtained in hydrogen assisted crack growth and those in air at room and liquid nitrogen temperatures are presented in Table 5.3.

It is seen from these results that there is no apparent correlation between the low temperature fracture mode and that obtained in hydrogen assisted cracking.

5.8. Location of Inclusions

It was noted in Section 5.2.5. that inclusions showed a tendency to be located at the prior austenite grain boundaries. This is an important factor in determining their role in hydrogen assisted crack growth especially when the fracture is along prior austenite grain boundaries. To confirm the observations made on fracture surfaces (Figure 5.13), a few specimens in the quenched and tempered condition were subjected to a repeated etching and polishing technique to develop the prior austenite grain boundaries. The etchant used was aqueous picric acid with a wetting agent added to it. The microstructure revealed by this procedure is shown in Figure 5.54. It is seen that there is a marked tendency for the inclusions to be associated with prior austenite grain boundaries.

Another important observation mentioned in Section 5.6 was that cracking occurred preferentially in the light etching regions of the banded structure. Microhardness measurements showed that the light etching region was harder by 40-50 HV compared to the rest of the matrix. Also, metallographic observation showed that MnS inclusions were preferentially associated with the light etching regions (Figure 5.55). This indicates that the latter correspond to the interdendritic regions in the original ingot and would therefore be expected to be enriched in substitutional solute elements such as P and Mn.

It may be concluded that the reasons for the light etching regions being the susceptible zone for cracking are three fold. These are

the embrittling effect and the hardening effect of the segregated elements and the more frequent occurrence of inclusions.

CHAPTER 6

ORIENTATION DEPENDENCE OF HYDROGEN TRANSPORT BEHAVIOUR

6.1. Introduction

Early observations on the strain rate sensitivity of hydrogen embrittlement indicated hydrogen transport to be an important step in the cracking process. The rate at which hydrogen could be transported to the site of embrittlement was considered to determine the rate of crack propagation. It is now well established that hydrogen diffusivity is sensitive to microstructural variables including the volume fraction of inclusions (Thompson and Bernstein, 1980). In the present investigation it is possible that anisotropy of crack growth rate could be due in part to anisotropy in the diffusivity of hydrogen, this being caused primarily by the presence of elongated MnS inclusions. For this reason it was decided to study the orientation dependence of diffusivity of hydrogen. Before presenting an account of the experimental details, the effect of microstructure on the transport behaviour of hydrogen in steel and its relevance to the study of hydrogen assisted cracking will be reviewed.

6.2. Diffusion of Hydrogen in Steel

Although the diffusivity of hydrogen in α iron is very high compared to many other interstitials, it is well known that the diffusivity values obtained at room temperature are much lower than those expected from extrapolating high temperature data (Fast, 1971). Also the measured diffusivity values show a very wide variation. For example reported values of diffusivity, D, in α iron at room temperature (25°C) range from 10^{-9} m^2sec^{-1} to 6×10^{-12} m^2sec^{-1} (Kumnick and Johnson, 1974). Two possible explanations have been put forward to account for this anomalous behaviour. One is that surface reactions and not volume diffusion is rate controlling and in most experiments surface conditions have not been identical (Fast, 1971). The alternative suggestion is that hydrogen is trapped at a number of internal sites thus leading to a lower apparent diffusivity (Darken and Smith, 1949). A number of microstructural features such as grain boundaries, dislocations and interfaces between the matrix and second phase particles have been considered to be possible trap sites. The wide variation in the diffusivity values has been attributed to the microstructural dependence of trap density, and there is now considerable experimental evidence to support this view.

6.3. Effect of Metallurgical Variables on the Transport Behaviour of Hydrogen

Grain size has been found to have little effect on the apparent diffusivity of hydrogen in pure iron (Radhakrishnan and Shreir, 1967; Bockris et al, 1965). In quenched and tempered plain carbon steels, the diffusivity of hydrogen reaches a minimum for steels tempered around 300°C and the hydrogen solubility reaches a maximum (Newman and Shreir, 1969). An increase in carbon content does not change this temperature but the maximum solubility increases and the corresponding diffusivity decreases. These observations lead to the conclusion that hydrogen is trapped at the carbide-matrix interface and tempering at 300°C produces a very fine dispersion of carbides resulting in a maximum density of traps. By using autoradiography it has recently been confirmed that hydrogen is strongly trapped at carbide-matrix interfaces and at grain boundaries (Asaoka et al, 1978).

Sulphide inclusions in steel have been found to retard hydrogen diffusion. However, it was observed that hydrogen was not retained permanently at the inclusion-matrix interface (Boniszewski and Moreton, 1967). These findings are in agreement with those of Evans and Rollason (1969a and b). It has also been found that diffusivity depends strongly on the thermomechanical history of the steel. Diffusivity measurements made using a thermal charging technique showed that cold rolling resulted in a drop in diffusivity. This drop was found to be associated with a decrease in the density of the steel. On subjecting the cold rolled material to a swaging treatment, the diffusivity and the density increased. By comparison, in pure iron the diffusivity values were relatively insensitive to deformation history and correspondingly little change in density was observed. From this it was concluded that voids forming around inclusions during working were acting as traps for molecular hydrogen. It also follows from the above observations that a direct correlation between sulphur content and diffusivity need not exist. The results obtained by Chew and Fabling (1972) confirm this. Evans and Rollason (1969a and b) also found that after prolonged annealing at high temperatures (1380°C), the diffusivity values of previously cold worked steels with different inclusion contents were similar and this was attributed to the elimination of voids. This implies that MnS per se has no affinity for hydrogen.

Both solubility and diffusivity of hydrogen have been reported to be orientation dependent in rolled steel plate (Ohnishi, 1971). The rate of hydrogen diffusion was found to be highest in the longitudinal direction and lowest in the short transverse direction. The solubility, as determined by the maximum amount of hydrogen absorbed during exposure to 5% acetic acid saturated with H_2S was found to be higher for specimens with the S plane exposed compared to those with the L plane exposed. Because solubility is a volume property it cannot be directional and therefore the reported effect must be due to the differences in the ease of blister formation on the exposed planes. It follows that the conclusions regarding the directionality of diffusivity are also invalid.

Directionality of hydrogen transport has also been observed in cylindrical bars by Smialowski (1977). The steady state permeation rate in the longitudinal direction was found to be higher than in the transverse direction. However, it should be noted that severe charging conditions were used and hence the apparent difference in permeation rate could have been caused by blister formation. These results should therefore be interpreted with caution.

It may appear from the above discussion that some progress has been made towards understanding the effect of microstructure on the transport behaviour of hydrogen. However, the same cannot be said about correlating trapping effects to hydrogen embrittlement susceptibility. While some trapping sites may be innocuous and hence have a beneficial role on cracking susceptibility, others like grain boundaries are detrimental. The effect of trapping could manifest itself as a change in stage II crack growth rate if bulk diffusion was rate controlling. However, any change in trap characteristics and density will almost invariably alter the failure criterion, with the result that it is difficult to isolate the effect of a change in diffusivity on crack growth rate. It is not surprising therefore that no correlation has been found between crack growth rate and apparent diffusivity (Kortovich and Steigerwald, 1972).

6.4. Experimental Method

Although a number of techniques have been used for studying hydrogen transport behaviour, those most widely used can be broadly divided into evolution or permeation techniques. To investigate the directionality of diffusivity caused by the presence of plate-like elongated inclusions, it is convenient to employ thin plate specimens.

Most permeation techniques utilise thin sheet specimens and hence a permeation technique was used. From among the many versions of the permeation method, the widely employed electrometric permeation technique developed by Devanathan and Stachurski (1962) was chosen because of its simplicity. In this technique a thin disc of the material of interest is sandwiched between two flanges (Figure 6.1). Hydrogen is generated on one side by cathodic polarisation under galvanostatic conditions. A small part of the hydrogen generated on this surface diffuses through the steel to the opposite side which is anodically polarised under potentiostatic conditions. This means that any hydrogen diffusing out is immediately oxidised. The current flowing in the anodic circuit is a direct measure of the hydrogen flux through the membrane. (The method of calculating diffusivity from rise and decay transients, will be discussed in the results section.)

Although the electrometric permeation technique may appear to be simple, experience has shown that a number of precautions have to be taken to ensure reproducible results. For a given current density, the steady state permeation current is influenced by the nature of the cathode surface, the purity of the electrolyte and the type of coating if any (Heidersbach et al, 1977). This implies that the effective hydrogen activity is sensitive to all these variables in addition to the current density. In the present investigation, the area of inclusion-matrix interface available to the environment is strongly dependent on orientation and this can influence the hydrogen activity. Therefore, to ensure identical conditions, the entry side of the specimen was coated with a thin layer of palladium. (It is normal practice to coat the exit side with Pd to prevent Fe dissolution.)

To ensure that diffusion along the radial direction is negligible, the diameter to thickness ratio must be greater than 10. However, if there is strong anisotropy in diffusivity, this ratio must be increased further. Also, in order to observe significant inclusion effects and to avoid the presence of pin holes, the thickness of the membrane should be several times the maximum inclusion dimension. In practice, the thickness is limited by the need to get a significant permeation current which reaches a steady state within a reasonable time. The cathode current density is also limited by the need to avoid blistering and internal damage. As a compromise solution, the thickness of the disc was 1 mm and the diameter of the area exposed to

the electrolyte was 50 mm.

6.5. Experimental Apparatus

A view of the permeation cell is shown in Figure 6.2. This is depicted diagrammatically in Figure 6.3. and the circuit diagram is shown in Figure 6.1. The thin disc is clamped between the two flanges of the cell compartments using O rings. Blackened platinum foil is used as counter electrode and for reference, a saturated calomel electrode (SCR) is employed with a Luggin capillary which terminated at the plane of the flange. Provision is also made for the continuous scavenging of the solution with oxygen-free-nitrogen. The permeation current is measured on a strip chart recorder by monitoring the voltage drop across a 100 Ω high stability resistor (50 ppm/°C).

6.6. Preparation of Experimental Materials

It would have been ideal to have studied the permeation characteristics of microstructures identical to those used in the study of crack growth behaviour. However, because of differences in the section thickness of the specimens employed in the two cases, this could not be achieved. Also, the primary aim of the permeation experiments was to study the anisotropy of diffusivity and not the effect of matrix microstructure on diffusivity. This objective would be accomplished as long as the microstructures for the different orientations were kept identical.

Discs having a diameter of 60 mm and 1.5 mm thickness were machined in the three orientations. They were austenitised at 840°C for 20 minutes and then quenched in normal oil. One set of specimens was tempered at 420°C for 4 hours and another set at 680°C for 24 hours. The specimens were then finish ground to 1 mm thickness. In En16, the pipe defect mentioned earlier (section 4.4.2.) could not be avoided on specimens taken parallel to the L plane. This resulted in cracking during heat treatment and hence this part of the investigation had to be restricted to the study of En16M alone.

Usually permeation specimens are polished to a mirror finish. In the present case this was not feasible because of the large surface area of the specimen. Also the specimens were slightly bowed which aggravated the problem. Therefore, the specimens were polished on a lathe with silicon carbide paper to a 800 grade finish. The specimens

were then degreased in alcohol and acetone and dried. They were then coated with a thin layer of palladium using an electroless palladium plating solution (DNS palladium plating solution from Johnson Matthey Chemicals). The specimens were successively rinsed in distilled water, alcohol and acetone and dried. The dried specimens were stored in a desiccator.

A 0.1 N solution of NaOH was prepared using AR NaOH and deionised water. The solution was deoxygenated for 24 hours by bubbling oxygen-free-nitrogen using a gas disperser.

6.7. Experimental Procedure

The prepared specimen was clamped between the two cells and the anode compartment was filled with 0.1N NaOH solution. The specimen was immediately anodically polarised to a potential of - 0.3 Volts (SCR). The background current in the anodic circuit was initially high but gradually decreased to reach a low value ($1\mu A/cm^2$) after 24 hours. Continuous bubbling of the solution with oxygen-free-nitrogen was maintained to remove dissolved oxygen. After the background current had attained a steady value, the cathode compartment was also filled with 0.1N NaOH solution. Immediately, cathodic polarisation of the specimen under galvanostatic conditions was commenced. The current density was maintained at 5 mA/cm^2. (This value may appear to be high and would have resulted in blister formation with poisoned acid solution. However, there is little risk of blistering with alkaline solutions (Smialowski, 1977). This was confirmed by visual examination after the tests which did not reveal any blister formation.)
After about 15-20 minutes hydrogen could be detected on the anodic side and the permeation current slowly increased to give a rise transient. After the permeation current had reached a steady value the cathodic polarisation of the entry side was immediately reversed to anodic polarisation under potentiostatic conditions. The potential was kept at - 0.3 Volts (SCR). After a few minutes the permeation current started to decrease, yielding a decay transient. A typical permeation transient is shown in Figure 6.4.

6.8. Analysis of Results

A number of methods based on classical diffusion theory exist for calculating diffusivity from rise and decay transients (Devanathan and Stachurski, 1962). Unfortunately the diffusivity values obtained by the various methods are significantly different (Heidersbach et al, 1977).

In the present case the diffusivities were calculated by plotting $-\ln\left(\frac{P_\infty - P_{tr}}{P_\infty}\right)$ against time t_r, where

P_∞ = steady state permeation current

P_{tr} = permeation at time t_r of the rise transient (Figure 6.4).

The slope of this straight line represents $\frac{\pi^2 D}{L^2}$ where D is the diffusivity and L is the membrane thickness. A similar plot of $-\ln\left(\frac{P_{td}}{P_\infty}\right)$ against the time, t_d, of the decay transient (Figure 6.4) yields a slope which corresponds to $\frac{\pi^2 D}{L^2}$.

The values of D obtained by the above procedure for the two extreme orientations, namely L and S are given in Table 6.1. It can be seen that there is no detectable orientation dependence of diffusivity either in the 420°C tempered condition or in the 680°C tempered condition. The diffusivity values of the 680°C tempered material are higher than those of the 420°C tempered condition. This behaviour has been observed by others (Newman and Shreir, 1969) and confirms the view that the carbide-matrix interface is a potent trapping site.

6.9. Discussion

The diffusivities calculated from the permeation transients are based on the assumption that standard diffusion theory is applicable to the characterisation of hydrogen transport in steel. Strictly speaking, this is not valid for the characterisation of diffusion in the presence of traps. Modified forms of the diffusion theory have been developed that take into account the effect of trapping, but their application requires a knowledge of the trap characteristics (McNabb and Foster, 1963). For these reasons the diffusivities calculated from the permeation transients should be considered as 'apparent' diffusivity values. This does not reduce their usefulness for characterising crack growth rate behaviour because a similar transient condition is prevailing ahead of the growing crack. However, the effect of plasticity at the crack tip and opening of the inclusion-matrix interface may render the use of these values invalid.

MnS inclusions are sites where hydrogen can be trapped in molecular form. As discussed above, voids may be formed during the deformation processing of the steel or they may arise from differences in thermal

expansion coefficients between the MnS inclusion and the matrix (Brooksbank and Andrews, 1968). The presence of voids associated with MnS inclusions can affect the transport behaviour of hydrogen in two ways. First, the voids have a large capacity for storing molecular hydrogen. Secondly, they can provide paths for the rapid transport of hydrogen. Whilst the former mechanism decreases apparent diffusivity, the latter increases it. (Because the activation energy of diffusion has been found to be unaffected by the presence of voids (Evans and Rollason, 1969b), the $H_2 \rightleftarrows 2[H]$ reaction can be assumed to be rapid compared to the diffusion of hydrogen through the matrix and the voids.)

All of the reported results show that MnS inclusions decrease the apparent diffusivity of hydrogen in steel (Evans and Rollason, 1969a and b; Boniszewski and Moreton, 1967). This means that the trapping effect of the voids is dominant. Any anisotropy of diffusivity caused by the presence of elongated MnS inclusions must arise solely from the contribution of the second mechanism. The absence of significant anisotropy of diffusivity, as shown by the present results, implies that this contribution to diffusivity is negligible.

It may be concluded from the results of the permeation experiments that anisotropy of crack growth rate does not arise from differences in hydrogen diffusivity.

CHAPTER 7

DISCUSSION

7.1. Introduction

The experimental results demonstrate that matrix strength, hydrogen activity of the environment and inclusion orientation and volume fraction exert a pronounced influence on crack growth behaviour. In the 1250/1300 MPa yield strength condition, both En16 and En16M exhibit anisotropy of crack growth behaviour in 3½% NaCl solution. The introduction of inclusions increases K_{TH} of the longitudinal and transverse orientations. In the short transverse orientations the presence of inclusions decreases K_{TH}. The crack growth rate is at a minimum in the longitudinal orientation and at a maximum in the short transverse orientation. The difference in crack growth rate between the extreme orientations increases with increasing inclusion volume fraction.

An increase in the yield strength of En16 to 1450 MPa increases crack growth rate and decreases K_{TH} for all orientations in 3½% NaCl solution. More importantly, there is little anisotropy in either crack growth rate or K_{TH}. A similar effect is shown by En16M in the 1300 MPa yield strength condition when the test environment is changed to 0.1 MPa H_2S gas.

A decrease in yield strength to 800-900 MPa necessitates the use of H_2S saturated 3½% NaCl solution to obtain significant cracking. The anisotropy of crack growth behaviour is similar to that observed for the 1250/1300 MPa yield strength condition in salt solution. However, in contrast to the continuous crack growth observed in 3½% NaCl solution, crack extension in H_2S saturated salt solution is discontinuous in the short transverse and transverse orientations. Fractographic observations show that in the short transverse orientations discontinuous crack growth is associated with the inclusion assisted nucleation and growth of subsidiary cracks ahead of the main crack.

The fracture mode in the high strength condition ($\sigma_{ys} \geq$ 1200 MPa) is predominantly intergranular. In the 800-900 MPa yield strength condition the mode of fracture is quasi-cleavage.

Permeation studies showed that hydrogen diffusivity does not depend on inclusion orientation.

7.2. Hydrogen Assisted Cracking in the Absence of Inclusions

Any attempt to explain the observed effects of inclusions on hydrogen assisted cracking necessarily requires an understanding of the effect of hydrogen on the fracture behaviour of the inclusion free material. The primary aim in this case is to gain insight into the micromechanism of fracture, so that it may be possible to predict K_{TH} and stage II crack growth rate from the material and environmental characteristics. The micromechanistic modelling approach has had considerable success in explaining carbide initiated transgranular cleavage fracture in mild steels and quenched and tempered steels. Because of its relevance to the understanding of hydrogen assisted cracking, this theory is examined here in some detail.

7.2.1. Carbide initiated cleavage fracture in steels

It is now well established that transgranular cleavage fracture in mild steel is initiated by the cracking of grain boundary carbides which can occur either by a dislocation pile-up mechanism or by a fibre loading mechanism. In a growth controlled situation, the critical event determining fracture is the propagation of the carbide microcrack into the ferrite matrix. The condition for propagating a carbide microcrack formed by a pile-up mechanism has been shown to be given by the following expression (Smith, 1966).

$$\left(\frac{\ell_o}{d}\right)\sigma_F^2 + \tau_{eff}^2\left[1 + \frac{4}{\pi}\left(\frac{\ell_o}{d}\right)^{\frac{1}{2}}\frac{\tau_i}{\tau_{eff}}\right]^2 \geq \frac{4E\gamma_p}{\pi(1-\nu^2)d} \qquad 7.1$$

where, σ_F = tensile stress across the nucleus
E = Young's modulus
ν = Poisson's ratio
d = grain diameter
ℓ_o = carbide thickness
γ_p = effective surface energy of ferrite
τ_i = lattice friction stress
τ_{eff} = effective shear stress acting on the slip band (Figure 7.1).

The first term in relationship 7.1 represents the effect of the applied tensile stress. The second term shows the contribution from the pile-up. The latter is much smaller than the effect of the applied tensile stress and hence it can be neglected. The relationship 7.1 then becomes

$$\sigma_F \geq \left[\frac{4E\gamma_p}{\pi(1-\nu^2)\ell_o}\right]^{\frac{1}{2}} \qquad 7.2.$$

This expression is the same as that for the propagation of a Griffith crack of length ℓ_o.

By testing notched bend specimens having various included angles, it has been shown that the initiation of cleavage fracture is coincident with the attainment of a critical tensile stress, σ_f, which is independent of the notch angle and the temperature of testing (Knott, 1966). These observations clearly proved that cleavage fracture in blunt notched specimens of mild steel, obeyed a critical tensile stress criterion.

In a blunt notched specimen, the peak stress is experienced over a distance encompassing several ferrite grains. Hence, when the critical stress for fracture is reached, it causes crack propagation from a number of nuclei.

The stress distribution ahead of a sharp crack is significantly different from that in the notched bar. In Figure 7.2. is shown the stress distribution ahead of a crack, obtained from the finite element analysis of Tracey (1976). Although very high stresses are attained immediately adjacent to the crack tip, they drop off rapidly with distance. An increase in K does not alter the range of crack tip stresses. However, the distance over which the elevated stresses act is increased.

In the case of a critical tensile stress controlled mode of fracture in a sharp cracked specimen, it can be seen that the required fracture stress can be attained at any K, provided the fracture stress, σ_f, is less than the maximum stress. It follows that for cleavage crack initiation from a sharp crack the attainment of a critical tensile stress is not a sufficient criterion for fracture and it is necessary to postulate that the required stress should also be exceeded over a

microstructurally significant distance. This is the basis of the Ritchie, Knott and Rice (1973a) model for cleavage fracture initiation in pre-cracked mild steel specimens.

Ritchie et al (1973a) found that the variation of cleavage fracture toughness of mild steel with temperature could be correctly predicted if the microstructurally significant critical distance X_o was taken to be two grain diameters. However, later work (Curry and Knott, 1976) has shown that there is no simple relationship between X_o and grain size. Hence it has become necessary to evaluate X_o for a specific material by measuring σ_f and K_{IC}.

For a material with a stress-strain relationship of the form

$$\frac{\varepsilon}{\varepsilon_y} = \frac{\sigma}{\sigma_{ys}} + \psi \left(\frac{\sigma}{\sigma_{ys}}\right)^N \qquad 7.3$$

where ε_y = strain at yield point
σ_{ys} = yield stress
ε = total strain
σ = stress
ψ = constant
*N = Work hardening exponent

Curry (1978) has shown that the cleavage fracture toughness can be related to X_o, σ_f, σ_{ys} and N by the following expression.

$$K_{IC} \alpha X_o^{\frac{1}{2}} \left[\frac{\sigma_f^{(N+1)/2}}{\sigma_{ys}^{(N-1)/2}}\right] \qquad 7.4$$

Here X_o is the critical distance and σ_f is the fracture stress given by equation 7.2.

*N in relationship 7.3 is inversely related to the work hardening exponent 'n' normally used for a power law hardening relationship.

Equation 7.4 shows that the important parameters which determine cleavage fracture toughness are σ_f, σ_{ys}, X_o and N. All these are sensitive to microstructure with σ_f being related to the carbide size ℓ_o and the effective surface energy γ_p of the matrix.

It also follows from equation 7.4 that an increase in K_{IC} can be obtained by increasing either X_o or σ_f. In many cases X_o and σ_f are microstructurally related to each other and it is not easy to alter them independently. For example, in mild steel, the carbide size, ℓ_o which determines σ_f, and the ferrite grain size which determines X_o, are related to each other. It follows that in most steels, any thermal/mechanical treatment will alter X_o and σ_f simultaneously, often in opposite directions, and hence it is difficult to predict the net effect on K_{IC}. This also implies that a change in microstructure need not produce a similar response in the behaviour of a pre-cracked specimen to that of a smooth or blunt notched specimen.

7.2.2. Fracture criterion in hydrogen embrittlement

To apply the concepts developed in the previous section for relating K_{TH} to microstructure, the primary requirement is to determine whether or not hydrogen assisted cracking obeys a critical stress criterion. The few experiments which have been performed on notched bend specimens have not led to any conclusive results (Lee et al, 1979). However, there is considerable circumstantial evidence to believe that hydrogen assisted cracking obeys a critical stress criterion. In the experiments of Johnson et al (1958), the region of crack nucleation in hydrogen charged notched tensile specimens was found to be below the notch root. More importantly, as the root radius was decreased, the point of crack initiation shifted towards the surface. These observations can be rationalised only if hydrogen assisted cracking is tensile stress controlled.

The fracture mode in high strength steels (>1250 MPa yield strength) during hydrogen assisted crack growth is almost invariably intergranular separation along prior austenite grain boundaries. A similar fracture mode is obtained in steels in the temper embrittled condition. Initial studies have suggested this mode of fracture to obey a critical tensile stress criterion (Ritchie et al, 1973b; Jokl et al, 1980), and arguments similar to those invoked to explain transgranular cleavage in mild steel, have been found to be applicable.

It is also well established that hydrogen embrittlement susceptibility is very sensitive to yield strength. This cannot easily be explained by anything other than a critical tensile stress criterion.

For these reasons, it is not unreasonable to assume that hydrogen assisted cracking is controlled by the attainment of a critical tensile stress.

7.2.3. Effect of hydrogen on σ_f

The embrittling effect of hydrogen must be through a reduction in the surface energy γ_s. For cleavage fracture in mild steel, the effective surface energy γ_p is around 14 J/m^2 (Oates, 1969). This is an order of magnitude greater than the surface energy γ_s of ferrite which is around 1 J/m^2. This discrepancy is considered to arise from the dislocation activity associated with crack propagation. It might be felt that any change in γ_s (brought about by the presence of an embrittling agent like hydrogen) should not have a large effect on the effective surface energy γ_p. However, a recent analysis by McMahon and Vitek (1979) has shown that γ_p is dependent on γ_s and therefore any small change in γ_s can have a large effect on γ_p and hence σ_f.

Although it is well recognised that hydrogen activity determines the severity of embrittlement, little is known about the exact form of the relationship between hydrogen concentration and σ_f. The effect of changes in γ_s on σ_f in temper embrittled steels has been confirmed by recent results relating σ_f to the concentration of embrittling elements at the prior austenite grain boundaries (Jokl et al, 1980). It is seen from Figure 7.3 that σ_f decreases rapidly with small impurity concentrations and tends to saturate at a reduced σ_f with increasing impurity concentration. It is reasonable to suppose that a similar relationship exists between σ_f and hydrogen concentration. However, this is unlikely to be a unique relationship because the coupling between γ_s and γ_p can be dependent on microstructure. Also, the relationship may be altered by temper embrittlement and trapping effects.

For small hydrogen concentrations, the initial part of the σ_f vs hydrogen concentration relationship can be approximated to a straight line. Therefore, following Oriani and Josephic (1974)

$$\sigma_f = \sigma_o - A[H] \qquad 7.5$$

where

σ_o = stress necessary for the operation of the same brittle fracture mode as obtained in hydrogen, at zero hydrogen concentration.

[H] = dissolved hydrogen concentration.

A = constant.

The hydrogen solubility is enhanced by the application of triaxial stresses, the effect of stress state on solubility being given by (Li et al, 1966)

$$c = c_o \text{ Exp } \frac{\bar{v}\ \sigma_{ii}}{3RT} \qquad 7.6$$

where c_o = concentration of hydrogen in the unstressed solid.

c = concentration of hydrogen in the stressed material.

$\bar{v}$ = partial molar volume of hydrogen in steel.

$\frac{\sigma_{ii}}{3}$ = hydrostatic stress = $\frac{\sigma_{11} + \sigma_{22} + \sigma_{33}}{3}$

If the effect of stress on solubility is taken into account then equation 7.5 becomes

$$\sigma_f = \sigma_o - A\ c_o \text{ Exp } \frac{\bar{v}\ \sigma_{ii}}{3RT} \qquad 7.7$$

By invoking Sievert's law to relate c_o to the partial pressure of hydrogen $P(H_2)$ equation 7.7 becomes

$$\sigma_f = \sigma_o - A' \left[P(H_2)\right]^{\frac{1}{2}} \text{ Exp } \frac{\bar{v}\ \sigma_{ii}}{3RT} \qquad 7.8$$

where A' = constant.

In the case of environments such as 3.5% NaCl solution and H_2S gas, $P(H_2)$ represents their effective hydrogen activity.

7.2.4. Size of crack nuclei and critical distance

In the case of transgranular cleavage in mild steel σ_f is determined by the carbide size as well as γ_p. In the case of hydrogen embrittlement, little is known about either the mechanism of crack nucleation or the nature of the crack nuclei. However, it is likely that any change in composition or microstructure will alter σ_f for a given hydrogen concentration and yield strength through an effect on the size of the crack nuclei.

Similar considerations apply to X_o, the characteristic distance.

The value of X_o is determined by the need to have a sufficient number of crack nuclei present within a sufficiently high stress field such that macroscopic crack growth can occur. The lower limit of X_o is determined by the slip distance, because plasticity is a necessary requirement for crack nucleation. For a given microstructure, X_o is likely to be a constant, independent of hydrogen activity, provided the fracture mode does not change. However, it is expected to decrease with increase in strength because the latter is normally achieved by microstructural refinement.

7.2.5. Relating K_{TH} to microstructural and continuum variables

The crack tip stress field shown in Figure 7.2. applies to a stationary crack subjected to a monotonically rising load. Hence, this is appropriate for the interpretation of K_{TH} measured using a rising load technique. In this investigation K_{TH} has been measured on a propagating crack and for this case it is necessary to consider the stress field ahead of a growing crack. Because there is no significant difference in K_{TH} values measured using rising load and crack arrest techniques, it would appear that the crack tip stress fields in the two cases should not be significantly different. Recent finite element results obtained by Sorensen (1979) show that the σ_{11} stress distribution ahead of a growing crack is essentially identical to the corresponding stress distribution for a monotonically loaded stationary crack (Figure 7.4).

Also shown in Figure 7.2. is the size of the plastic zone. In the crack plane this extends to a distance of $0.04\ (\frac{K}{\sigma_{ys}})^2$. However, the maximum size occurs at an angle of 70° to the crack plane and is approximately $0.13 - 0.15\ (\frac{K}{\sigma_{ys}})^2$. Because the σ_{11} stress is a maximum in the crack plane, it is the size of the plastic zone in the plane of the crack that is important for stress controlled fracture.

It is seen from Figure 7.4. that work hardening influences the maximum stress attainable at the crack tip and generally elevates the stress levels within the plastic zone. The maximum σ_{11} stress is $3\sigma_{ys}$ when there is no work hardening. However, even a small work hardening effect (n = 0.1) increases the maximum σ_{11} stress to $4.4\ \sigma_{ys}$. In the range of yield strengths encountered in this investigation (800 - 1450 MPa), the work hardening exponent, n, is likely to be between 0.12 - 0.07 (Rosenfield and Hahn, 1966). It is appropriate therefore to consider the stress distribution corresponding

to a n value of 0.1.

A knowledge of stress triaxiality within the plastic zone is required to calculate the extent of the enhancement of hydrogen solubility. This can be estimated in the case of the rigid plastic material. At the crack tip $\frac{\sigma_{ii}}{3} \simeq 2.5\ \sigma_{ys}$ and at the elastic plastic interface, it decreases to approximately $1.5\ \sigma_{ys}$. The effect of work hardening will be to increase the stress triaxiality and this cannot be easily estimated. The important point to be noted is that stress triaxiality within the plastic zone is directly dependent on yield strength. Therefore, the following approximation can be made.

$$\frac{\sigma_{ii}}{3} = \alpha\ \sigma_{ys} \qquad 7.9$$

where α is a function of distance from the crack tip, stress intensity and work hardening exponent.

Combining equations 7.9 and 7.8

$$\sigma_f = \sigma_o - A'[P(H_2)]^{\frac{1}{2}}\ \mathrm{Exp}\ \frac{\alpha\ \sigma_{ys}\ \bar{v}}{RT} \qquad 7.10$$

For crack growth two conditions should be satisfied. First, the σ_{11} stress at a distance X_o must exceed the fracture stress σ_f given by equation 7.10

i.e. at $X = X_o$, $\sigma_{11} \geq \sigma_f$ 7.11

Equation 7.11 is the requirement for propagation. Secondly, since all initiation processes require dislocation activity i.e. plasticity, the plastic zone size must be equal to or greater than X_o, the critical distance

i.e. $0.040\ (\frac{K}{\sigma_{ys}})^2 \geq X_o$ 7.12

The ideas developed in the foregoing section show that the important factors that determine hydrogen embrittlement susceptibility as characterised by K_{TH}, are the inherent fracture strength of the matrix (represented by σ_o), yield strength, work hardening exponent, hydrogen activity and critical distance X_o.

7.2.6. Variation of K_{TH} with hydrogen activity

The expected form of the dependence of K_{TH} on hydrogen activity, as represented by the partial pressure of hydrogen, is schematically shown in Figure 7.5.

The condition for crack growth as given by equation 7.10 and 7.11

is shown by the line AB which represents the K necessary to meet the stress requirements at $X = X_o$ for crack growth in an embrittled mode (possibly intergranular).

At very low hydrogen activities the K needed to operate the brittle mode of fracture will be higher than that required for fibrous fracture, which is the mode that is normally obtained in a hydrogen free, inert environment. In such cases there is likely to be no effect of hydrogen in reducing K_{IC} unless hydrogen is able to influence ductile fracture processes.

At increased hydrogen activities, the embrittling effect begins to be manifested, because the necessary stress requirements are satisfied at K values less than K_{IC}. Further increases in hydrogen activity result in a progressive decrease of K_{TH} because of the adverse effect of hydrogen on σ_f.

At very high hydrogen activities, the stress requirement can be satisfied before plasticity has spread over the distance X_o. In this case the latter requirement, as given by equation 7.12 becomes the controlling factor and crack growth in this region is mechanism controlled. Hence, K_{TH} becomes increasingly insensitive to hydrogen activity and reaches a saturation value. Such behaviour has been observed (Clark, 1975; Walter and Chandler, 1973). Another possible contributory factor for the saturation behaviour is that σ_f reaches a limiting value (Figure 7.3) and hence any further increase in $P(H_2)$ does not significantly alter K_{TH}.

The effects of changing σ_{ys}, X_o and σ_o on the relationship shown in Figure 7.5. can now be considered. At a given K and critical distance X_o, a decrease in yield strength results in a reduction of the σ_{11} stress and the triaxiality at $X = X_o$ within the plastic zone. Additionally, a decrease in yield strength is likely to be accompanied by an increase in the critical distance X_o and this results in a further reduction in σ_{11} stress and stress triaxiality. It follows that the hydrogen activity necessary to initiate cracking at a given K increases as the yield strength is decreased. In other words the line representing "growth control" is shifted to higher K_{TH} values. The K at which mechanism control takes over will be determined by the net result of the two opposing influences arising from the increase in X_o and the decrease in σ_{ys}. All the available evidence in the literature suggests that the net result is likely to be an increase

in the K_{TH} at which crack growth changes over to mechanism control. Another effect which normally accompanies a decrease in yield strength is an increase in K_{IC}. The overall result of a reduction in the yield strength of the matrix is seen to be an upward shift of the entire curve (Figure 7.6a).

The effect of increasing the critical distance, X_o, at a given σ_{ys} is to shift both the growth control line and the mechanism control line upwards (Figure 7.6b).

If the matrix is in a temper embrittled condition then σ_o is reduced. Consequently the hydrogen concentration required to initiate crack growth at a given K is reduced and hence the line representing growth control is shifted to lower K_{TH} values. However, the K_{TH} at which crack growth changes over to mechanism control is likely to remain unaffected (Figure 7.6c).

7.2.7. Variables determining crack growth rate

From the previous model relating K_{TH} to hydrogen activity, it follows that as K increases, the hydrogen concentration necessary to initiate crack growth decreases. Hence, the crack growth rate at a K above K_{TH} will be determined by the rate at which the required hydrogen concentration is achieved ahead of the crack tip.

Most high strength steels show K independent stage II behaviour. This is usually attributed to surface reactions controlling the rate of transport of hydrogen to the stressed region. However, the local hydrogen concentration required for crack advance depends on K. Hence, even if surface reactions are controlling the rate of supply of hydrogen, this need not necessarily result in K independent stage II behaviour.

To determine the effect of material and environmental variables on crack growth rate and its K dependence, a crack can be considered growing under constant K conditions at a $K > K_{TH}$, such that crack growth is predominantly by an embrittlement mechanism. Let the steady state crack growth rate at this K be V. The hydrogen source at the crack tip can be treated as a moving line source. The solution to the diffusion problem is the same as that for a moving line source of heat in an infinite solid and the reduced concentration profile in the crack plane is given by (Johnson, 1974)

$$\frac{C}{C_o} = \frac{k_o\left(\frac{Vr}{2D}\right) \text{Exp}\left(-\frac{Vr}{2D}\right)}{k_o\left(\frac{Vr_o}{2D}\right) \text{Exp}\left(-\frac{Vr_o}{2D}\right)} \qquad 7.13$$

where V = Crack growth rate.

D = Diffusivity.

C = Concentration of hydrogen at a distance r ahead of the crack tip.

C_o = Concentration very near the tip of the crack.

k_o = Modified Bessel function of second kind of order zero.

r_o = Distance ahead of the crack tip over which the concentration is C_o.

C_o is determined by the hydrogen activity of the environment and the solubility of hydrogen in the steel. r_o represents the distance over which equilibrium between the environment and the steel is established instantaneously and a value of 5×10^{-7} mm is used.

The reduced concentration C/C_o at a distance 10 μm ahead of the growing crack tip is plotted as a function of V/D in Figure 7.7. In this analysis the effects of stress triaxiality and plasticity at the crack tip have not been considered. However, this is unlikely to alter the conclusions significantly.

The criterion for crack growth at a given K is the attainment of a critical hydrogen concentration C_{Cr} at a distance X_o from the crack tip. The velocity at this K is however determined by C_{Cr}/C_o and D. An increase in hydrogen activity increases C_o and hence decreases C_{Cr}/C_o. It follows from Figure 7.7 that the crack growth rate V must increase. Similarly a decrease in yield strength increases C_{Cr} and hence C_{Cr}/C_o. Although a reduction in strength normally increases D, the increase in C_{Cr}/C_o is dominant. Hence, the net effect is to reduce the crack growth rate.

The more intriguing aspect of the K dependence of velocity can now be considered. This is determined not only by the fractional change in C_{Cr}/C_o with K but also by the absolute values of C_{Cr}/C_o. It is seen from Figure 7.7 that the change in velocity for a given fractional change in C_{Cr}/C_o decreases as the range of C_{Cr}/C_o values over which the change occurs is decreased. In those cases where C_{Cr} is very small or C_o is very large such as severely embrittled steels and severely embrittling environments respectively, C_{Cr}/C_o is necessarily

small. It follows that fractional changes in C_{Cr} are likely to have a small effect on crack growth rate. Consequently it is to be expected that the change in crack growth rate with K will be small in severely embrittled steels and severely embrittling environments.

7.3. Mechanisms by which Inclusions Influence Crack Growth Behaviour

Having discussed the behaviour of the inclusion free steel, it is appropriate now to consider the mechanisms by which inclusions may affect susceptibility to hydrogen assisted cracking.

(i) In wet environments inclusions may alter the effective hydrogen activity at the crack tip by affecting the corrosion reactions which lead to the generation of hydrogen at the crack tip.

(ii) The crack tip stress/strain field may be modified by the presence of inclusions. The nature and effect of the interaction will depend strongly on inclusion orientation.

(iii) Because of their weak nature, inclusion-matrix interfaces are favoured sites for the accumulation of molecular hydrogen. The resultant pressurisation may again modify the stress/strain field at the crack tip.

(iv) Inclusions may provide paths for rapid hydrogen transport. Hence diffusivity of hydrogen may be anisotropic.

Unlike (i), (ii), and (iii) which can affect both K_{TH} and crack growth rate, (iv) is likely to affect only the latter.

7.4. Effect of MnS Inclusions on Electrochemical Reactions at the Crack Tip

MnS inclusions are known to be potent sites of corrosion in steels (Wranglen, 1975). However, the reasons for this behaviour are not well understood. According to Wranglen, one reason is that the matrix adjacent to the MnS inclusion is contaminated by sulphur and hence is anodic with respect to both the MnS inclusion and the rest of the matrix. Therefore, the presence of inclusions leads to enhanced localised corrosion with a consequent increase in the rate of hydrogen generation. Once the contaminated matrix has been consumed, corrosion can be expected to become general unless fresh contaminated matrix is exposed in the process of dissolution.

A different mechanism operates in situations where MnS can dissolve significantly and generate H_2S. This is true in acid solutions and forms the basis of the well known 'Sulphur Printing' technique. Once generated, H_2S poisons the hydrogen recombination reaction, this resulting in increased hydrogen activity.

Pumphrey (1980) has studied the effect of inclusion orientation and volume fraction on hydrogen permeation behaviour through thin (0.5 - 2 mm) disc specimens under conditions of cathodic charging in 1N H_2SO_4. The results of his investigations are shown in Figure 7.8. It is seen that the steady state permeation rate increases with increasing volume fraction in all orientations. Also, the permeation in the longitudinal direction (L) is much higher than in the transverse direction (T). However, when 10 ppm H_2S is added to the electrolyte there is very little dependence of permeation on either orientation or volume fraction. It may be concluded that the directionality of permeation behaviour in the former case arises solely from the differences in the volume of inclusions exposed to the electrolyte and hence available for H_2S generation. This is larger in the longitudinal orientation and smaller in the transverse orientation. Consequently the local H_2S concentration and hence the effective hydrogen activity can be orientation dependent. In this context it is interesting to note that a sulphur print obtained from a wrought steel bar is normally more intense on a transverse section than on a longitudinal section, if all other conditions are kept identical.

Similar directionality in hydrogen permeation rate is possible with the mechanism suggested by Wranglen (1975) although the effect is likely to be small.

The effect of MnS inclusions in affecting hydrogen activity at the crack tip has to be considered only in aqueous environments like 3.5%NaCl solution which do not contain H_2S. However, the present experimental results suggest that the effect if present, is small and is certainly not a dominant factor determining anisotropy of crack growth behaviour in 3.5% NaCl solution.

Examination of nickel plated sections of uncleaned fracture surfaces showed that inclusions exposed to the crack tip environment had suffered very little chemical attack (Figure 5.15 and 5.19). It follows that in the absence of inclusion dissolution, no significant effect of inclusion orientation and volume fraction on hydrogen activity can be expected. It is a well established fact that the pH at the

crack tip is acidic (3-4) (Smith et al, 1970) and this should favour dissolution of MnS inclusions. Thus the retention of MnS inclusions on the fracture surface is not easily explained. However, Lees (1977) has also found that MnS inclusions exposed to acidic environments (pH 3-4) did not suffer chemical attack.

If the effect of inclusions on hydrogen activity was a dominant factor, then it follows that K_{TH} should decrease and crack growth rate should increase with increasing volume fraction of MnS for all orientations. In fact, such an effect was observed only in the ST and SL orientations, inclusions having a favourable effect in the LT and TL orientations. The crack plane intersects the maximum number of inclusions in the LT orientation and the least in the SL and ST orientation. Hence, if a hydrogen activity effect were dominant, the LT orientation would be expected to be least resistant and ST and SL should show maximum resistance to cracking. This is also contrary to the observed behaviour.

Having concluded that any effect of inclusions on hydrogen activity at the crack tip cannot be a significant factor in determining the orientation dependence of crack growth behaviour, it is now appropriate to consider the role of inclusions in affecting the stress or strain distribution at the crack tip.

7.5. Effect of Inclusions on the Crack Tip Stress and Strain Distribution

Because hydrogen assisted cracking is considered to be a critical tensile stress controlled event, any change in the stress field at the crack tip can result in a change in K_{TH} and crack growth rate. Most of the previous studies on the role of inclusions in fracture processes have been confined to their effect on fibrous fracture which is known to obey a critical strain criterion. Consequently, the effect of inclusion orientation and volume fraction on K_{TH} may be different from that on K_{IC}. As pointed out in section 5.2.3. this difference is in fact observed.

7.5.1. Behaviour of the LT orientation in the 1250-1300 MPa yield strength condition in 3½% NaCl solution

The behaviour of the 1250-1300 MPa yield strength condition in 3½% NaCl solution is taken as the base line for the following discussions.

In the LT orientation, inclusions were observed to promote repeated branching of the crack into the short transverse plane (Figure 5.14).

Thus in this orientation, inclusions effectively act as crack dividers. Under the influence of the σ_{33} stress (Figure 7.2) the matrix separates from the inclusions present within the plastic zone because of the weakness of the boundary. It is suggested that the resultant introduction of numerous delaminations in the short transverse plane causes a local relaxation of plane strain conditions. It follows that, in this orientation, the stress elevation and stress triaxiality within the plastic zone at a given K will be less for a material containing elongated inclusions than for an inclusion free material. Also the local stress intensification is expected to decrease as the sulphur content increases.

From Figure 5.3. it is seen that the apparent K_{TH} of the inclusion free steel is around 25 MN $m^{-3/2}$. Therefore, at a K of 25 MN $m^{-3/2}$ the σ_{11} stress at $X = X_o$ is just sufficient to satisfy the failure criterion. For the LT orientation, the introduction of inclusions is seen to result in an increase of K_{TH}. It follows that in the LT orientation at a K of 25 MN $m^{-3/2}$, the σ_{11} stress at $X = X_o$ is no longer sufficient to initiate crack growth because of inclusion induced stress relaxation. Also the extent of hydrogen concentration at the crack tip is less because of the reduction in stress triaxiality. Consequently the σ_{11} stress necessary to initiate crack growth is greater than that for the inclusion free material. It follows that the K_{TH} of the LT orientation must be higher than it is for the inclusion free material.

The above explanation is consistent with the observed effect of inclusion volume fraction on K_{TH} in 3.5% NaCl solution (Figure 5.3). It also supports the assumption of a critical stress criterion for hydrogen embrittlement and hence explains why the response of K_{IC} and K_{TH} in the LT orientation to changes in inclusion volume fraction are different. The observed occurrence of high energy fracture modes in the LT orientation, even near the threshold, is also consistent with the proposition of inclusions relaxing stress triaxiality.

A number of other cases exist where an improvement in resistance to a critical stress controlled fracture has been obtained by utilising weak interfaces to reduce triaxiality. Embury et al (1967) observed that the impact transition temperature (ITT) of laminated mild steel in the crack divider mode was less than that of mild steel in bulk form (Figure 7.9). The decrease in ITT increased with the number of layers

of the laminate. The behaviour of the laminated composite specimen was found to be the same as that of the thin specimens that constituted it.

The ITT has also been found to be affected by inclusion orientation and volume fraction as shown in Figure 7.10. (Pickering, 1979). ITT increases with inclusion content up to 0.05%S, but there is a favourable effect at higher sulphur contents. While it is difficult to explain the rising part of the curve, the drop in ITT with sulphur content can be attributed to the inclusions relaxing stress triaxiality. It is also interesting to note that the effect of inclusion volume fraction is more pronounced in the longitudinal orientation than in the transverse orientation. The same orientation dependence is observed with the effect of inclusion volume fraction on K_{TH} (Figure 5.3). A very similar effect of inclusion orientation and volume fraction on ITT has been reported by Gladman (1979).

Having suggested a mechanism by which inclusions can affect K_{TH} in the LT orientation, it is now possible to consider the variables that determine the magnitude of the effect shown in Figure 5.3.

If σ_{11} is the stress at a distance $X = X_o$ within the plastic zone for the inclusion free material and σ_{11i} is the corresponding stress in the presence of inclusions, then the extent of stress relaxation can be characterised by:

$$\beta = \frac{\sigma_{11} - \sigma_{11i}}{\sigma_{11}} \qquad 7.14$$

Consider an ellipsoidal inclusion whose axes in the longitudinal, transverse and short transverse directions are 2a, 2b and 2c respectively such that $a > b > c$ (Figure 7.11). The factors that determine the severity of stress relaxation are the number of potential sites causing stress relaxation and the size of the delamination from each site as represented by the projected area of the inclusion on the short transverse plane. The number of inclusions per unit area of the fracture plane (L plane) is given by $2a\ N_v$ where N_v is the number of inclusions per unit volume, and the projected area of each inclusion on the short transverse plane is πab. Hence, as a first approximation,

$$\beta \alpha (2a\ N_v)\ (\pi ab)$$
$$\alpha 2\pi a^2 b\ N_v \qquad 7.15$$

But volume fraction $V_f = (4/3)\pi abc\ N_v$ 7.16

Substituting for N_v from 7.16 in 7.15

$$\beta \alpha V_f\ (a/c) \qquad 7.17$$

Relationship 7.17 emphasises the importance of inclusion volume fraction as well as shape in determining the severity of the stress relaxation effect.

The effect of inclusions in the LT orientation is to reduce the triaxiality of stress state locally within the plastic zone. This is similar to the macroscopic effect obtained by reducing the thickness of the specimen. The dependence of any critical K property, such as fracture toughness K_c on specimen thickness B is of the form shown in Figure 7.12. This is well established in the case of fracture toughness and a similar thickness effect has been observed with K_{TH} in hydrogen embrittlement (Gerberich, 1974). When the fracture mode is fibrous the improvement in critical K with decreasing thickness is due to shear lips occupying an increasing fraction of the fracture surface. A similar thickness dependence can be expected for a critical stress controlled brittle fracture event, which always gives a flat fracture because the maximum tensile stress ahead of the crack tip is a function of stress triaxiality. The important point is that irrespective of the mode of fracture, the extent of the improvement in critical K for a given reduction in thickness depends on both K and σ_{ys}. If a similar argument is extended to the effect of inclusions in reducing triaxiality and σ_{11} stress, it follows that the effectiveness of a given inclusion dispersion will depend on $(K/\sigma_{ys})^2$. This is an important conclusion and its implication is that the extent of improvement in K_{TH} for a given inclusion dispersion will be a function of the K_{TH} of the inclusion free material and the yield strength. In other words, as the severity of embrittlement increases, the beneficial effect of inclusions in the LT orientation decreases.

7.5.2. Behaviour of the TL orientation in the 1250-1300 MPa yield strength condition in 3.5%NaCl solution

Fractographic examination and the appearance of fracture surface profiles on nickel plated sections showed that the behaviour of the TL orientation is very similar to that of the LT orientation (Compare Figure 5.14 and 5.18). Again repeated crack branching along the inclusions into the short transverse plane is observed (Figure 5.19).

These observations, together with the nature of the volume fraction dependence of K_{TH}, lead to the conclusion that the mechanism for the improvement in K_{TH} in the TL orientation is not significantly different from that suggested for the LT orientation. The only difference in ß for the TL and LT orientations is the number of inclusions threading through unit area of the crack plane. In the TL orientation, the number is 2b N_v, this being much lower than 2a N_v, the value for the LT orientation. Hence, for the TL orientation the stress relaxation factor ß is proportional to V_f (b/c). This argument correctly predicts the order of orientation dependence of K_{TH} between the LT and TL orientations, but the difference in K_{TH} between the two orientations is not as marked as the model would suggest.

7.5.3. Behaviour of the short transverse orientations in the 1250-1300 MPa yield strength condition in 3.5% NaCl solution

The effect of inclusions in the SL and ST orientation is to reduce K_{TH} (Figure 5.3). If it is assumed that inclusion orientation and volume fraction do not affect the critical distance X_o, the decrease in K_{TH} implies that the presence of inclusions results in a σ_{11} stress that is greater than the value attained in the absence of inclusions. It is well known that inclusions lead to decreased ductile fracture toughness in this orientation by causing local strain intensification. There is, however, no information on the role of elongated inclusions on the fracture behaviour in the short transverse orientation when a critical stress controlled fracture mechanism is operative. Hence, it is necessary to deduce the mechanism responsible for the reduction in K_{TH}, from the fractographic observations and the measured effects of yield strength and hydrogen activity.

The tendency for the crack to grow preferentially via inclusions is suggested by a number of observations. Fractographic examination shows that the apparent area fraction of inclusions on the fracture surface is much higher than the area fraction on a random section. As already mentioned, the area fraction of inclusions on the fracture surface was found to be dependent on K and the inclusion volume fraction at a given strength. The maximum number of inclusions that can be present on a fracture surface is limited by the size of the plastic zone. This accounts for the K dependence of the area fraction of inclusions. The effect is most noticeable when the plastic zone size ranges from several times the inclusion spacing to less than an inter-inclusion spacing. If inclusions were not actively participating in

the fracture process then the area fraction of inclusions should be small and independent of K.

It might be argued that when a fibrous fracture mechanism dominates hydrogen assisted crack growth as it does at high K values, a large area fraction of inclusions would be expected (Figures 5.7 and 5,8). However, large area fractions of inclusions persist even when the matrix fails in a predominantly intergranular mode (Figure 5.6) and this is clear evidence for the active participation of inclusions in hydrogen assisted fracture.

Nickel plated sections of the fracture surface showed branched intergranular cracks to be associated with closely spaced inclusions (Figure 5.11). This implies that the inclusions act as crack nucleating sites. If inclusions are to directly participate in an intergranular fracture phenomenon, it is essential for them to be located at the grain boundaries. If not, any cracking via the inclusions must involve transgranular fracture and when the latter is not the favoured fracture mode, inclusions are likely to inhibit cracking rather than promote it. Fractographic observations did not indicate the existence of transgranular fracture regions around inclusions. Therefore, it has to be concluded that at least those inclusions that were seen on the fracture surface were located at the prior austenite grain boundaries. This is supported by the fractographic and metallographic observations (Figures 5.13 and 5.54).

The enhancement of the σ_{11} stress to a level above that obtained in the absence of inclusions is feasible in the short transverse orientation, due to at least two different mechanisms. First, strain intensification at the periphery of the inclusions can lead to a local elevation of the σ_{11} stress within the plastic zone if work hardening effects are significant. The work hardening exponent, n, for the 1250-1300 MPa yield strength range is around 0.07 (Rosenfield and Hahn, 1966), and this can result in significant stress enhancement within the plastic zone. The severity of this effect will increase with the size of the plastic zone, especially when the latter is of the order of the inter-inclusion spacing.

Secondly, inclusions near the elastic-plastic boundary will extend into a region of high elastic stress. The strain concentration at the periphery of the inclusions can give rise to local yielding and hence the net effect will be to increase the size of the plastic zone and

the distance over which the elevated stresses act. At a given stress intensity this effect will be more pronounced as the yield strength is raised because the region exposed to high elastic stresses is greater at higher yield strengths. This implies that the effect of the inclusions should become more pronounced as strength increases, in fact the opposite is observed. It follows that, in order to explain the observed effects of inclusion volume fraction, strength and hydrogen activity, the first proposed mechanism must be dominant.

Figure 5.3. suggests that the K_{TH} of the inclusion free material is about 25 MN $m^{-3/2}$. Around this stress intensity, the fracture surface of the ST orientation in En16M shows active participation of the inclusions in the fracture process (Figure 5.6). If these inclusions lead to stress elevation as suggested, it follows that crack growth can continue to lower values of K. Under these conditions, K_{TH} occurs when the local stress ahead of the crack tip as determined by the applied K and inclusion induced stress intensification is no longer capable of satisfying the critical stress criterion. Hence, in the region of arrest, a significant area fraction of inclusions must still be observed on the fracture surface. Also in the region of crack arrest, for different inclusion volume fractions, other factors remaining constant, the area fraction of inclusions on the fracture surface should be similar. Both of these conclusions are supported by the fractographic observations (Compare Figures 5.5, 5.9 and 5.10).

Several similarities must be noted between the fracture behaviour of the two short transverse orientations, ST and SL, in both air and hydrogen assisted cracking. The results of the present investigation show that in hydrogen assisted cracking the crack growth behaviour (Figure 5.2) and fracture surface appearance are similar for the two orientations at comparable stress intensities and inclusion volume fractions. A corresponding similarity in both fracture surface appearance and initiation toughness has been observed for the two short transverse orientations in the case of fibrous fracture (Baker, 1972).

For the short transverse orientations, increasing the inclusion volume fraction has an adverse influence on both the susceptibility to hydrogen assisted cracking and initiation toughness. The low initiation toughness of the short transverse orientations is attributed to the inclusions promoting strain concentration. To account for the

adverse effect of inclusions on K_{TH} in these orientations, it has been suggested that a similar strain localisation mechanism results in stress elevation through work hardening.

The effect of inclusion variables on the initiation toughness of the short transverse orientation has been shown to correlate with the projection parameter, P, which is given by $\frac{\sqrt{6}\, V_f}{\pi c}$ (Baker, 1972). The 'P' parameter which represents the total length of the inclusions per unit area on the transverse plane emphasises the adverse effect of inclusion deformation and volume fraction on toughness. The previously cited similarities in the fracture behaviour of the short transverse orientations in air and in hydrogen assisted cracking suggest that the 'P' parameter is also likely to characterise the susceptibility of the short transverse orientation to hydrogen assisted cracking.

7.6. Anisotropy of Crack Growth Rate of the 1250-1300 MPa Yield Strength Condition in 3.5% NaCl Solution

The differences in K_{IC} and K_{TH} between the various orientations mean that it is not possible to compare crack growth rates at the same K and fracture mode. However, the arguments developed below provide a basis for explaining the observed anisotropy of crack growth rate shown in Figures 5.1 and 5.2.

The differences in crack growth rate in a given environment between the different orientations at a given K could arise from differences in either hydrogen concentration requirements for fracture, or diffusivity. The results of the permeation experiments in this investigation and those of Pumphrey (1980) show that there is no significant orientation dependence of diffusivity. Hence, anisotropy of crack growth rate must be due entirely to differences in local hydrogen concentration requirements for fracture.

Because inclusions decrease the σ_{11} stress in the LT and TL orientations, the hydrogen concentration required for crack growth in these orientations must be higher than that for an inclusion free steel. By comparison, in the ST and SL orientations the hydrogen concentration requirements are reduced because of the stress concentrating effect of the inclusions. Hence the crack growth rate in the matrix in the ST and SL orientations is higher than in the LT and TL orientations.

An additional effect arises from the fact that inclusions are preferred crack paths and cracking via inclusions must be more rapid than cracking through the matrix. This inclusion contribution is expected to be strongly dependent on K as inclusion participation is observed to be sensitive to K. The significance of the contribution from the inclusions to the anisotropy of crack growth rate will also depend on the difference between the crack growth rates through the matrix and along the inclusions.

3½%NaCl solution is not a very active environment and hence C_o (the maximum hydrogen concentration representing the intensity of the hydrogen source) is small. The pronounced orientation dependence of K_{TH} in the 1250-1300 MPa yield strength condition suggests that C_{Cr} values for the various orientations at a given K are significantly different. Assuming a diffusivity value of 5×10^{-12} m^2/sec (from Table 6.1) and an estimated stage II crack growth rate for the inclusion free steel to be 2×10^{-4} mm/sec (from Figure 5.4), a value of $40mm^{-1}$ is obtained for V/D. From Figure 7.7 the corresponding C_{Cr}/C_o value is found to be around 0.1. It is seen from Figure 7.7 that any change in C_{Cr}/C_o around this region must result in a significant change in crack growth rate.

The orientation dependence of stage II crack growth rate and K_{TH} are such that those orientations which show maximum crack growth rate also show minimum K_{TH} and vice versa. However, in those cases where the introduction of inclusions decreases K_{TH}, the stage II crack growth rate need not necessarily increase. This is because inclusion volume fraction can influence crack growth rate through two independent effects. One is through an effect on the hydrogen concentration requirements for crack growth, the direction of this effect having been shown to be dependent on inclusion orientation. The other is through an effect on diffusivity which is known to be sensitive to inclusion volume fraction. In the latter case, an increase in inclusion volume fraction can lead to a decrease in diffusivity and this in turn will result in a reduction of crack growth rate for all orientations.

The results of the present investigation suggest that the effect of inclusion volume fraction on stage II crack growth rate is similar to the effect on K_{TH} (compare Figures 5.3 and 5.4). This implies that the dominant mechanism by which inclusions influence stage II growth rate is through an effect on C_{Cr} and not through D.

7.7. Effect of Increasing Matrix Strength

At a yield strength of 1450 MPa, En16 showed reduced K_{TH} values and increased crack growth rates for all orientations in 3.5% NaCl solution compared to the 1250 MPa yield strength condition in the same environment. More significantly, there was little anisotropy in either crack growth rate or K_{TH}. Also, the fracture mode for this condition, in air, was intergranular indicating that it was in an embrittled condition.

The absence of anisotropy in K_{TH} under these conditions can be rationalised as follows. The effect of increasing yield strength is to increase the σ_{11} stress and triaxiality at $X = X_o$ for a given K. Also, an increase in yield strength is likely to result in a decrease in X_o. For a given hydrogen activity of the environment, the increased triaxiality reduces the critical stress required for crack growth. The decrease in critical distance means that the fracture stress has to be exceeded over a smaller distance. The net effect of the increased yield strength is that the criterion for crack growth is satisfied at a smaller K value. Therefore, it follows that the K_{TH} of the inclusion free material in the 1450 MPa yield strength condition is less than that of the 1250 MPa yield strength condition. As discussed in Section 7.5.1, the combination of a decrease in K_{TH} of the inclusion free steel and increase in σ_{ys} means that the effect of inclusions in relaxing triaxiality will be very small in both the LT and TL orientations. Hence the K_{TH} of these two orientations ($\simeq 16 MNm^{-3/2}$ from Fig.5.20) will approach the K_{TH} of the inclusion free material. The plastic zone size at a K of 16 MN $m^{-3/2}$ is also very small ($\simeq 4\mu m$) compared to the inclusion spacing. Hence the plastic zone does not contain a sufficient number of inclusions to result in any significant stress elevating effect in the short transverse orientations. This is confirmed by the fractographic observations which show that in the region of arrest there are no inclusion features to be seen on the fracture surface (Figure 5.22). The net result is that there is no significant orientation dependence of K_{TH} in En16 in the 1450 MPa yield strength condition.

A contributory factor may be that the K_{TH} of all the orientations has decreased to such an extent that crack growth is now under mechanism control. Inclusions have no significant effect on yield strength and hence K_{TH} determined by mechanism control cannot be sensitive to inclusion orientation and volume fraction.

The very high crack growth rates that are observed in 3.5% NaCl solution and the fact that the material is in an inherently embrittled condition, even in the absence of hydrogen, imply that the hydrogen concentration required to initiate crack growth in the environment is very small in relation to the intensity of the hydrogen source. In other words, C_{Cr}/C_o is very small and therefore it follows from Figure 7.7 that any small difference in C_{Cr} for the various orientations will not lead to significant anisotropy of crack growth rate.

7.8. Effect of Decreasing Matrix Strength

In the 800 MPa yield strength condition of En16M, the stress levels attained within the plastic zone are much less than those associated with the 1250 MPa yield strength condition. Also the elevation of hydrogen concentration arising from stress triaxiality is less pronounced. The net result is that the maximum attainable σ_{11} stress is less than the σ_f necessary for crack growth in a low hydrogen activity environment such as 3½% NaCl solution. In order to permit cracking, σ_f must be decreased to the σ_{11} stress levels encountered within the plastic zone. This can be achieved by using a high hydrogen activity environment like H_2S saturated NaCl solution.

In spite of the increased hydrogen activity, the stress intensities over which significant crack growth is encountered are higher than in the case of the 1250 MPa yield strength condition tested in 3½% NaCl solution. Also the occurrence of a quasi-cleavage fracture mode instead of the intergranular mode observed in the high strength condition indicates that embrittlement is less severe. These observations are evidence for the dominant effect of yield strength in determining susceptibility to cracking.

7.8.1. Conditions for crack growth by a pressurisation mechanism

Hydrogen can assist crack growth by two different mechanisms when the hydrogen activity of the environment is high. One is the embrittlement mechanism and the role of inclusions in this has already been discussed. The other possibility is a pressurisation mechanism caused by the accumulation of molecular hydrogen within the material. In addition to an intense hydrogen source, the operation of the latter mechanism requires the fulfilment of the conditions explained below.

For hydrogen to accumulate in molecular form, suitable sites or interfaces must be present. If accumulation of molecular hydrogen is

to result in cracking, such sites must also be present as shapes which favour crack initiation. Inclusion-matrix interfaces are usually the weakest interfaces in steel and hence are the preferred sites for the accumulation of molecular hydrogen. When the inclusions are large and plate-like, the large pressures developed at the interface can result in cracking in the short transverse plane.

If pressurisation is necessary for crack advance, the required pressures need to be established over a region which encompasses several inclusions ahead of the crack tip. Because the inclusions do not assist hydrogen diffusion, the required concentration profile must be achieved over these distances throughout the matrix.

When a pressure assisted microcrack propagates from an inclusion, the pressure necessary to maintain a certain K decreases as the length of the microcrack increases. However, the amount of hydrogen necessary to meet the decreasing pressure requirement, will be determined by the relationship between stress intensity, internal pressure, volume of the pressurised crack and crack length. In Appendix 2, the variation of stress intensity with crack length has been analysed for a Griffith crack internally pressurised by a constant amount of an ideal gas and it is shown that K decreases with crack length. It follows that in order to maintain a constant K, which is required for sustained microcrack growth, more and more hydrogen has to accumulate at the inclusion-matrix interface. Even in the presence of external stress, the above sequence of events must be true up to the point when the inclusion initiated microcrack joins back to the main crack, thus resulting in macroscopic crack growth.

The overall implication of the above arguments is that because large hydrogen concentrations have to be maintained over distances spanning several inclusions and the amount of hydrogen required to maintain microcrack growth increases, crack growth by a pressurisation mechanism must be a slow process and hence requires the maintenance of an intense hydrogen source at a near stationary crack for extended periods.

7.8.2. Nature of crack growth in the short transverse orientation by a pressurisation mechanism

With the ideas developed in the foregoing section it is possible to interpret in broad terms most aspects of the crack growth behaviour of the short transverse orientation in H_2S saturated salt water.

At high stress intensities the crack grows predominantly by an embrittlement mechanism. Crack growth is too rapid for any significant hydrogen pressures to be developed over the required distances ahead of the crack tip. The crack apparently arrests at a K which represents the K_{TH} of the material in the absence of the operation of a pressurisation mechanism. For subsequent crack growth, the applied stress has to be supplemented by pressurisation at the inclusion-matrix interfaces. Metallographic examination of the arrest region revealed the existence of long secondary cracks ahead of the main crack and apparently not connected to it. These secondary cracks were invariably associated with inclusions (Figure 5.35a and b). Crack growth following apparent arrests took place in bursts with the growth increment varying between 0.5 mm and 2 mm. Each burst was preceded by long periods (4-12 hrs) during which there was little crack advance. Both of these important observations cannot be accounted for by any mechanism other than pressurisation assisted crack growth.

A number of important aspects of the mechanism of cracking caused by pressurisation at the inclusion-matrix interface can be understood by studying the crack path in unstressed specimens exposed to H_2S saturated salt water. In this case, crack initiation must necessarily be from inclusions. If a plate-like inclusion is considered to be an elliptical crack under internal pressure, the maximum stress intensity is at the transverse position T (Figure 7.11). Hence crack growth will first be in the transverse direction. Amongst a group of inclusions, in the absence of a strong concentration gradient, the largest inclusion will nucleate the first crack. As discussed in the previous section, the pressure required to keep this crack growing decreases with crack growth. However, to meet the decreasing pressure requirements for crack growth, more hydrogen has to accumulate. The existence of a pressure gradient between the inclusion with the first nucleated crack and the neighbouring inclusions will result in the migration of hydrogen from the latter to the former. This favours the continued growth of the first nucleated crack in the same plane in preference to nucleating cracks from neighbouring inclusions.

The experimental observations suggest that the initial crack nucleation may be assisted by the interaction of two closely spaced inclusions (Figure 5.51). However it does not necessarily follow that subsequent propagation need be preferentially via inclusions. The observation of cracks deviating to propagate preferentially via inclusions

(Figure 5.50) implies that crack propagation is in fact assisted by interaction with inclusions. The factors that govern the interaction between a crack and an adjacent inclusion are the spacing between them and their relative disposition. The problem is very similar to the linkage between an elongated inclusion and a crack in the fibrous fracture of the short transverse plane analysed by Baker (1972). When the crack is propagating on the short transverse plane, the favoured direction for inclusion interaction will be towards the transverse direction. Therefore, from considerations of both local stress intensity and disposition of neighbouring inclusions, crack propagation in the transverse direction is encouraged. This accounts for the fact that most of the cracks were seen on the transverse section, whilst very few could be seen on the longitudinal section (Section 5.6). The important conclusion from these observations is that crack propagation by an inclusion assisted pressurisation mechanism is strongly favoured by the presence of closely spaced inclusions.

The factors that govern the advance of an apparently arrested crack can now be considered. Following apparent arrest, a number of subsidiary cracks nucleate at inclusions and propagate ahead of the main crack. These ultimately link up with the main crack to cause macroscopic crack advance. Several factors determine the location of these subsidiary cracks. From the point of view of applied stress, the favoured location for cracking is directly ahead of the crack tip in the crack plane. However, the crack faces where the $H_2S + Fe \rightarrow FeS + 2[H]$ reaction takes place constitute a plane hydrogen source. Therefore, the maximum hydrogen pressures are not developed directly ahead of the crack tip in the crack plane. As indicated earlier, crack nucleation and propagation by a pressurisation mechanism is determined by the presence of closely spaced large inclusions. Metallographic examination showed that these inclusions were present in clusters (Figure 5.55) with the spacing between the clusters being of the order of 200μm. The net result of these constraints is that pressurisation assisted cracks which nucleate and grow ahead of the main crack rarely lie on the plane of the main crack. This is clearly seen from Figures 5.35a, 5.37 and 5.49a. (The latter two cases refer to different strength conditions, but they represent similar situations and hence are relevant to the present discussion.) The subsidiary cracks which nucleate at a number of points along the crack front also lie on different planes.

It is also of note that the subsidiary cracks are found only ahead of the crack tip. They are not formed below that part of the fracture surface which had been caused primarily by external stress. Also there was no evidence of blistering or crack formation elsewhere on the specimen surface exposed to the environment. This demonstrates that the disconnected cracks observed ahead of the main crack tip could not have been formed by pressurisation alone.

If the high hydrogen activity is maintained around the crack tip region, the secondary cracks grow at a number of points along the crack front. The small crack growth rate (10^{-4} - 10^{-5} mm/sec) associated with an apparently arrested crack need not represent the movement of the main crack tip. It may well be caused by the formation and propagation of subsidiary cracks because this can also result in a drop in load cell output. It was mentioned earlier that clusters of inclusions around the crack tip were the favoured sites of secondary crack nucleation and growth. These subsidiary cracks tend to be separated from the original crack tip by inclusion free material (Figures 5.35 and 5.49). In such cases the secondary crack grows away from the crack tip leaving an unbroken ligament of inclusion free material. The presence of a long secondary crack (> 200μm) not lying in the same plane as the main crack results in a redistribution of stresses at the original crack tip. Under conditions of constant displacement, the stress and strain intensification at the original crack tip is thereby decreased. Also the ligament connecting the two cracks must fracture by a shear mechanism and pressurisation cannot significantly assist this process because of the large size of the ligament.

Propagation of the subsidiary crack towards the main crack by a normal opening mode, i.e. mode I growth, is also not favoured because of its proximity to the free surface. However, pressurisation may still favour the growth of the subsidiary crack in the opposite direction. The latter favours the shear failure of the unbroken ligaments, which takes place in rapid succession when sufficient damage has occurred ahead of the original crack tip. This corresponds to a burst of crack growth. The cycle is repeated when further damage accumulates ahead of the crack tip. With this mechanism of crack extension the growth increments must encompass a number of inclusion clusters.

7.8.3. Nature of the hydrogen source provided by H_2S saturated salt solution and its consequences

In developing the arguments of the previous section, it has been tacitly assumed that a H_2S saturated 3½% NaCl solution maintains a constant high hydrogen activity on the steel surface exposed to it. This assumption appears to be consistent with the observation of extensive blistering and internal cracking on pipeline steels ($\sigma_{ys} \simeq 450$ MPa) exposed to a similar environment. However, if this assumption were true, then intermittent growth should continue to occur up to the point where the stress intensity reaches a sufficiently low value that crack extension has to be entirely by a pressurisation mechanism. At this stage the entire volume of the specimen would have had to have suffered extensive blistering and internal cracking. It follows that this mechanism of crack growth should result in a stage I behaviour in which crack growth rate varies gradually with K, there being no indication of the existence of a true K_{TH}. By comparison, in the absence of a pressurisation mechanism, a stage I behaviour with a pronounced K dependence is normally obtained. The former stage I behaviour was observed to a large extent in those cases where discontinuous growth was observed (Figures 5.27 and 5.28). However, all the intermittent growth took place within the first 150 hours of exposure to the environment with there being very little crack advance during the subsequent 150 hours. Also there was no evidence of surface blistering or internal cracking in the bulk of the specimen. However, when thinner specimens of En16 and En16M (<5 mm) were exposed to the same environment, blistering and internal cracking could be noticed even after 96 hours. All of these observations indicate that H_2S saturated salt solution provides a high hydrogen activity only in the initial stages and thereafter the hydrogen activity gradually decreases to a low value. This view is supported by the results of Skei et al (1953) who monitored the hydrogen pressure within steel capsules which had their outer surface exposed to a H_2S saturated aqueous environment. The rate of change of hydrogen pressure was high in the initial stages but it gradually decreased to a steady low value (Figure 7.13). On replacement with fresh solution, there was an abrupt increase in hydrogen flux (Figure 7.14).

In aqueous solutions containing H_2S, hydrogen is generated through the reaction $H_2S + Fe \rightarrow FeS + 2[H]$. The presence of H_2S poisons the

hydrogen recombination reaction $2[H] \rightarrow H_2$. This produces effectively a large surface coverage of atomic hydrogen which in turn results in a large dissolved hydrogen concentration in the matrix and a high hydrogen pressure at the inclusion-matrix interface. The observed decay in the hydrogen flux is likely to be caused by the build up of an adherent FeS film on the surface which begins as soon as the solubility product of FeS is exceeded. The formation of this film then hinders the hydrogen generation reaction. Replacing with fresh solution allows the previously formed protective film to dissolve and hence leads to an increase in flux. The film formation then recommences and the flux again starts to decrease. As would be expected a decrease in pH favours greater hydrogen flux for longer periods because of the increased solubility of FeS.

The occurrence of several bursts of discontinuous crack growth in En16M in the 800 MPa yield strength condition at stress intensities greater than 40 MN $m^{-3/2}$ suggests that the hydrogen activity and the period for which it is maintained are sufficient to cause crack growth by a pressurisation mechanism. A reduction in yield strength to 600 MPa increases the resistance of the matrix to cracking and hence the hydrogen pressures needed to assist crack growth are greater. Because the increased pressure requirements could not be met by H_2S saturated salt solution, the short transverse orientation of En16M in the 600 MPa yeild strength condition showed no significant crack growth even at a K of 60 MN $m^{-3/2}$ in this environment. By employing the modified testing procedure, in which the notch tip is continuously fed with fresh acidified salt solution saturated with H_2S, an increased hydrogen activity is maintained over long periods. Under these conditions crack growth is favoured even when the stress intensity is 40 MN $m^{-3/2}$. However, as the crack grows away from the notch, the increased hydrogen source intensity cannot move with it and hence the crack arrests.

The quantity of hydrogen that can be introduced into the steel during exposure to a H_2S saturated salt solution depends on the surface area exposed to the environment. The overall concentration of hydrogen in the material will hence depend on the ratio of specimen surface area to volume. Also, for a given concentration of hydrogen, susceptibility to cracking is influenced by the inclusion volume fraction. This affects cracking behaviour through two opposing influences. For a given specimen thickness and period of exposure to the environment,

the pressures developed at the inclusion-matrix interface will decrease as the inclusion volume fraction increases. However, because of inclusion-inclusion interactions, the pressures required to initiate and propagate cracks will be less. Also the amount of matrix which has to be fractured for a given increment of crack growth can be less. If inclusion parameters other than volume fraction remain unchanged, then in the range of sulphur contents normally encountered in commercial steels, the former effect tends to be dominant and cracking kinetics should be slowed down by an increase in inclusion volume fraction. Such an effect has been observed under electrolytic charging (Figure 7.15). The effect of inclusion volume fraction on cracking kinetics should be even more pronounced with H_2S saturated aqueous solutions. Hence, it is not surprising that blisters and internal cracks were not observed in 25 mm thick WOL specimens of En16 and En16M when exposed to this environment whereas commercial pipeline steels where the sulphur content is kept low (< 0.02%) and the specimen thickness is around 10 mm showed extensive blistering and internal cracking.

7.8.4. The applicability of fracture mechanics to the characterisation of macroscopic crack growth by a pressurisation mechanism

The mechanism of crack extension by pressurisation of the inclusion-matrix interface involves the nucleation and growth of a number of subsidiary cracks ahead of the main crack. These are large (> 200μm) in comparison to the plastic zone sizes encountered and hence are bound to perturb the stress/strain fields at the original crack tip. The presence of a number of such cracks along the crack front in different planes raises considerable doubt as to whether conventional fracture mechanics can be applied to the characterisation of macroscopic crack growth in this regime. Also under these circumstances definition of crack length itself becomes ambiguous.

In order to apply fracture mechanics to the characterisation of hydrogen assisted crack growth behaviour, an implicit requirement is that the nature of the hydrogen source should at least have a unique relationship with K for a given material-environment system. In practice a constant hydrogen activity is usually assumed. Even in this case it is essential that the nature and configuration of the hydrogen source should approximate to that of a line source at the crack tip, with hydrogen entering only through the crack tip. In the case of H_2S

saturated salt solution, hydrogen activity changes with time. Also it is possible that hydrogen may enter through the sides of the specimen and through the crack faces.

All of these factors, namely the presence of long subsidiary cracks ahead of the main crack, the time dependence of hydrogen activity and the entry of hydrogen through the crack faces can invalidate the application of fracture mechanics to the characterisation of macroscopic crack growth by a pressurisation mechanism.

7.8.5. Effect of inclusion volume fraction on crack growth behaviour of the 800-900 MPa yield strength condition

The effect of inclusion volume fraction on the anisotropy of crack growth rate at high stress intensities is similar to that obtained with the 1250-1300 MPa yield strength conditions in 3½% NaCl solution. The reasons for this behaviour are similar to those given in Section 7.6. However, the K_{TH} of En16 specimens in the short transverse orientations are lower than those of En16M in similar orientations. Possible reasons for this somewhat unexpected behaviour are the differences in yield strength and matrix composition. The higher yield strength of En16 (900 MPa) compared to that of En16M (800 MPa) makes it more susceptible to embrittlement. Also as mentioned in Section 5.2.3. the matrix composition of En16, because of higher Mn and C contents, favours greater susceptibility to embrittlement. The occurrence of increased amounts of intergranular fracture in En16 as compared to En16M supports this view.

7.9. Effect of Increasing Hydrogen Activity on the Crack Growth Behaviour of En16M in the High Strength Condition (σ_{ys} = 1200 - 1300 MPa)

7.9.1. Anisotropy of crack growth rate

Changing the test environment from 3.5% NaCl solution to 0.1 MPa H_2S gas results in the elevation of crack growth rate for all orientations in En16M in the 1300 MPa yield strength condition. More significantly there is very little anisotropy in crack growth rate in H_2S gas, whereas in 3½% NaCl solution there was a large difference in crack growth rate between the extreme orientations (Compare Figures 5.2 and 5.39). These observations can be rationalised as follows. H_2S gas is an environment of high hydrogen activity and this corresponds to a high value

of C_o. Therefore C_{Cr}/C_o decreases for crack growth in an inclusion free steel at a $K > K_{TH}$. It is seen from Figure 7.7 that a decrease in C_{Cr}/C_o leads to an increase in crack growth rate. Using a crack growth rate value of 2.5×10^{-3} mm/sec in 0.1 MPa H_2S gas (from Figure 5.39) and a D value of 5×10^{-12} m^2/sec (Table 6.1), (V/D) is found to be 5×10^2 mm^{-1}. From Figure 7.7 the corresponding value of C_{Cr}/C_o is 10^{-3}. By comparison in 3½% NaCl solution C_{Cr}/C_o was shown to be around 10^{-1} (Section 7.6). It is seen from Figure 7.7 that by using H_2S gas, C_{Cr}/C_o is shifted to a region over which a given fractional change in C_{Cr} will have a small effect on velocity whereas in 3½% NaCl solution a similar change C_{Cr} would result in a large difference in crack growth rate. The contribution to anisotropy of crack growth rate arising from preferential crack propagation via the inclusions in the short transverse orientations is also decreased in 0.1 MPa H_2S gas because the crack growth rate through the matrix has increased. The overall consequence of these two effects will be to reduce the differences in crack growth rate between the different orientations.

On reducing the yield strength of En16M to 1200 MPa, the crack growth rates in H_2S saturated 3½% NaCl solution show a general decrease in all orientations and anisotropy of crack growth rate begins to reappear (Figure 5.43). The reappearance of anisotropy following a reduction in strength is identical to the behaviour of En16 when tested in 3½% NaCl solution. In the 1450 MPa yield strength condition it did not show any anisotropy of crack growth rate but showed significant anisotropy in the 1250 MPa yield strength condition. In the present case the use of a higher hydrogen activity environment has postponed the development of anisotropy of crack growth rate to a lower strength level.

7.9.2. Threshold behaviour

Valid K_{TH} values in 0.1 MPa H_2S could not be measured for En16M in the 1300 MPa yield strength condition. However, the indications are that the anisotropy in K_{TH} is much less than for the same strength condition in 3½% NaCl solution. The absence of anisotropy in K_{TH} for the 1200 MPa yield strength condition in H_2S saturated salt solution confirms this indication.

An increase in hydrogen activity decreases the K_{TH} of an inclusion free steel. As discussed in Section 7.5.1. the stress relaxing effect of the inclusions in the LT and TL orientations will decrease as the K_{TH} of the inclusion free steel is decreased. Because of the decrease in the size of the plastic zone resulting from the reduced K_{TH} of the inclusion free material, the number of inclusions causing stress elevation in the short transverse orientations is decreased. Hence, anisotropy in K_{TH} should decrease as hydrogen activity is increased.

In the case of the 1200 MPa yield strength condition $^*K_{TH}$ is nearly the same for all orientations but there is anisotropy of crack growth rate. As pointed out earlier, anisotropy of crack growth rate can arise solely from differences in the hydrogen concentration required for crack growth at a given K. This implies that there should be a corresponding difference in K_{TH}. The fact that there is no significant difference in K_{TH}, leads to the conclusion that in this case K_{TH} may be mechanism controlled. The very low value of K_{TH} for this strength level supports this view.

7.9.3. Crack growth by a pressurisation mechanism

If the arguments advanced in Section 7.8.1. are correct then in environments of high hydrogen activity, crack growth by a pressurisation mechanism, should be observed in the short transverse orientations even in the high strength condition. Although H_2S gas and H_2S saturated salt solution are both high hydrogen activity environments, in the former there is no mechanism for the removal of the FeS film. It follows that H_2S gas is likely to maintain a high hydrogen activity for much shorter periods compared to H_2S saturated 3½% NaCl solution.

The specimens tested in H_2S gas were not kept in the environment for a sufficiently long time after arrest to detect any subsequent crack growth. Also, by this stage the cracks had grown too far towards the back face of the specimen (a/W > 0.8). All these factors make crack growth by a pressurisation mechanism in 0.1 MPa H_2S gas unlikely.

$^*K_{TH}$ here refers to the value that would be obtained in the absence of the operation of a pressurisation mechanism. Crack growth by a pressurisation mechanism was observed only in the SL orientation. If this is not taken into account K_{TH} of the SL orientation is approximately 20 MN $m^{-3/2}$ (Figure 5.43).

In the case of H_2S saturated 3½% NaCl solution, crack extension by a pressurisation mechanism is to be expected in the short transverse orientations. This was in fact observed (Figure 5.42). In the ST orientation, metallographic examination of the arrested crack showed evidence of a developing pressurisation crack, although no burst of crack growth following apparent arrest was recorded (Figure 5.49a and b). In the SL orientation there was clear evidence for the nucleation and propagation of cracks associated with inclusions ahead of the main crack (Figures 5.44 to 5.47).

7.10. Fractographic Features

7.10.1. Fracture modes

A number of factors such as strength, stress intensity, hydrogen activity and inclusion orientation and volume fraction determine the modes of fracture and their relative proportions. Intergranular fracture along prior austenite grain boundaries corresponds to the occurrence of severe embrittlement. This is followed by quasi-cleavage. The presence of a fibrous fracture mode implies the absence of significant embrittlement.

En16 in the 1450 MPa yield strength condition shows a completely intergranular fracture at all stress intensities in 3½% NaCl solution (Figure 5.21 and 5.22). This is consistent with the observation of an intergranular fracture mode in air. The same steel at a yield strength of 1250 MPa showed predominantly intergranular fracture at arrest with some tearing component which increased with K (Figure 5.10). This effect of K on fracture mode was pronounced with En16M in the short transverse orientation of the 1300 MPa yield strength condition (Figures 5.5, 5.6 and 5.7).

Increasing amounts of fibrous fracture with increasing K have been observed by others (McIntyre, 1973). The occurrence of intergranular cracking at a number of points along the crack front results in strain concentration in the remaining ligaments. The extent of strain concentration will increase with both the amount of intergranular cracking and the applied K. Therefore, the amount of intergranular fracture necessary to cause the failure of the remaining ligaments by a fibrous mechanism will depend on the applied K in relation to K_{IC} (assuming that the mode of fracture in air is fibrous).

This explains the increasing amount of fibrous fracture with K observed in the short transverse orientations.

A large increase in hydrogen activity, obtained by using H_2S gas, decreases the amount of fibrous fracture in all orientations in the 1300 MPa yield strength condition. Near the arrest region there is very little tearing to be seen (Figure 5.41) and even at high stress intensities the amount of fibrous fracture was small when compared to that in salt solution. Also the fibrous mode observed in salt solution tended to be replaced by quasi-cleavage (compare Figures 5.40 and 5.7). Although the reduction in the amount of fibrous fracture reflects the severity of embrittlement by H_2S, the change in fracture mode from fibrous to quasi-cleavage is not so easily explained.

When tested in H_2S saturated salt solution at a yield strength of 800 MPa, the amount of intergranular fracture is decreased and is replaced by quasi-cleavage (Figures 5.29a and b). In the 600 MPa yield strength condition there is no evidence of intergranular cracking (Figure 5.53). This trend of decreasing amounts of intergranular fracture with decreasing strength reflects a large reduction in the severity of embrittlement.

The factors that may determine whether the fracture mode is intergranular or transgranular are as follows:

(i) Enrichment of the prior austenite grain boundaries by impurity elements.

(ii) Enrichment of the prior austenite grain boundaries by hydrogen (trapping mechanism).

(iii) A synergistic interaction between impurities and hydrogen which favours an intergranular fracture mode even if hydrogen is uniformly distributed.

The fact that there is no unique relationship between the crack path in hydrogen and in air at low temperature (-196°C) (Refer Table 5.3) implies the operation of mechanism (ii) and/or (iii). The presence of closely spaced coarse carbides at the prior austenite grain boundaries can be a factor favouring an intergranular fracture path because carbide matrix interfaces are known to be potent trapping sites for hydrogen (Asaoka et al, 1978).

7.10.2. Inclusion participation in the short transverse orientation

In Figure 7.16 is shown a plot of the apparent area fraction of inclusions on the fracture surface of the short transverse orientation against $(K/\sigma_{ys})^2$ x% Sulphur. The latter is related to the number of inclusions that could participate in the fracture process. These data have been collected from fractographs and include different environments, strength levels and steels. Although a statistically significant number of measurements have not been made, the trend in the behaviour is apparent. The area fraction of inclusions is seen to depend only on the number of inclusions within the plastic zone (assuming other inclusion parameters like size and aspect ratio are held constant). It is also worth noting the absence of a significant area fraction of inclusions at very small plastic zone sizes and a tendency towards saturation at large plastic zone sizes and inclusion volume fractions.

7.11. The Consequences of the Association Between Inclusions and Interdendritic Segregation

It is an inevitable consequence of the solidification behaviour of steel that MnS inclusions are distributed in regions of interdendritic segregation. This association is not easily destroyed by any subsequent processing. As far as hydrogen assisted cracking is concerned, this is an unfavourable effect. It promotes clustering of inclusions in a region that is inherently more susceptible to embrittlement than the rest of the matrix. This difference in susceptibility is caused by an increase in hardness (about 50 HV in the present case) as compared to the rest of the matrix, and by the enrichment of these regions in elements like Mn and P which are well known to promote embrittlement. The difference in susceptibility becomes a significant factor in low strength steels, and in high strength steels when exposed to low hydrogen activity environments.

The association with inclusions is unfavourable to the cracking resistance of the short transverse orientations even if the cracking mechanism is solely restricted to embrittlement. However, when pressurisation is the dominant mechanism of cracking, the unfavourable effect will manifest itself to a much greater extent. In this case, the clustering of inclusions will aggravate the situation because of the detrimental effect of inclusion-inclusion interaction in assisting crack initiation and growth.

CHAPTER 8

CONCLUSIONS

8.1. Summary of Results

The role of elongated non-metallic inclusions in hydrogen assisted cracking has been studied as a function of yield strength, hydrogen activity and inclusion orientation and volume fraction by employing two medium carbon hardenable steels En16 and En16M of sulphur content 0.038% and 0.15% respectively.

In the 1250-1300 MPa yield strength range, both steels showed anisotropy of crack growth rate and K_{TH} in 3½% NaCl solution. The stage II crack velocity was greatest in the short transverse orientation and smallest in the longitudinal orientation. The K_{TH} was lowest in the short transverse orientation and greatest in the longitudinal orientation. Increasing the volume fraction of inclusions had a pronounced favourable effect on K_{TH} in the longitudinal orientation, a less pronounced although still beneficial effect in the transverse orientation and a detrimental effect in the short transverse orientation. The difference in stage II crack growth rate between the extreme orientations also increased with inclusion volume fraction.

An increase in the yield strength of En16 to 1450 MPa resulted in increased crack growth rates and decreased K_{TH} for all orientations in 3½% NaCl solution. More significantly there was little anisotropy in either crack growth rate or K_{TH}.

An increase in hydrogen activity of the environment obtained by using 0.1 MPa H_2S gas, resulted in a general elevation of crack growth rate and depression of K_{TH} of En16M in the 1300 MPa yield strength condition. The orientation dependence of crack growth rate and K_{TH} was again reduced to a large extent.

When the yield strength was reduced to 800-900 MPa, H_2S saturated 3½% NaCl solution had to be employed as the test environment in order to obtain significant crack advance. In spite of using a high hydrogen activity environment, there was an increase in K_{TH} for all orientations. This was accompanied by a reappearance of anisotropic crack growth behaviour similar to that observed in the 1250-1300 MPa yield strength condition in 3½% NaCl solution. However, the nature of crack growth in the H_2S bearing environment was quite different from that in 3½% NaCl solution, With the high strength steels tested in 3.5% NaCl solution crack growth was continuous leading to a

smooth transition to crack arrest after a period of constant crack growth rate. In the low strength steels tested in H_2S saturated 3½% NaCl solution, similar behaviour was observed at high stress intensities. However, in this case an apparent arrest was followed by discontinuous growth in the short transverse and transverse orientations. The size of the growth increment was between 0.5 mm and 2 mm and each burst of crack growth was preceded by 4-12 hour periods over which there was little crack advance. The occurrence of discontinuous crack growth resulted in a gradually decreasing stage I behaviour giving no clear indication of the existence of a true threshold.

En16M in the 1200 MPa yield strength condition, when tested in H_2S saturated NaCl, also showed discontinuous crack growth in the short transverse orientation. Although there was no significant anisotropy of K_{TH} corresponding to apparent arrest, crack growth rates showed anisotropy similar to that observed in 3½% NaCl solution in the 1300 MPa yield strength condition.

The mode of fracture in the environment was found to be dependent on a number of factors such as yield strength, stress intensity, hydrogen activity and inclusion orientation. In the 1250-1300 MPa yield strength conditon, the fracture mode in 3½% NaCl in the arrest region of the short transverse orientations was predominantly intergranular with a small amount of tearing. At high stress intensities fibrous fracture was the dominant mechanism of failure. In the stage I region of the LT and TL orientations, the amount of intergranular fracture was less than in the corresponding regions of the short transverse orientations, there being an increased contribution from quasi-cleavage and fibrous modes of fracture. Repeated deflection of the crack into the short transverse plane by inclusions could also be seen in the longitudinal and transverse specimens. In all of the specimens tested in salt solution there was no significant chemical attack of MnS inclusions on the fracture surface.

When the environment was changed from 3.5% NaCl solution to 0.1 MPa H_2S gas, the fibrous fracture observed at high stress intensities in the former environment was replaced by quasi-cleavage. Similarly, in the arrest region cracking was fully intergranular with very little tearing being observed.

When the yield strength of En16 was increased to 1450 MPa, the fracture mode in 3.5% NaCl solution was fully intergranular at all

stress intensities and in all orientations.

On reducing the yield strength to 800-900 MPa, the predominant fracture mode in H_2S saturated 3½% NaCl solution was quasi-cleavage.

Cracking in the short transverse orientations was preferentially via elongated MnS inclusions. The extent of inclusion participation, as measured by their area fraction on the fracture surface, was found to be related to the number of inclusions within the plastic zone.

A number of disconnected subsidiary cracks were observed ahead of the main crack in the arrest region of the short transverse specimens tested in H_2S saturated 3.5% NaCl solution. These subsidiary cracks were invariably associated with inclusion clusters.

The apparent diffusivity of hydrogen measured using the electrometric permeation technique showed little orientation dependence.

The criterion for hydrogen assisted fracture is assumed to be the attainment of a critical tensile stress. It is suggested that the embrittling effect of hydrogen results in a reduction of the fracture stress σ_f, the extent of the reduction being dependent on local hydrogen concentration. It is postulated that hydrogen assisted crack growth takes place when the fracture criterion is satisifed over a microstructurally significant distance X_o. By treating the hydrogen source at the crack tip as a moving line source and by applying the same failure criterion, the crack growth rate is found to be related to the hydrogen diffusivity and the relative concentration C_{Cr}/C_o where C_{Cr} is the local concentration of hydrogen necessary for crack growth at a distance X_o ahead of the crack and C_o is related to the intensity of the hydrogen source. With this model it is possible to explain the observed effect of strength and hydrogen activity of the environment on the crack growth behaviour of an inclusion free steel.

It is shown that inclusions affect crack growth behaviour primarily by perturbing the crack tip stress field within the plastic zone. In the LT and TL orientations, inclusions increase K_{TH} by reducing the stress triaxiality within the plastic zone and hence are beneficial. In the short transverse orientations SL and ST, the presence of elongated inclusions leads to strain intensification which enhances the stress levels within the plastic zone as a result of work hardening and therefore decreases K_{TH}.

The extent to which inclusions affect the stress field is shown to increase with increasing K_{TH} of an inclusion free steel and decreasing yield strength. Thus, at very high strength levels, there is little anisotropy of K_{TH} even in a weak environment like 3½% NaCl solution. On reducing strength, anisotropic behaviour in K_{TH} is manifested in weak environments, but not in high hydrogen activity environments containing H_2S. A further reduction in strength leads to the reappearance of anisotropy even in H_2S bearing environments.

Anisotropy in crack growth rate arises from differences in C_{Cr}, the critical local hydrogen concentration required for crack growth at a given K in the various orientations. It has been shown that for a given difference in C_{Cr}, the resulting anisotropy in crack growth rate is higher when C_{Cr}/C_o is large than when it is small. In the very high strength condition (σ_{ys} = 1450 MPa) both the absolute values of C_{Cr} and the differences in C_{Cr} between the various orientations are very small. Therefore, there is little anisotropy of crack growth rate even in a weak environment like 3.5% NaCl solution (Small C_o). A decrease in yield strength to 1250-1300 MPa results in an increase in both C_{Cr} and the differences in C_{Cr} between different orientations. This leads to anisotropy of crack growth rate in salt solution but there is no significant orientation dependence in H_2S gas (large C_o). A further reduction in strength to 800 MPa results in the reappearance of anisotropy even in H_2S bearing environments because of the increase in both C_{Cr} and the differences in C_{Cr}.

It is proposed that hydrogen assisted crack growth takes place by matrix embrittlement and by hydrogen pressurisation of the inclusion-matrix interface. The latter mechanism is manifested only in environments of high hydrogen activity like H_2S saturated 3.5% NaCl solution and assists crack growth in the short transverse orientations. Crack growth in these orientations in H_2S saturated 3.5% NaCl solution is by an embrittlement mechanism at high stress intensities. Following an apparent crack arrest several subsidiary cracks nucleate and grow ahead of the main crack by pressurisation of the inclusion-matrix interface. These cracks link with the main crack causing a burst of crack growth. This cycle is repeated several times leading to discontinuous crack growth before final arrest.

8.2. Some Practical Implications of the Present Work

It is an often held belief that an increase in plane strain fracture toughness K_{IC} at a given strength also increases K_{TH} and conversely any decrease in K_{IC} also decreases K_{TH}. The present work shows that this argument has no basis. For example an increase in inclusion volume fraction decreases K_{IC} in the LT and TL orientations whereas it can increase K_{TH}. Also, in the short transverse orientation the detrimental effect of inclusions on K_{TH} is not as severe as it is on K_{IC}.

It has been suggested by McIntyre and Priest (1972) that H_2S gas can be used as an accelerated test environment to obtain K_{TH}. The results of the present work indicate that in high strength steels, H_2S gas, because of its extreme hydrogen activity, gives very conservative estimates of K_{TH} and is unable to detect small differences in susceptibility between steels. For example, whereas a modified composition or microstructure can give a significant increase in K_{TH} and a decrease in crack growth rate with a test environment such as 3½% NaCl solution, which represents a service environment like sea water, the same improvement may not be revealed if 0.1 MPa H_2S gas is used.

In the case of low strength steels, a fracture mechanics approach to testing is fraught with serious practical problems. Crack growth in these steels invariably requires the maintenance of a high hydrogen activity at the crack tip for extended periods, but because of the inaccessibility of the crack tip this cannot be achieved by chemical or electrochemical means.

Pressurisation assisted macroscopic crack growth in the short transverse orientations involves the formation of several inclusion assistednon-co-planar subsidiary cracks ahead of the main crack. Also, these subsidiary cracks are large in comparison to the plastic zone sizes encountered. Both of these factors can invalidate the application of conventional fracture mechanics to the characterisation of macroscopic crack growth.

The presence of elongated inclusions improves resistance to cracking in weak environments in the LT and TL orientations. However, this cannot be exploited in practice because of the detrimental effect of inclusions on K_{IC} in all orientations and on crack nucleation kinetics in wet environments. The adverse influence of plate-like inclusions

on resistance to hydrogen embrittlement in the short transverse orientations in weak environments should also be a factor favouring efforts towards their elimination.

With regard to the pipelines that failed in service, the steels from which they were manufactured, contained type II MnS inclusions. Although the inclusion volume fractions were generally low (≈ 0.02% S), the individual inclusions were thin and highly elongated and occurred in groups of co-planar arrays, the spacing between the inclusions in each array being very small. This condition is ideal for cracking by pressurisation at the inclusion-matrix interface because of the small lateral spacing between the elongated inclusions. Also, the small inclusion volume fraction hastens cracking kinetics. Had the inclusions been of the more uniformly distributed type I morphology, they would have been less detrimental even if they were elongated. It is, therefore essential to prevent the formation of type II inclusions. Unfortunately, the deoxidation practice employed in the production of pipeline steels is such that MnS inclusions are likely to be present in the type II morphology. Therefore, to obtain increased resistance to cracking in steels containing normal sulphur contents (≈ 0.02%), it is necessary to employ sulphide inclusion modifiers such as rare earth metals, Ti and Zr. Besides eliminating the adverse type II MnS, these modifiers lead to the formation of hard sulphide inclusions which are almost non-deformable during hot working. However, results obtained by Miyoshi et al (1976) show that cerium treatment can result in the formation of clusters of closely spaced spherical inclusions which can be equally detrimental as the elongated inclusions and hence complete freedom from cracking susceptibility is not obtained. It is possible that inclusion clustering is a less serious problem with Ti or Zr based modifiers and it is suggested that the effectiveness of these alternative modifiers should be investigated more thoroughly. In the absence of inclusion modification, reducing the inclusion volume fraction to very low levels seems to be the surest way to obtain freedom from cracking. As pointed out in the introductory chapter, this approach has been used successfully by Japanese steel manufacturers and sulphur contents in Japanese pipeline steels are currently held below 0.005%.

8.3. Suggestions for Further Work

An essential prerequisite for modelling hydrogen assisted cracking is to establish whether or not the fracture process obeys a critical tensile stress criterion. The second requirement is a knowledge of the size of the process zone in terms of the microstructural parameters, and matrix strength. Available data on the effect of hydrogen activity on K_{TH} suggest the existence of a lower limit to K_{TH}. It is necessary to determine whether this is associated with a limiting fracture stress σ_f, or with the need for the spread of plasticity over the microstructurally significant critical distance.

The role of elongated inclusions in fibrous fracture has been well studied. However, their influence on critical stress controlled fracture phenomena has received little attention. Since it is now well established that carbide initiated cleavage in steels is controlled by the attainment of a critical stress, a study of the effect of inclusion orientation and volume fraction on cleavage fracture toughness would be a convenient way of assessing their role in stress controlled fracture phenomena. This would also test the validity of the explanations proposed to account for the role of inclusions on crack growth behaviour in hydrogen embrittlement.

The weak nature of the inclusion-matrix interface is the primary factor responsible for the role of inclusions in fracture. Although this interface is known to be weak, a detailed knowledge of the nature of the interface is lacking. The effect of inclusion orientation and volume fraction on Young's modulus, determined as a function of total strain in tension and compression would give useful information on the nature of the inclusion-matrix interface.

APPENDIX 1

DEVELOPMENT OF AN AC POTENTIAL DROP SYSTEM FOR MONITORING CRACK LENGTH

A.1.1. Introduction

Monitoring of crack length forms a vital part of any experiment designed for studying sub-critical crack growth. A number of crack length measuring techniques have been developed and their relative merits have been reviewed in detail (McIntyre and Priest, 1971; Ritchie, 1972; Deans and Richards, 1979). The following discussion is confined to the Potential Drop (PD) technique which is based on the principle that the resistance of a cracked body is a function of the crack length. Although DC and AC versions of the PD technique have been developed, it is the former that has found widespread use.

In the following, the sources of error associated with the use of the DCPD technique are discussed. The development of an ACPD system which overcomes some of these problems is then outlined and the performance of this system in monitoring sub-critical crack growth is assessed. (The factors which favoured the development of this system have already been stated in Section 4.6.)

A.1.2. Sources of Error in the DCPD Technique

Most of these errors are characteristic of those encountered in the measurement of small resistances. The resistance of a steel specimen is typically a few microohms and therefore to get a detectable signal across the crack, high currents have to be employed (30-50 amps). If the potential drop is to give a direct measure of the resistance of the specimen, the current has to be maintained constant to a high degree. Commercial current sources employed for crack length monitoring maintain the current constant to within 0.01%. Thermal emfs developing at dissimilar metal junctions introduce errors which subsequently get amplified. They occur at the specimen-potential lead junction and at the amplifier input terminals. The use of iron wire for potential leads can eliminate the problem at the specimen end. However, it still persists at the amplifier input terminals. The second source of error arises from the drift of the input offset voltage of the amplifier. However, the most significant and often overlooked error is caused by the large temperature coefficient of resistance of steel ($5 \times 10^{-3}/°C$).

A modified DCPD system developed by Cottis (1978) eliminates all of these errors. In this method two successive measurements of the potential drop across the crack are made with and without current flowing through the specimen (V and V_o respectively). Similarly two other measurements are made at a region of the specimen where potential drop is largely unaffected by crack growth (V_R and V_{Ro} respectively). The quotient $(V - V_o)/(V_R - V_{Ro})$ can be used as a measure of crack length.

A.1.3. Distinguishing Features of the ACPD Technique

When an alternating current passes through a conductor, current flow is restricted to the regions near the surface of the conductor and this is known as the 'skin effect'. The severity of this effect is given by the depth of penetration δ, which is also known as the skin depth and

$$\delta = \left(\frac{\rho}{\pi\mu f}\right)^{\frac{1}{2}} \qquad \text{A.1.1.}$$

where ρ = resistivity

μ = magnetic permeability

f = frequency

The AC impedance, Z, of a cylindrical conductor of length ℓ and radius r is given by

$$Z = \frac{\rho\ell}{2\pi r\delta} \quad \text{if } \delta << r \qquad \text{A.1.2.}$$

Thus the impedance depends on frequency, magnetic permeability, effective cross-sectional area and resistivity. In a ferromagnetic material like mild steel where the skin effect is strong, the AC impedance is much larger than the DC resistance even at low frequencies. For example 2 amps of AC at 100 Hz gives a 1-2 mV potential drop. The same value of DC results in a signal of a few microvolts only. Thus the use of AC improves the signal to current ratio enormously.

Because current flow is restricted to the surface, the impedance of the specimen across the crack varies linearly with crack length and such a variation has obvious advantages.

Most of the sources of error mentioned in the DCPD system are DC voltages and in an AC system these can be effectively removed by using AC coupled amplifiers.

A.1.4. Development of an ACPD system

If the PD is to give a direct measure of the impedance of the specimen then in the case of an ACPD system both current and frequency have to be maintained constant to a high degree. Whereas keeping the frequency constant is not a serious problem, the design of a constant AC current source is more complex than its DC counterpart. Even if a constant current source could be used, the errors due to variation in μ and ρ with temperature would still be present. To overcome the above problems it was decided to use a comparison technique. Potential drops across the specimen (V_{sp}) and a reference (V_{ref}) connected in series are measured. The dimensionless quotient V_{sp}/V_{ref} can be correlated to crack length provided frequency, current and temperature remain constant over the period during which the division is performed. It is convenient to use an identical passive specimen as the reference for it effectively removes the errors arising from the variation of μ and ρ with temperature.

The dual slope integration technique used for Analogue to Digital (A-D) conversion in modern Digital Volt Meters provides a convenient means for carrying out the division electronically in a very short time (fraction of a second). The converter compares the input voltage with an internal reference voltage ratiometrically (Motorola, 1975). Thus a dual slope integration A-D converter IC (integrated circuit) can be adapted to perform the division of two external voltages, in this case an external voltage being used in place of the internal reference. The high accuracy, linearity and noise immunity of the DVM IC, make it an ideal choice for performing the division operation. A large variety of such ICs are available at low cost because of their application for DVMs.

A.1.5. Circuit Details

In Figure A.1.1. is shown the block diagram of the ACPD system. The current source is provided by an AC power amplifier (2). A Wien bridge oscillator (1) provides the input for the power amplifier. The specimen (5) is connected in series with the reference (4) and a load resistor (3) across the output of the power amplifier. The output signal from the specimen is fed into an AC coupled signal amplifier (7). The amplified signal is rectified using a synchronous switching technique (9). The signal from the reference is also amplified (6) and rectified (8) in an identical fashion. The rectified

outputs from the specimen (V_{sp}) and the reference (V_{ref}) are fed into the A-D converter which performs the division and gives the quotient V_{sp}/V_{ref} as a digital output.

Because frequency was an important parameter in the ACPD technique, it was decided to experiment with a range of frequencies. Although the signal/current ratio increases with frequency, at very high frequencies the output becomes sensitive to fracture surface roughness. Also, because of the capacitance between the crack faces which becomes dominant at high frequencies, the output signal varies with crack face separation (Carlsson, 1962). A frequency range of 150 Hz - 10 kHz was therefore selected. The frequency of the Wien bridge oscillator could be varied in 12 steps within this range. By using silvered-mica and polycarbonate capacitors for the Wien bridge, frequency could be maintained stable to within 0.01% (Ferranti, 1970). Such a high stability of frequency is not required with a comparison technique, whereas with a constant current technique it would be essential to have high stability because voltage output varies with the square root of frequency.

The power amplifier was capable of delivering up to 3A current. The desirable characteristics of a power amplifier suitable for the ACPD application were found to be a high mains frequency rejection (50 Hz) and a low crossover distortion. The purpose of the load resistor was to reduce the power dissipation across the driving transistors.

A detailed circuit diagram of the signal amplifier and rectifier is shown in Figure A.1.2. The signal from the specimen is amplified by a differential amplifier with a gain of 1000. Because the source impedance was low, it was felt that the input impedance of the single IC differential amplifier was adequate. The IC 725 was chosen for its good high-frequency response and large open loop gain. The first amplification stage is AC coupled to a non-inverting amplifier of a gain of ≈6 through a 10μF polycarbonate capacitor.

Initially, a precise rectification technique (Clayton, 1980) was tried. However, it was found to have poor linearity at high frequencies and voltages. Because a high linearity is essential for the success of the division technique, it was decided to try an alternative technique (synchronous switching) for rectification and this is described below.

Rectification by synchronous switching is achieved using the analogue switch (RS) 4053B. The signal for operating the gate of the switch is obtained from the oscillator and this is first amplified by a non-inverting amplifier of a gain of ≈3 before being fed into a phase shifter. (Because the voltage from the specimen leads the voltage from the amplifier by 45°, a phase shifter is necessary.) The output of the phase shifter drives a high speed comparator (319) which operates the gate of the switch 4053B. The amplified signal output from the specimen and its inverted counterpart constitute the input to the switch. The phase relationships of the two input signals and the comparator output are shown in the inset of Figure A.1.2. The rectified output is fed into a smoothing circuit. Besides having better linearity over the precise rectification technique, the synchronous switching technique also gave superior noise rejection.

The signal from the reference was also processed through an identical stage of amplification and rectification. A 12 bit (3½ digit) A-D converter (MC 14433) IC was used to perform the division.

A.1.6. Results and Discussion

A.1.6.1. Calibration using simulated crack

For initial calibration a specimen with a saw-cut of 0.75 mm width was used to simulate crack extension. The current and sensing leads were connected to the WOL specimen with 4BA screws at the positions shown in Figure A.1.3. A Tufnul strip was placed between the bolt and the loading pin to prevent current flow across them. Preliminary trials showed that the output signal from the specimen and the reference was sensitive to the position of the leads in the vicinity of the specimen. Therefore, in order to maintain the same configuration of leads during calibration, current and sensing leads were connected to the specimen through rigid copper bars. The current in the specimen was adjusted to obtain an output of approximately 1 Volt from the specimen after amplification. At 1 kHz, this current was approximately 200 mA.

The results of the calibration are presented in Figure A.1.4. Two important points should be noted. First, the calibration is linear up to very large crack lengths ($a/W > 0.9$). This is in contrast to the calibration for the DCPD, where linearity is observed only up to an a/W of 0.7 (McIntyre and Priest, 1971). In steel the skin

effect occurs at relatively low frequencies because of its high μ. Therefore, in the case of ACPD linearity is observed over a much larger range of a/W. Secondly, the calibration is almost independent of frequency between 150 Hz and 10 kHz. The observed signal from the specimen, V, is made up of the contribution from the skin effect in the specimen (V_s) and the induced emf between the sensing and the current leads (V_p).

(i.e.) $V = V_s + V_p$ A.1.3.

However, from A.1.1. and A.1.2.

$V_s \alpha f^{\frac{1}{2}}$ A.1.4.

But $V_p \alpha f$ A.1.5.

The absence of significant frequency dependence of calibration implies that induced emfs are small in the frequency range 150 Hz - 10 kHz.

A.1.6.2. Stability

In order to check the stability of the ACPD system, the output V_{sp}/V_{ref} of a specimen with a simulated crack was monitored over a period of 5 days. It was found that the output of the A-D converter did not change by more than 1 count. This corresponded to a stability of 0.1%. Halving the current through the specimen resulted in the output V_{sp}/V_{ref} changing by 0.1%. The insensitivity of the output to the current variation of this magnitude shows the effectiveness of the division technique.

In practice current variations are likely to be within ±5% and this variation will cause no detectable change in the output. The foregoing results of stability of the ACPD system demonstrate that the division technique is very effective in eliminating the errors caused by changes in temperature and current.

A.1.6.3. Monitoring fatigue crack growth

In order to assess the performance of the ACPD system in monitoring the length of real cracks, it was employed to monitor fatigue crack length in a WOL specimen. Crack length was also measured by a compliance technique in which a clip gauge was used to measure the mouth opening displacement. The lead positions were the same as those shown in Figure A.1.3. The specimen was insulated from the machine by using Teflon coated pins. The results of the experiments revealed several features of the ACPD system which could not be observed during

calibration with the simulated crack and these are discussed below.

Crack length, as measured by the compliance technique, is compared with the normalised output of the ACPD (Figure A.1.5.). Although the relation between the two is linear, the calibration of Figure A.1.5, is different from that shown in Figure A.1.4. for a simulated crack. The presence of the specimen grips, which were ferromagnetic, affected the output signal from the specimen, resulting in a different calibration.

It was also found that the output from a fatigue cracked specimen showed a marked load dependence. A typical trace of output vs load is shown in Figure A.1.6. Initially PD increases with load and this increase is caused by the elimination of the electrical shorting of the crack faces. After the complete opening of the crack, the output decreases slowly. The decrease in output with load could be due to either the very high stresses at the crack tip or the stressing of the crack faces. In order to determine which of the two was causing the drop in PD, the output across the gauge length of a plain tensile specimen was measured as a function of load. At a stress of 240 MPa, the output decreased by 2% and the effect was reversible. The results from the experiment with the plain tensile specimen showed that the drop in output with load shown in Figure A.1.6. was primarily due to stressing of the crack faces.

The foregoing results show that the ACPD system has certain disadvantages when compared to DCPD , namely, the configuration of the leads and the presence of ferromagnetic materials in the vicinity of the specimen influence the calibration. However, linearity of calibration is preserved under all conditions. Therefore, provided the leads are held rigid during a test the calibration plot can be constructed from the outputs corresponding to the initial and final crack lengths. Thus, the absence of a unique calibration does not constitute a serious practical problem. However, the dependence of output on load is a problem which is more difficult to overcome and limits the exploitation of the inherently high sensitivity, stability and linearity of the ACPD system.

*A.1.6.4. Application of ACPD to the determination of R curves

The adverse effect of elastic strain on permeability was considered

*This part of the investigation was carried out in collaboration with Dr. N. Okumura.

to be the likely cause of the drop in PD with load. It was expected that plasticity at the crack tip would also have a detrimental effect on μ and hence it would result in a similar drop in voltage output. This behaviour of the ACPD should be contrasted with that of the DCPD where both plasticity and crack growth result in an increase in output. If ACPD could thereby distinguish between plasticity and crack growth, it might have a useful role in monitoring crack initiation and growth during slow stable crack extension.

In order to determine the suitability of the ACPD technique for detecting crack initiation and monitoring crack extension during slow crack growth, side-grooved Charpy size specimens were tested in three point bending. Because stability was not an important consideration in the application of PD to the study of slow crack growth, only one amplifier-rectifier channel of the previously described ACPD system was used. The variation of PD and load with clip gauge opening displacement (CGOD) is shown in Figure A.1.7. The most important feature of the PD-CGOD trace is the occurrence of a minimum. A number of specimens were tested so that initiation COD, δ_i, could be determined using the recommended multispecimen technique. The COD corresponding to the minimum point, δ_{min}, was also evaluated for all the specimens. These results are presented in *Table A.1.1. and it is seen that δ_{min} obtained from ACPD closely agrees with the δ_i value obtained by the recommended multispecimen technique.

By measuring the amount of slow crack growth on the specimens broken open at the completion of testing and by assuming a linear relationship between voltage change (ΔV in Figure A.1.7.) and crack extension, COD-R curves could be constructed using the PD-CGOD trace of a single specimen. The R curve obtained from the multispecimen technique is compared with those calculated by using ACPD on single specimens in Figure A.1.8. It is seen that close agreement exists between the results obtained from the two methods.

---

*The results shown in Table A.1.1. form only a small part of the more detailed investigation reported by Okumura et al where several steels covering a wide range of δ_i values have been tested.

A.1.7. Conclusions

An ACPD system has been developed, which by using a division technique overcomes the effects of variations in specimen current and temperature.

The inherently high sensitivity, stability and linearity of the ACPD system could not be fully exploited because the PD output is affected by stress and configuration of the sensing and current leads.

In the case of ACPD, plasticity results in a decrease in PD output whereas crack growth leads to an increase in PD. This contrasts with the behaviour of DCPD where both plasticity and crack growth result in an increase in output.

By exploiting the difference in the response of ACPD to plasticity and crack growth, it has been applied successfully to the detection of crack initiation in side-grooved Charpy size mild steel specimens tested in three point bending. Both δ_i and COD-R curves determined from single specimens using ACPD agree closely with those obtained by the recommended multispecimen technique.

APPENDIX 2

VARIATION OF STRESS INTENSITY WITH CRACK LENGTH FOR A GRIFFITH CRACK PRESSURISED BY A CONSTANT AMOUNT OF AN IDEAL GAS

Consider a Griffith crack of length 2a in an infinite sheet of thickness B under plane strain conditions. When the crack is subjected to a uniform internal pressure 'p', it assumes the shape of an ellipse (Figure A.2.1.) The displacement in the y direction, u_y is given by (Sneddon and Lowengrub, 1969)

$$u_y = 2 \frac{(1 - \nu^2)}{E} p \sqrt{a^2 - x^2} \qquad \text{A.2.1.}$$

where E is Young's modulus and ν is Poisson's ratio.

The volume of the crack 'v' is given by

$$v = \frac{8\ Bp}{E'} \int_0^a \sqrt{a^2 - x^2}\ .\ dx$$

where $E' = \dfrac{E}{1 - \nu^2}$

But

$$\int \sqrt{a^2 - x^2} = \frac{1}{2} \left[x \sqrt{a^2 - x^2} + a^2 \sin^{-1} \frac{x}{|a|} \right]$$

$$\therefore \quad v = \frac{2Bp}{E'} \pi a^2 \qquad \text{A.2.2.}$$

For an ideal gas, $pv = nRT$ A.2.3.

Eliminating v from A.2.2. and A.2.3.

$$p^2 = \frac{nRTE'}{2\pi a^2 B} \qquad \text{A.2.4.}$$

The Mode I stress intensity for a crack under internal pressure 'p' is

$$K_I = p \sqrt{\pi a} \qquad \text{A.2.5.}$$

Substituting for p from A.2.4. in A.2.5.

$$K_I = \sqrt{\frac{nRTE'}{2aB}} \qquad \text{A.2.6.}$$

It is seen from A.2.6. that for a constant amount of ideal gas expanding under isothermal conditions, the stress intensity decreases with crack length.

REFERENCES

Ahmad, S.A., Ryder, D.A. and Davies, T.J. (1975), Eng. Fract. Mechanics, 7, 357.

Akhurst, K.N. (1979), Ph.D. Thesis, Imperial College, University of London.

Asaoka, T., Lapasset, G., Aucouturier, M. and Lacombe, P. (1978), Corrosion, 34, 39.

ASTM D1141-75 - Specification for Substitute Ocean Water.

Baker, R.G. and Watkinson, F. (1961), "Hydrogen in Steel", ISI Special Report No. 73, p.123.

Baker, T.J. (1972), Ph.D. Thesis, University of Cambridge.

Barraclough, K.C. (1961a), "Hydrogen in Steel", ISI Special Report No. 73, p.101.

Barraclough, K.C. (1961b), "Hydrogen in Steel", ISI Special Report No. 73, p.143.

Barth, C.F., Steigerwald, E.A. and Troiano, A.R. (1969), Corrosion, 25, 353.

Bernstein, I.M. and Thompson, A.W. (1976), Int. Met. Rev., 269.
BIRKLE, A.J., WEI, R.P. and PELLISIER, G.E. (1966) Trans. A.S.M, 59, 981.

Bockris, J. O'M., McBreen, J. and Nanis, L. (1965), Journal of Electrochemical Soc., 112, 1025.

Bockris, J. O'M., Beck, W., Genshaw, M.A., Subramanyan, P.K. and Williams, F.S. (1971), Acta Met., 19, 1209.

Boniszewski, T. and Baker, R.G. (1965), British Welding J., 12, 349.

Boniszewski, T. and Moreton, J. (1967), British Welding J., 14, 321.

Briant, C.L., McMahon, C.J. Jr. and Feng, H.C. (1978), Met. Trans., 9A, 625.

Briant, C.L. and Banerji, S.K. (1978), Int. Met. Rev., 164.

British Petroleum Test Procedure for Evaluating Hydrogen Induced Cracking, Revision 3, October 1973.

Brown, B.F. (1968), Int. Met. Rev., 171.

Carlsson, J. (1962), Trans. Royal Institute of Technology, Stockholm, Sweden, 189.

Carter, C.S. (1969), Corrosion, 25, 423.

Chew, B. and Fabling, F.T. (1972), Metal Construction and British Welding Journal, 19, 132.

Clark, Jr., W.G. (1975), Westinghouse Research Laboratories, Scientific Paper 75-1E7-MSLRA-P1.

Clark, W.G., Jr., and Landes, J.D. (1976), "Stress Corrosion - New Approaches", ASTM STP610, p.108.

Clayton, G.B. (1980), "Operational Amplifiers", p.320, Butterworths.

Colangeló, V.J. and Heiser, F.A. (1974), "Analysis of Metallurgical Failures", p.226, John Wiley.

Cottis, R. (1978), Private Communication.

Curry, D.A. and Knott, J.F. (1976), Met. Science, 10, 1.

Curry, D.A. (1978), CERL Lab. Note RD/L/N64/78.

Darken, L.S. and Smith, R.P. (1949), Corrosion, 5, 1.

Davis, R.A. (1963), Corrosion, 19, 45t.

Deans, W.F. and Richards, C.E. (1979), Journal of Testing and Evaluation, 7, 147.

Devanathan, M.A.V. and Stachurski, Z. (1962), Proc. Roy. Soc., A270, 90.

Doig, P. and Flewitt, P.E.J. (1978), Met. Trans. A, 9A, 357.

Embury, J.D., Petch, N.J., Wraith, A.E. and Wright, E.S. (1967), Trans. AIME, 239, 114.

Evans, G.M. and Rollason, E.C. (1969a), JISI, 207, 1484.

Evans, G.M. and Rollason, E.C. (1969b), JISI, 207, 1591.

Farrar, J.C.M. (1977), Welding Research International, 7, 120.

Farrell, K. and Quarrell, A.G. (1964), JISI, 202, 1002.

Fast, J.D. (1971), "Interaction of Metals and Gases", Vol. II, Macmillan, sec. 2.13 .

Ferranti E line Transistor Applications (1970), p.35.

Gerberich, W.W., Garry, J. and Lessar, J.F. (1976), "Effect of Hydrogen on Behaviour of Materials", Ed. Bernstein, I.M. and Thompson, A.W. p.70, AIME.

Gerberich, W.W. (1974), "Hydrogen in Metals", ed. Bernstein, I.M. and Thompson, A.W., p.115, ASM.

Gilbreath, W.P. and Adamson, M.J. (1976), "Stress Corrosion - New Approaches", ASTM STP 610.

Gladman, T. (1979), "Inclusions" ed, Pickering, F.B., p.157, Institution of Metallurgists.

Hancock, G.G. and Johnson, H.H. (1966), Trans. AIME, 236, 513.

Harrison, R.D. (1978), "Book of Data", p.119, Nuffield Foundation.

Hart, P.H.M. and Brooks, T.L. (1977), Welding Institute Report 43/1977/M.

Haynes, A.G. (1961), "Hydrogen in Steel", ISI Special Report No. 73, p.102.

Heidersbach, R., Jones, J. and Surkein, M. (1977), Second International Congress on Hydrogen in Metals, Paris.

Hewitt, J. (1961a) "Hydrogen in Steel" ISI Special Report No. 73, p.149.

Hewitt, J. (1961b), "Hydrogen in Steel", ISI Special Report No. 73, p.104.

Hewitt, J. and Murray, J.D. (1968), British Welding J. 15, 151.

Hughes, P.C., Lamborn, I.R. and Liebert, B.B. (1965), JISI, 203, 154.

Inagaki, H., Tanimura, M., Matsushima, I. and Nishimura, T. (1978), Trans. ISIJ, 18, 149.

Interrante, C.G. and Hicho, G.E. (1976), "Stress Corrosion - New Approaches", ASTM STP 610, p.349.

Johnson, H.H., Morlet, J.G. and Troiano, A.R. (1958), Trans. AIME, 212, 528.

Johnson, H.H. (1974), "Hydrogen in Metals", ed. Bernstein, I.M. and Thompson, A.W., p.35, ASM.

Jokl, M.L., Kameda, J., McMahon, Jr., C.J. and Vitek, V. (1980), "Micromechanisms of Crack Extension", Cambridge, paper 10, (preprint).

Jonas, O. (1977), "Fracture 1977", Proceedings of International Conference on Fracture, Vol. 2, p.269, Waterloo, Canada.

Kazinczy, F. De (1959), Acta Met., 7, 525.

Knott, J.F. (1966), JISI, 204, 104.

Kortovich, C.S. and Steigerwald, E.A. (1972), Eng. Fracture Mechanics, 4, 637.

Kumnick, A.J. and Johnson, H.H. (1974), Met. Trans. 5, 1199.

Landes, J.D. and Wei, R.P. (1973), Int. Journal of Fracture, 9, 277.

Lee, T.D., Goldenberg, T. and Hirth, J.P. (1979), Met. Trans. A, 10A, 439.

Lees, D.J. (1977), "Mechanisms of Environment Sensitive Cracking of Materials", ed. Swann, P.R. et al, p.557, TMS.

Lessar, J.F. and Gerberich, W.W. (1976), Met. Trans. A, 7A, 953.

Li, J.C.M., Oriani, R.A. and Darken, L.S. (1966), Z. Phys. Chem. (N.F.), 49, 271.

Loginow, A.W. and Phelps, E.H. (1975), J. Eng. Ind., Trans. ASME, Series B, 97, 275.

McIntyre, P. and Priest, A.H. (1971), BISRA Report MG/54/71.

McIntyre, P. and Priest, A.H. (1972), British Steel Corporation Report MG/3/72.

McIntyre, P. (1973), "Mechanics and Mechanisms of Crack Growth", Proceedings of Conference held at Cambridge, p.130, British Steel Corporation.

McIntyre, P. and Walker, E.F. (1977), Second International Congress on Hydrogen in Metals, Paris.

McIntyre, P. (1977), "Stress Corrosion Cracking and Hydrogen Embrittlement of Iron Base Alloys", ed. Staehle, R.W. et al, p.788, NACE, Houston.

McIntyre, P. and Banks, T.M. (1978), Preprints of Select Seminars on European Offshore Steels Research, 2, 459.

McMahon, Jr. C.J. and Vitek, V. (1979), Acta Met., 27, 507.

McNabb, A. and Foster, P.K. (1963), Trans. AIME, 227, 618.

Miyoshi, E., Tanaka, T., Terasaki, F. and Ikeda, A. (1976), J. Eng. Industry, Trans. ASME, Series B, 98, 1221.

Moore, E.M. and Warga, J.J. (1976), Materials Performance, 15, 17.

Motorola application note AN-317 (1975).

Nelson, H. and Williams, D.P. (1977), "Stress Corrosion Cracking and Hydrogen Embrittlement of Iron Base Alloys", ed. Staehle, R.W. et al, p.390, NACE, Houston.

Newman, J.F. and Shreir, L.L. (1969), JISI, 207, 1369.

Novak, S.R. and Rolfe, S.T. (1969), Journal of Materials, 4, 701.

Oates, G.J. (1969), JISI, 207, 353.

Ohki, T., Tanimura, M., Kinoshita, K. and Tenmyo, G. (1975), "Stress Corrosion - New Approaches", ASTM STP 610, p.399.

Ohnishi, K. (1971), Trans. Japan. Inst. Metals, 12, 329.

Okumura, N., Venkatasubramanian, T.V., Unvala, B.A. and Baker, T.J., To be published in Eng. Fracture Mechanics.

Oriani, R.A. and Josephic, P.H. (1974), Acta Met., 22, 1065.

Oriani, R.A. (1977), "Stress Corrosion Cracking and Hydrogen Embrittlement of Iron Base Alloys", ed. Staehle, R.W. et al., p.351, NACE, Houston.

Petch, N.J. and Stables, P. (1952), Nature, 169, 842.

Petch, N.J. (1956), Phil. Mag., Ser. B., 1, 331.

Pickering, F.B. (1979), "Inclusions", Institution of Metallurgists, p.108.

Proctor, R.P.M. and Paxton, H.W. (1969), Trans. ASM, 62, 989.

Pumphrey, P.H. (1980), CEGB Report RD/L/N22/80.

Radhakrishnan, T.P. and Shreir, L.L. (1967), Electrochemica Acta, 12, 889.

Ritchie, R.O. (1972), Report on Crack Growth Monitoring, Department of Metallurgy and Materials Science, University of Cambridge.

Ritchie, R.O., Knott, J.F. and Rice, J.R. (1973a), J. Mech. Phys. Solids, 21, 395.

Ritchie, R.O., Geniets, L.C.E. and Knott, J.F. (1973b), Proc. Int. Conference on the Microstructure and Design of Alloys, Vol. 1, p.124, Inst. of Metals, London.

Rosenfield, A.R. and Hahn, G.T. (1966), Trans. ASM, 59, 962.

Sandoz, G. (1972), Met. Trans. 3, 1169.

Sawicki, Jr., V.R. (1971), Ph.D. Thesis, Cornell University.

Skei, T. Wachter, A., Bonner, W.A. and Burnham, H.D. (1953), Corrosion, 9, 163t.

Smialowski, M. (1977), "Stress Corrosion Cracking and Hydrogen Embrittlement of Iron Base Alloys", ed. R.W. Staehle, et al., p.405, NACE, Houston.

Smith, E. (1966), Proc. Conf.'Physical Basis of Yield and Fracture', 36, Inst. Phys. and Phys. Soc., Oxford.

Smith, N. and Bagnall, B.I. (1968), British Welding J. 15, 63.

Smith, J.A., Peterson, M.H. and Brown, B.F. (1970), Corrosion, 26, 539.

Snape, E. (1968), Corrosion, 24, 261.

Sneddon, I.N. and Lowengrub, M. (1969), "Crack Problems in the Classical Theory of Elasticity", p.28, John Wiley.

Sorensen, E.P. (1979), "Elastic-Plastic Fracture", ASTM STP 668, p.151.

Steigerwald, E.A., Schaller, F.W. and Troiano, A.R. (1959), Trans. AIME, 215, 10481

Tetelman, A.S. (1973), "Hydrogen in Metals", ed. Bernstein, I.M. and Thompson, A.W., p.17, ASM.

Thompson, A.W. and Bernstein, I.M. (1980), Advances in Corrosion Science and Technology, Vol. 7, Plenum Press, New York.

Tracey, D.M. (1976), Trans. ASME, Journal of Engineering Materials and Technology, 98, 146.

Troiano, A.R. (1960), Trans. ASM, 52, 54.

Unvala, B.A. and Green, A.K. (1974), Journal of Strain Analysis, 9, 88.

Van der Sluys, W.A. (1969), Eng. Fracture Mechanics, 1, 447.

Walter, R.J. and Chandler, W.T. (1973), NASA Report CR-124410.

Webster, D. (1969), Trans. ASM, 62, 759.

Wei, R.P., Novak, S.R. and Williams, D.P. (1972), Materials Research and Standards, 9, 12.

Wranglen, G. (1975), "Sulfide Inclusions in Steel", ed. DeBarbadillo, J.J. and Snape, E., p.361, ASM.

Wriedt, H.A. and Oriani, R.A. (1970), Acta Met. 18, 753.

Yoshino, K. and McMahon, C.J., Jr. (1974), Met. Trans., 5, 363.

Zapffe, C. and Sims, C. (1941), Trans. AIME, 145, 225.

Zapffe, C. (1947), Trans. ASM, 39, 191.

TABLE 4.1.

CHEMICAL COMPOSITION OF En16 AND En16M

Element wt %	En16		En16M	
	Actual	Specified	Actual	Specified
Carbon	0.37	0.3 - 0.4	0.32	0.3 - 0.4
Silicon	0.26	0.1 - 0.35	0.21	0.25 max
Manganese	1.35	1.3 - 1.8	1.32	1.3 - 1.8
Sulphur	0.038	0.05 max	0.15	0.12 - 0.2
Phosphor us	0.009	0.05 max	0.009	0.05 max
Molybdenum	0.24	0.2 - 0.35	0.23	0.2 - 0.35

TABLE 5.1.

DETAILS OF HEAT TREATMENT AND MECHANICAL PROPERTIES

Set	Steel	Austenitising Temperature °C	Quenching Medium	Tempering Temperature °C	*Ultimate Tensile Strength σ_{UTS} (MPa)	*0.2% Proof Stress σ_{ys} (MPa)	Test Environment
A	En16	840	Normal Oil	400	1450	1250	3½% NaCl solution
B	En16M	860	Fast Oil	300	1500	1300	(a) 3½% NaCl solution (b) 0.1 MPa H_2S gas
C	En16	840	Normal Oil	300	1750	1450	3½% NaCl solution
D	En16M	840	Water	580	900	800	3½% NaCl solution saturated with H_2S gas
E	En16	840	Normal Oil	600	990	900	do.
F	En16M	840	Water	680	†680	†600	do.
G	En16M	840	Water	430	1280	1200	do.

*Determined on Hounsfield No. 11 and No. 13 Test pieces. Values are averages of at least three tests.

†Obtained by hardness conversion.

TABLE 5.2.

ORIENTATION DEPENDENCE OF K_{IC} FOR En16M AT A YIELD STRENGTH OF 1300 MPa

Orientation	K_{IC} (MN $m^{-3/2}$)
LT	60
TL	47
SL	45
ST	48

TABLE 5.3.

COMPARISON OF FRACTURE MODES IN HYDROGEN ASSISTED CRACKING WITH THOSE IN AIR AT ROOM AND LIQUID NITROGEN TEMPERATURES

Set	Steel	0.2% Proof Stress MPa	Fracture Mode in Hydrogen Assisted Cracking	Fracture Mode in Air at Room Temperature	Fracture Mode in Air at Liquid Nitrogen Temperature
A	En16	1250	IG	Fibrous	TGC
B	En16M	1300	IG	Fibrous	TGC
C	En16	1450	IG	IG	IG
D	En16M	800	Quasi-cleavage	Fibrous	TGC
E	En16	900	IG + Quasi-cleavage	Fibrous	TGC
F	En16M	600	Quasi-cleavage	Fibrous	TGC
G	En16M	1200	IG	Fibrous	TGC

IG = Intergranular Fracture; TGC = Transgranular Cleavage Fracture.

TABLE 6.1.

ORIENTATION DEPENDENCE OF APPARENT DIFFUSIVITY OF HYDROGEN

Orientation	Apparent Diffusivity m^2 sec^{-1}			
	Condition 1 - Tempered at 420°C		Condition 2 - Tempered at 680°C	
	From Rise Transient	From Decay Transient	From Rise Transient	From Decay Transient
L	8.1×10^{-12} 7.2×10^{-12} 8.8×10^{-12}	5.0×10^{-12} 4.2×10^{-12} 6.2×10^{-12}	1.8×10^{-10} 2.0×10^{-10}	1.2×10^{-10} 1.3×10^{-10}
S	8.9×10^{-12} 10.0×10^{-12} 9.6×10^{-12}	5.5×10^{-12} 8.2×10^{-12} 4.1×10^{-12}	1.7×10^{-10} 1.8×10^{-10}	1.2×10^{-10} 1.0×10^{-10}

TABLE A.1.1.

COMPARISON OF COD CORRESPONDING TO THE MINIMUM OF THE PD-CGOD TRACE AND INITIATION COD OBTAINED BY THE MULTISPECIMEN TECHNIQUE

Material: En7A Orientation: Longitudinal

Specimen No.	Frequency	δ_{min} (mm)
1	4.7 kHz	0.090
2	"	0.110 ± 0.010
3	"	0.120
4	"	0.084
5	"	0.130
6	"	0.110
7	"	0.093 ± 0.010
8	"	0.093
9	150 Hz	0.093
10	"	0.120
11	"	0.100
12	"	0.097

Average δ_{min} = 0.103 mm

Multispecimen δ_i = 0.11 mm

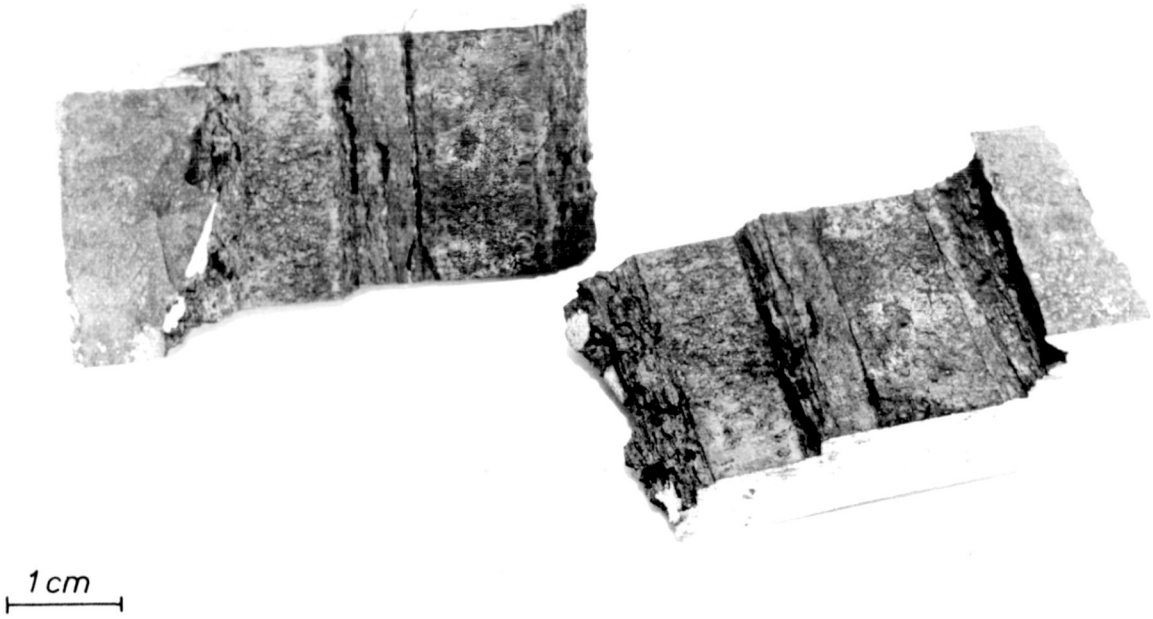


Fig.1.1 Fracture appearance of a cracked pipe.



Fig.1.2 Quasi-cleavage between MnS inclusions.

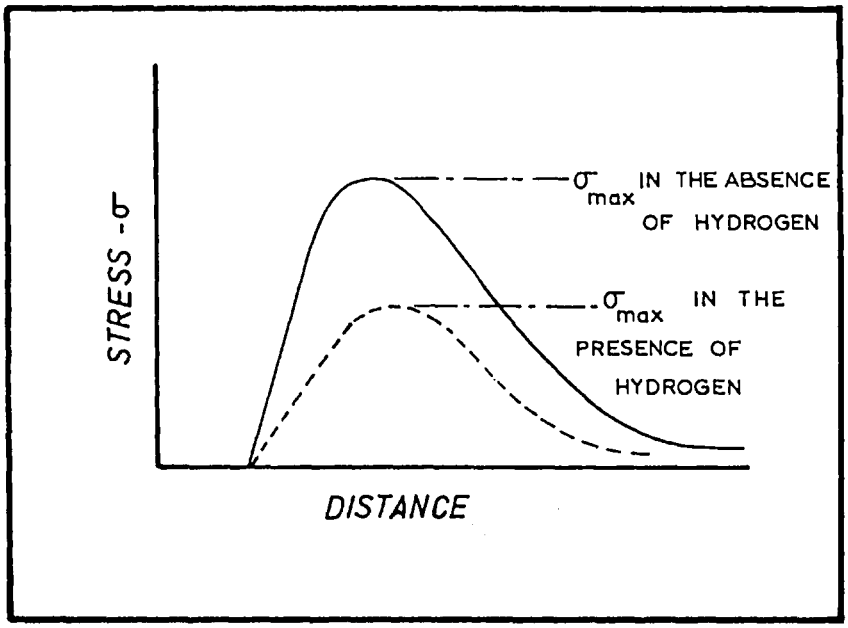


Fig. 2·1 Effect of hydrogen on the interatomic stress-distance curve

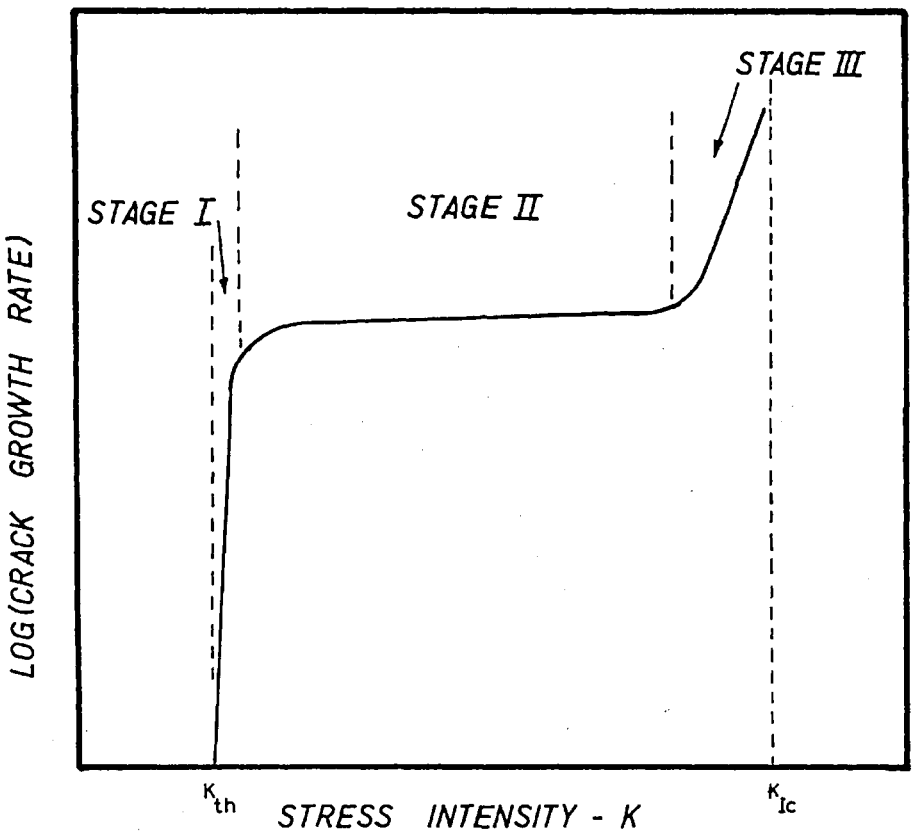


Fig. 2·2 Dependence of crack growth rate on stress intensity

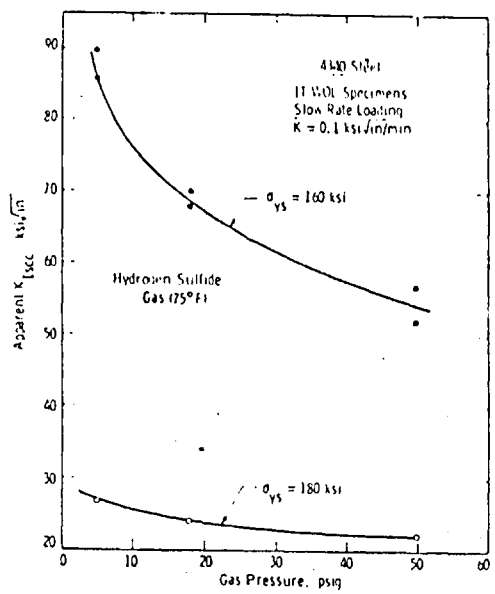


Fig. 2.3 Effect of H_2S pressure on K_{TH} (CLARK & LANDES, 1976)

Details of Figure 2.4. (over)

	Alloy	Yield Strength (MPa)	Source
A	4340	1723	Oriani and Josephic (1974)
B	1/2NiCrMoV	1370	Ahmad et al (1975)
C	5CrVMo	1800	"
D	4130	1330	Nelson and Williams (1977)
E	4340	1350	Gerberich et al (1976)
F	H-11	1590	Sawicki (1971)
G	4340	-	Walter and Chandler (1973)
H	Inconel 718	-	"
I	4340	1250	Clark (1975)
J	Several steels	586-779	Loginow and Phelps (1975)
K	Several steels	869-1055	"

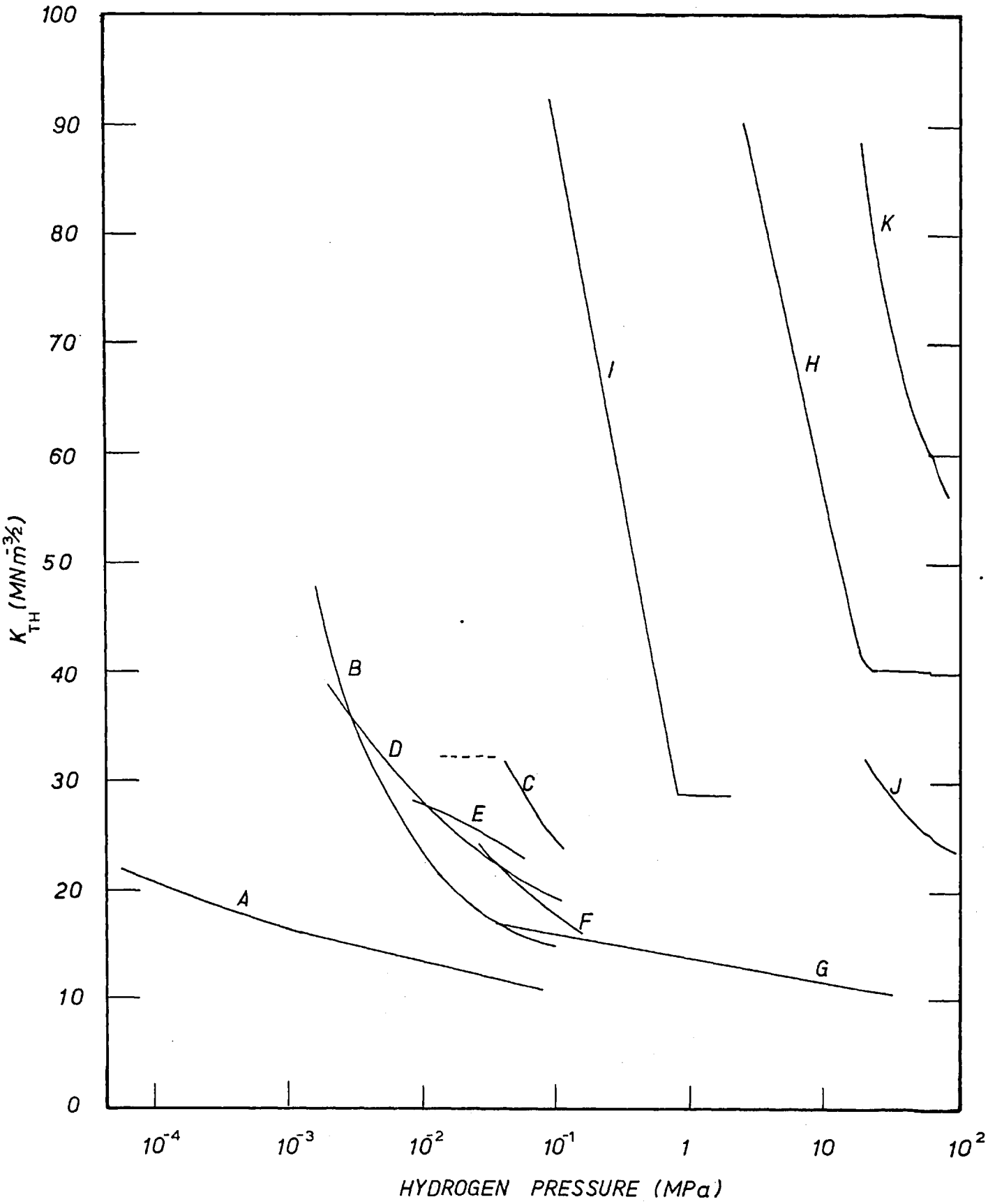


Fig.2.4 Effect of hydrogen pressure on K_{TH}. FROM AKHURST (1979)

(DETAILS ON PREVIOUS PAGE)

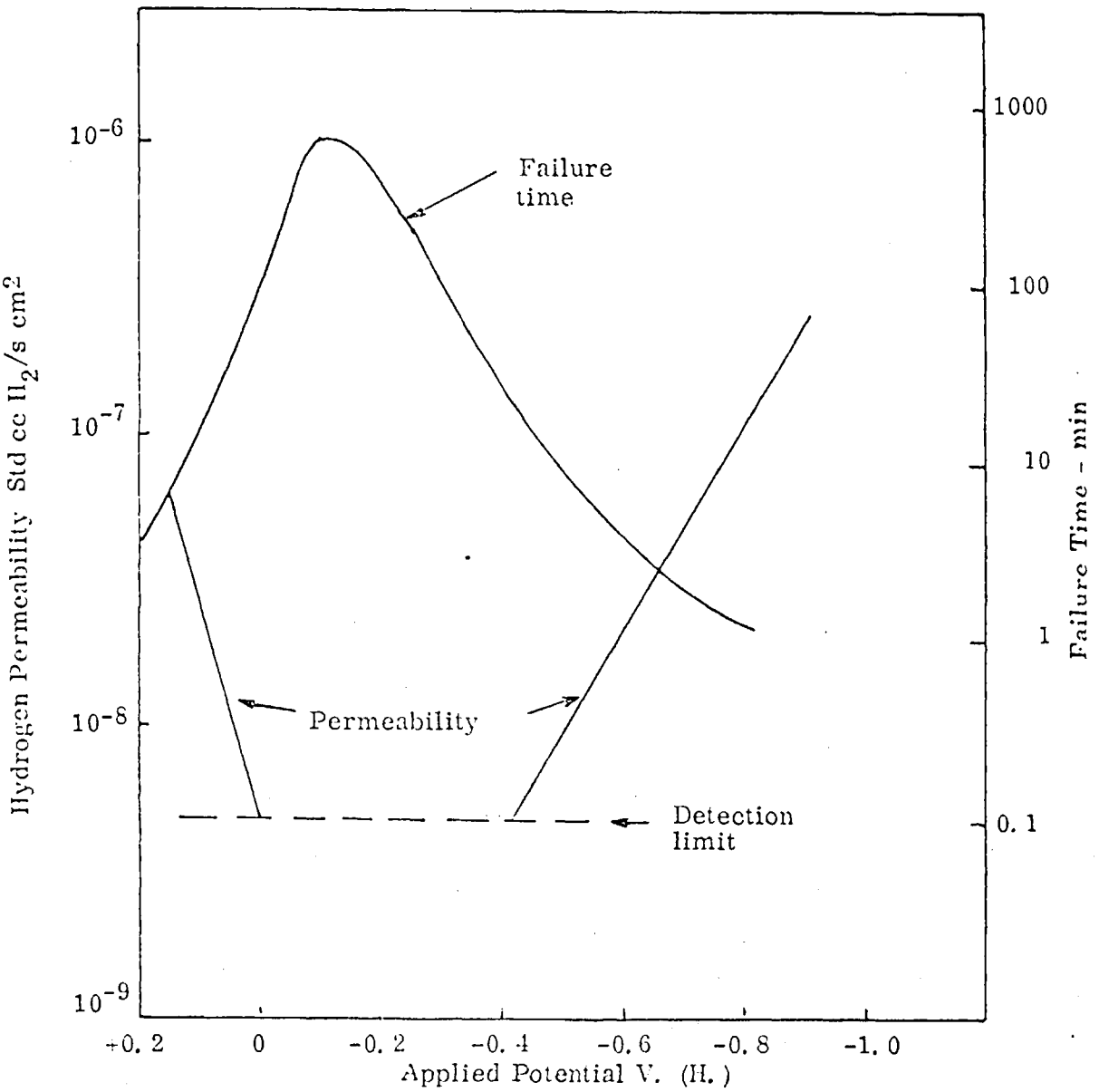


Fig.2·5 Relationship between hydrogen permeability and embrittlement susceptibility (BARTH et al, 1969)

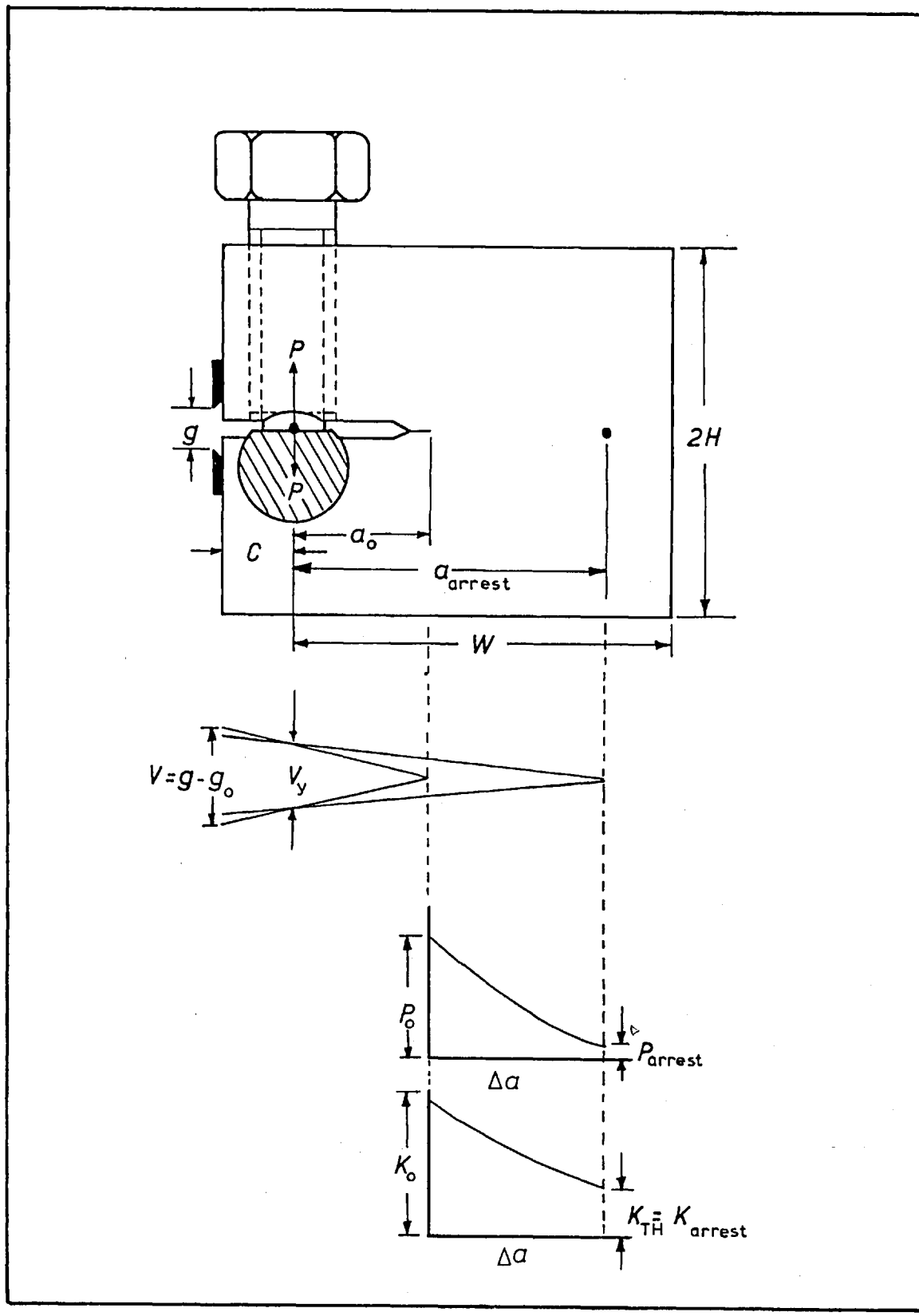


Fig. 4.1 Principle of the crack arrest technique using modified self loaded WOL specimen (DETAILS ON NEXT PAGE)

V = Mouth opening displacement (MOD)

V_y = Loading point displacement

P = Load

P_o, K_o = Initial values of load and stress intensity

$$V_y = V\left(\frac{a}{a+C}\right)$$

DETAILS OF FIGURE 4.1 OF THE PREVIOUS PAGE

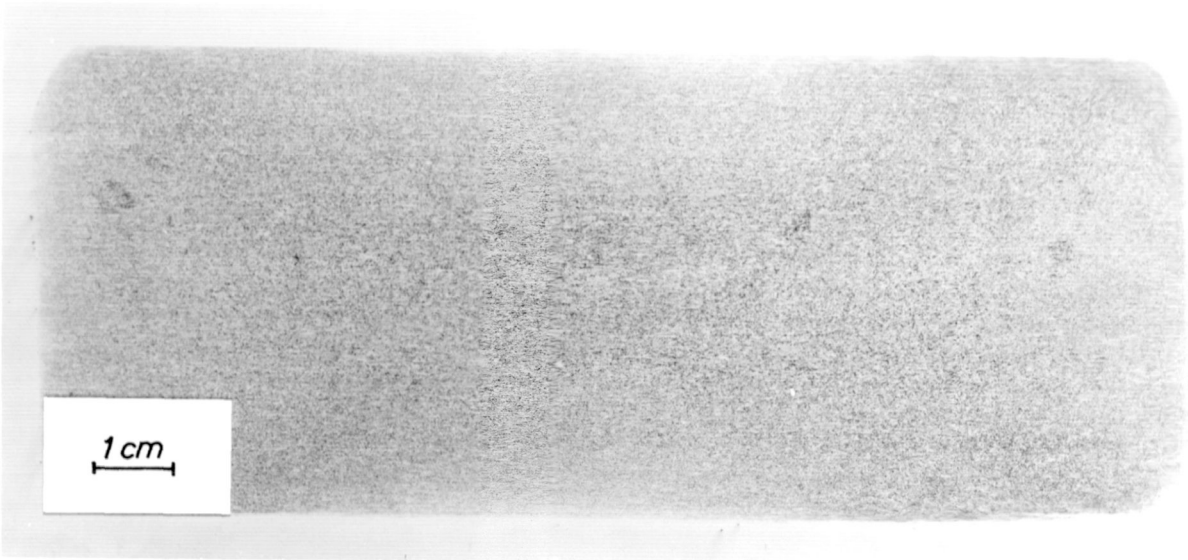


Fig. 4.2 Sulphur print of a transverse section of En 16.

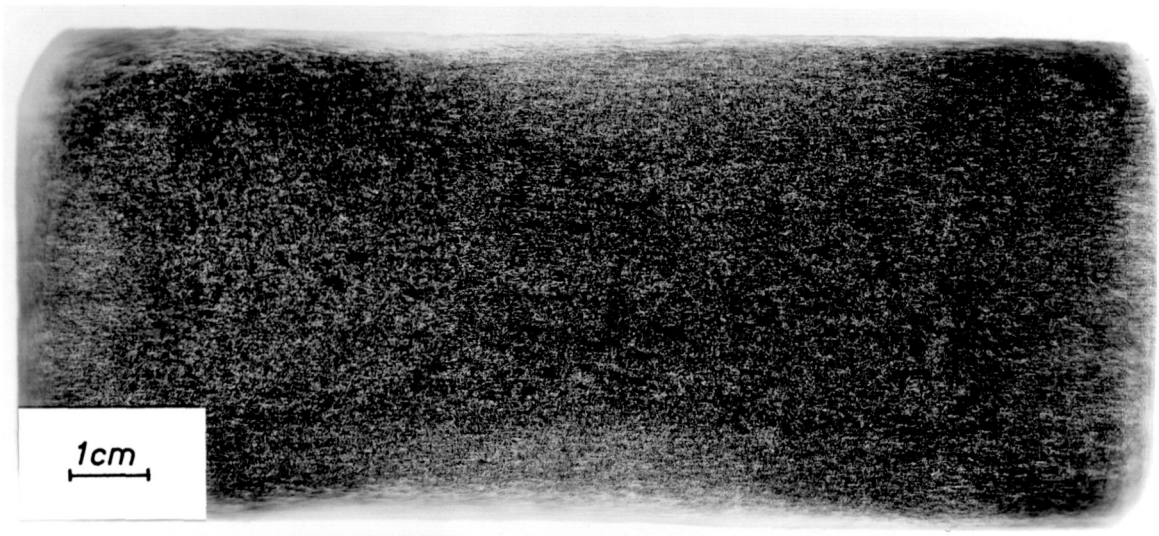


Fig. 4.3 Sulphur print of a transverse section of En 16M.



Fig. 4.4a MnS inclusions in En16. Plane of view T.



Fig. 4.4b MnS inclusions in En16. Plane of view L.



Fig.4.5a MnS inclusions in En16M. Plane of view T.



Fig.4.5b MnS inclusions in En16M. Plane of view L.

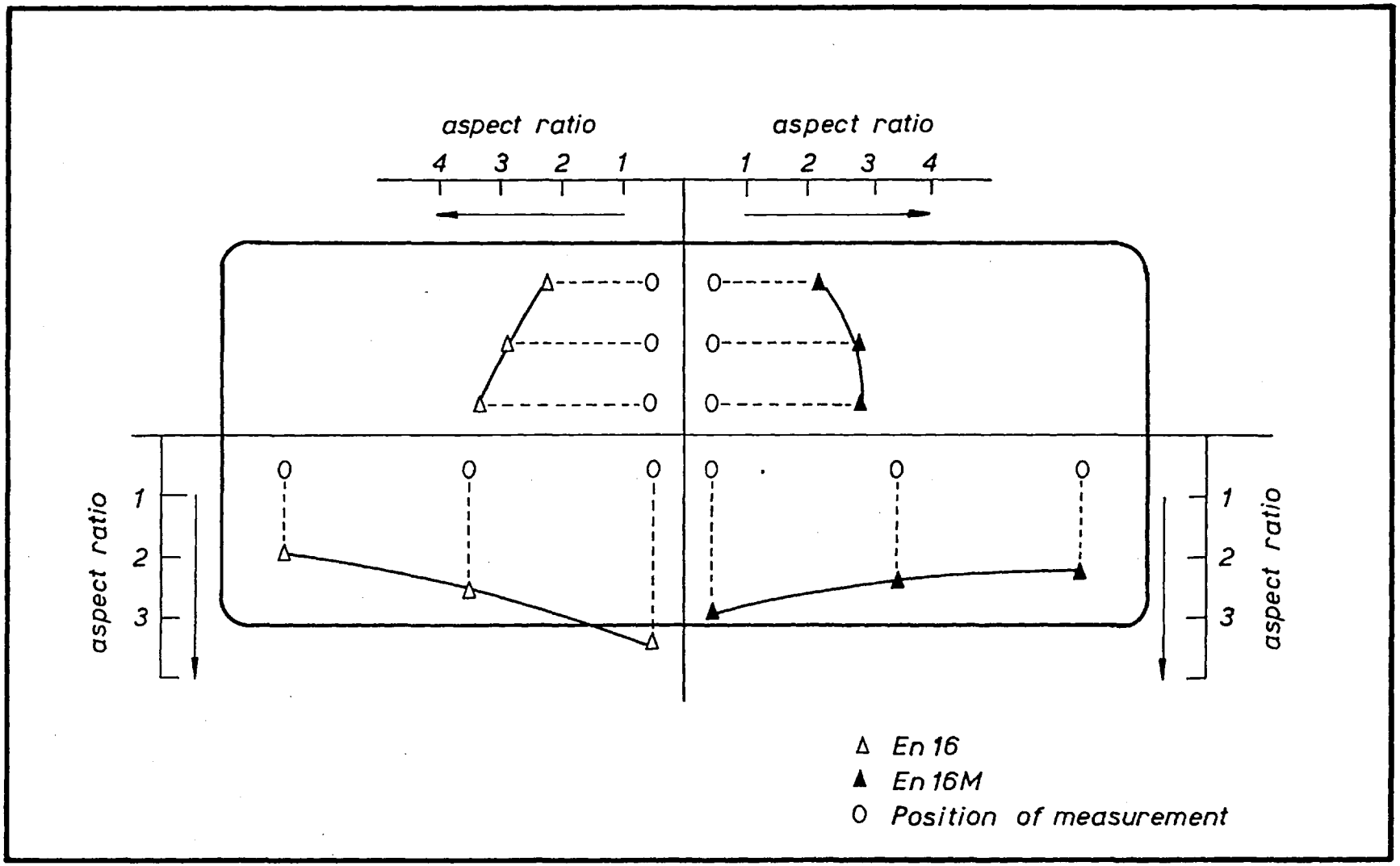


Fig. 4.6 Variation in lateral spread of MnS inclusions across the width and thickness of the billet.

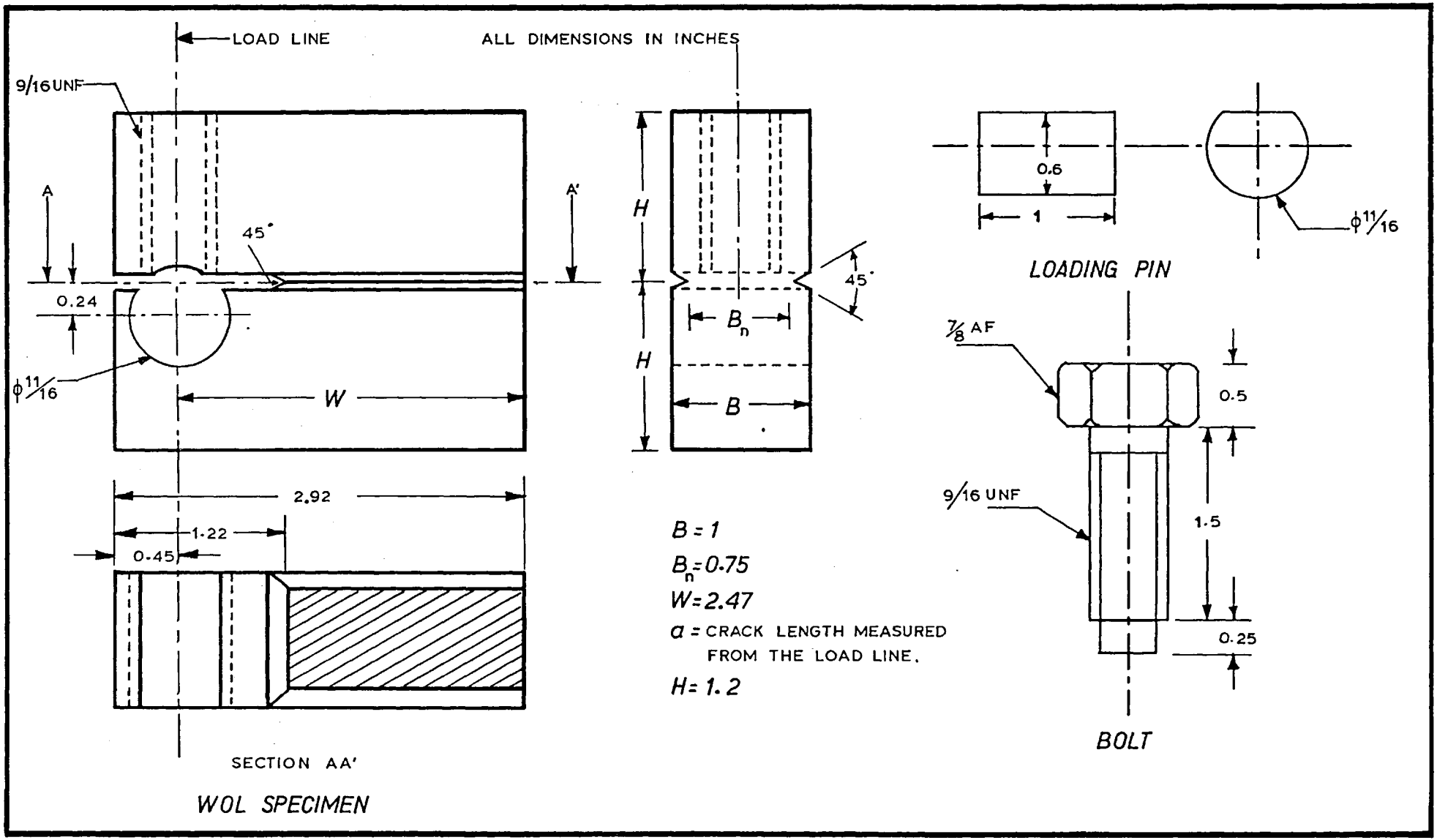


Fig. 4.7 WOL Specimen, Bolt and Loading Pin.

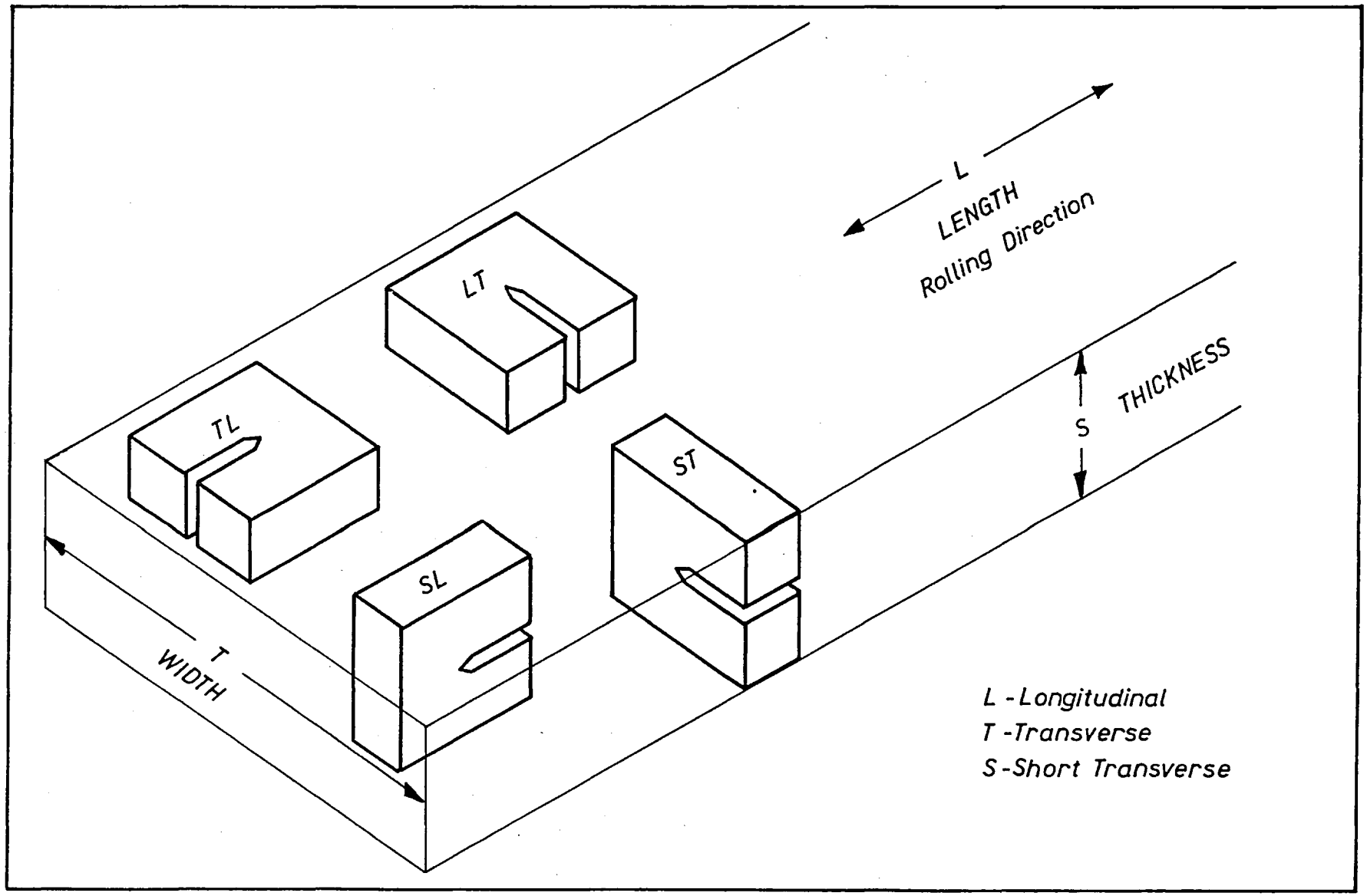


Fig. 4.8 Crack Plane Orientation Identification.

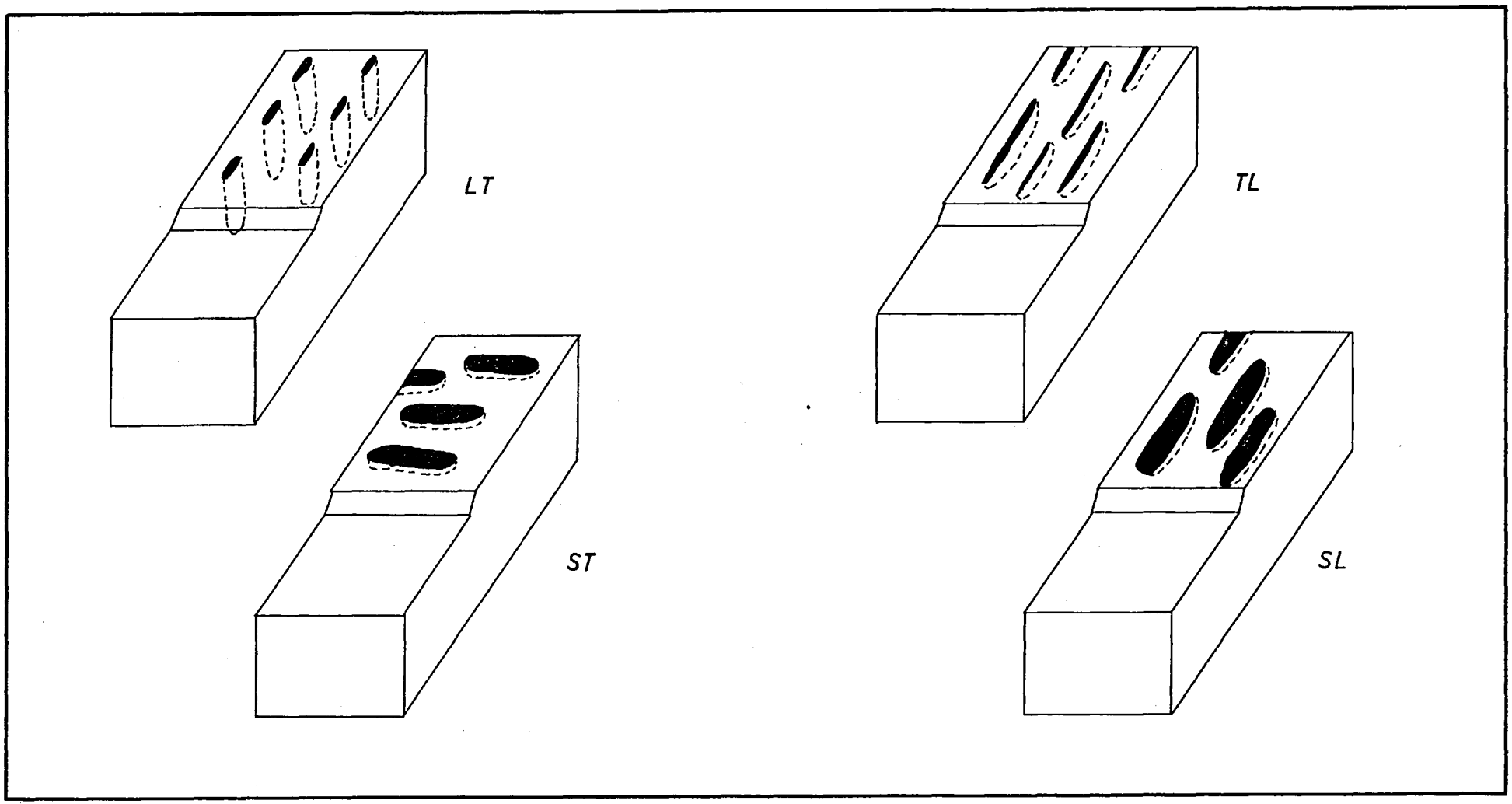


Fig. 4.9 Inclusion orientation in relation to the specimen orientation.

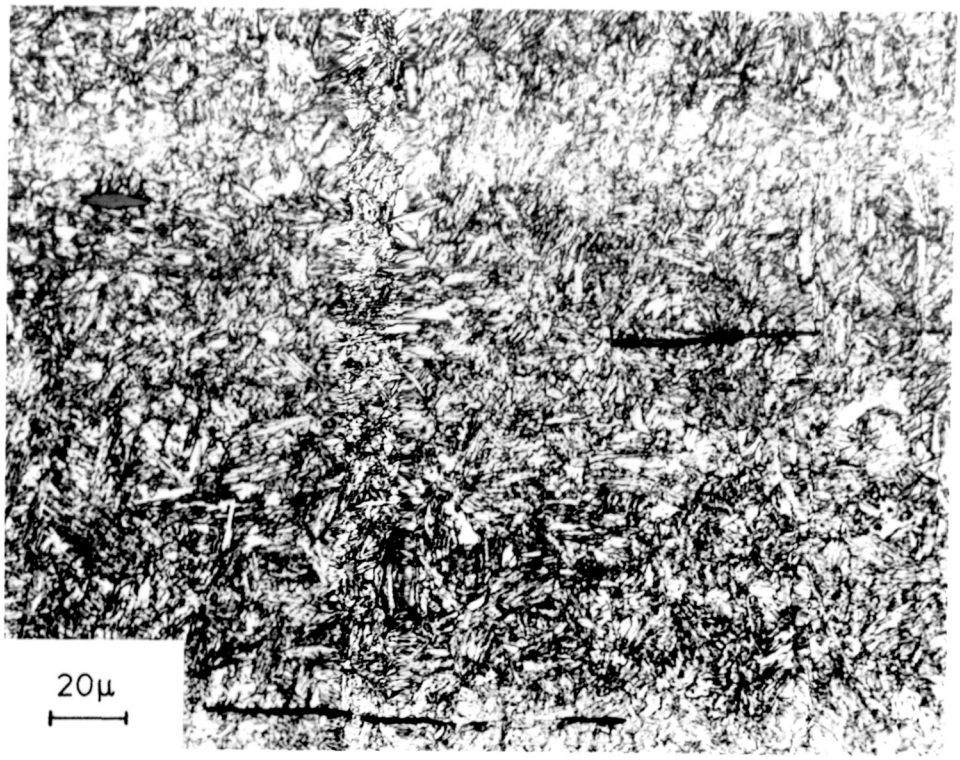


Fig. 4.10 Microstructure of En 16 at the mid-section after quenching in normal oil and tempering at 400°C

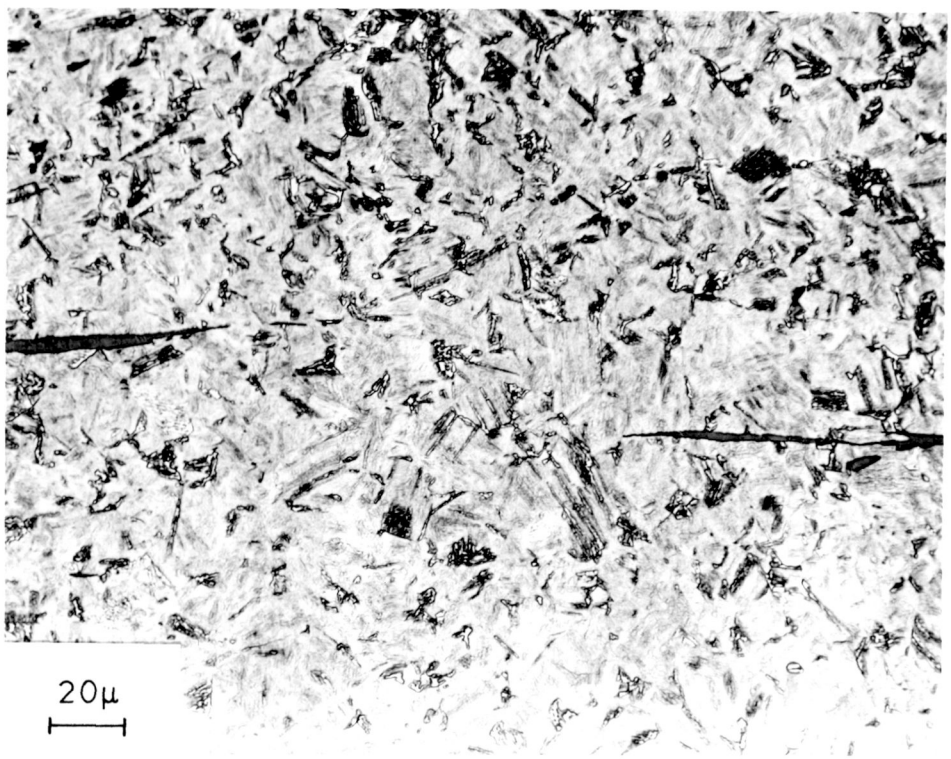


Fig. 4.11 Microstructure of En16M at the mid-section after quenching in fast oil and tempering at 300°C

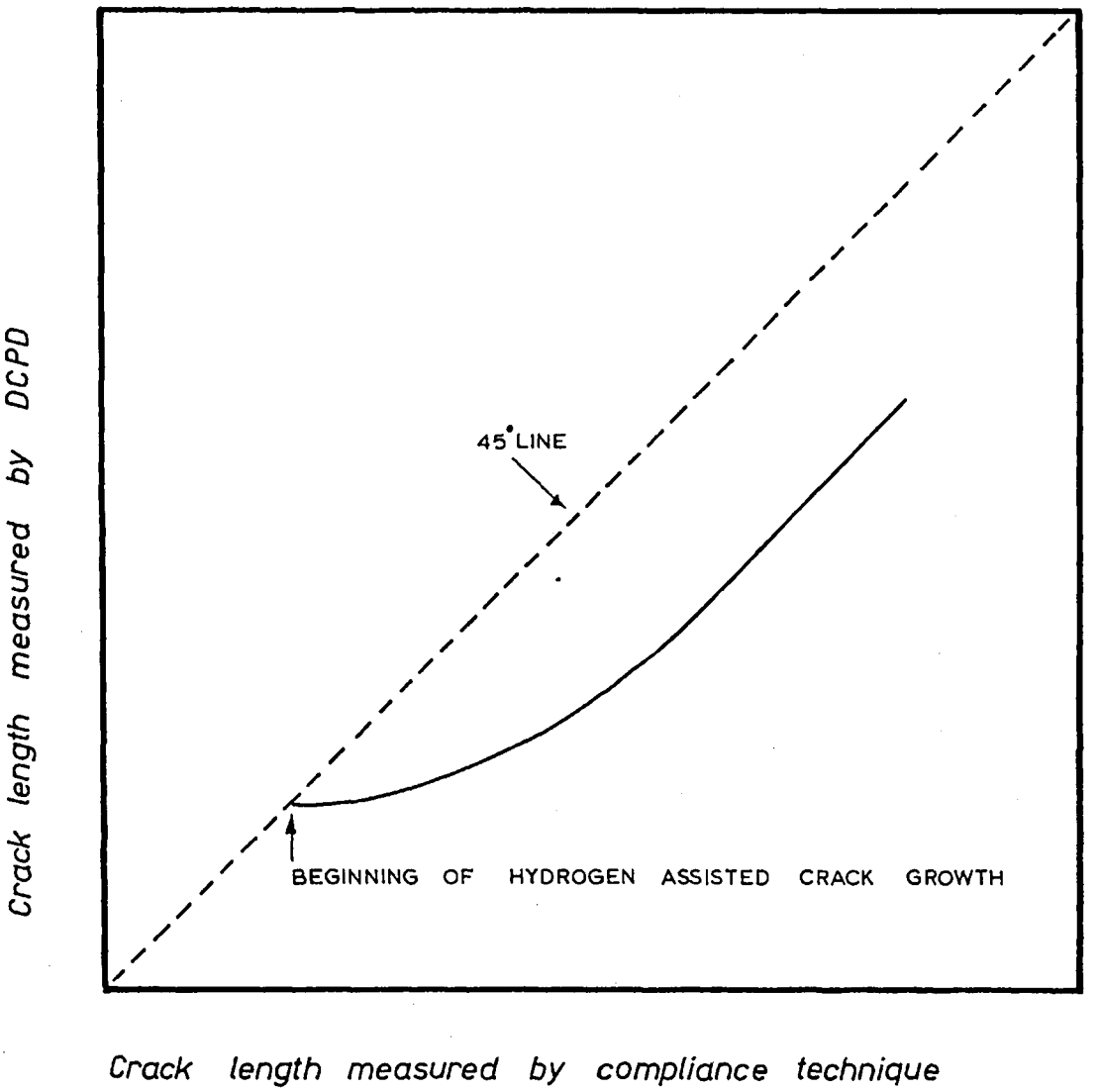


Fig. 4·12 Comparison of crack lengths measured by DCPD and compliance technique for a CKS specimen under constant load

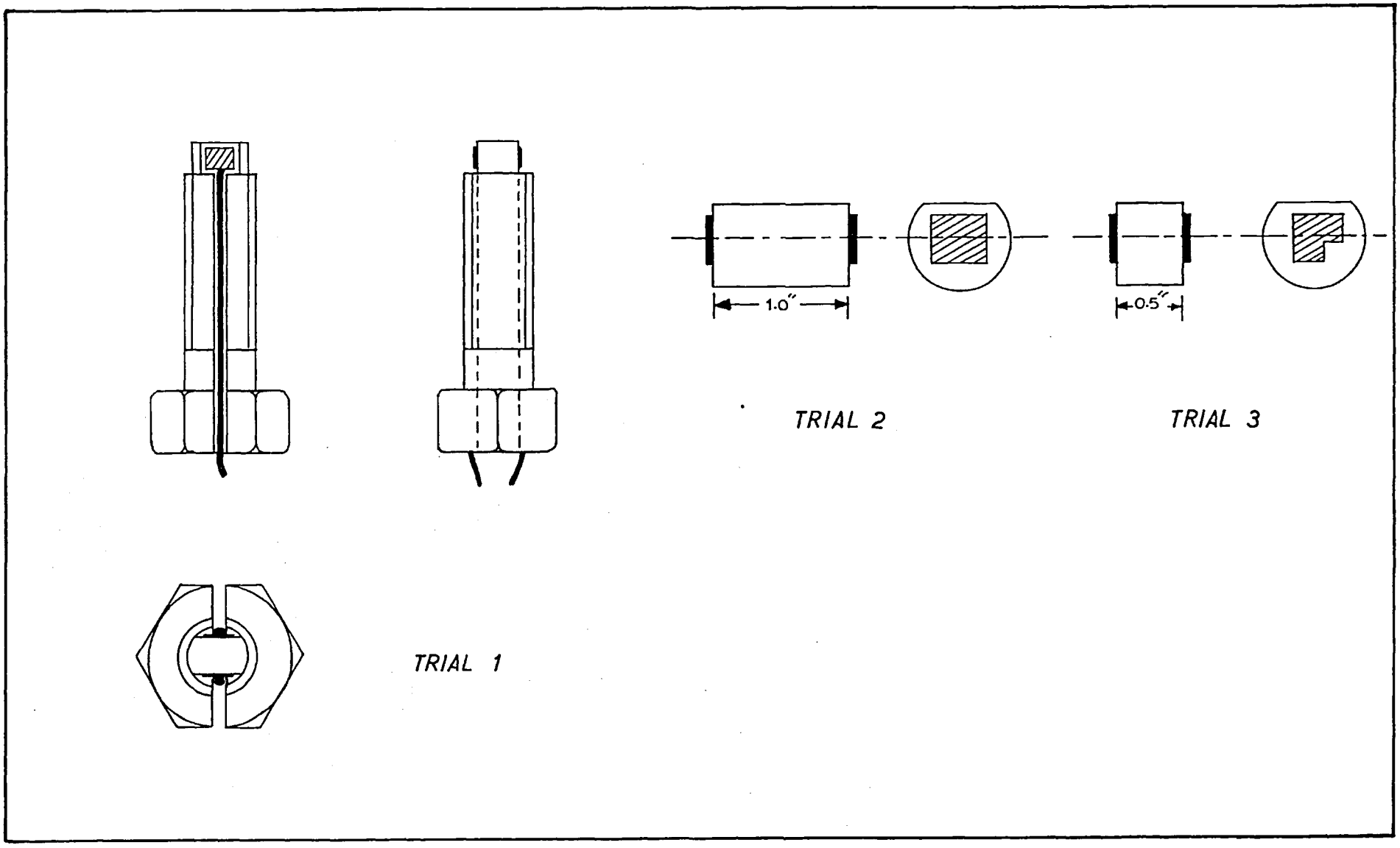


Fig. 4.13 Strain gauge locations evaluated for monitoring load.

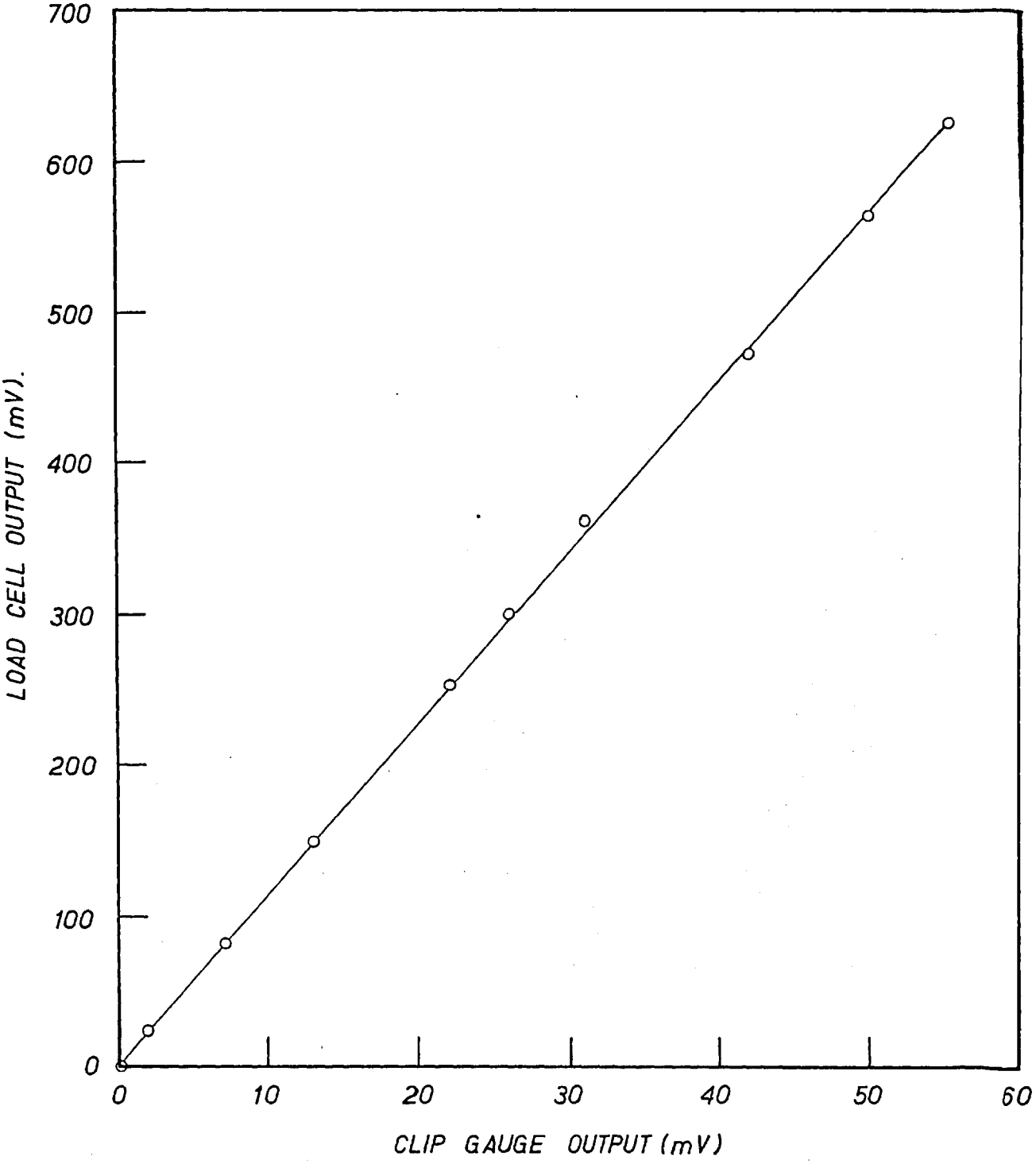


Fig.4.14 Variation of load cell output with clip gauge output.

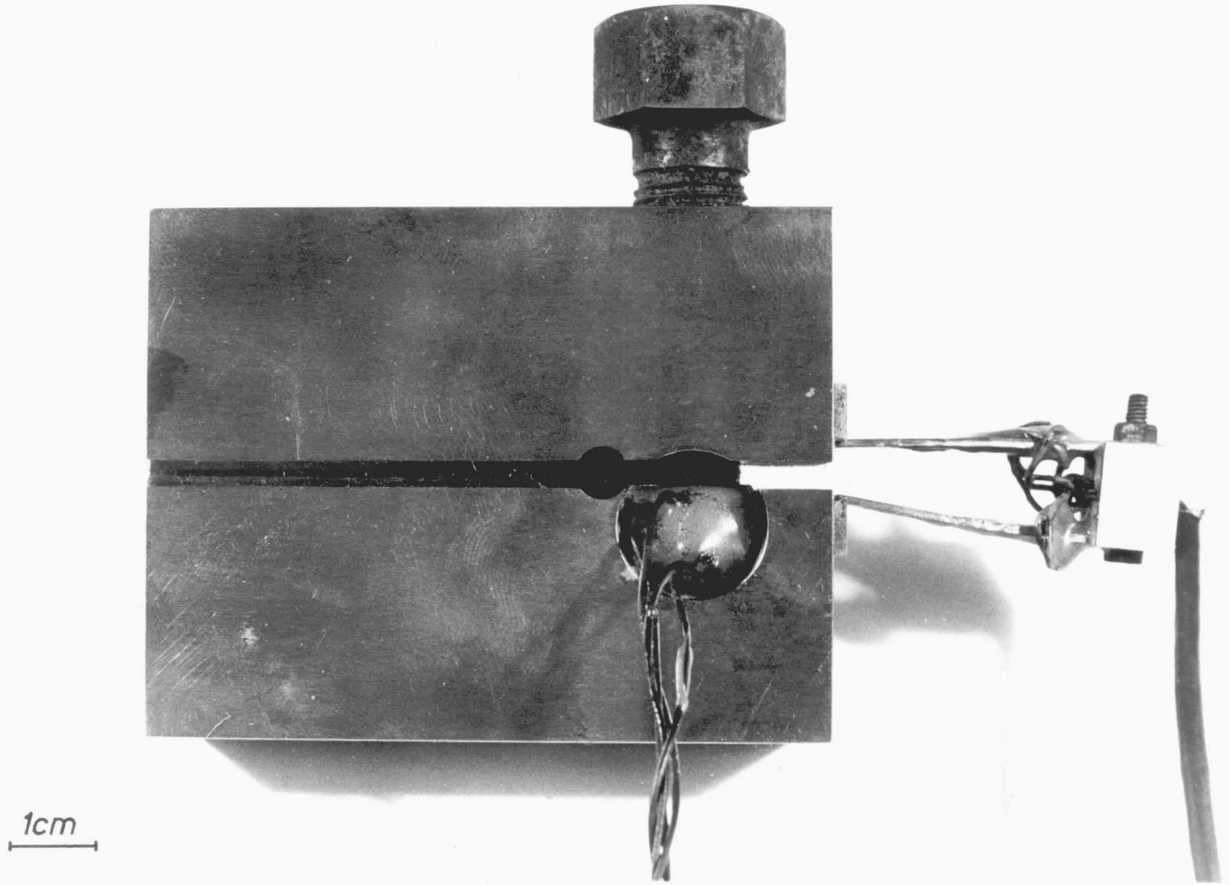


Fig. 4.15 WOL specimen with load cell and clip gauge.

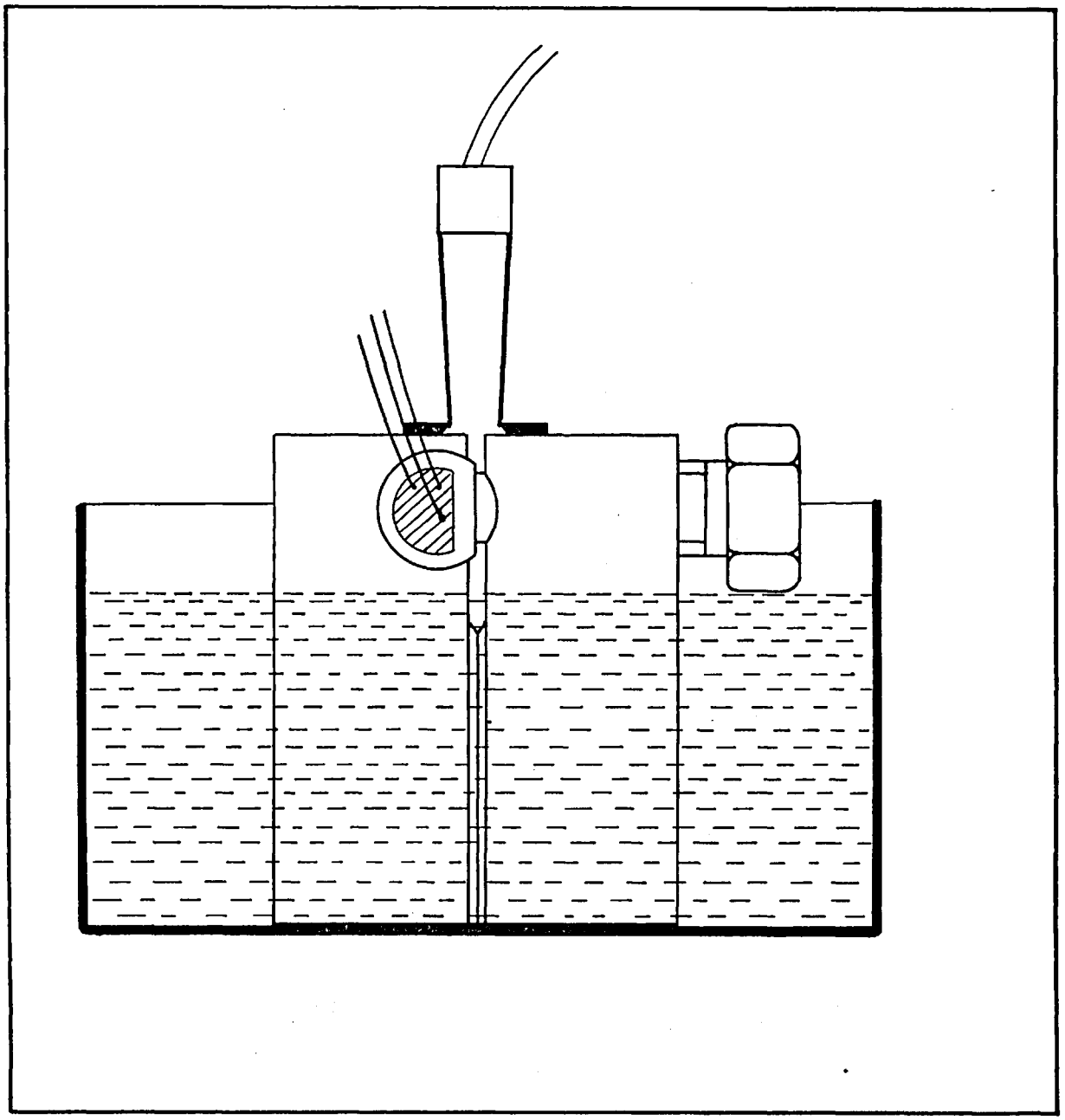


Fig. 4.16 Testing in 3.5% NaCl solution.

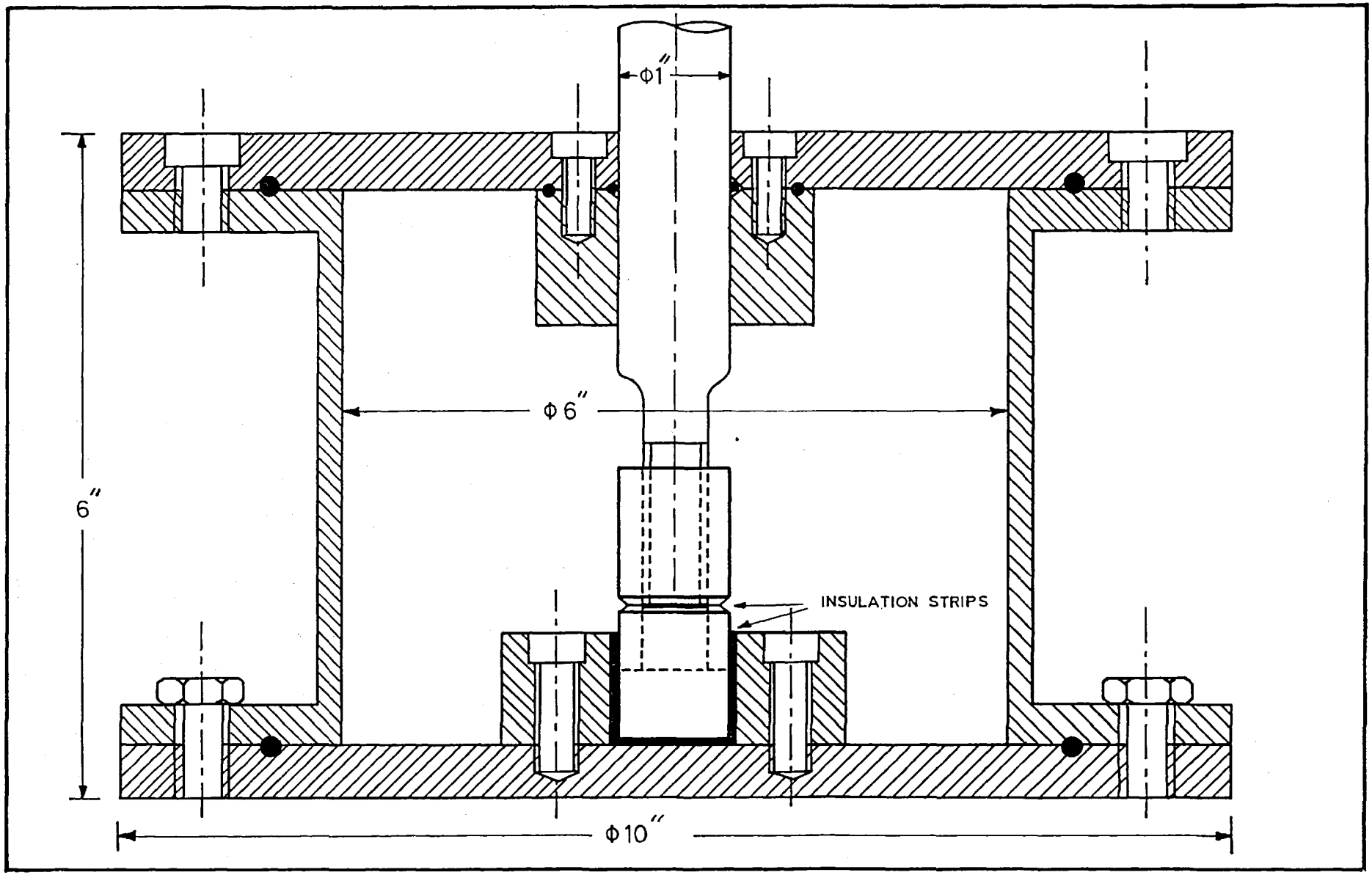


Fig 4.17 Sectional view of the chamber used for testing in H_2S gas

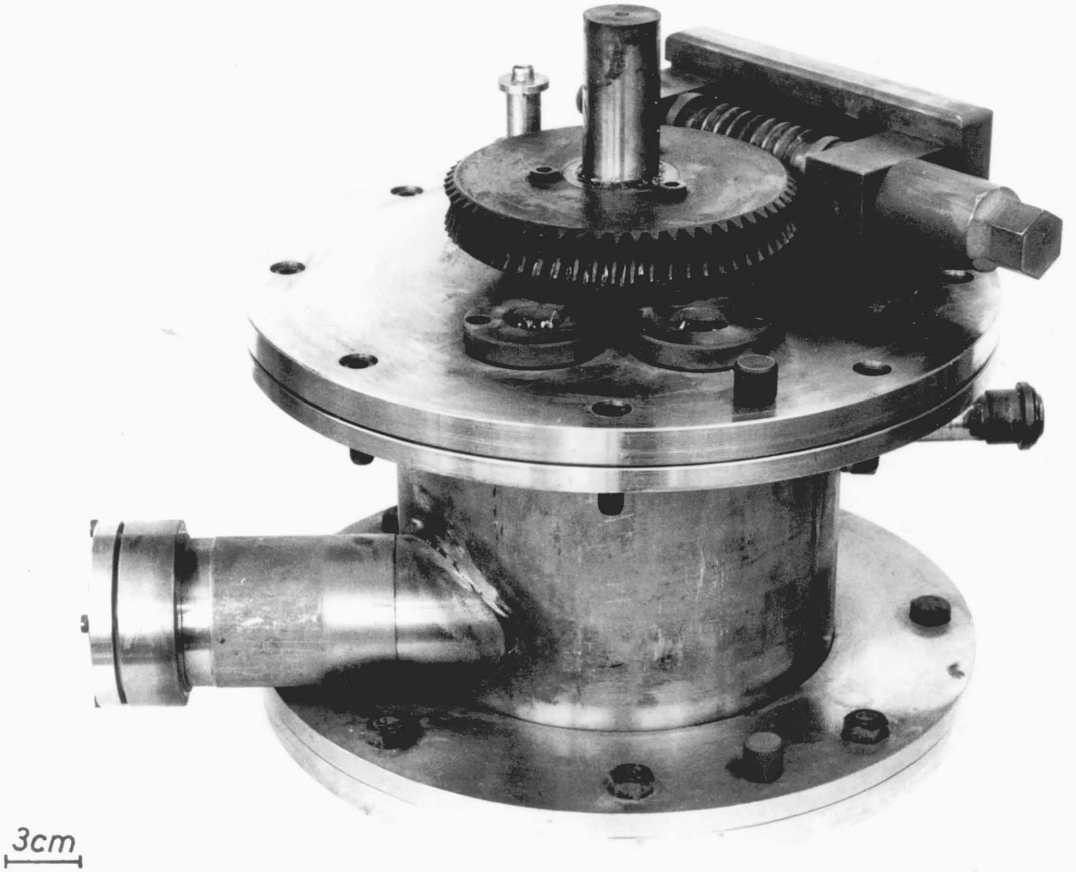


Fig. 4.18 Chamber employed for testing in hydrogen sulphide gas.

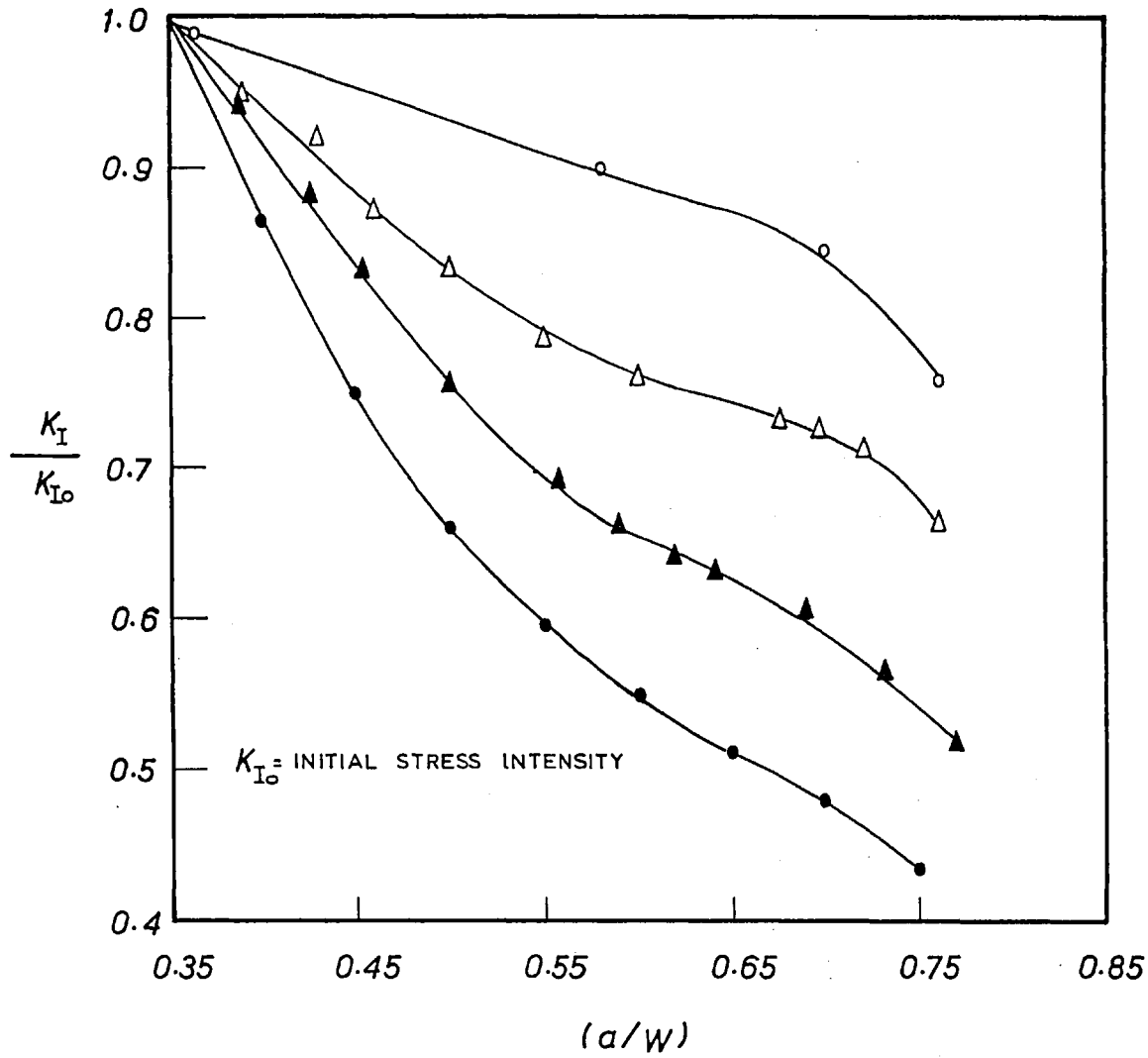


Fig. 4·19 Variation of 'K' with crack growth under different testing conditions

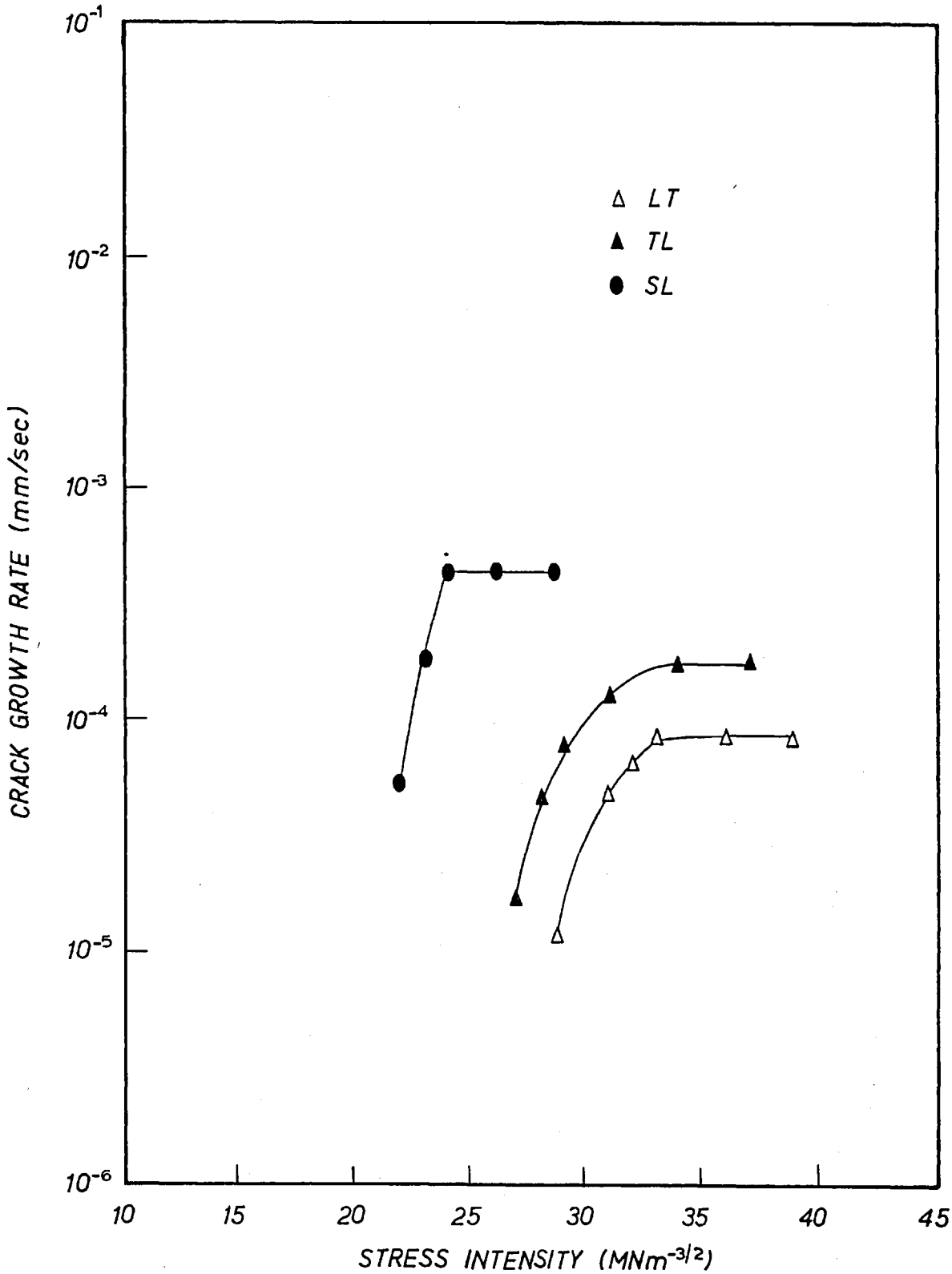


Fig 5·1 Crack growth behaviour of En16 at a yield strength of 1250MPa in 3·5% NaCl solution

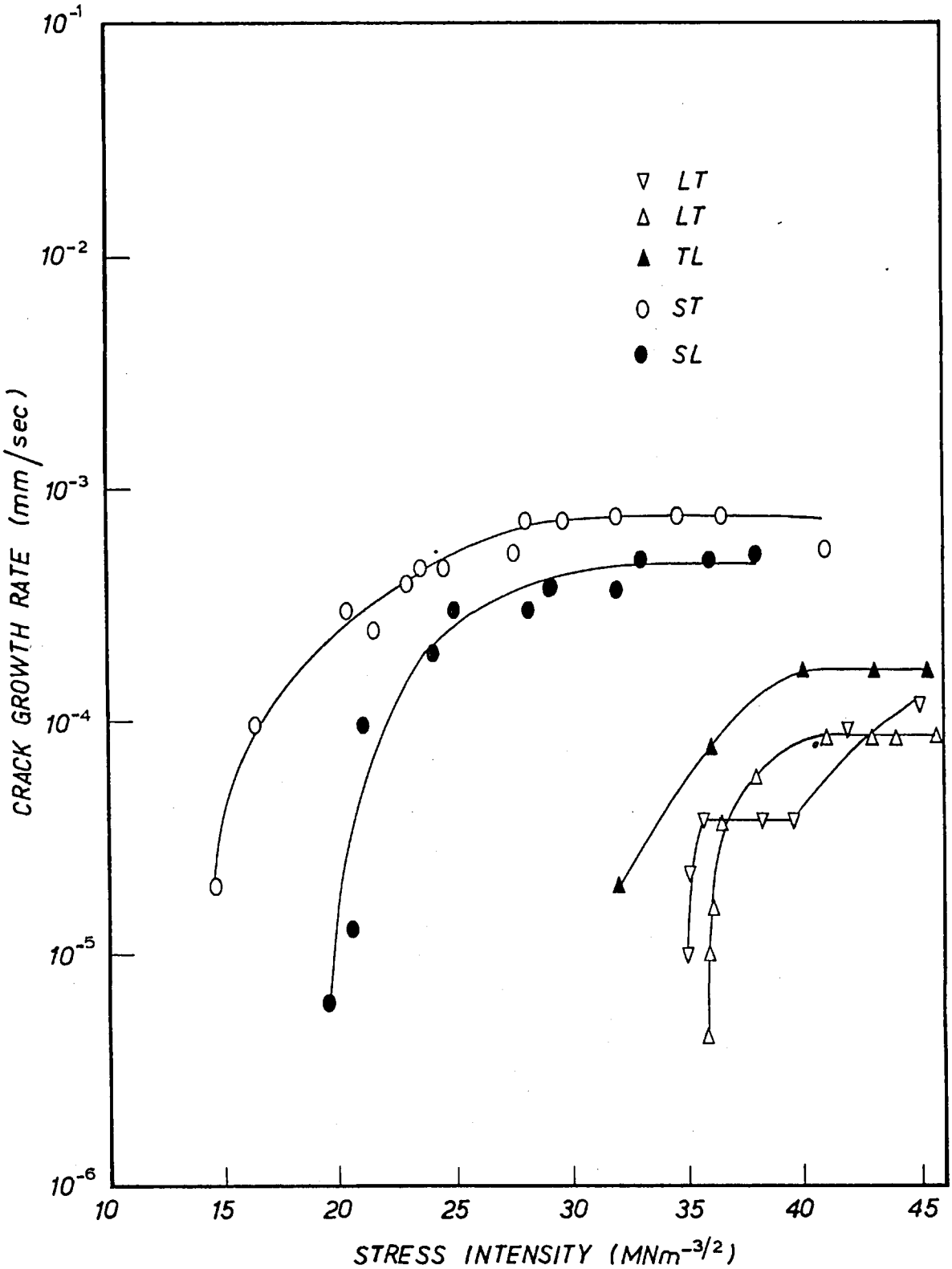


Fig 5·2 Crack growth behaviour of En 16M at a yield strength of 1300MPa in 3·5% NaCl solution

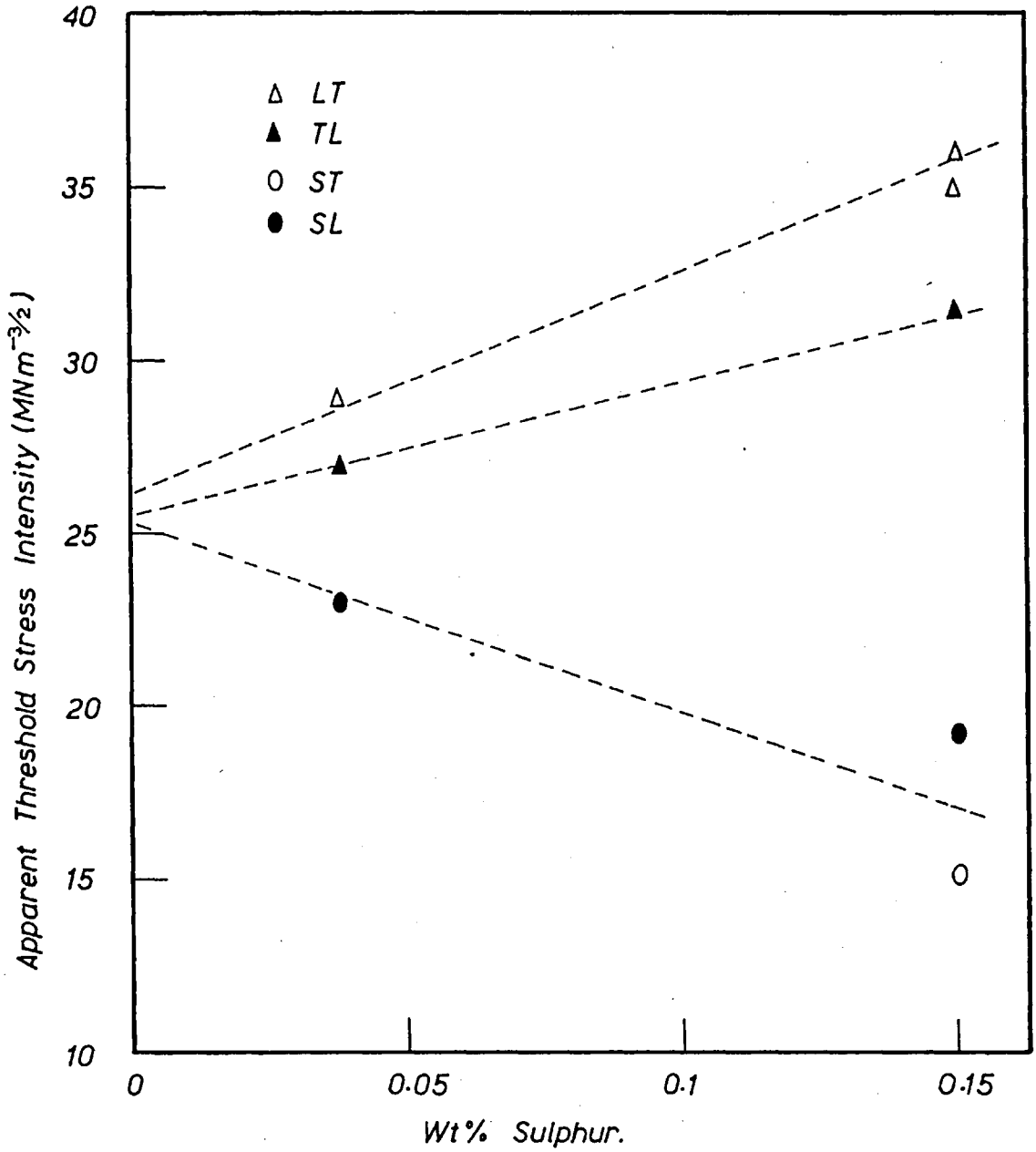


Fig. 5·3 Effect of inclusion volume fraction on K_{TH} in 3·5% NaCl solution (σ_{ys} = 1250 - 1300 MPa)

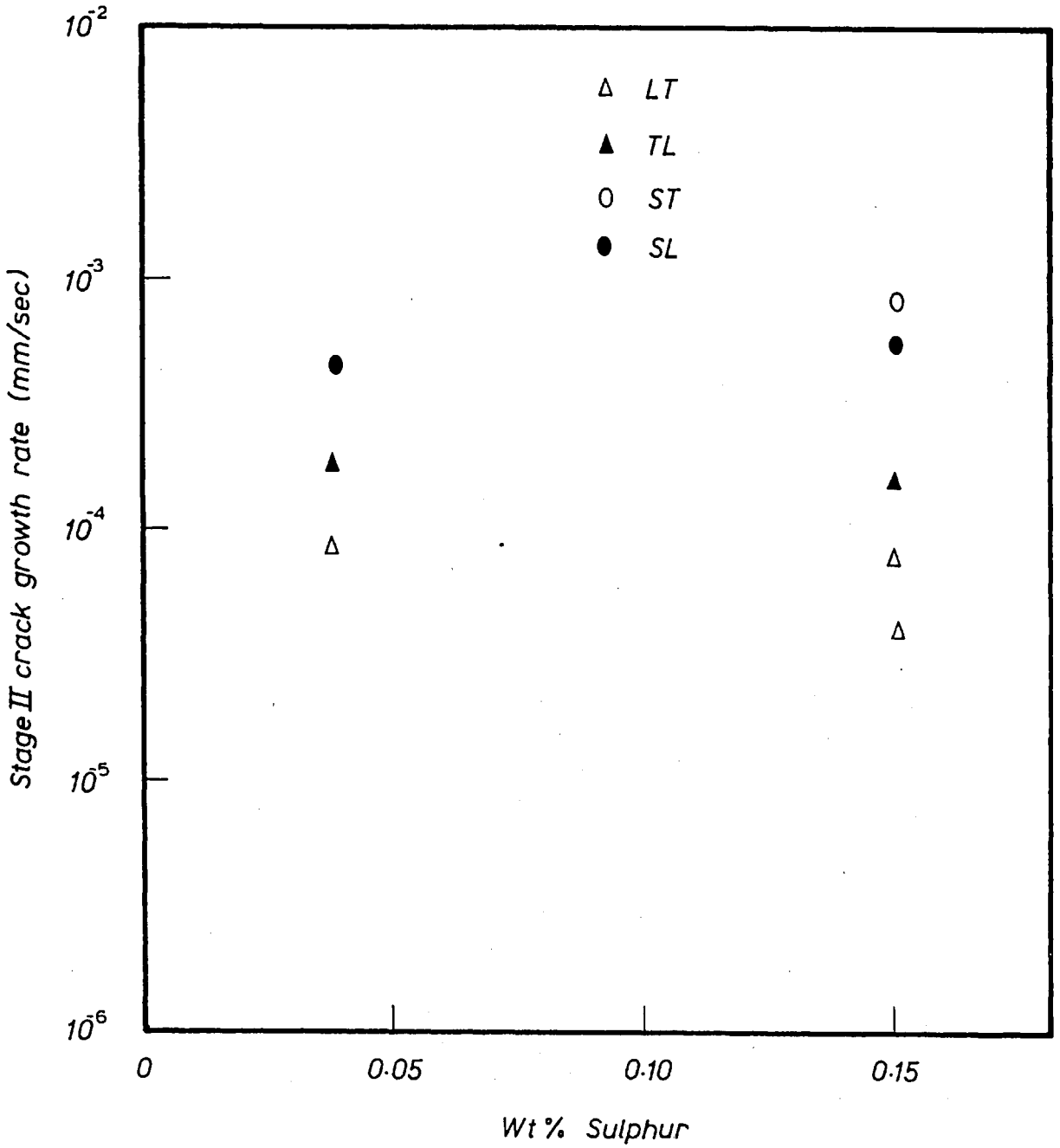


Fig 5·4 Effect of inclusion volume fraction on stage II crack growth rate in 3·5% NaCl solution (σ_{ys} = 1250 - 1300 MPa)

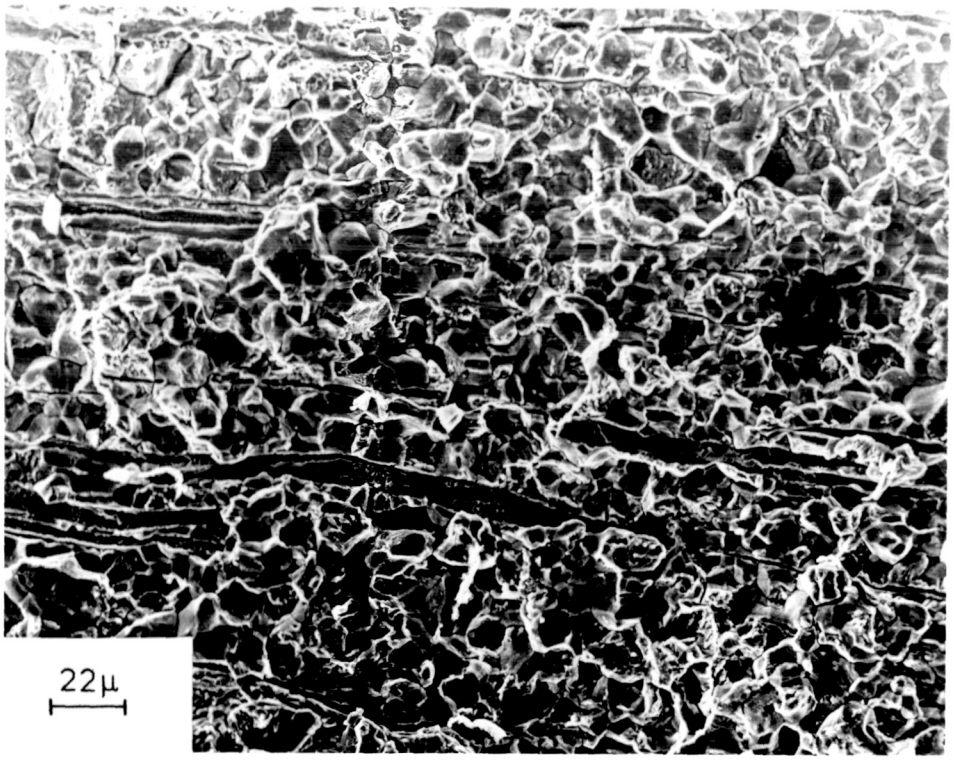


Fig. 5.5 *Fracture surface of En16M tested in 3.5% NaCl solution. Orientation ST.* σ_{ys} *= 1300MPa.* $K \simeq 17 MNm^{-3/2}$

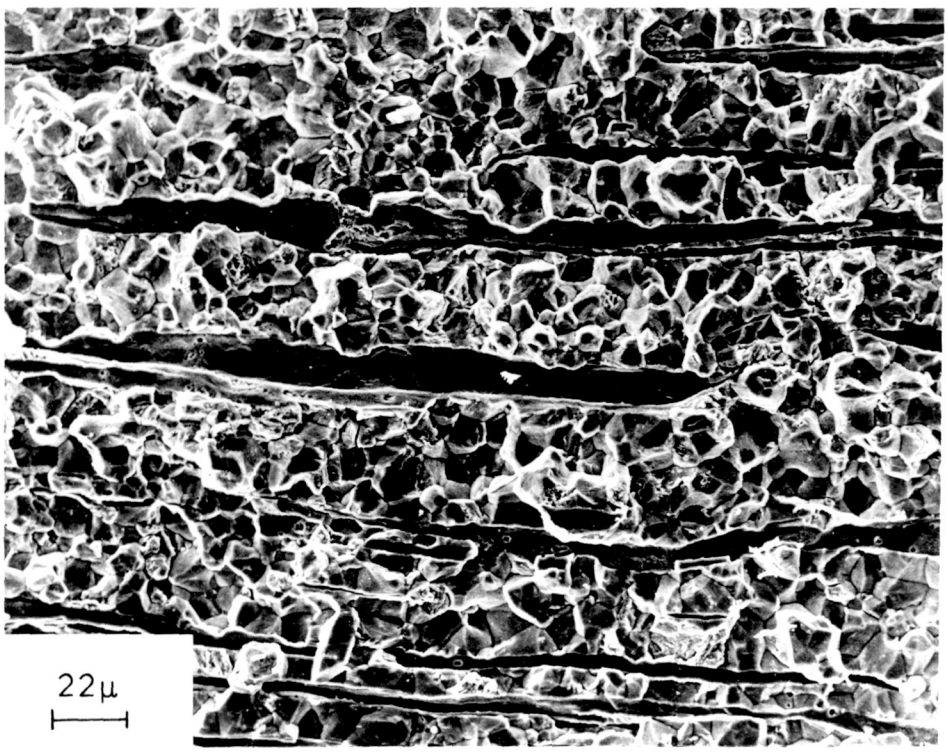


Fig. 5.6 *Fracture surface of En16M tested in 3.5% NaCl solution. Orientation ST.* σ_{ys} *=1300MPa.* $K \simeq 28 MNm^{-3/2}$

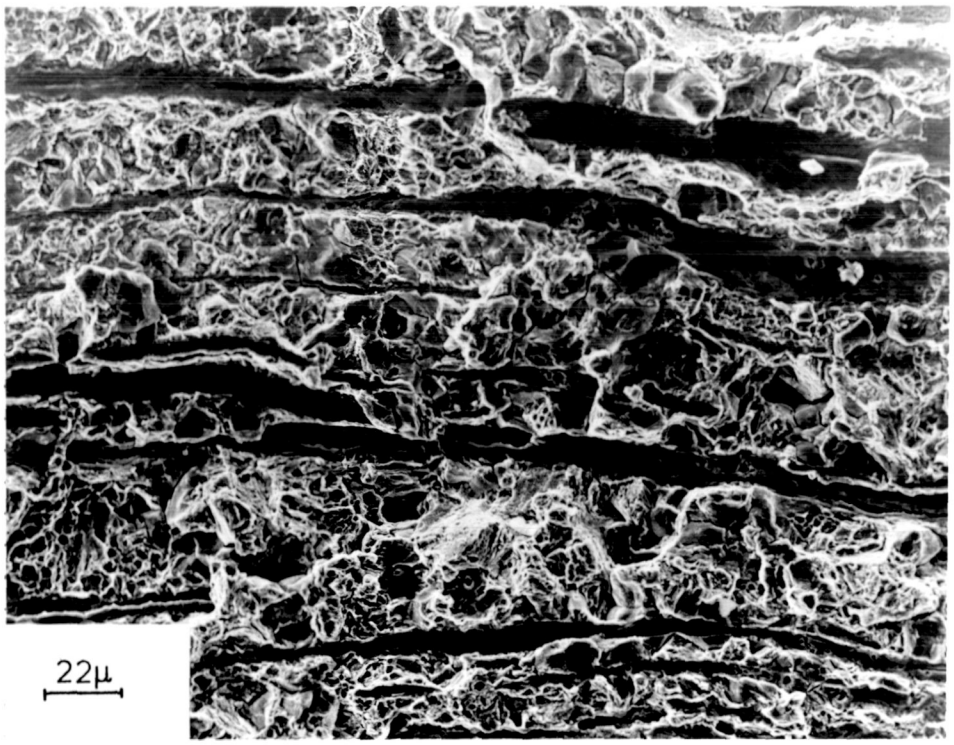


Fig. 5·7 Fracture surface of En16M tested in 3·5% NaCl solution. Orientation ST. σ_{ys} = 1300MPa. $K \simeq 35 MNm^{-3/2}$.

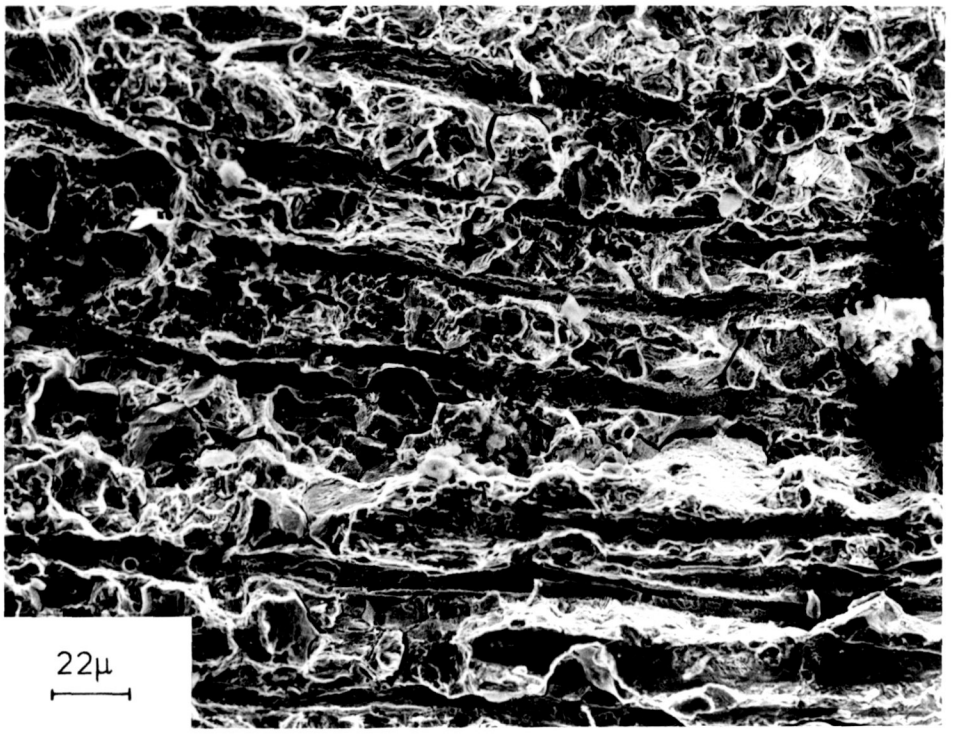


Fig. 5·8 Fracture surface of En16M tested in 3·5% NaCl solution. Orientation SL. σ_{ys} = 1300MPa. $K \simeq 35 MNm^{-3/2}$.

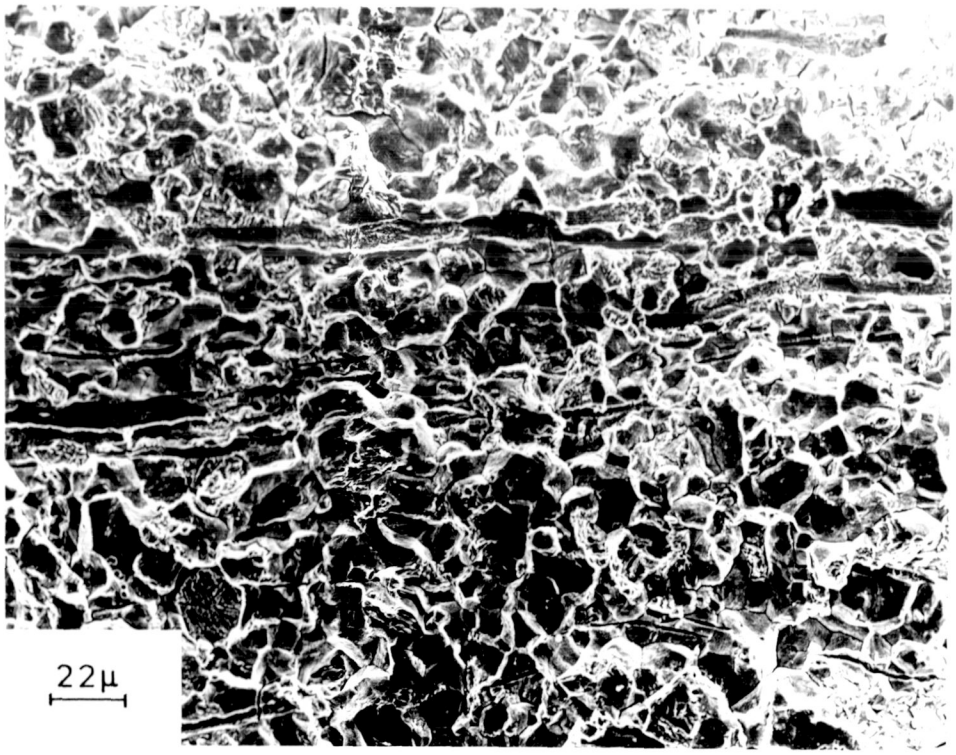


Fig. 5.9 Fracture surface of En16M tested in 3.5% NaCl solution. Orientation SL. σ_{ys}=1300MPa. K ≃ 20MNm$^{-3/2}$.

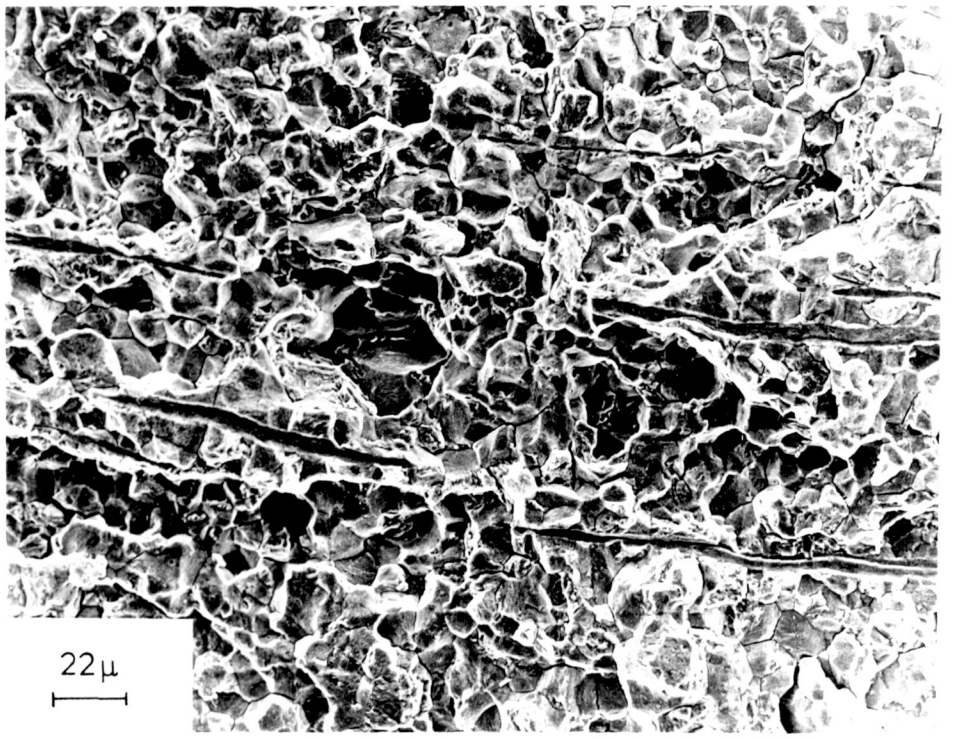


Fig. 5.10 Fracture surface of En16 tested in 3.5% NaCl solution. Orientation SL. σ_{ys} = 1250 MPa. K ≃ 22 MNm$^{-3/2}$.



Fig. 5·11 *Nickel plated section of the fracture surface of En16M tested in 3·5% NaCl solution showing inclusion assisted intergranular cracking. Plane of view L. Orientation ST.* $\sigma_{ys} = 1300MPa$.

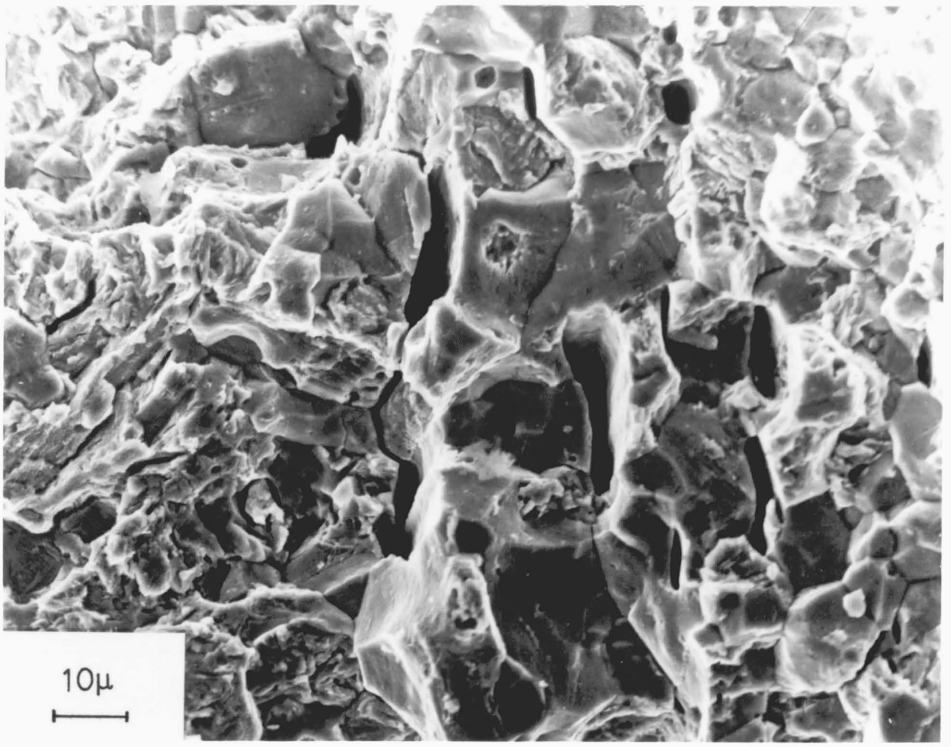


Fig. 5.12 *Fracture surface of En16M tested in 3.5% NaCl solution. Orientation LT. σ_{ys} = 1300MPa. K ≃ 45MNm$^{-3/2}$.*

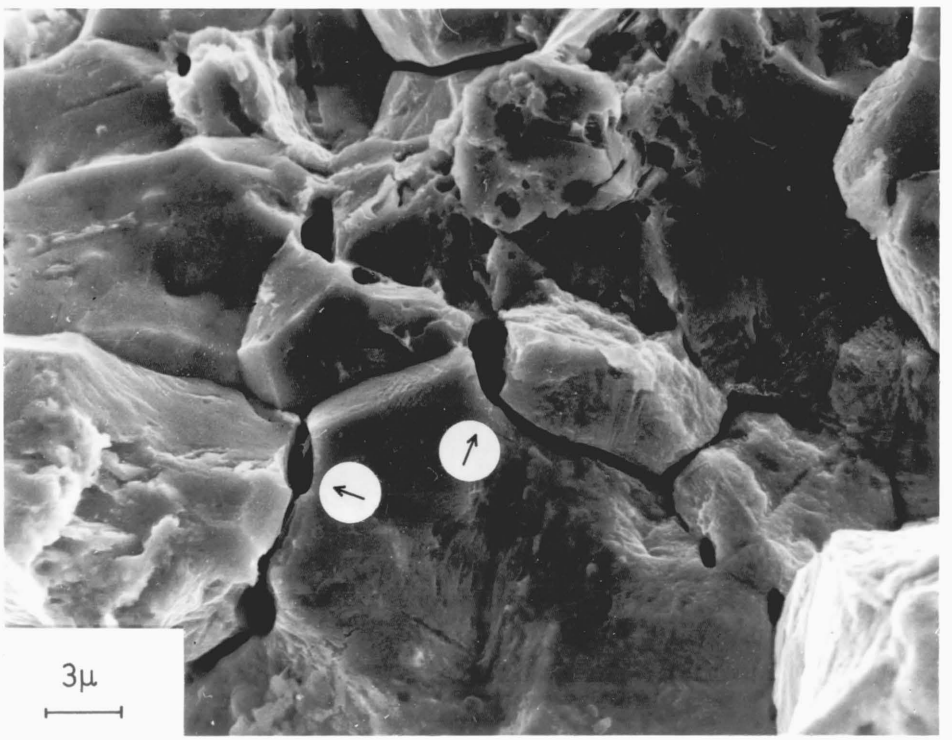


Fig. 5.13 *Fracture surface of En16M tested in 3.5% NaCl solution. Orientation LT. σ_{ys} = 1300MPa. K ≃ 35MNm$^{-3/2}$. The holes(arrowed) represent the position of MnS inclusions.*



Fig. 5.14 Nickel plated section of the fracture surface showing cracking along inclusions in En16M tested in 3.5% NaCl solution. Plane of view T. Orientation LT. σ_{ys} = 1300MPa.

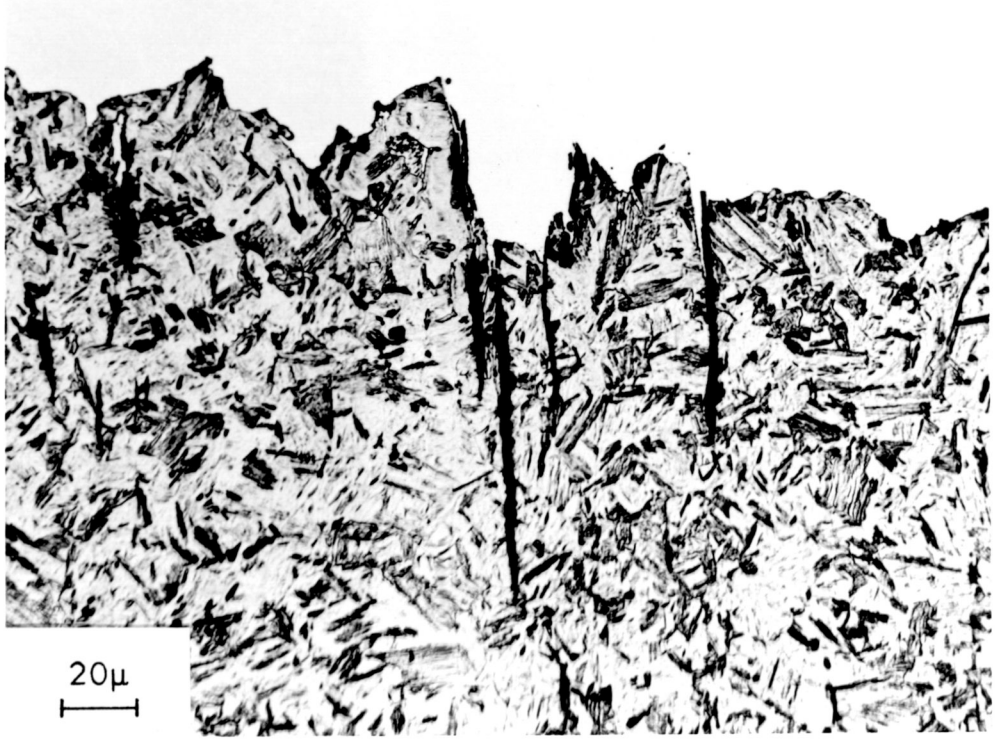


Fig. 5.15 Nickel plated section of the fracture surface showing opening of the inclusion matrix interface and the retention of MnS inclusions exposed to the environment. All other details same as in the previous figure.

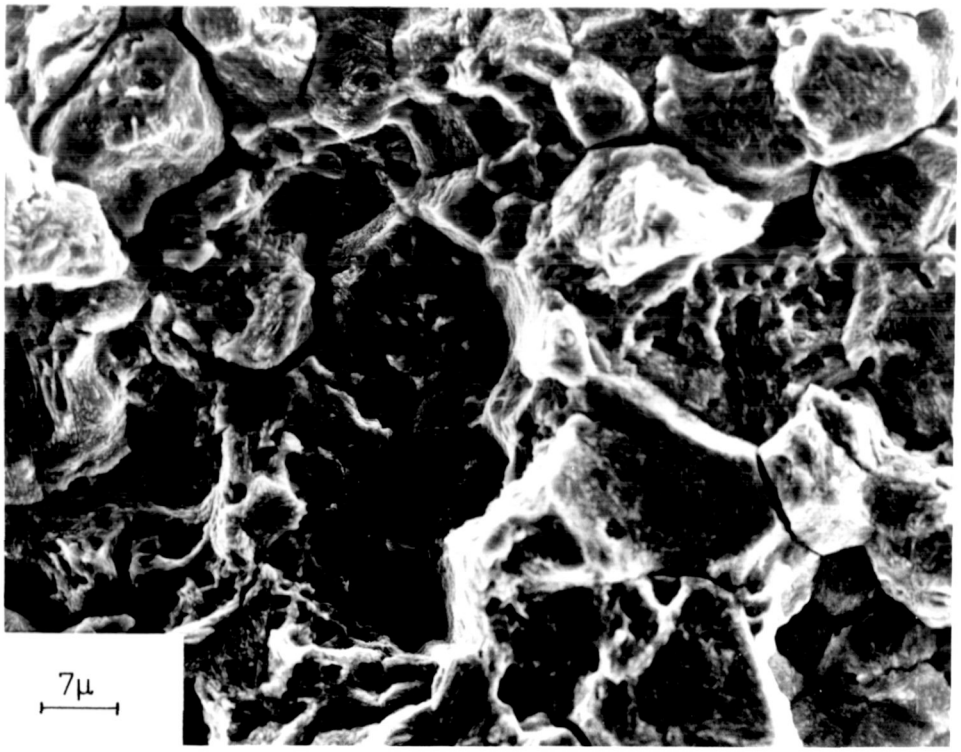


Fig. 5.16 Fracture surface of En16 tested in 3.5% NaCl solution. Orientation LT. σ_{ys} *= 1250MPa.* $K \approx 32 MNm^{-3/2}$.

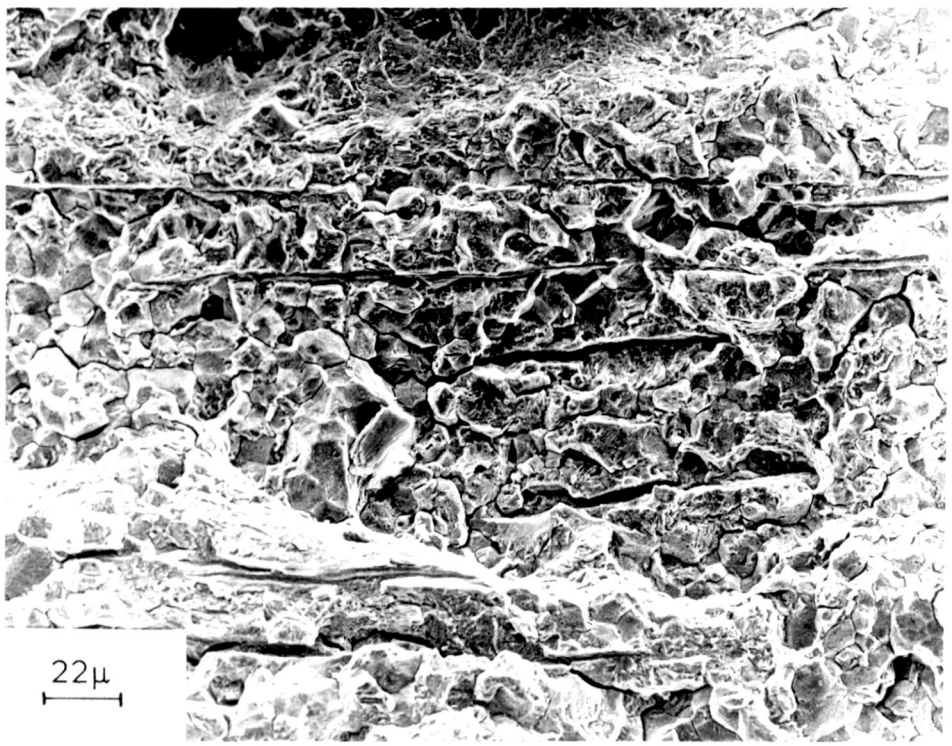


Fig. 5.17 Fracture surface of En16 tested in 3.5% NaCl solution. Orientation TL. σ_{ys} *= 1250MPa.* $K \approx 33 MNm^{-3/2}$.

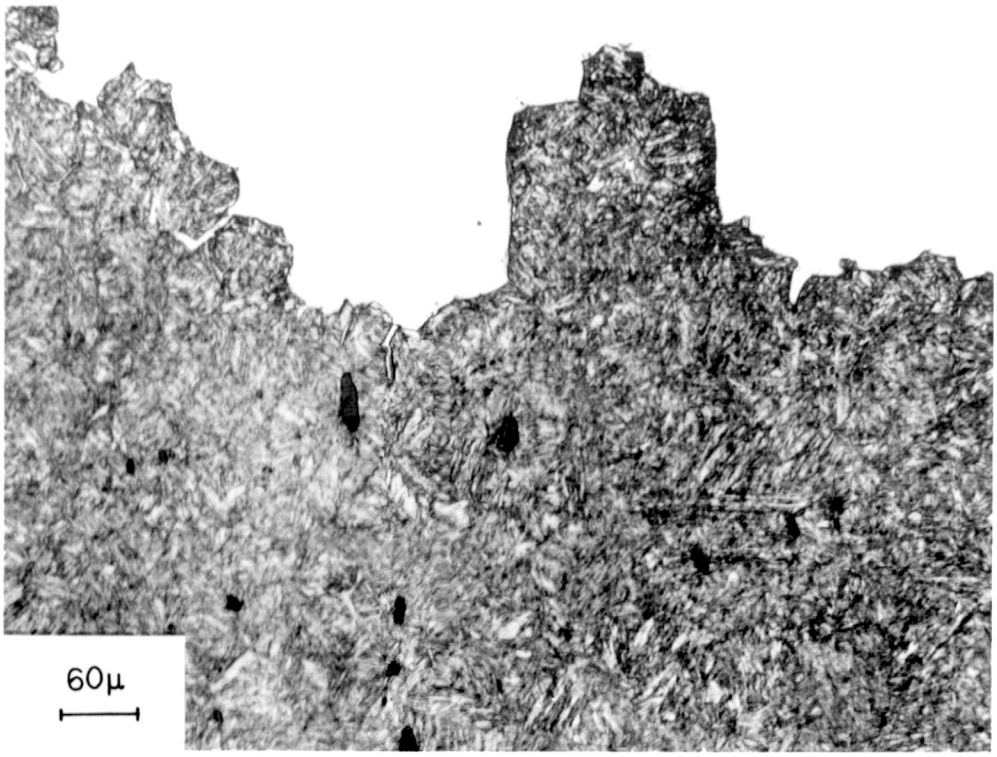


Fig. 5.18 Nickel plated section of the fracture surface of En16 tested in 3.5% NaCl solution. Plane of view L. Orientation TL. σ_{ys} = 1250 MPa.

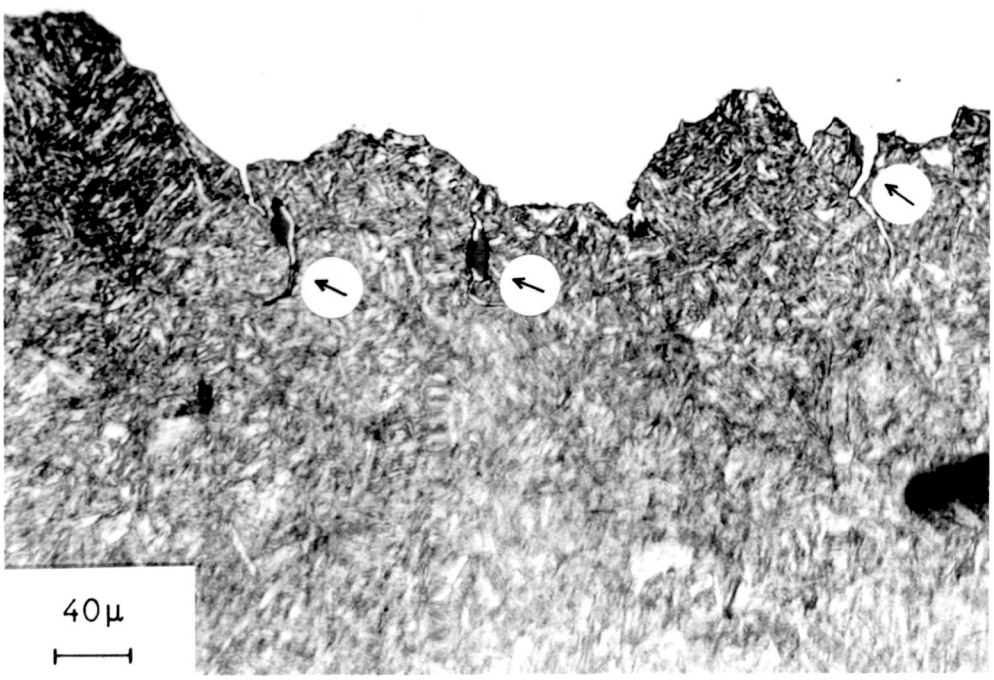


Fig. 5.19 Arrows indicate cracking along inclusions. Other details same as in previous figure.

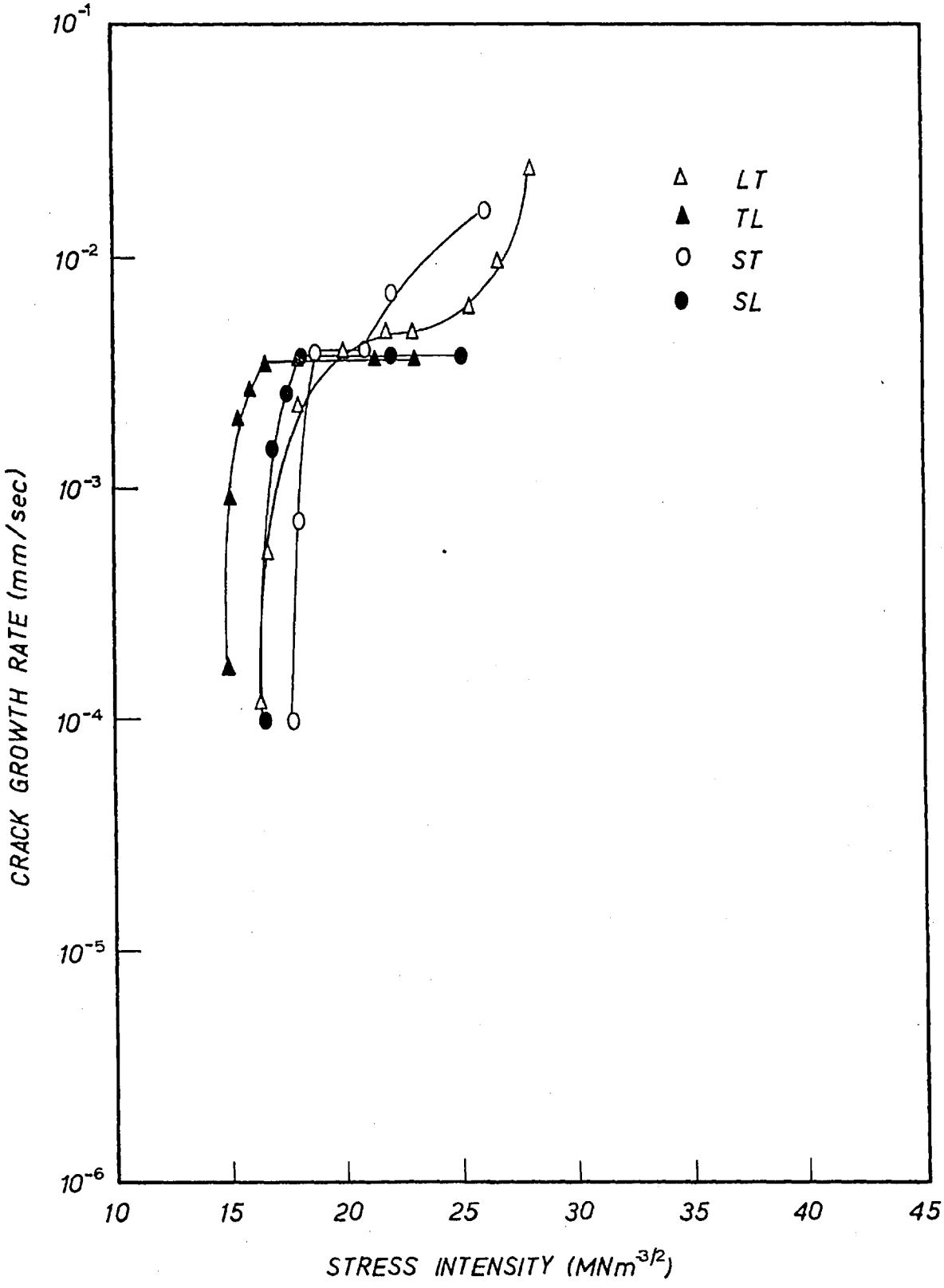


Fig.5·20 Crack growth behaviour of En16 at a yield strength of 1450MPa in 3·5%NaCl solution

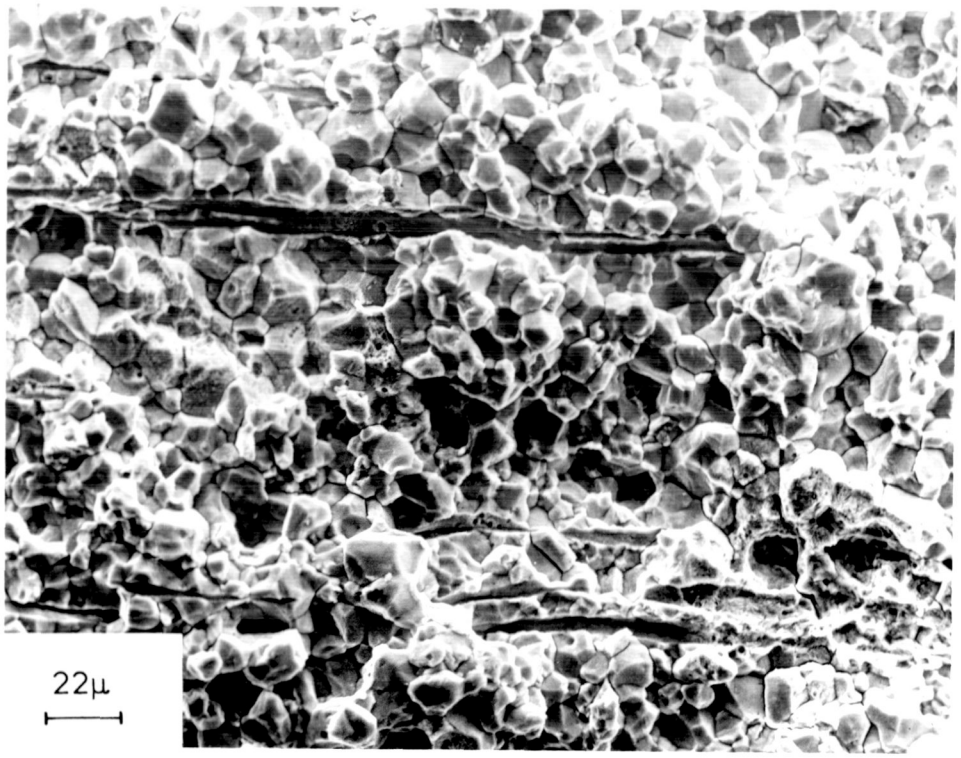


Fig.5.21 Fracture surface of En16 tested in 3.5% NaCl solution. Orientation ST. σ_{ys} =1450MPa. K = 23MNm$^{-3/2}$.

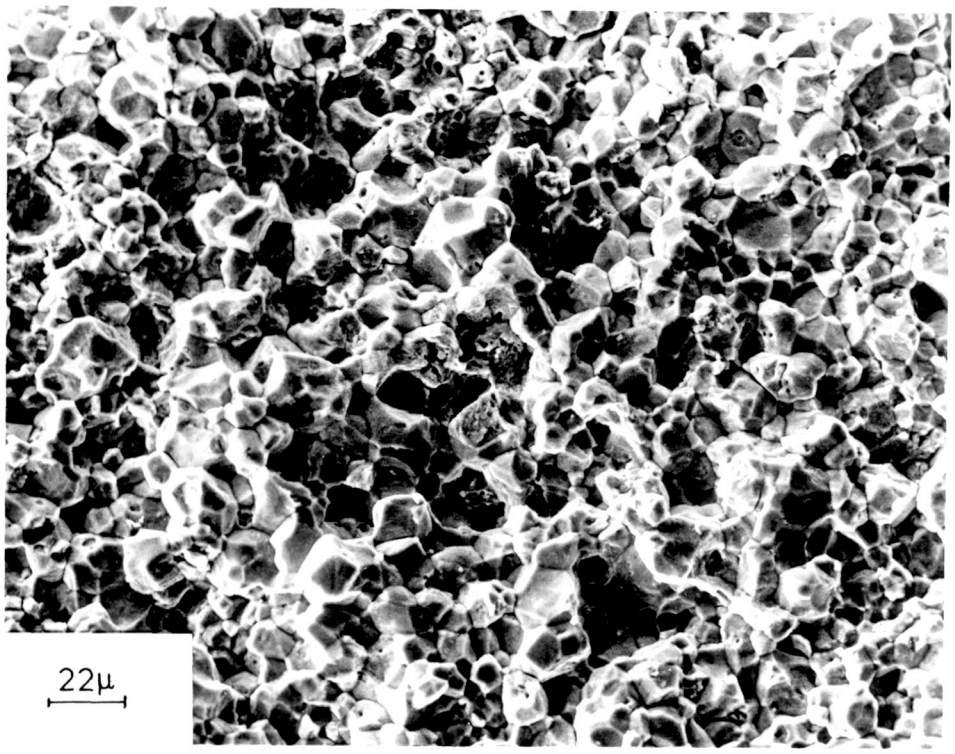


Fig.5.22 Fracture surface of En16 tested in 3.5% NaCl solution. Orientation ST. σ_{ys} =1450MPa. K≃17MNm$^{-3/2}$.

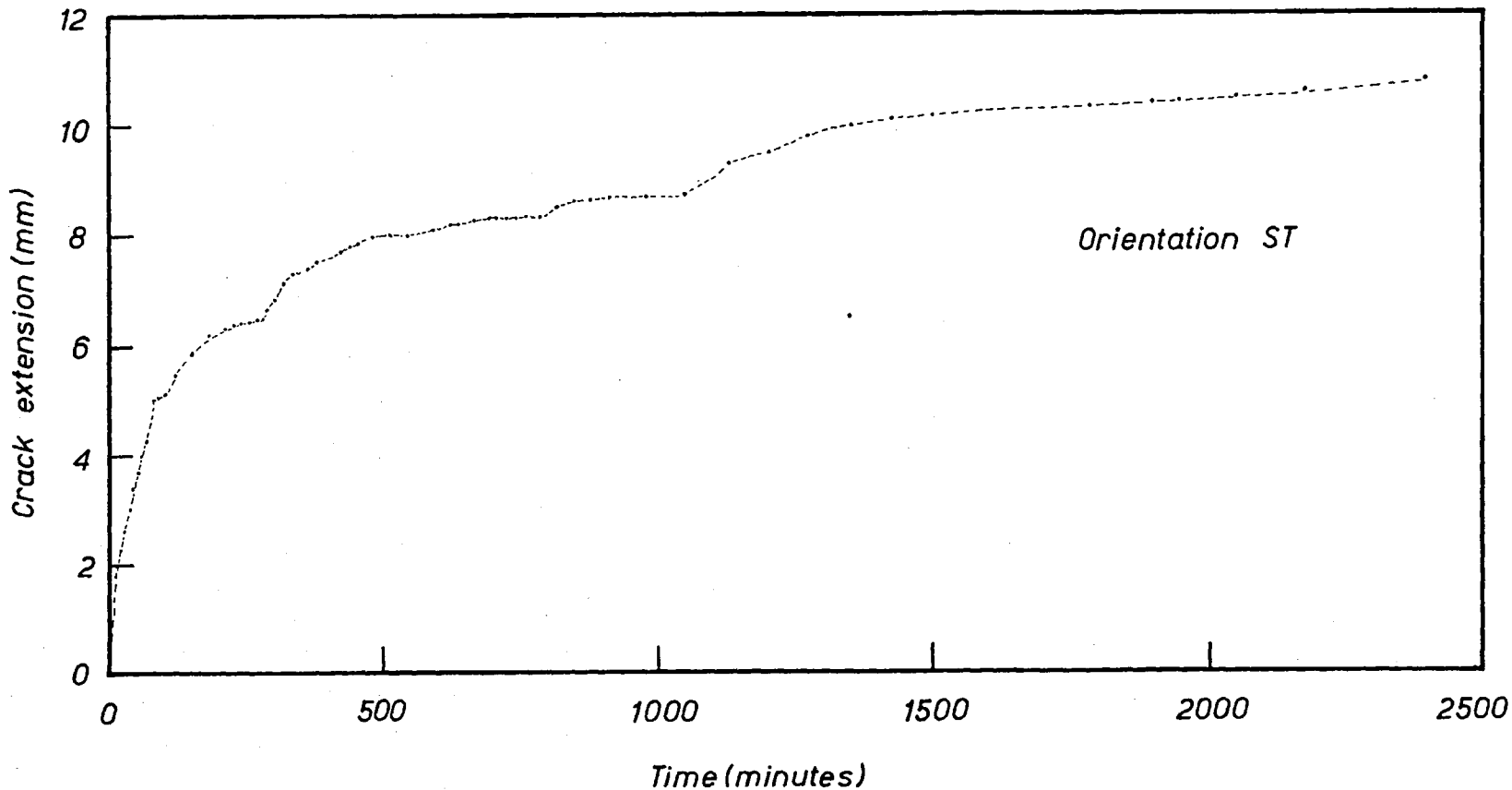


Fig. 5·23 Discontinuous crack growth in En16M at a yield strength of 800MPa in H_2S saturated 3·5% NaCl solution.

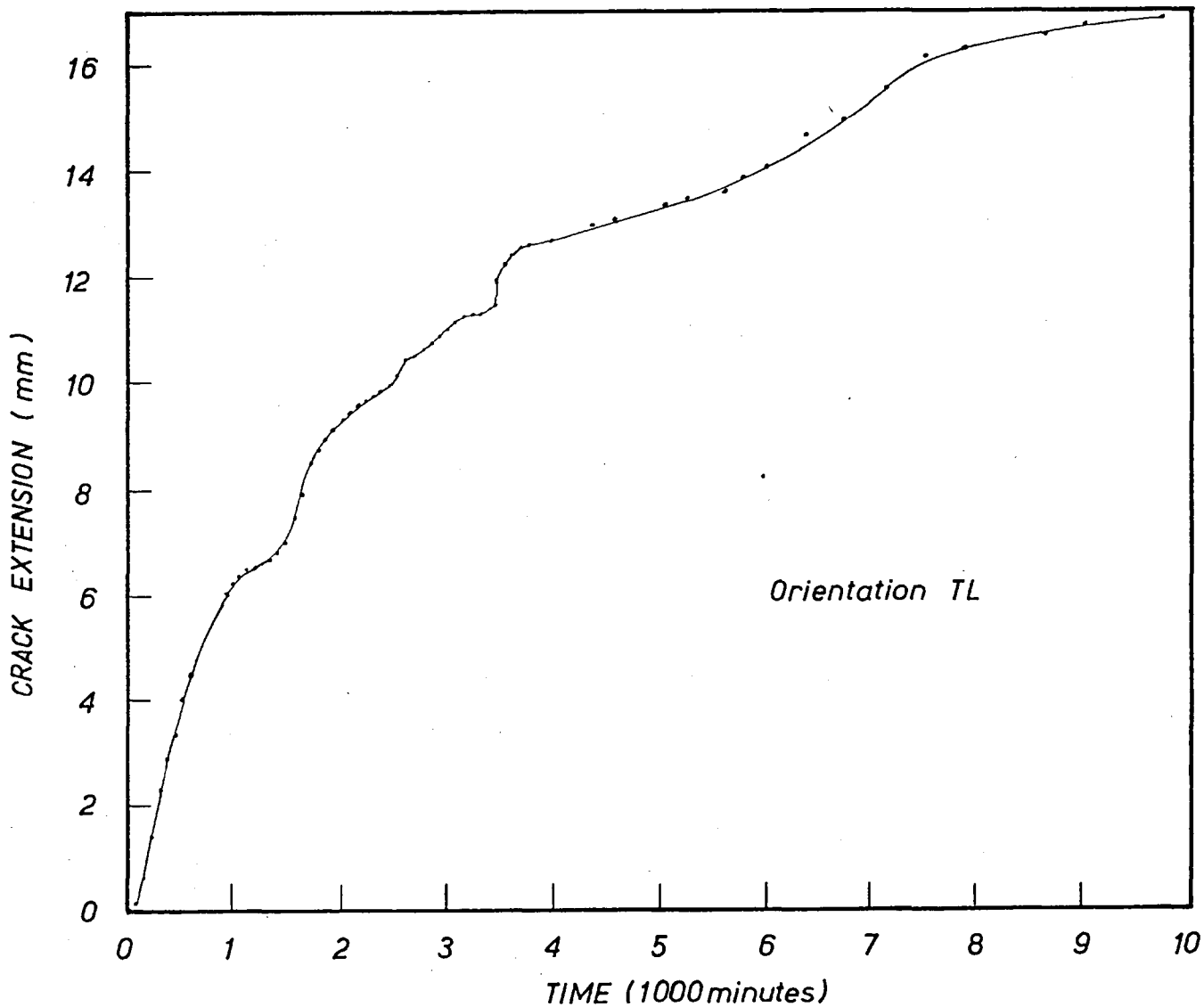


Fig. 5.24 Discontinuous crack growth in En16M at a yield strength of 800MPa in H_2S saturated 3·5% NaCl solution

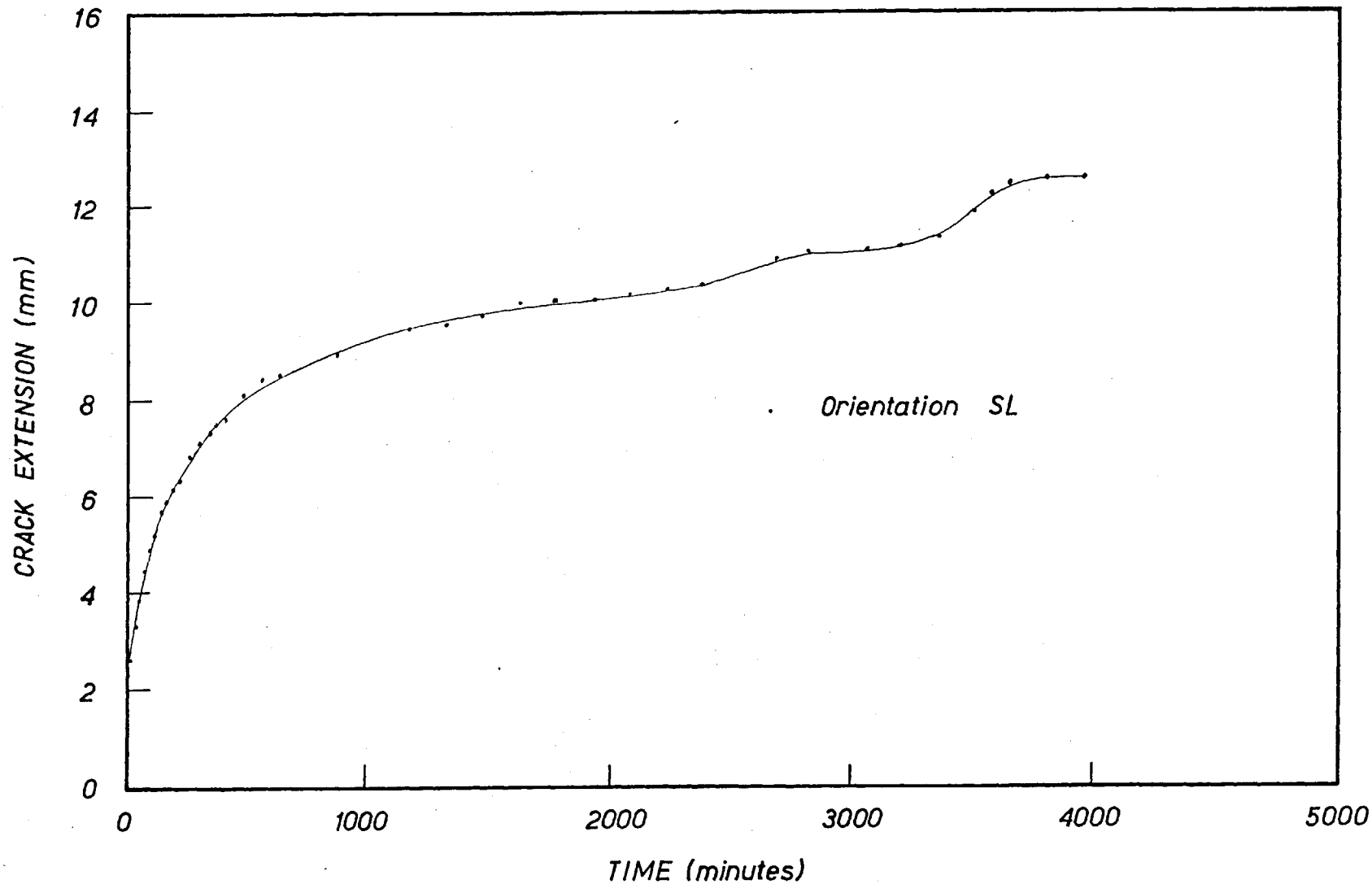


Fig. 5·25 Discontinuous crack growth in En16M at a yield strength of 800MPa in H_2S saturated 3·5% NaCl solution

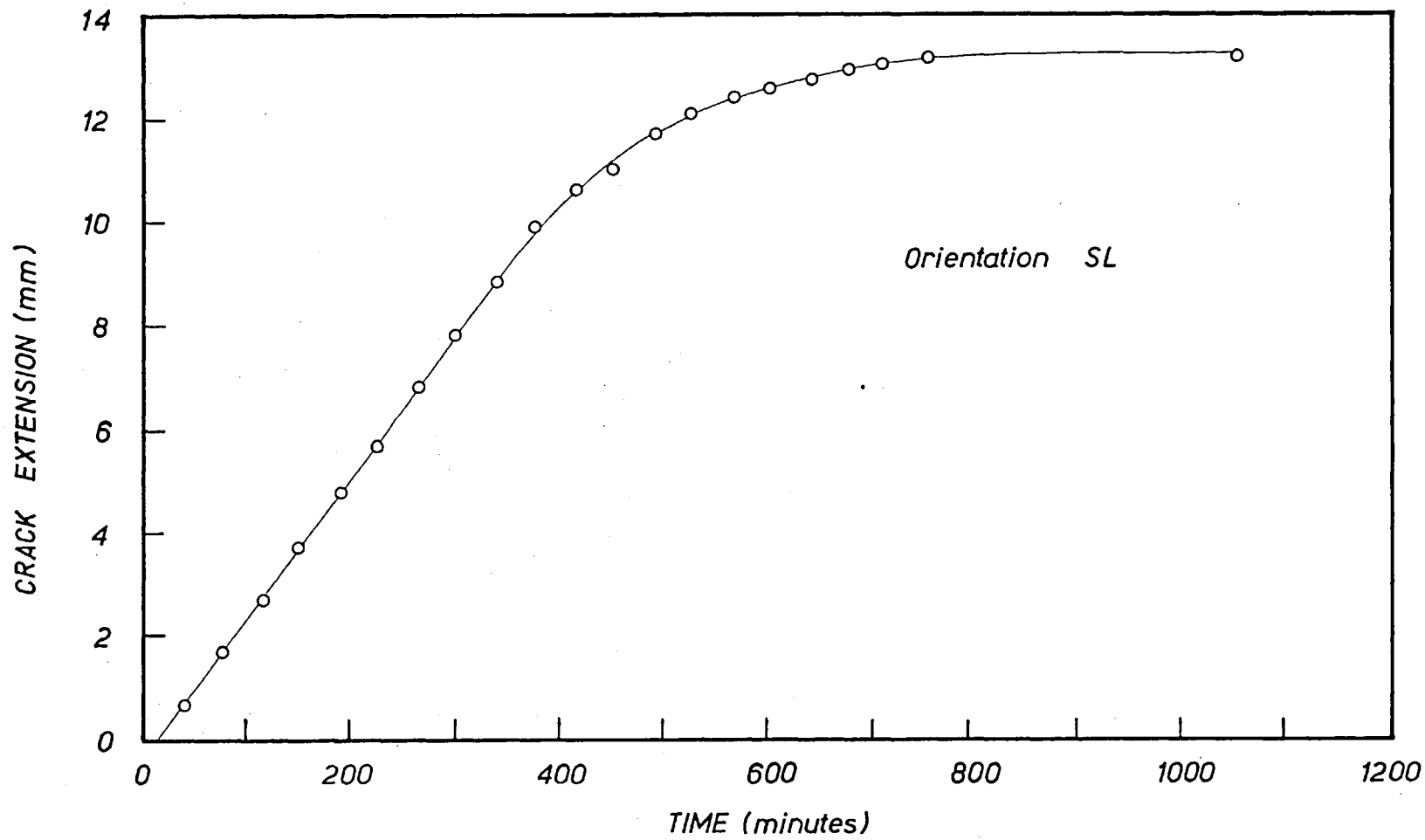


Fig 5.26 Continuous crack growth in En16 at a yield strength of 1250MPa in 3.5% NaCl solution

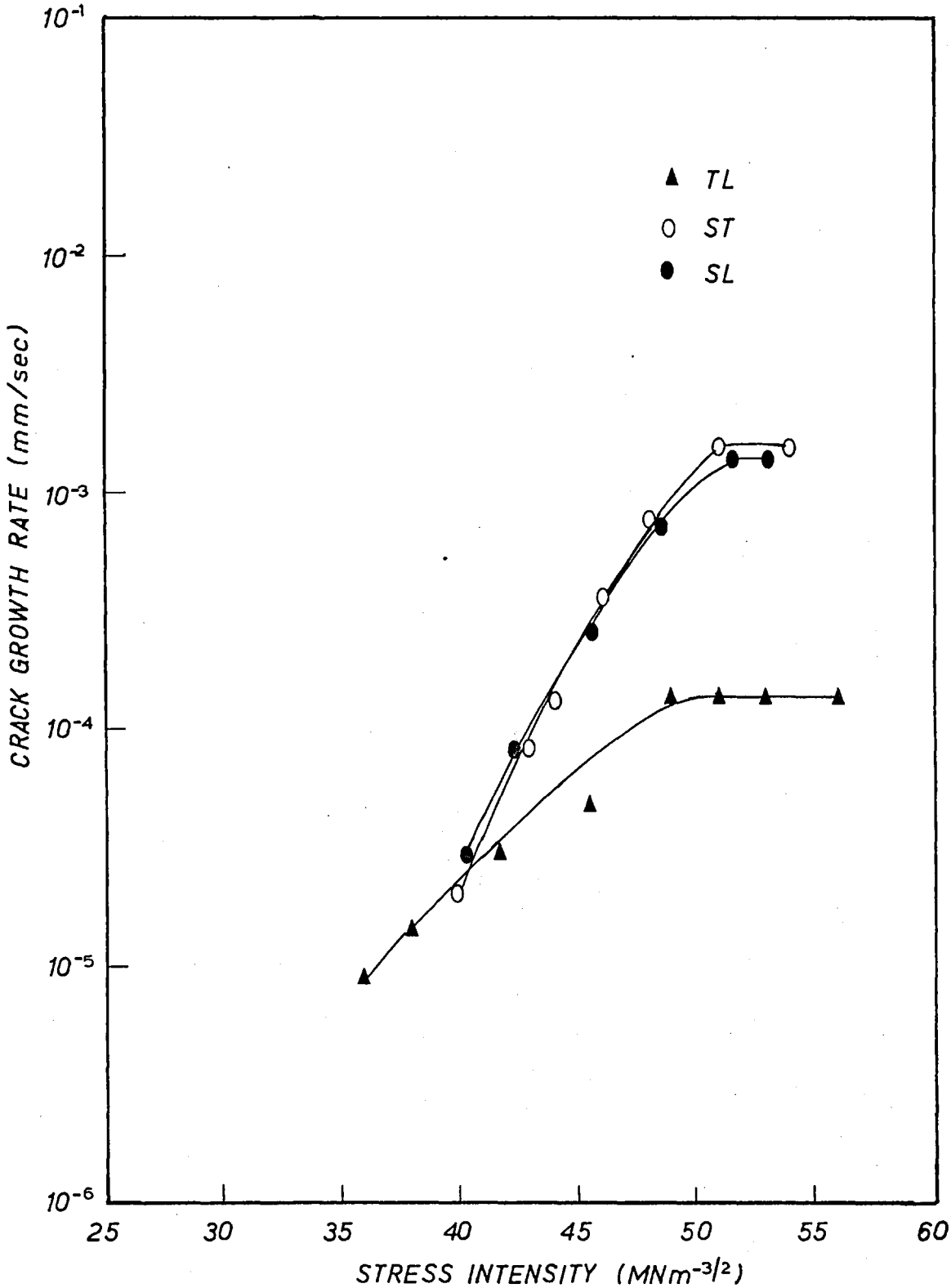


Fig. 5·27 Crack growth behaviour of En16M at a yield strength of 800MPa in H_2S saturated 3·5% NaCl solution

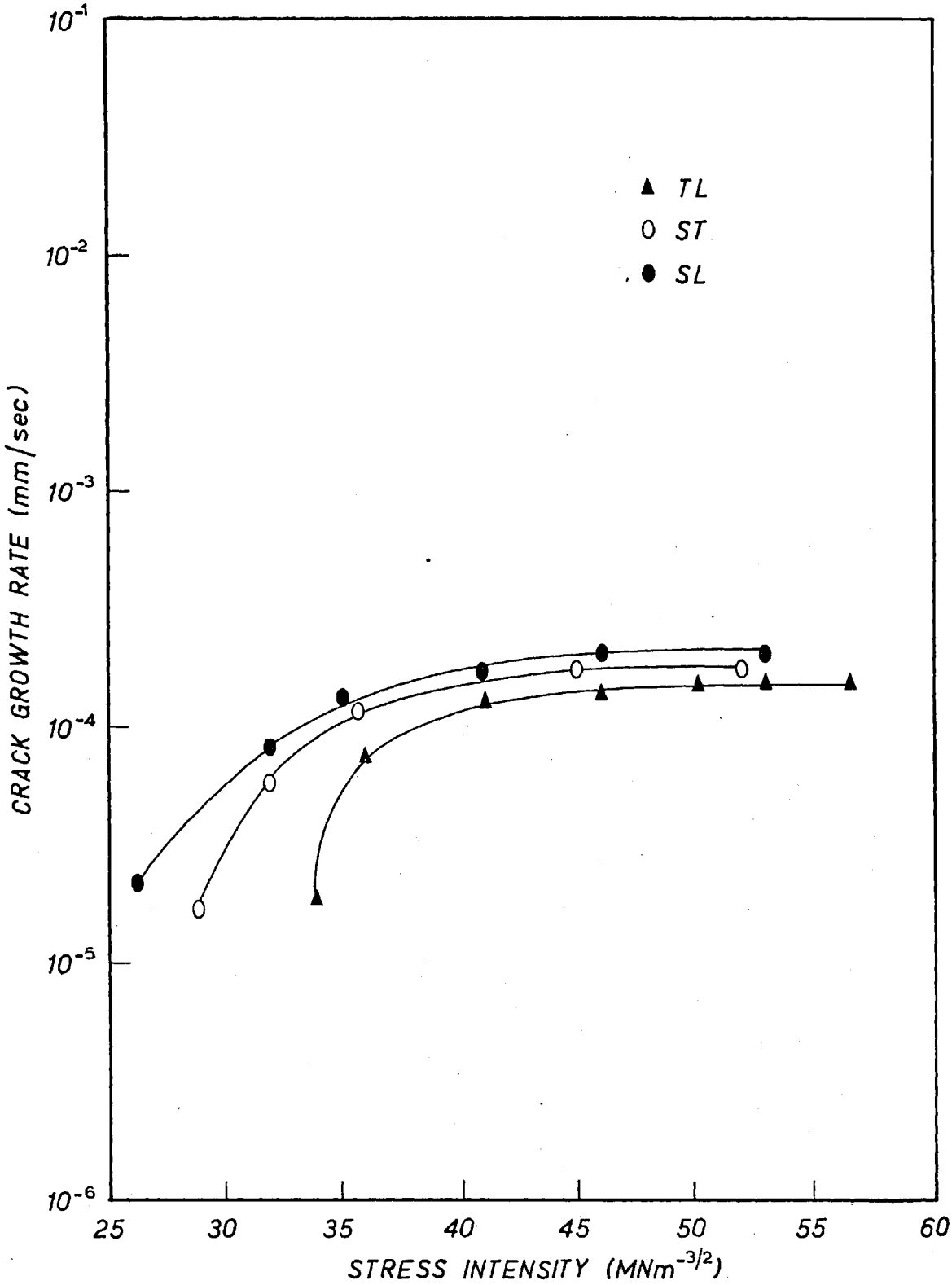
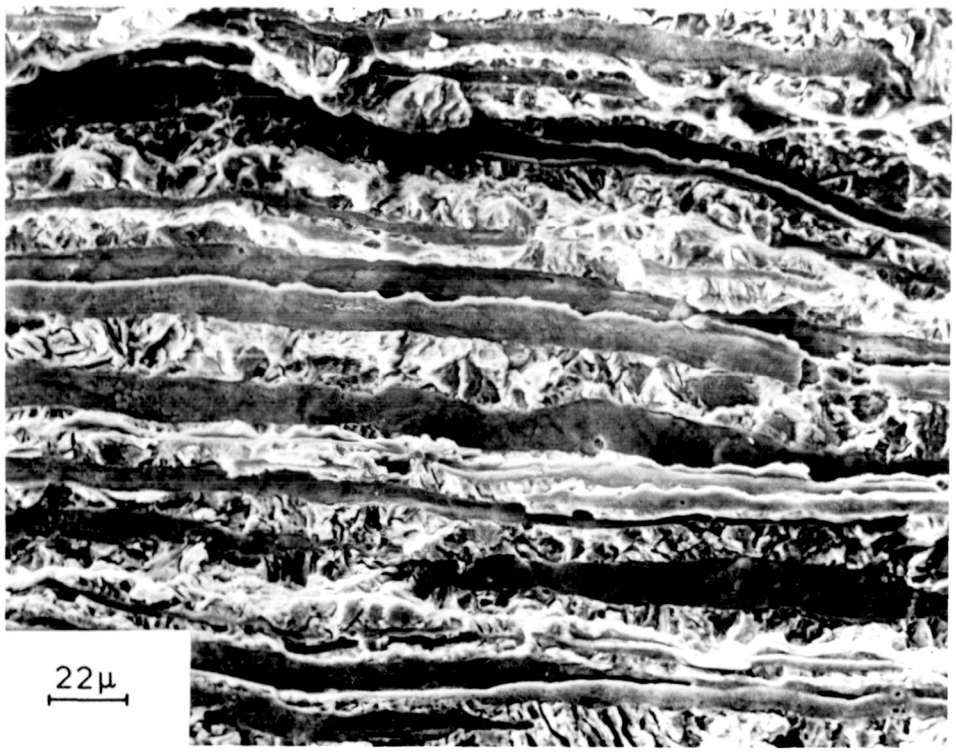
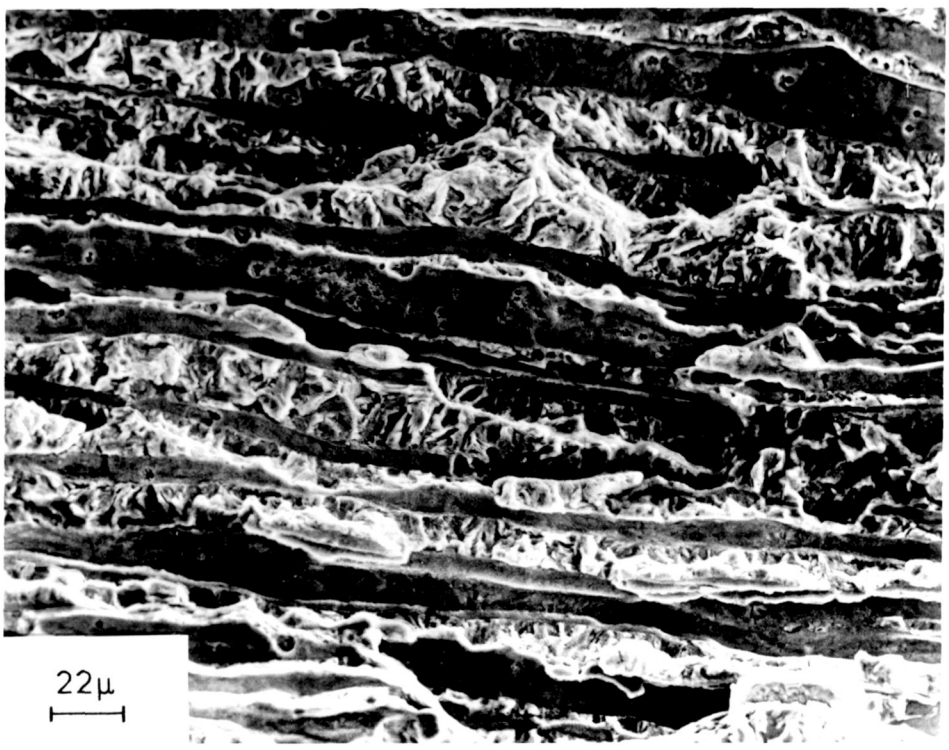


Fig. 5·28 Crack growth behaviour of En16 at a yield strength of 900MPa in H_2S saturated 3·5% NaCl solution



(a)



(b)

Fig 5.29 *Fracture surface of En16M tested in H_2S saturated 3.5% NaCl solution. Orientation ST. σ_{ys} = 800 MPa. $K \simeq 40 MNm^{-3/2}$.*

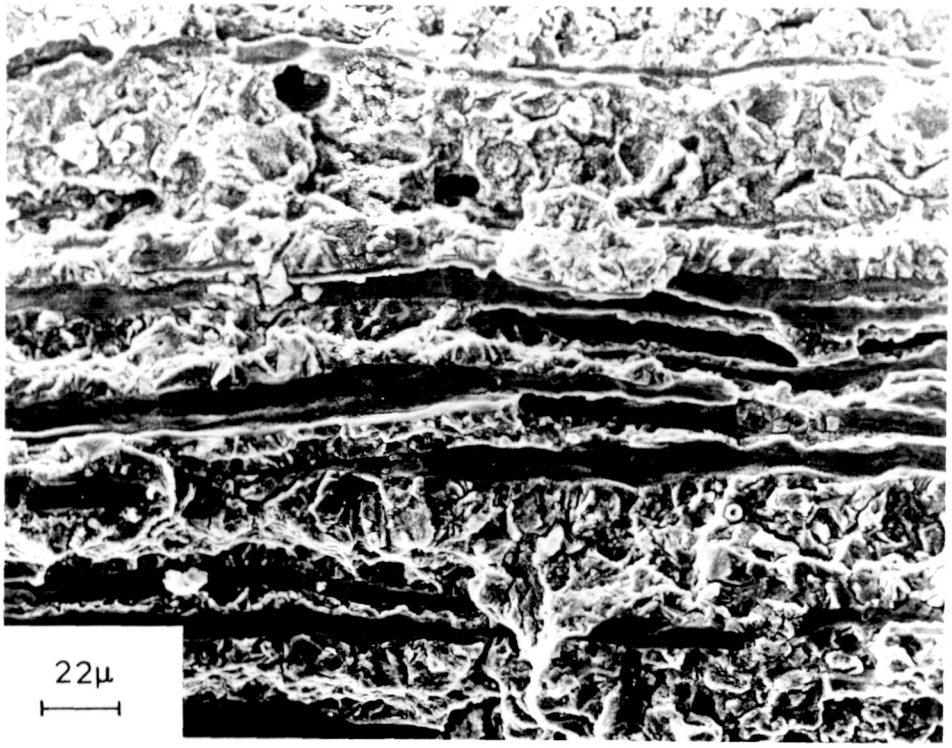


Fig.5.30 *Fracture surface of En16M tested in H_2S saturated 3.5% NaCl solution. Orientation SL. σ_{ys} =800MPa. K ≈ 40MNm$^{-3/2}$.*

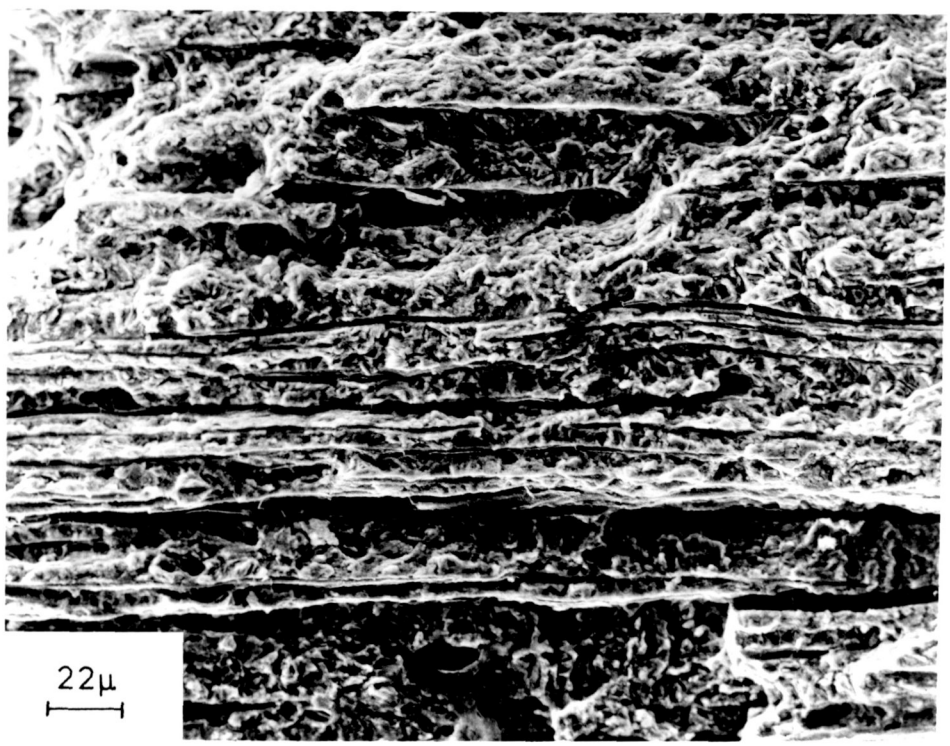


Fig.5.31 *Fracture surface of En16M tested in 3.5% NaCl solution saturated with H_2S. Orientation TL. σ_{ys} = 800MPa. K ≈ 40MNm$^{-3/2}$.*

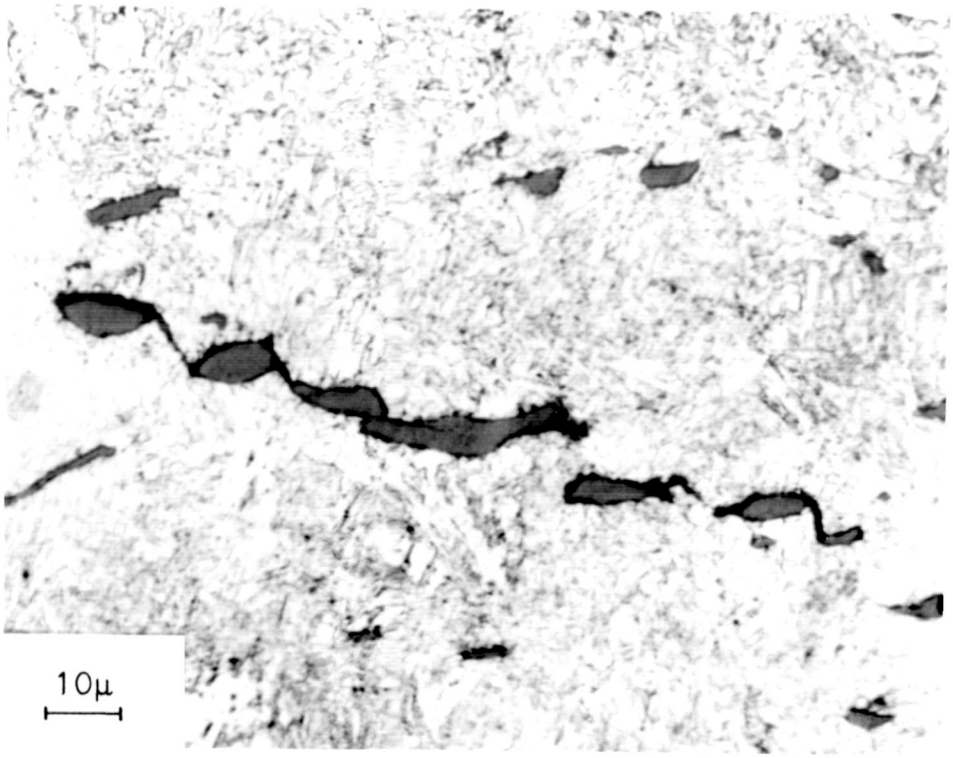


Fig. 5.32 Secondary crack observed below the fracture surface in En16M tested in H_2S saturated 3½ % NaCl solution. Plane of view L. Orientation ST. σ_{ys} = 800 MPa.

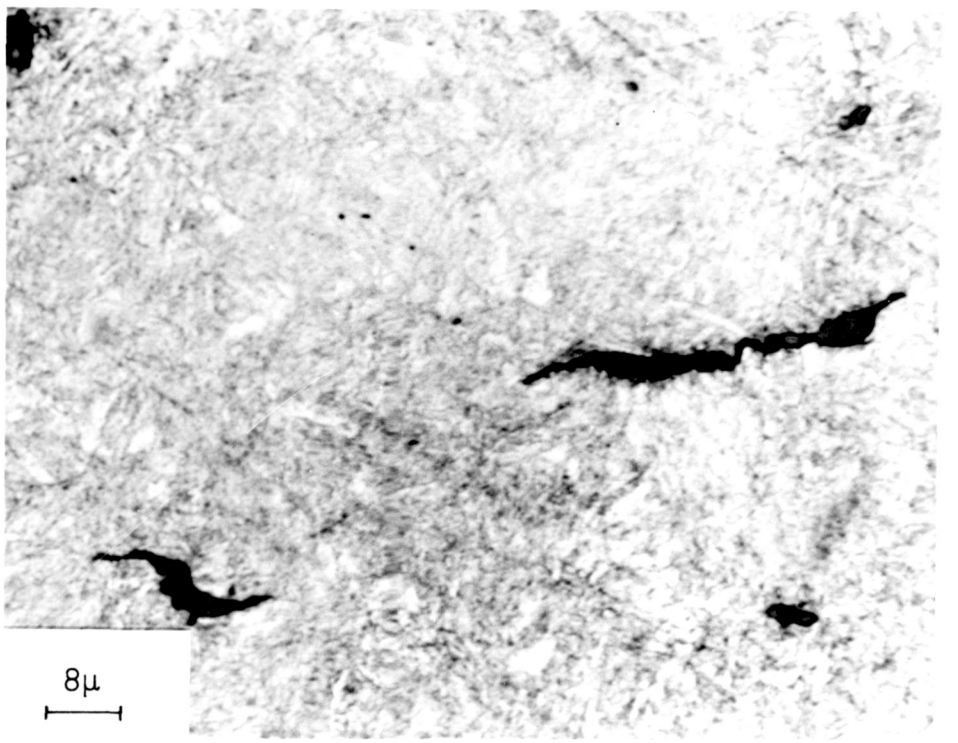


Fig. 5.33 Sub-surface cracks originating from inclusions in En16 tested in H_2S saturated 3½ % NaCl solution. Plane of view L. Orientation ST. σ_{ys} = 900 MPa.

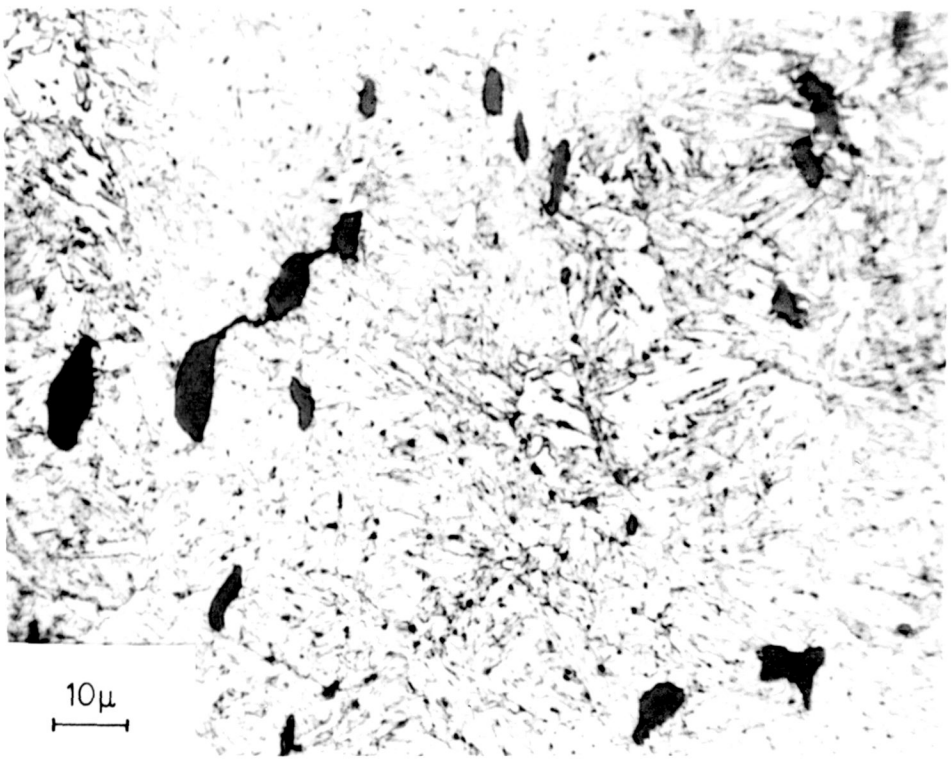


Fig. 5.34 Sub-surface crack in En16M formed by the linkage of closely spaced inclusions. Environment H_2S saturated 3·5% NaCl solution. Plane of view L. Orientation TL. σ_{ys} = 800 MPa.

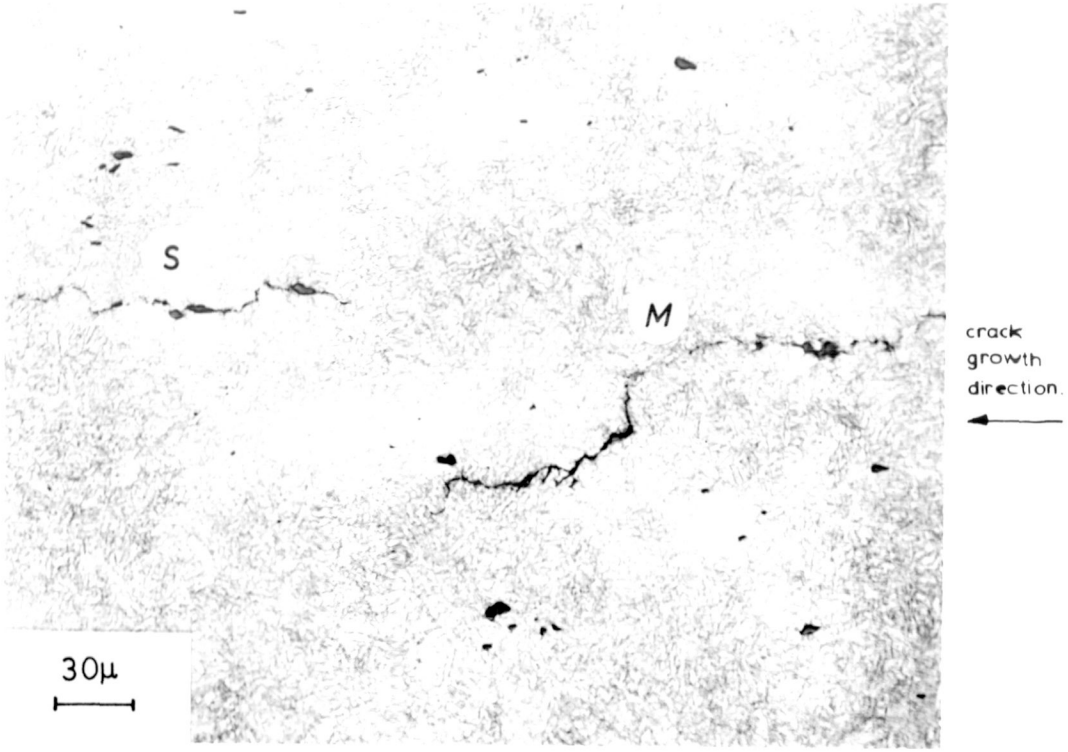


Fig.5.35a Secondary crack (S) developing ahead of the main crack (M) in En16 tested in H_2S saturated 3½% NaCl solution. Plane of view L. Orientation ST. σ_{ys} *= 900MPa*

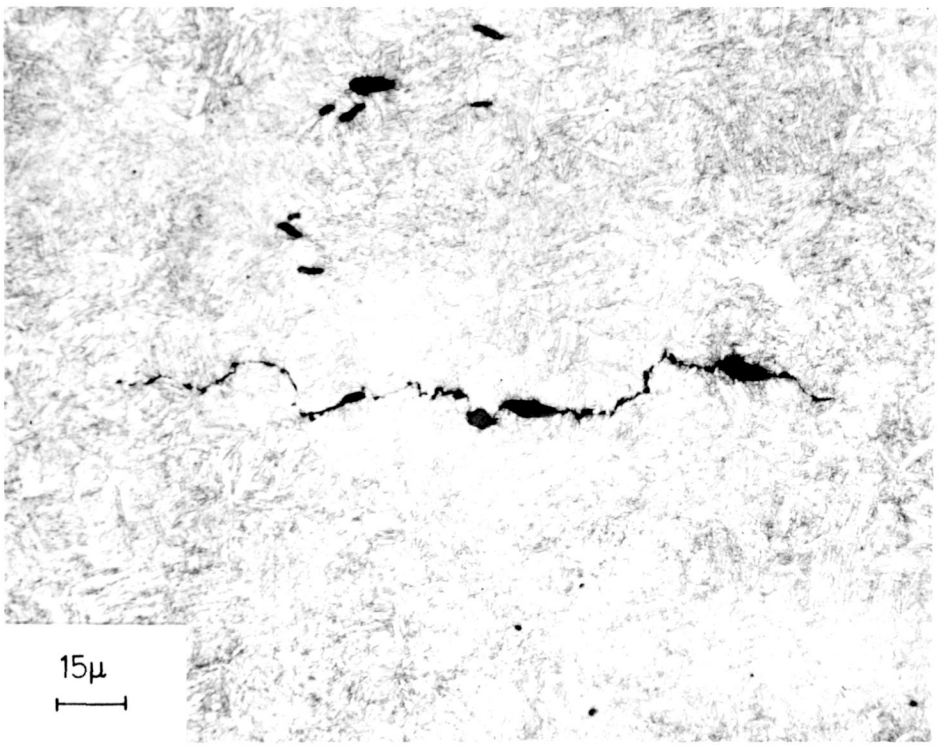


Fig.5.35b Enlarged view of the secondary crack of the previous figure showing preferential crack propagation via inclusions.

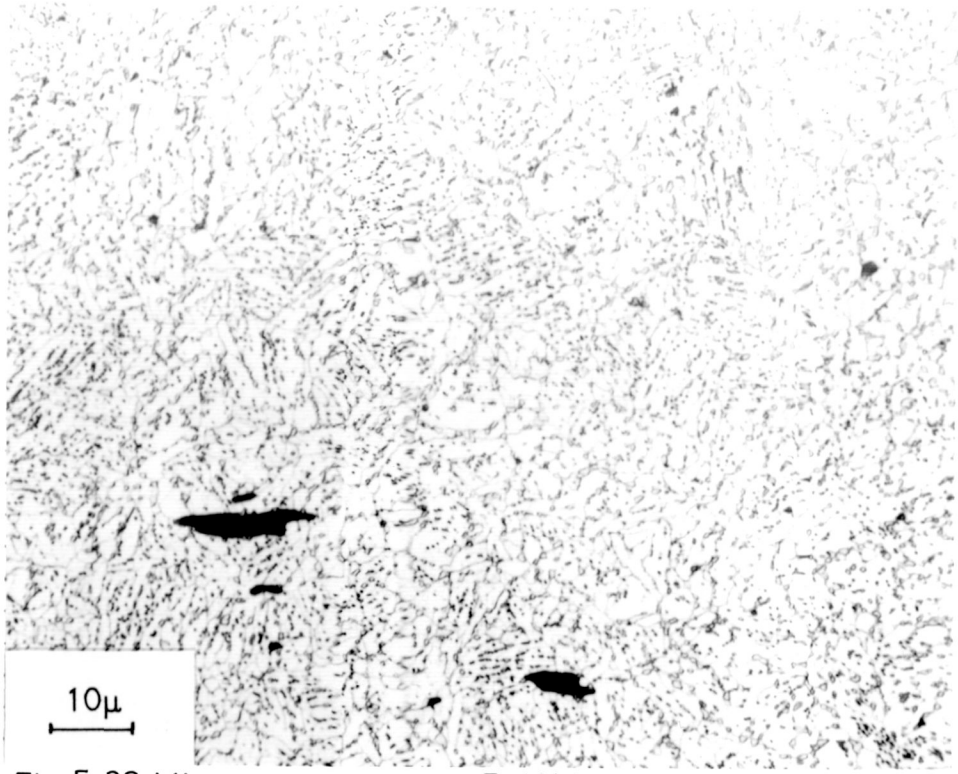


Fig. 5.36 *Microstructure of En16M after hardening and tempering at 690°C.*

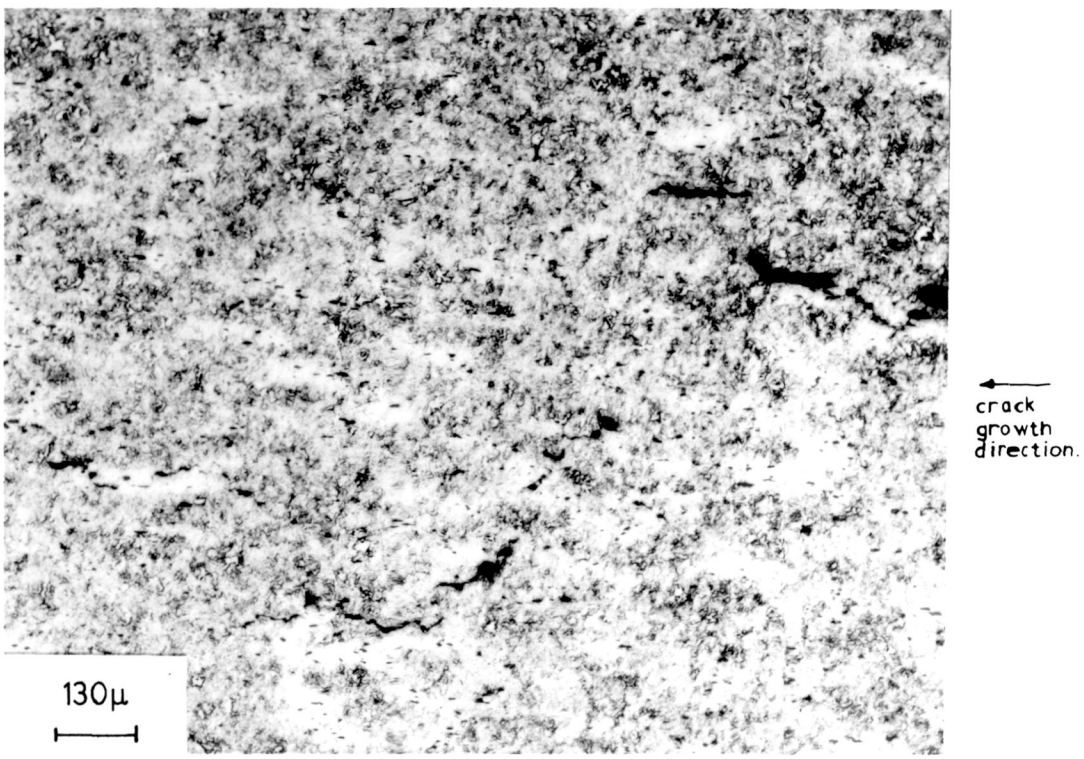


Fig. 5.37 *Cracks in En16M tested in acidified 3.5% NaCl solution saturated with H_2S. Plane of view L. Orientation ST. $\sigma_{ys} \approx 600$MPa.*

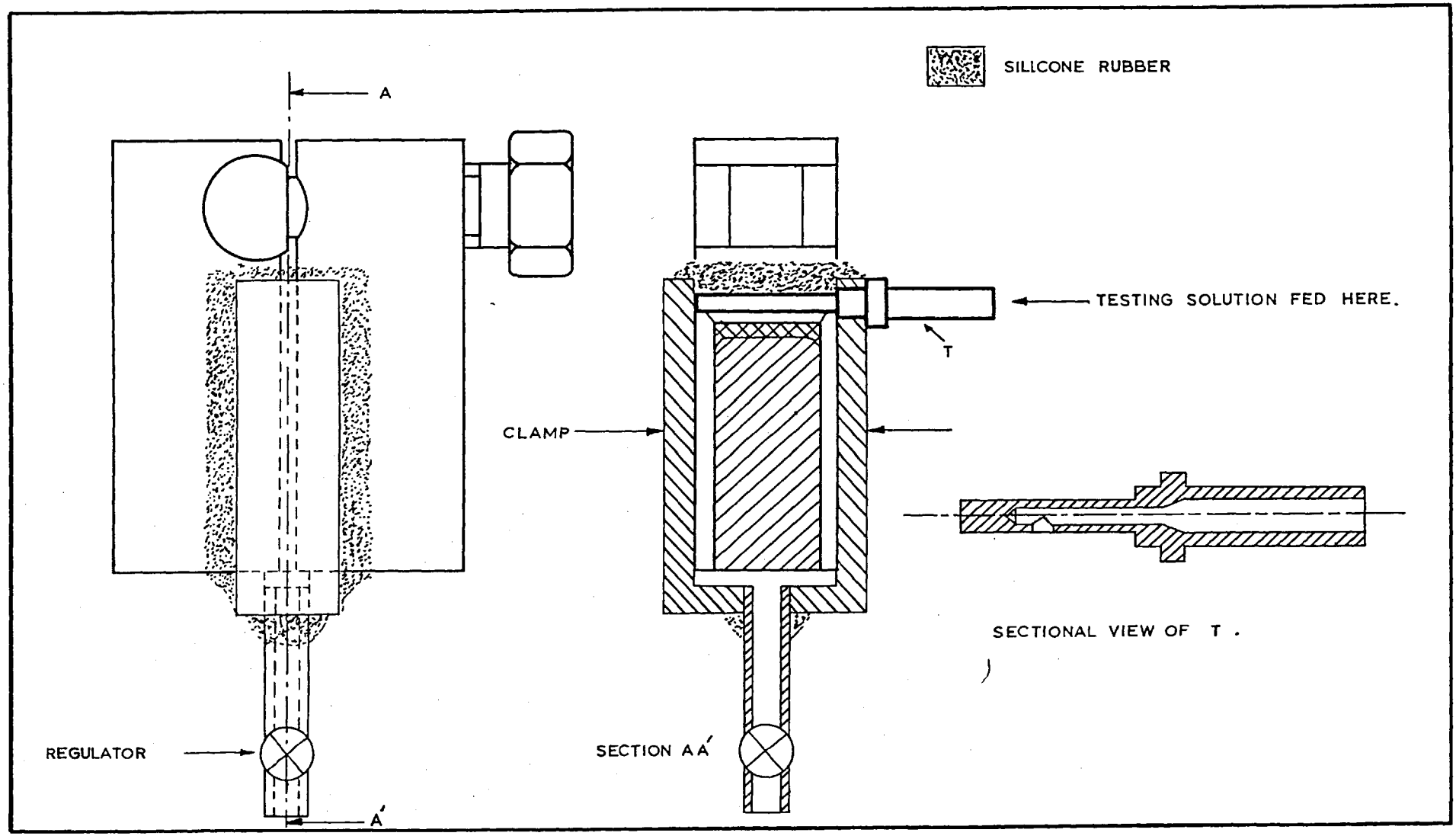


Fig. 5.38 Modified procedure for testing in H_2S saturated 3.5 % NaCl solution.

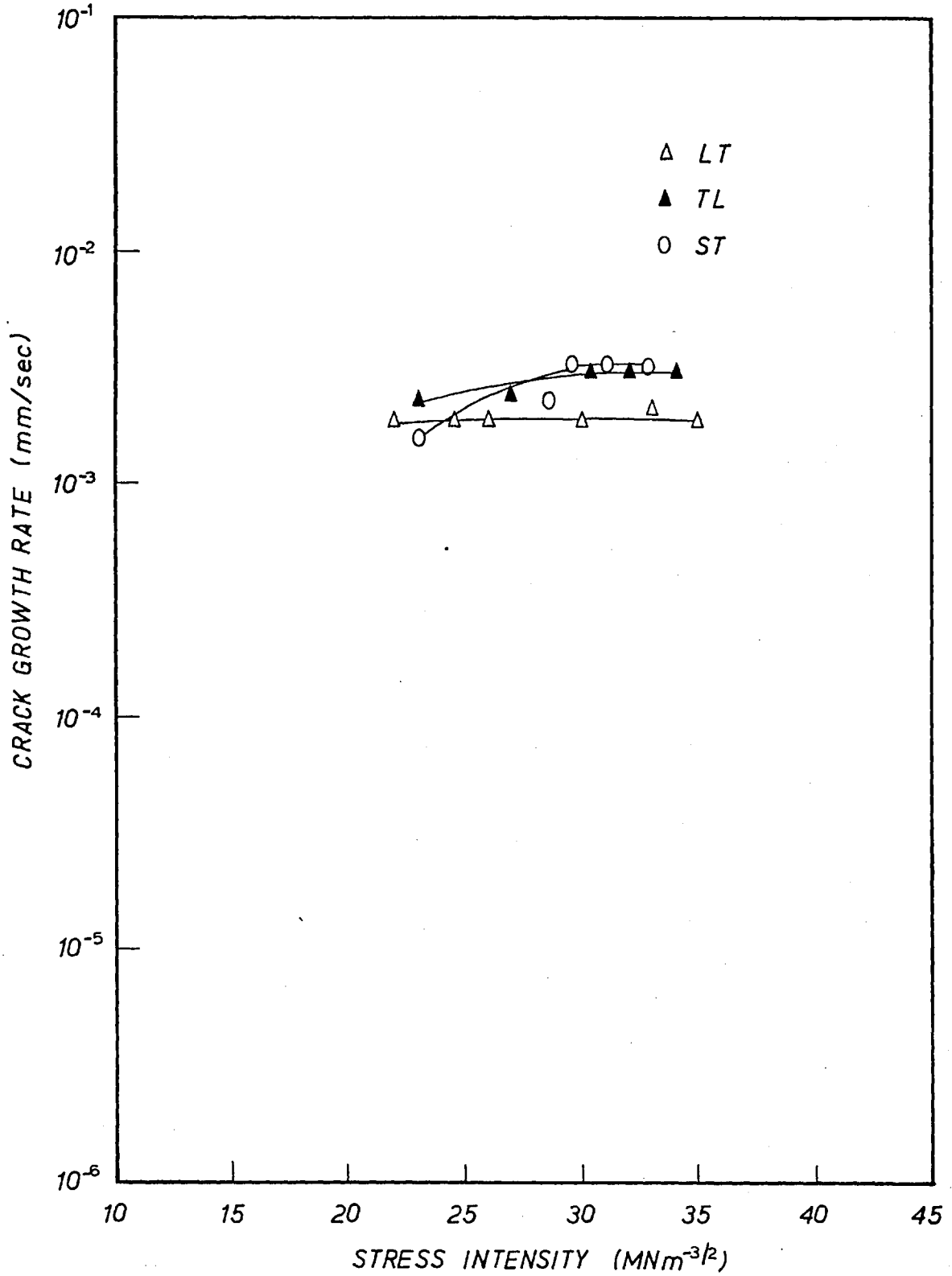


Fig. 5·39 Crack growth behaviour of En 16M at a yield strength of 1300MPa in 0·1MPa H_2S gas

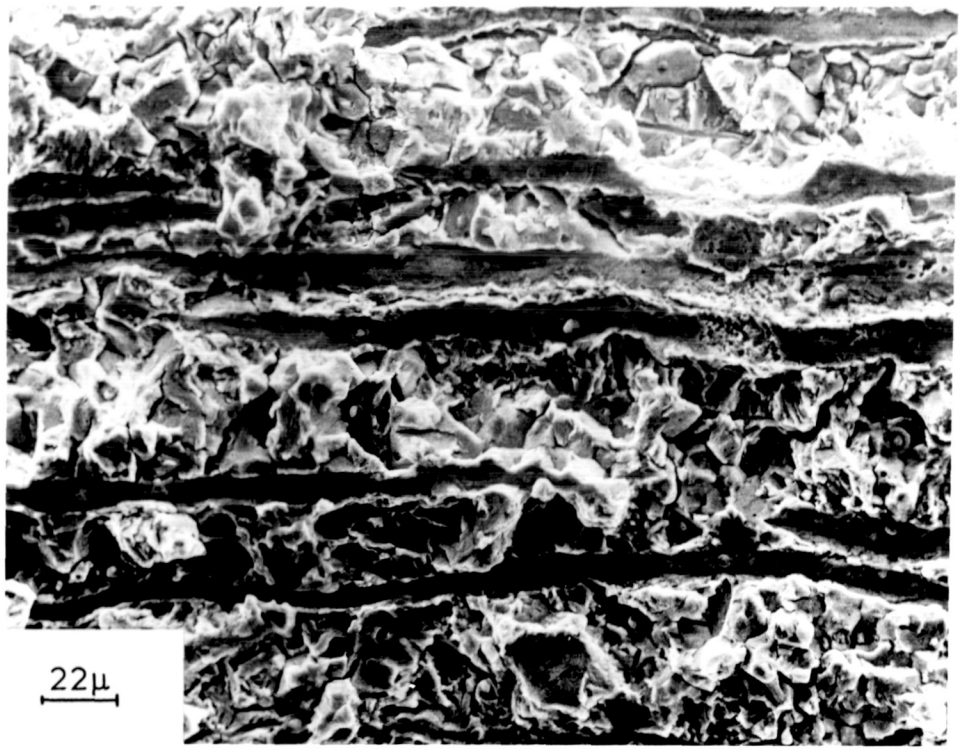


Fig.5·40 *Fracture surface of En16M tested in 0·1MPa H_2S gas. Orientation ST. σ_{ys} = 1300MPa. $K \simeq 33 MNm^{-3/2}$.*

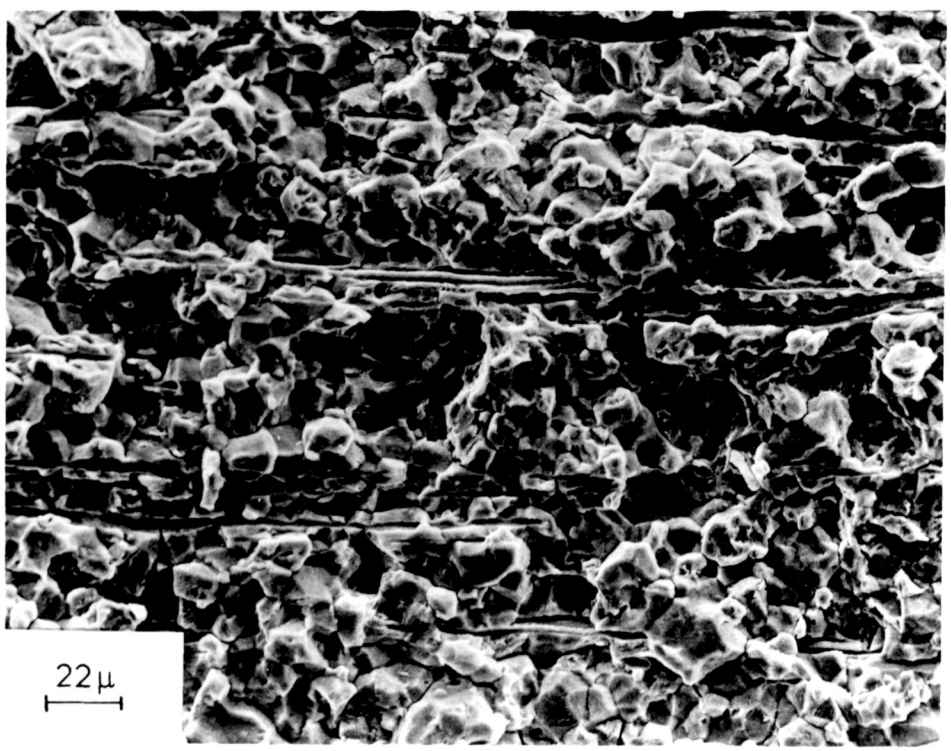


Fig.5·41 *Fracture surface of En16M tested in 0·1MPa H_2S gas. Orientation ST. σ_{ys} = 1300MPa. $K \simeq 20 MNm^{-3/2}$.*

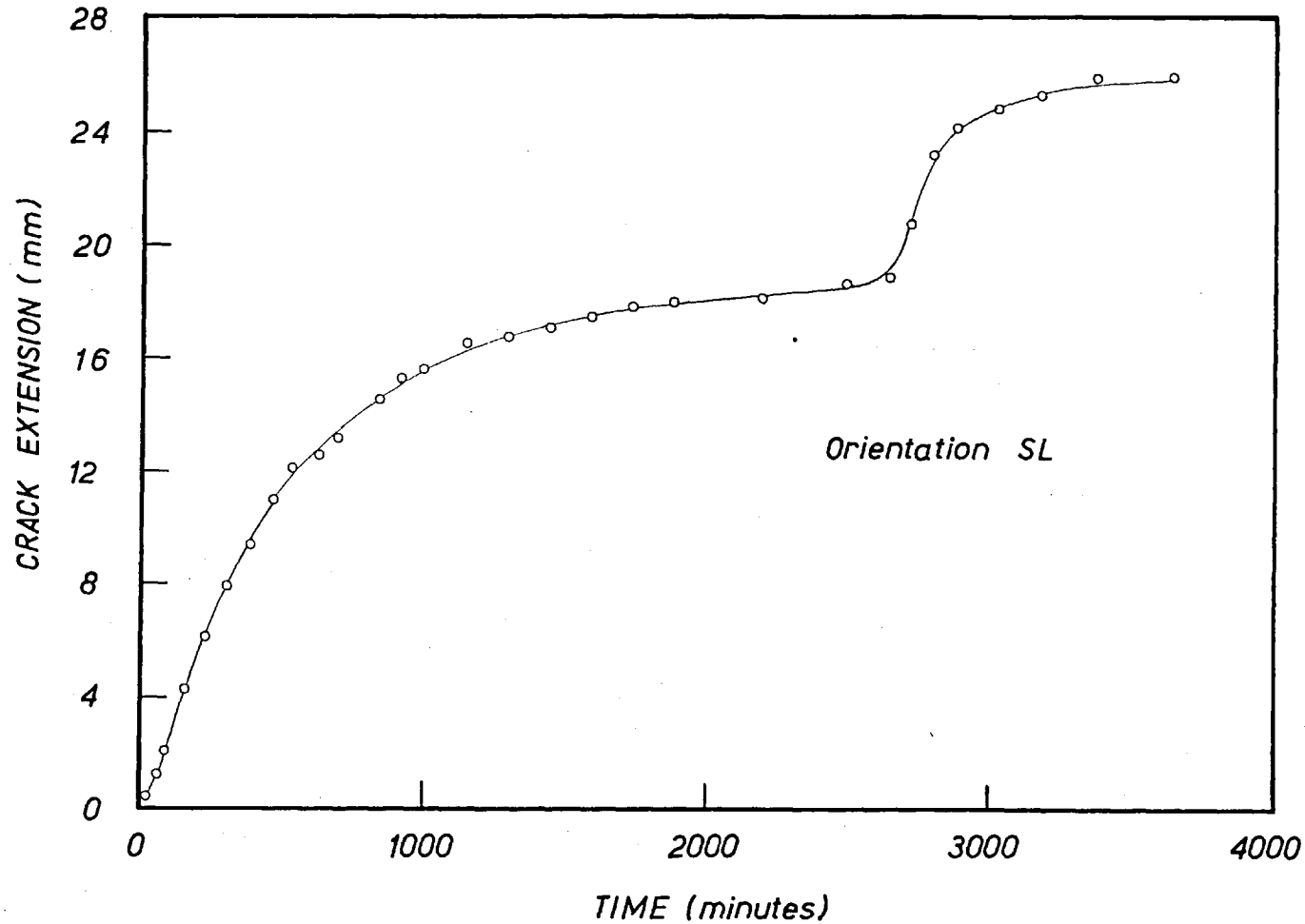


Fig. 5.42 Discontinuous crack growth in En16M at a yield strength of 1200MPa in H_2S saturated 3.5% NaCl solution

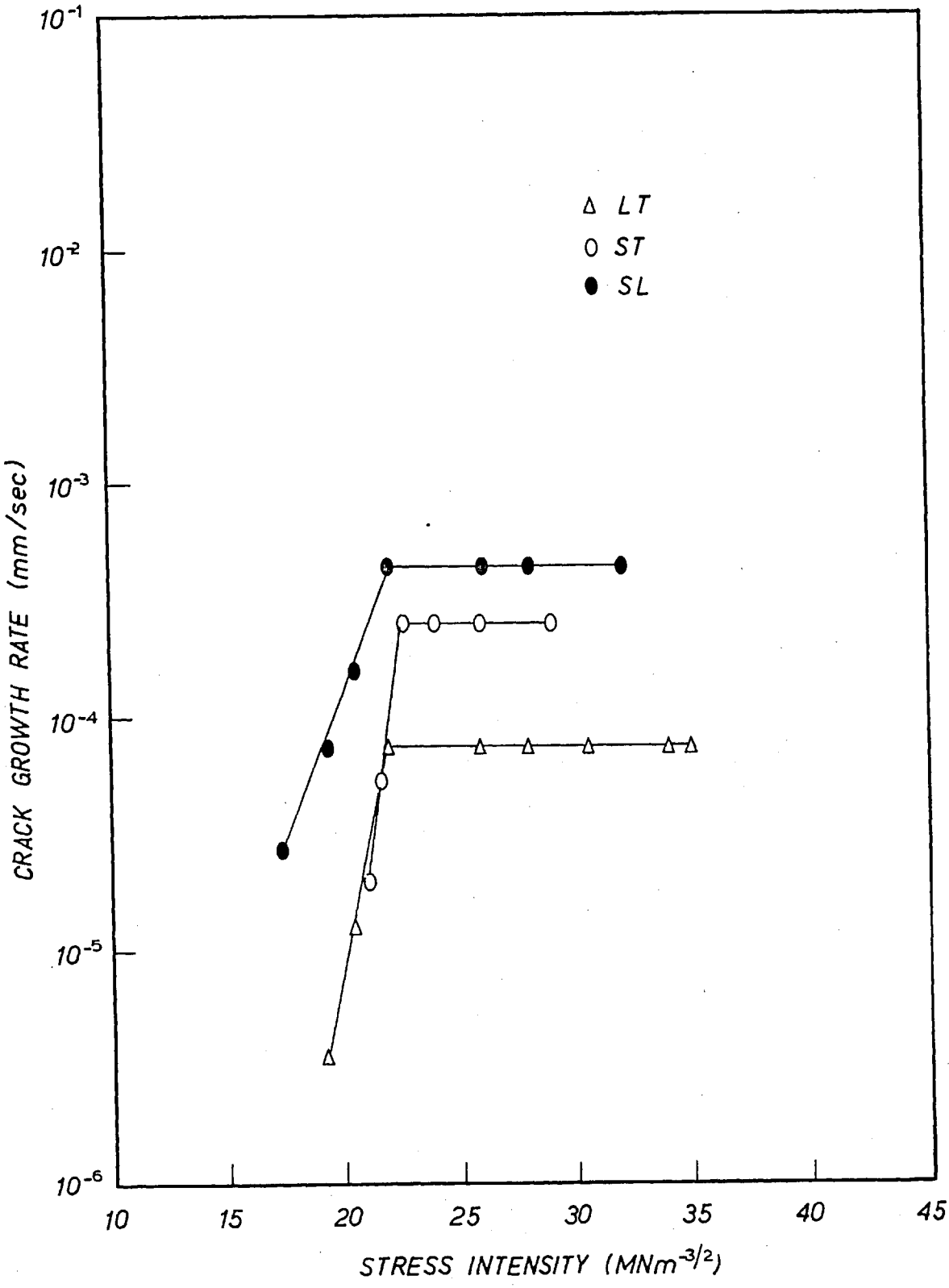


Fig. 5·43 Crack growth behaviour of En 16M at a yield strength of 1200MPa in H_2S saturated 3·5% NaCl solution

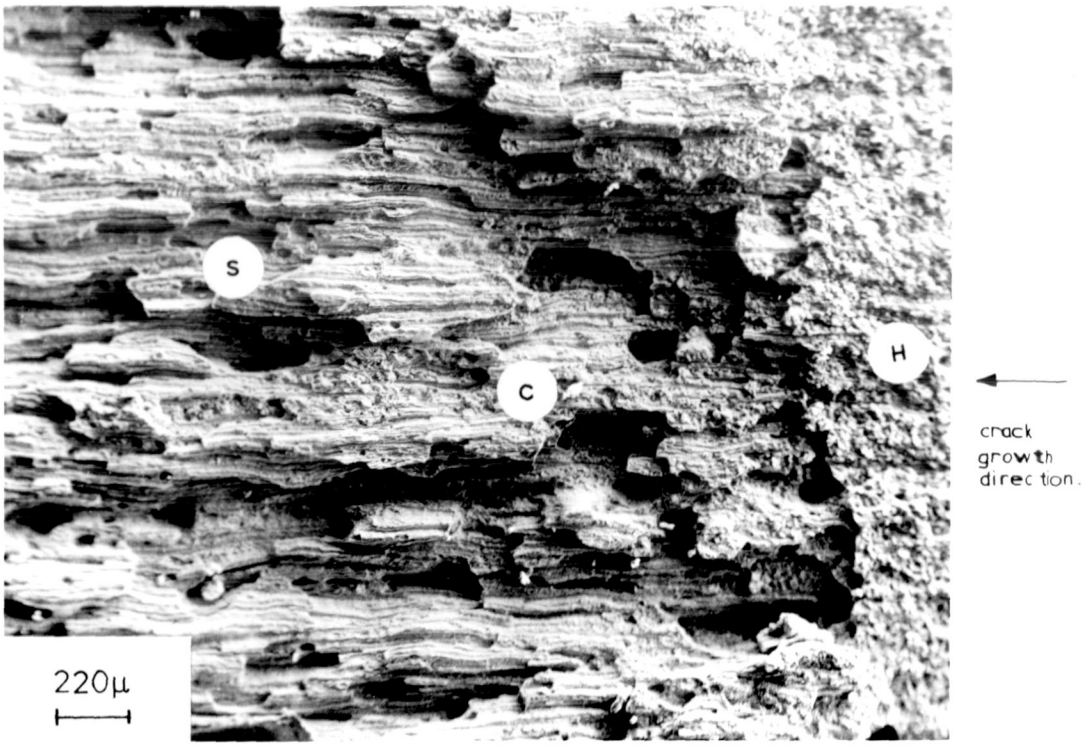


Fig.5.44a Region of crack arrest in En16M tested in H_2S saturated 3.5% NaCl solution. Orientation SL. σ_{ys} = 1200MPa. Region H and S represent respectively zone of hydrogen assisted crack growth and fast fracture in air.

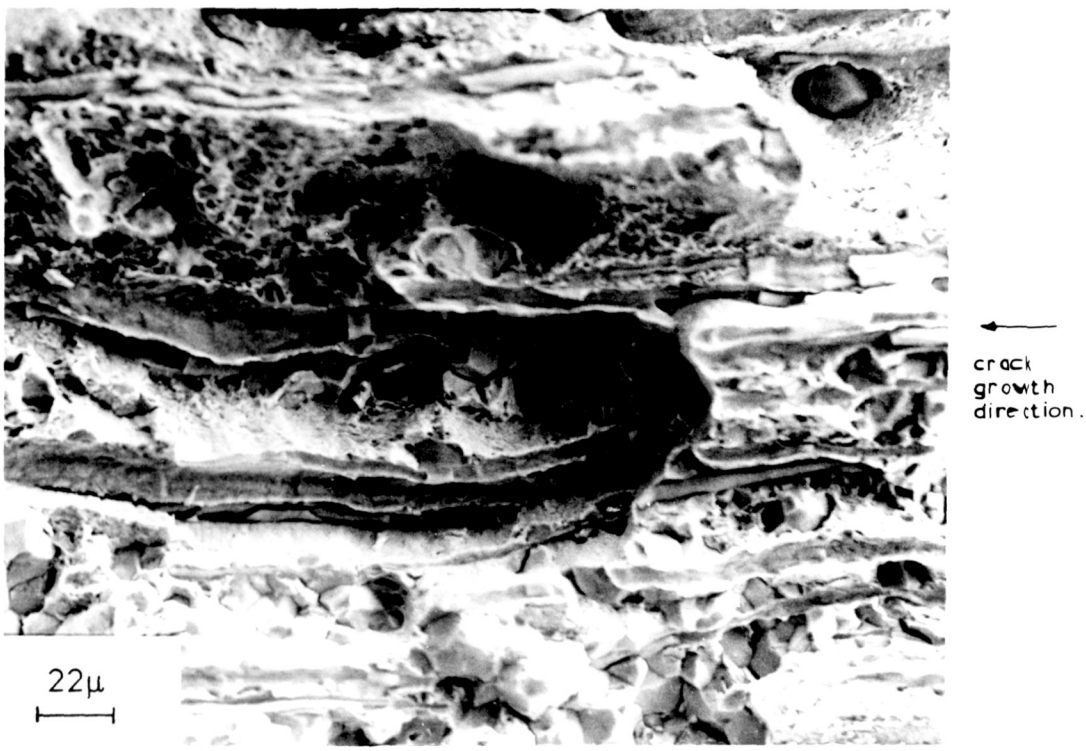


Fig.5.44b Enlarged view of region C of the previous figure.

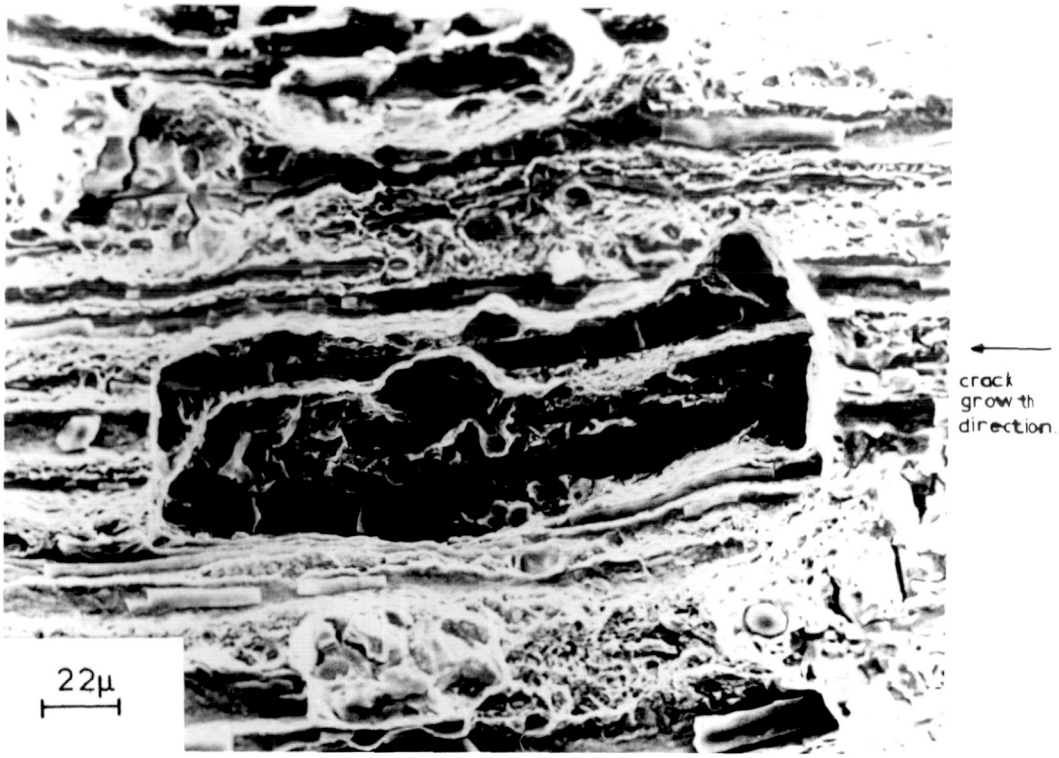


Fig. 5.45 *Isolated region of intergranular fracture lying ahead of the main crack in En16M tested in H_2S saturated 3·5% NaCl solution. Orientation SL. σ_{ys}=1200MPa.*

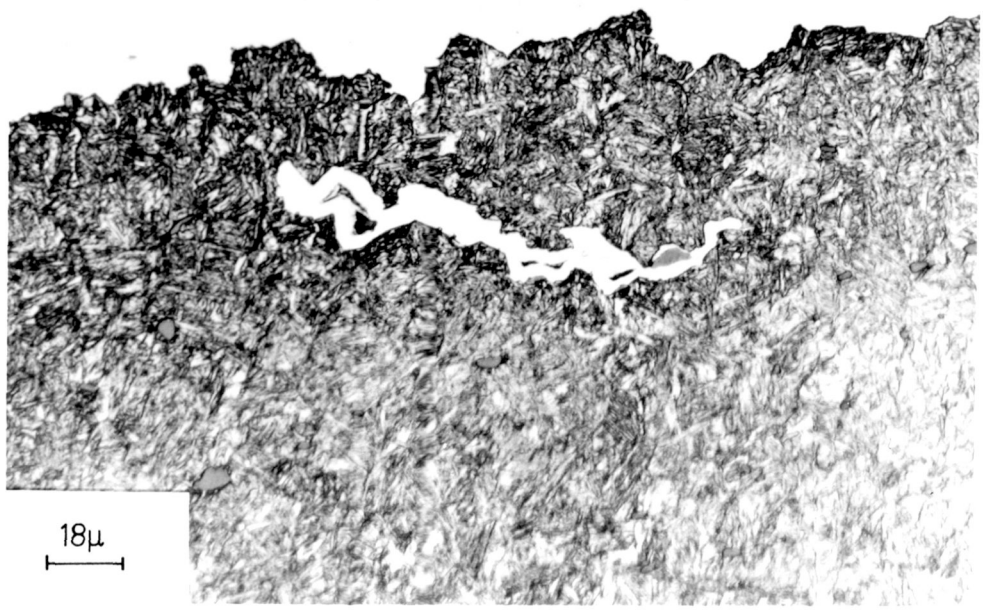


Fig. 5.46 *Cracking ahead of the main crack as seen on a nickel plated section of the same specimen as in previous figure. Plane of view L.*

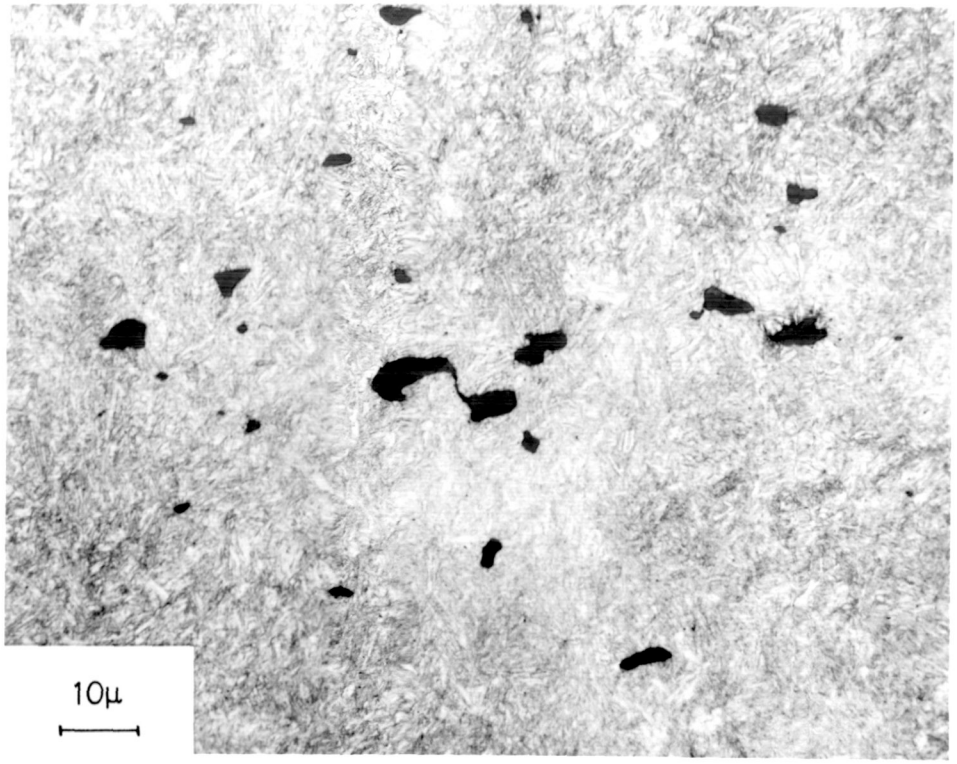


Fig.5.47 Cracking ahead of the main crack in En16M tested in 3.5% NaCl solution saturated with H_2S. Plane of view L. Orientation SL. σ_{ys}=1200MPa.

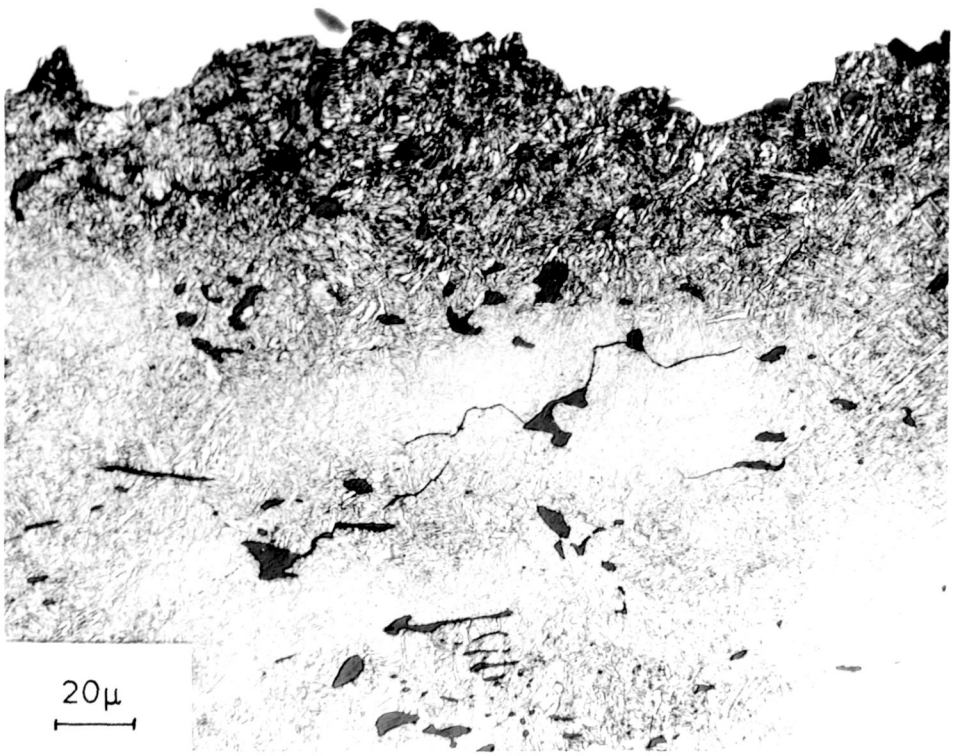


Fig.5.48 Sub-surface crack in En16M. Specimen details same as in previous figure.

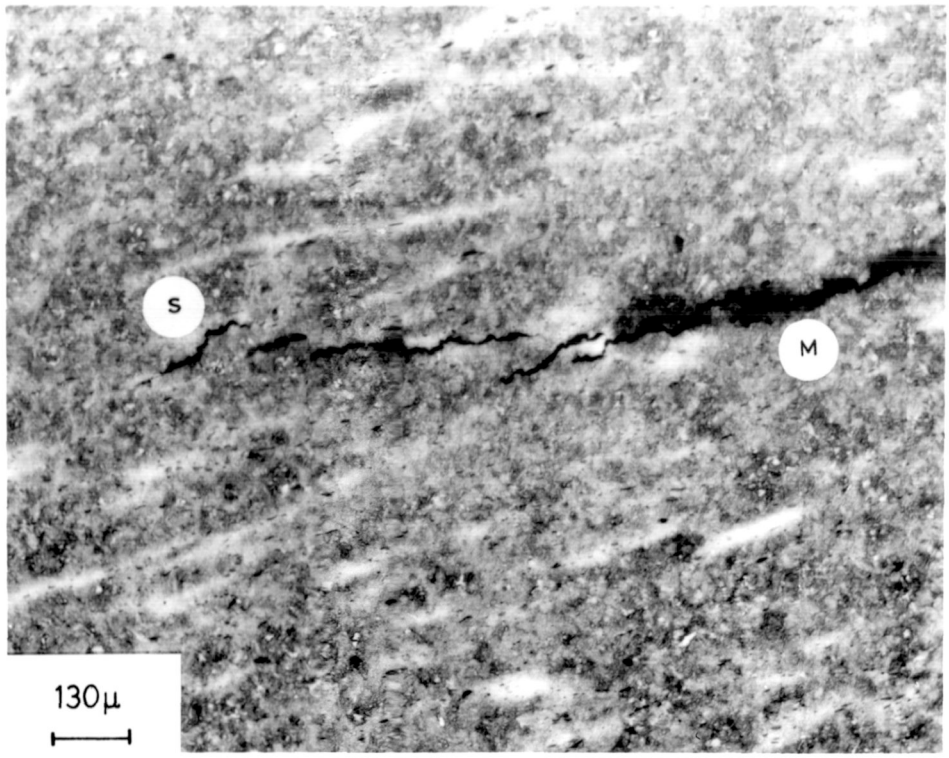


Fig.5.49a Secondary cracks ahead of the main crack(M) in En16M tested in H_2S saturated 3·5% NaCl solution. Plane of view L. Orientation ST. σ_{ys}=1200MPa.

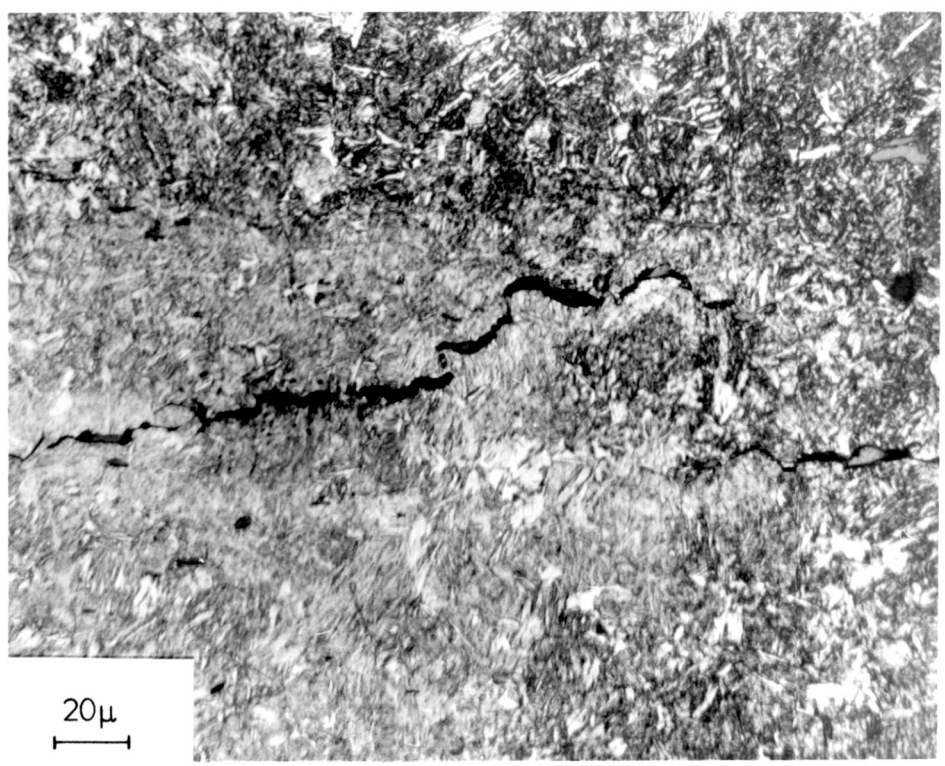


Fig.5.49b Enlarged view of one of the cracks shown in the previous figure(marked S) indicating active participation of inclusions.

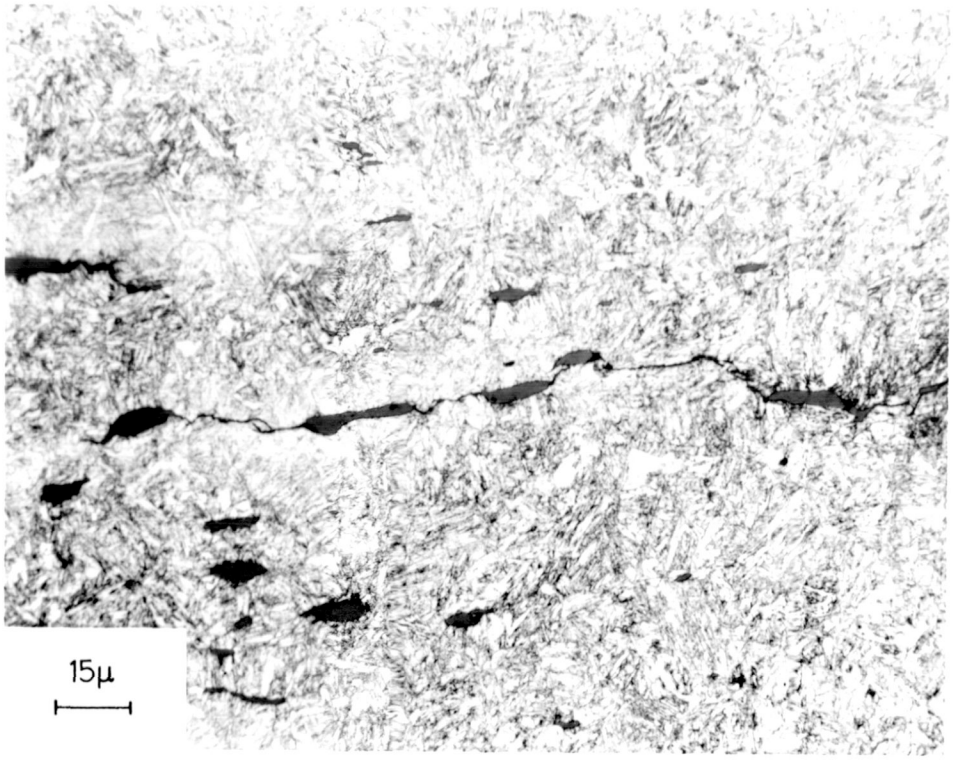


Fig.5.50 Inclusion induced cracking in En16M exposed to H_2S saturated 3.5% NaCl solution. Plane of view L. σ_{ys} = 800MPa.

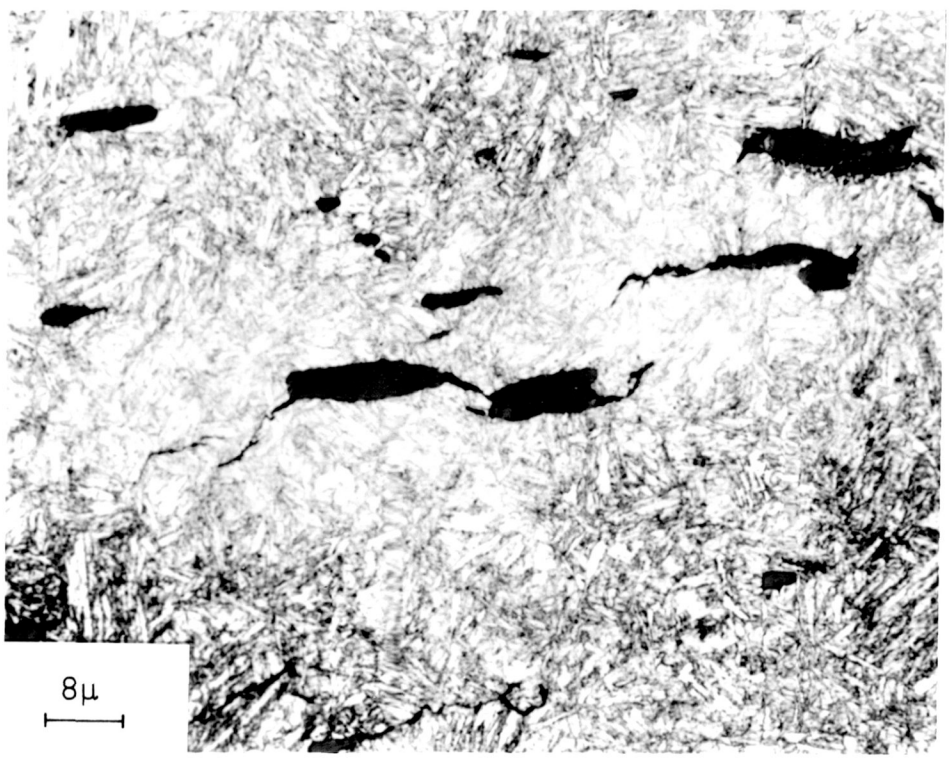


Fig.5.51 Effect of interaction between inclusions on cracking in En16M exposed to H_2S saturated 3.5% NaCl solution. Plane of view L. σ_{ys} = 800MPa.

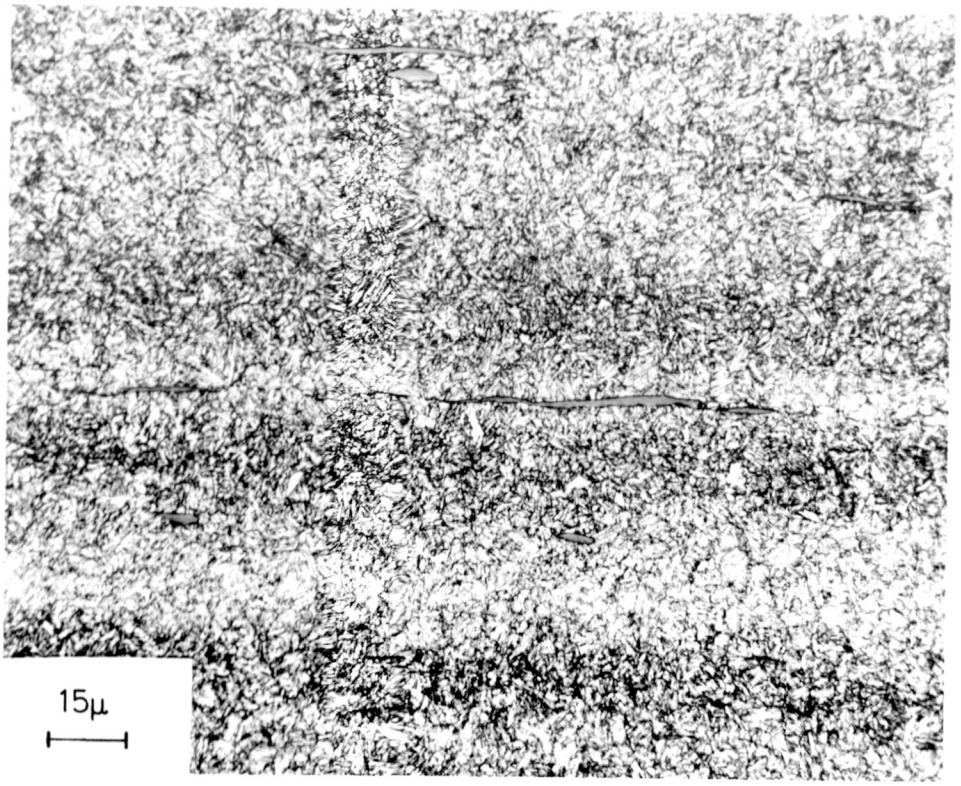


Fig.5.52 Cracks emanating from inclusions in En16 exposed to H_2S saturated 3.5% NaCl solution. Plane of view T. σ_{ys}=900MPa.

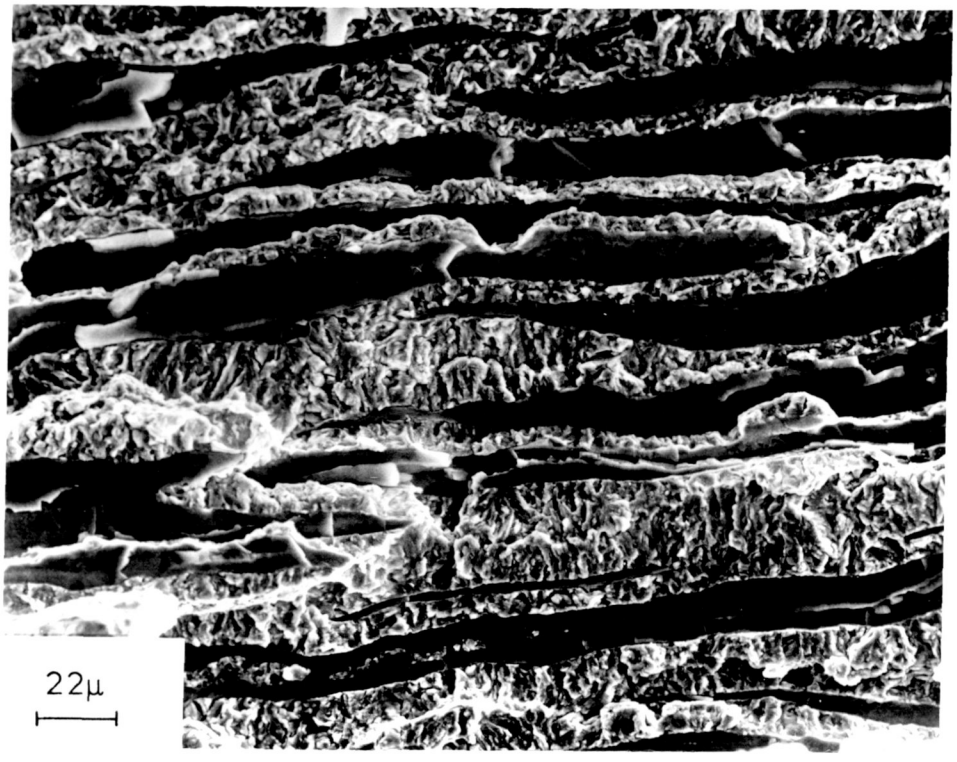


Fig.5.53 Fracture surface associated with an internal crack in En16M exposed to H_2S saturated 3.5% NaCl solution. σ_{ys}=600MPa.

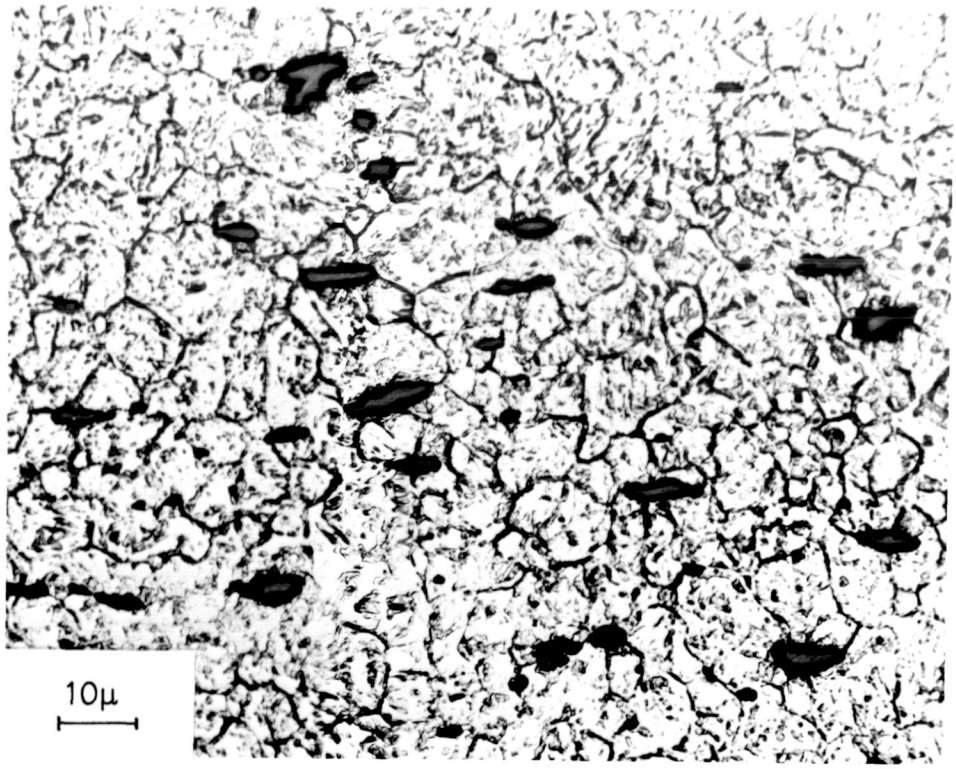


Fig. 5.54 Location of MnS inclusions in relation to the prior austenite grain boundaries in En16M. Plane of view L.

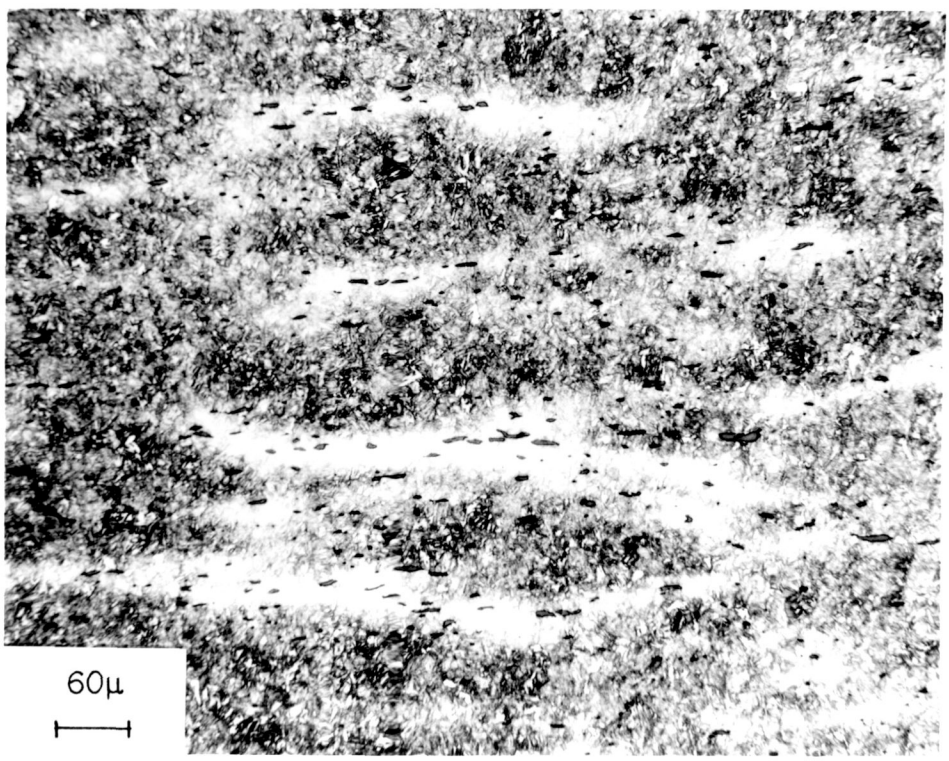


Fig. 5.55 Association of MnS inclusions with inter-dendritic segregation in En16M. Plane of view L

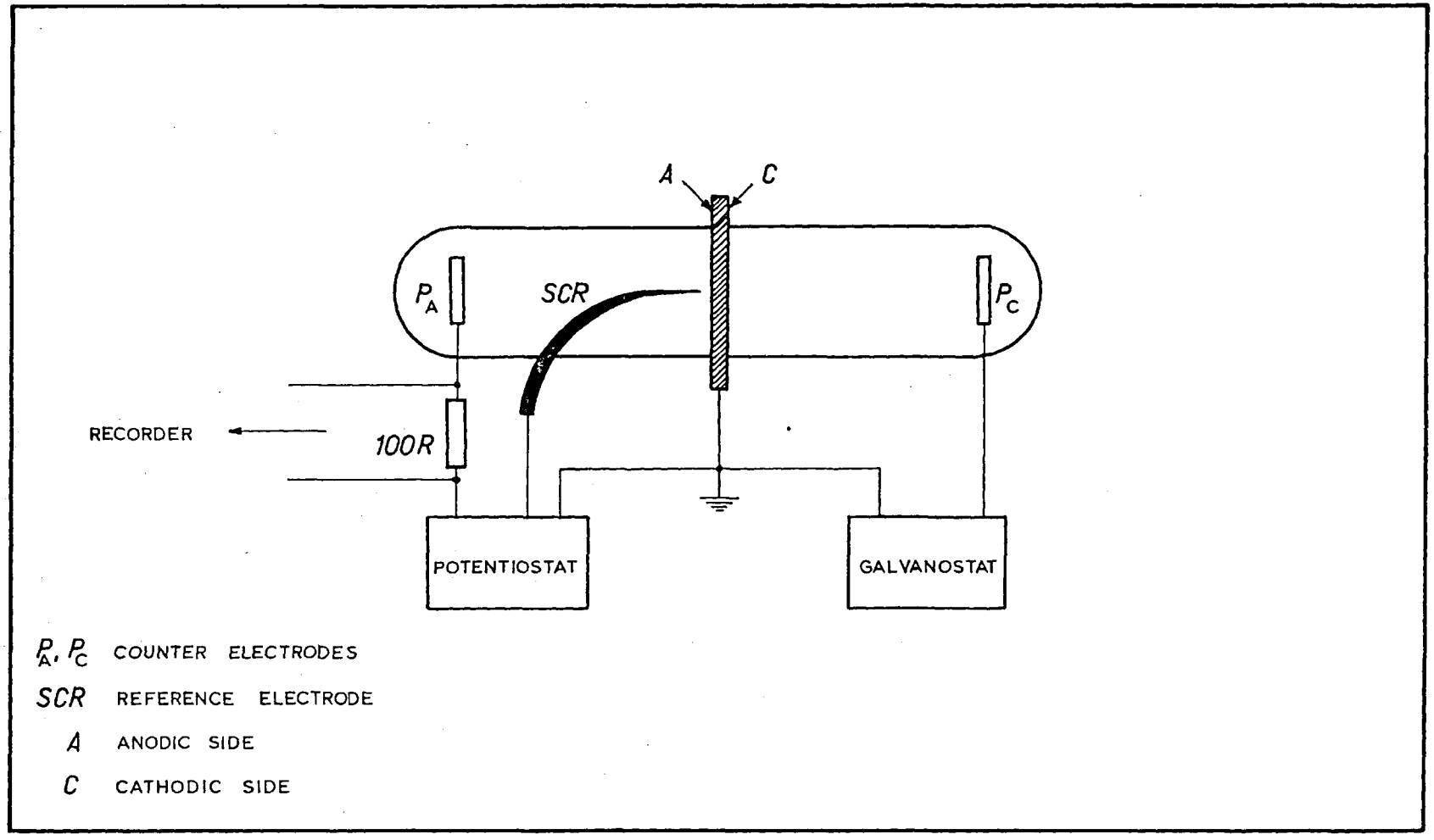


Fig. 6·1 Electrical Circuit For Studying Permeation Behaviour.

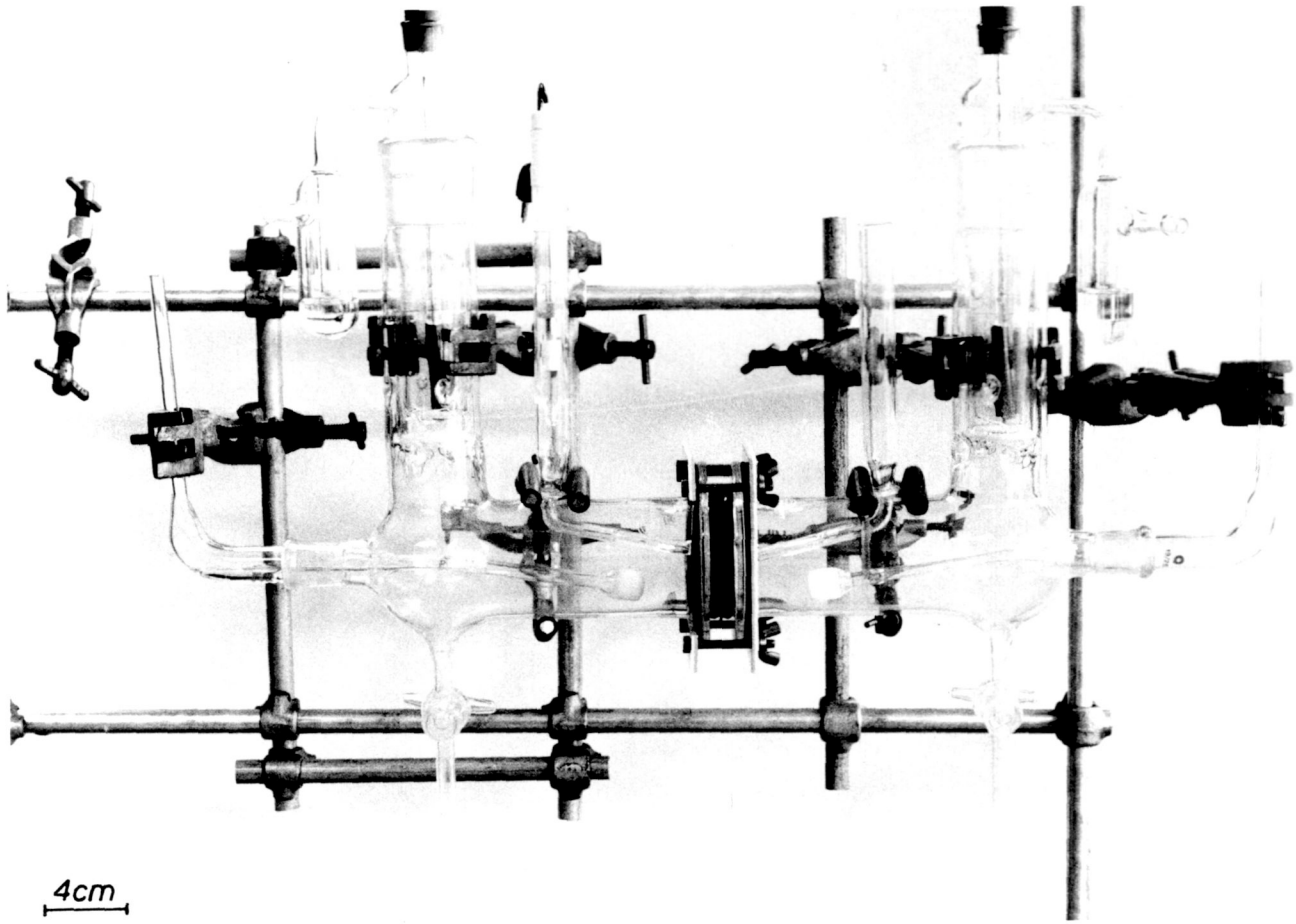


Fig. 6·2 Permeation apparatus used for studying hydrogen transport behaviour.

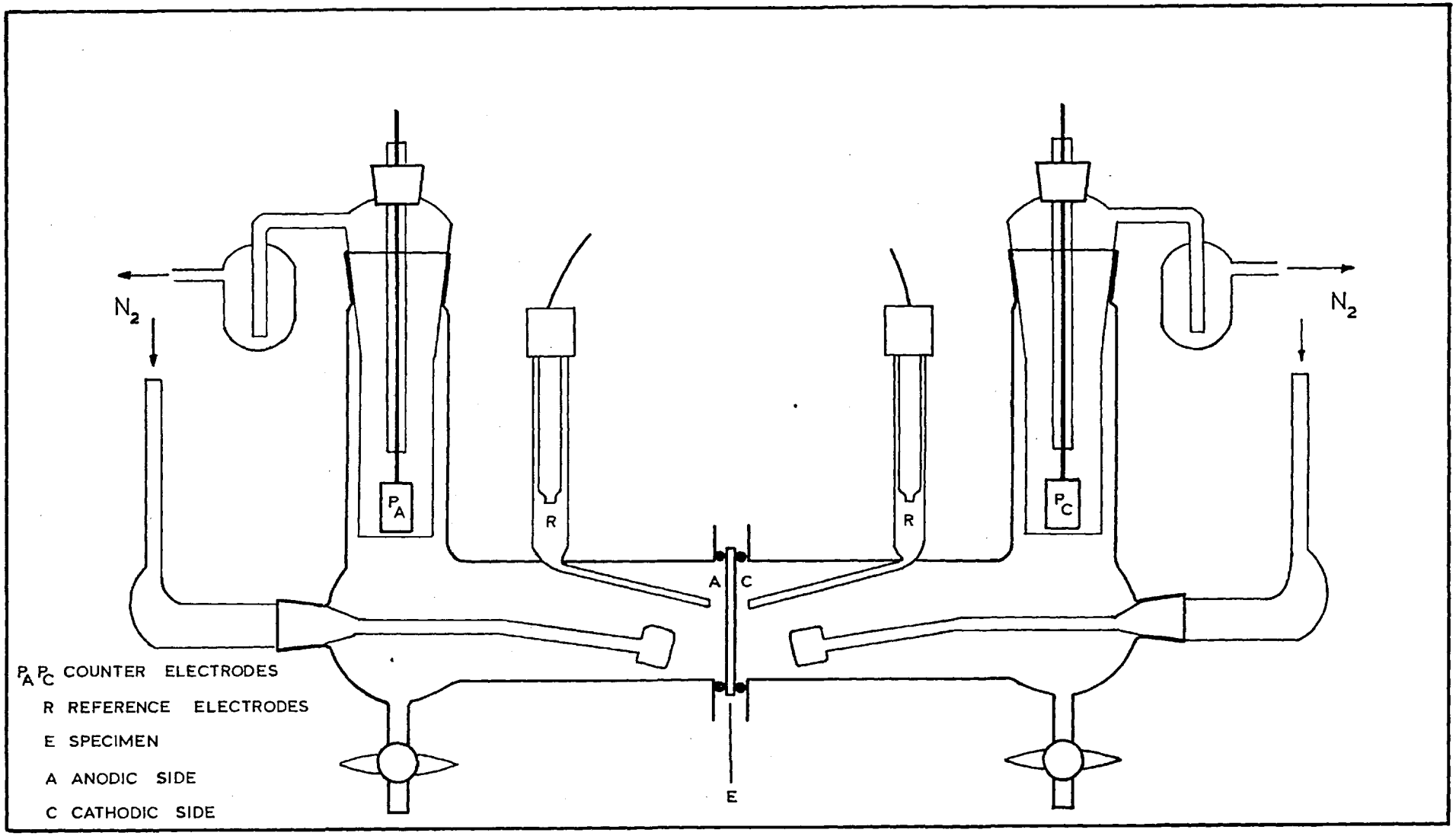


Fig. 6·3 Permeation Cell.

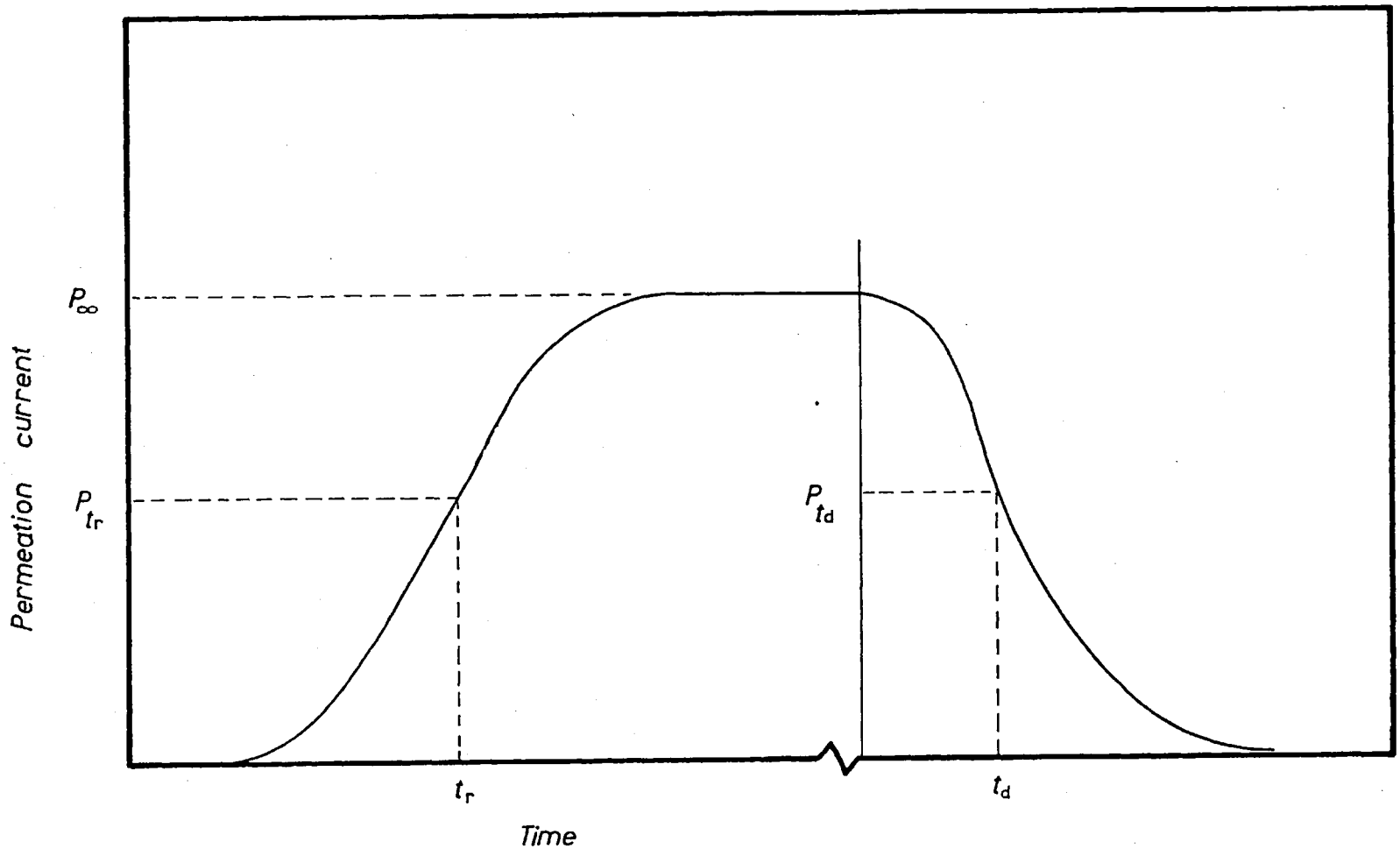


Fig. 6·4 Schematic rise and decay transients

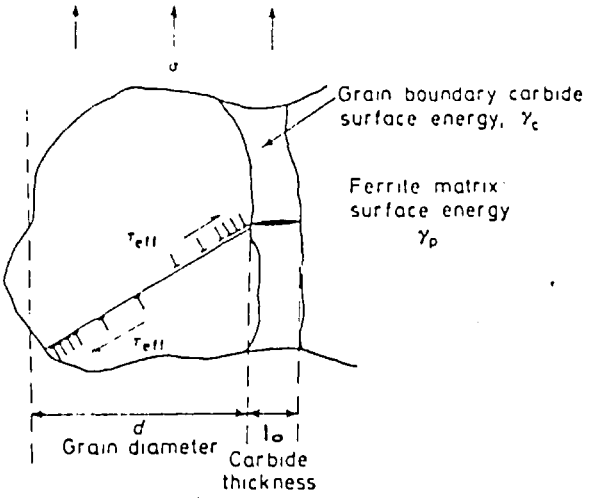


Fig. 7.1 Smith's model for cleavage fracture in mild steel (SMITH, 1966)

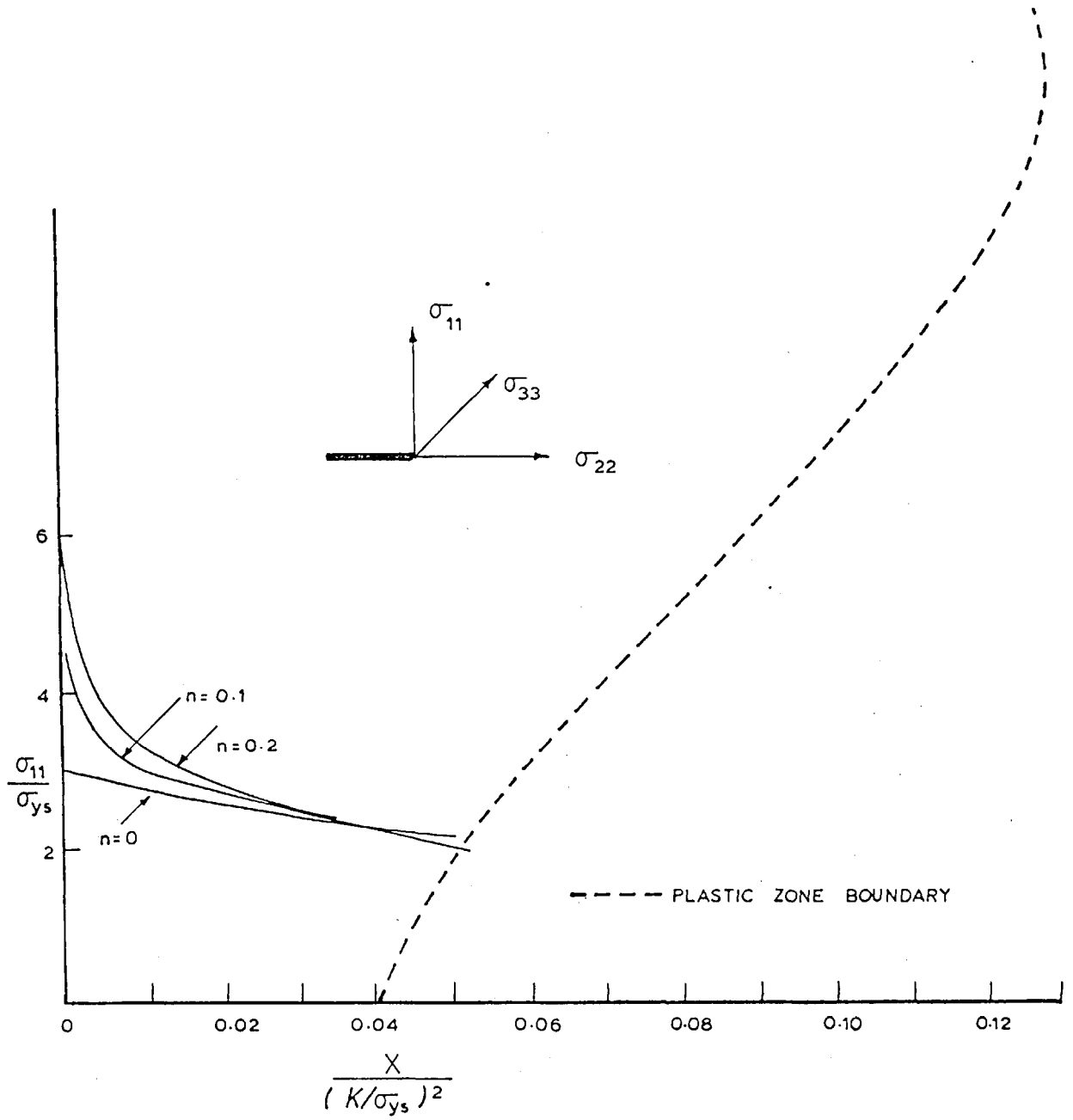


Fig. 7.2 $\bar{\sigma}_{11}$ *stress distribution ahead of a stationary crack under monotonic loading.* (TRACEY, 1976)

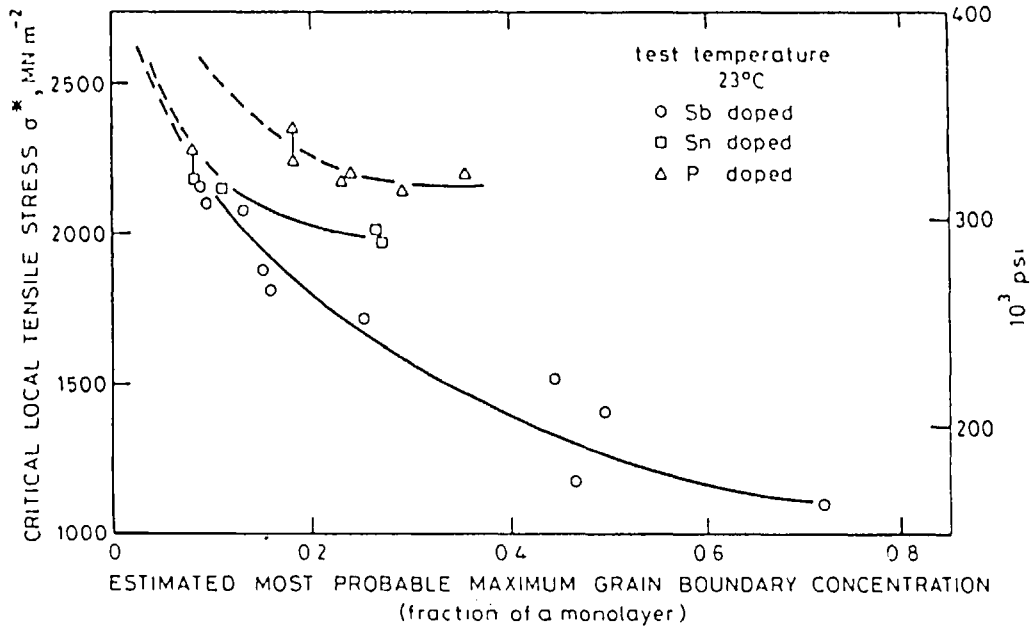


Fig. 7.3 Variation of fracture stress with local intergranular concentration of Sb, Sn and P (JOKL et al, 1980)

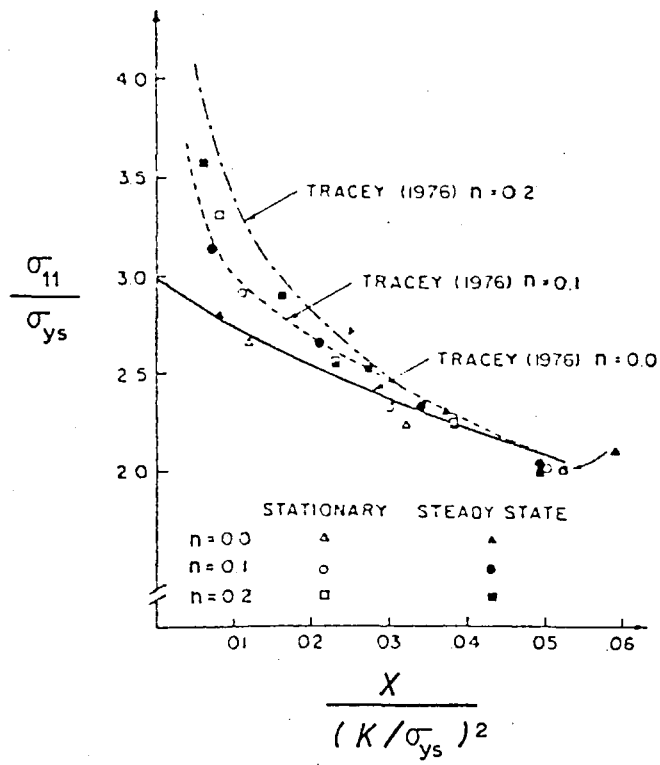


Fig. 7.4 Comparison of σ_{11} stress distribution ahead of a growing crack and a stationary crack (SORENSEN, 1979)

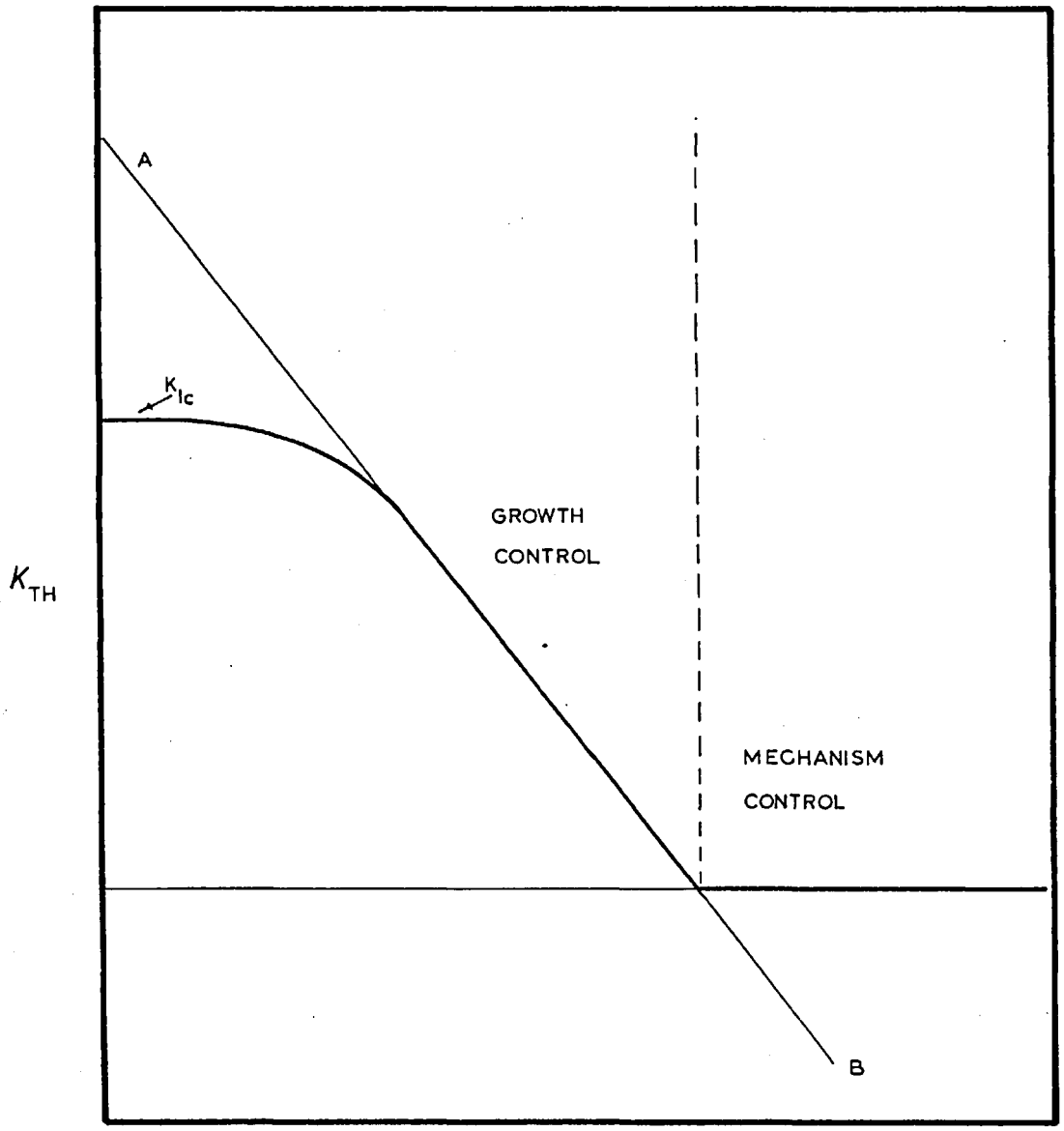


Fig. 7·5 Effect of hydrogen activity on K_{TH}

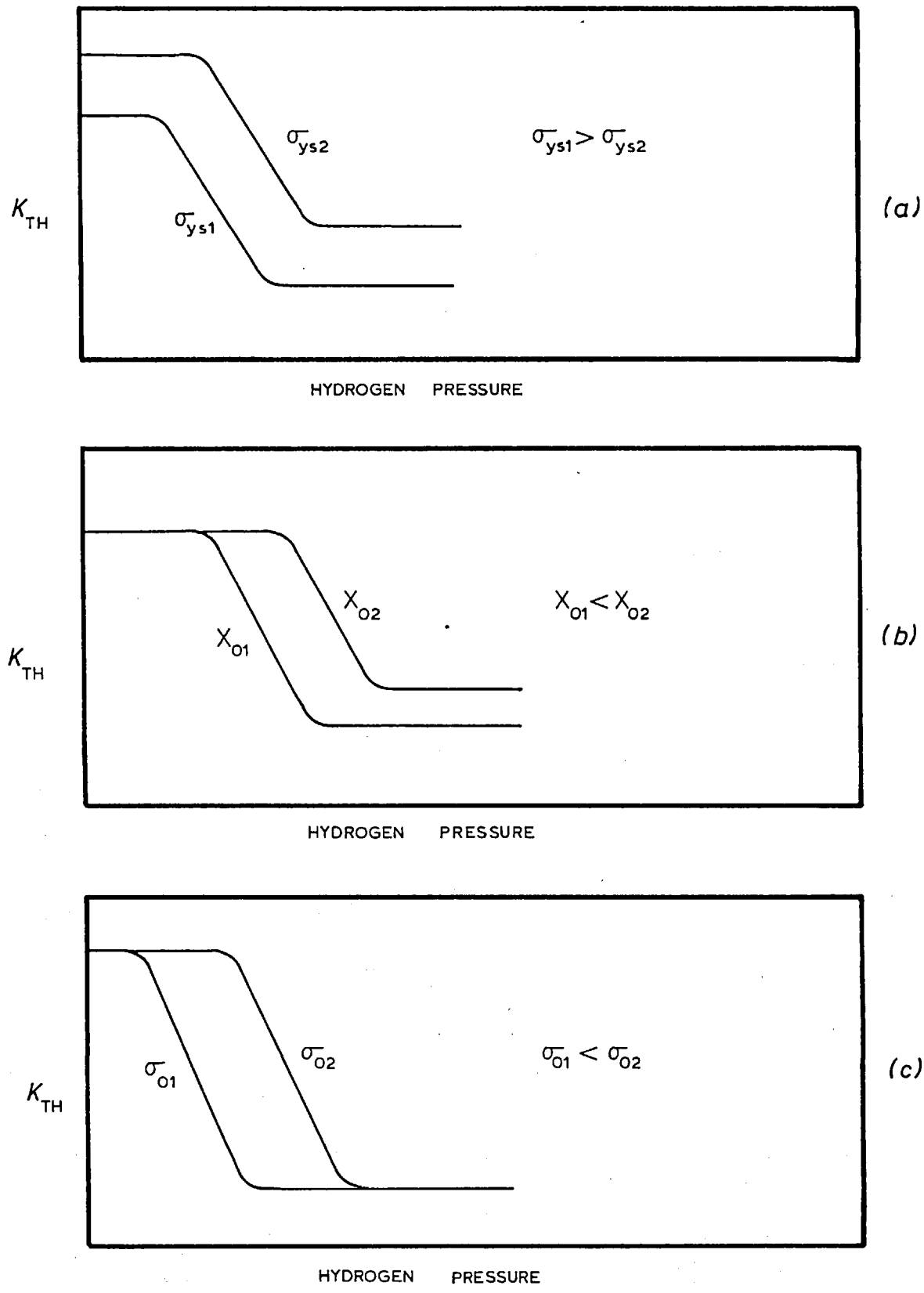


Fig. 7·6 Effect of changing yield strength (σ_{ys}), critical distance (X_o) and the inherent fracture strength of the matrix (σ_o) on the K_{TH} vs hydrogen activity relationship

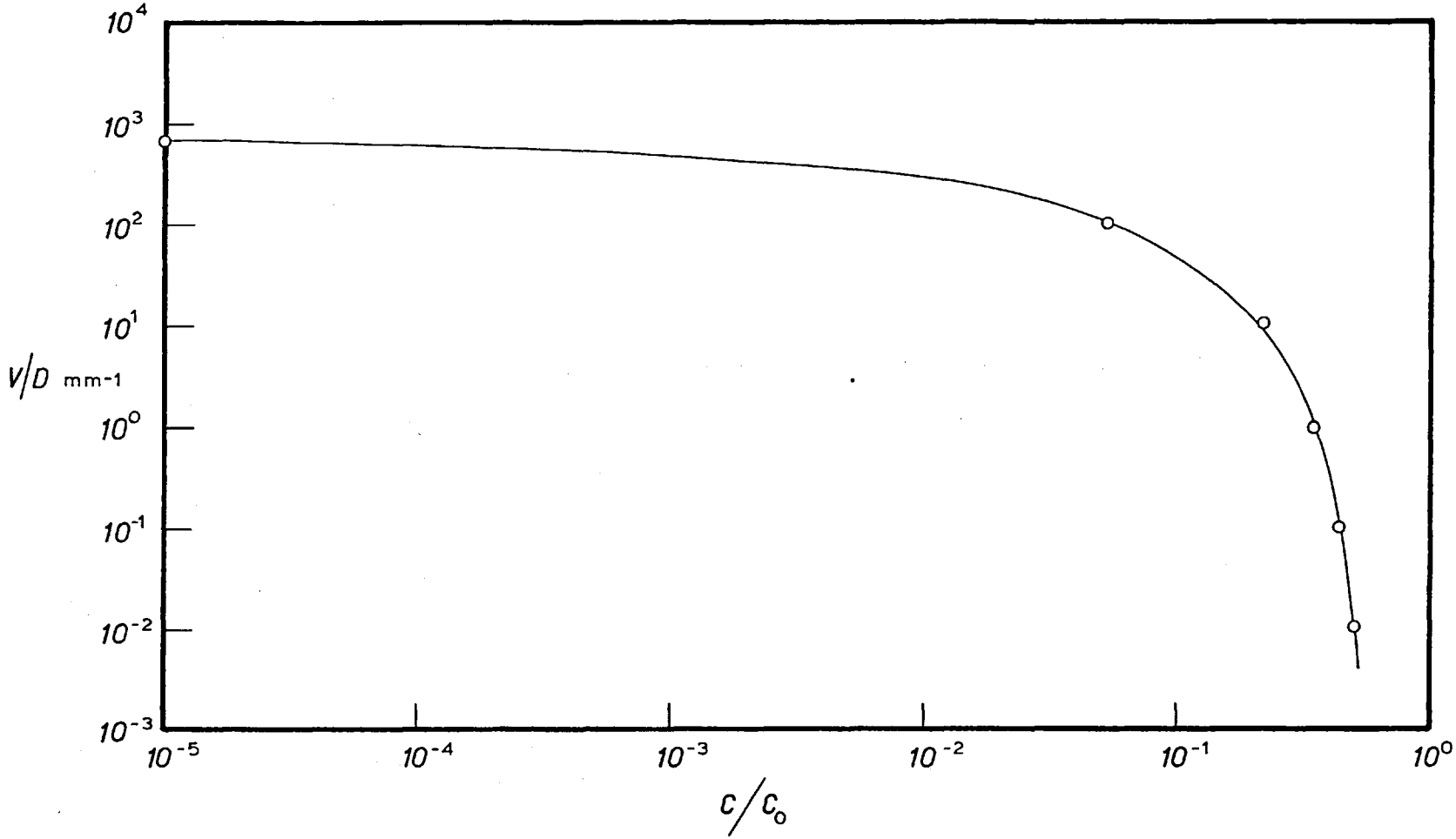


Fig. 7.7 Relative hydrogen concentration ahead of a growing crack as a function of V/D

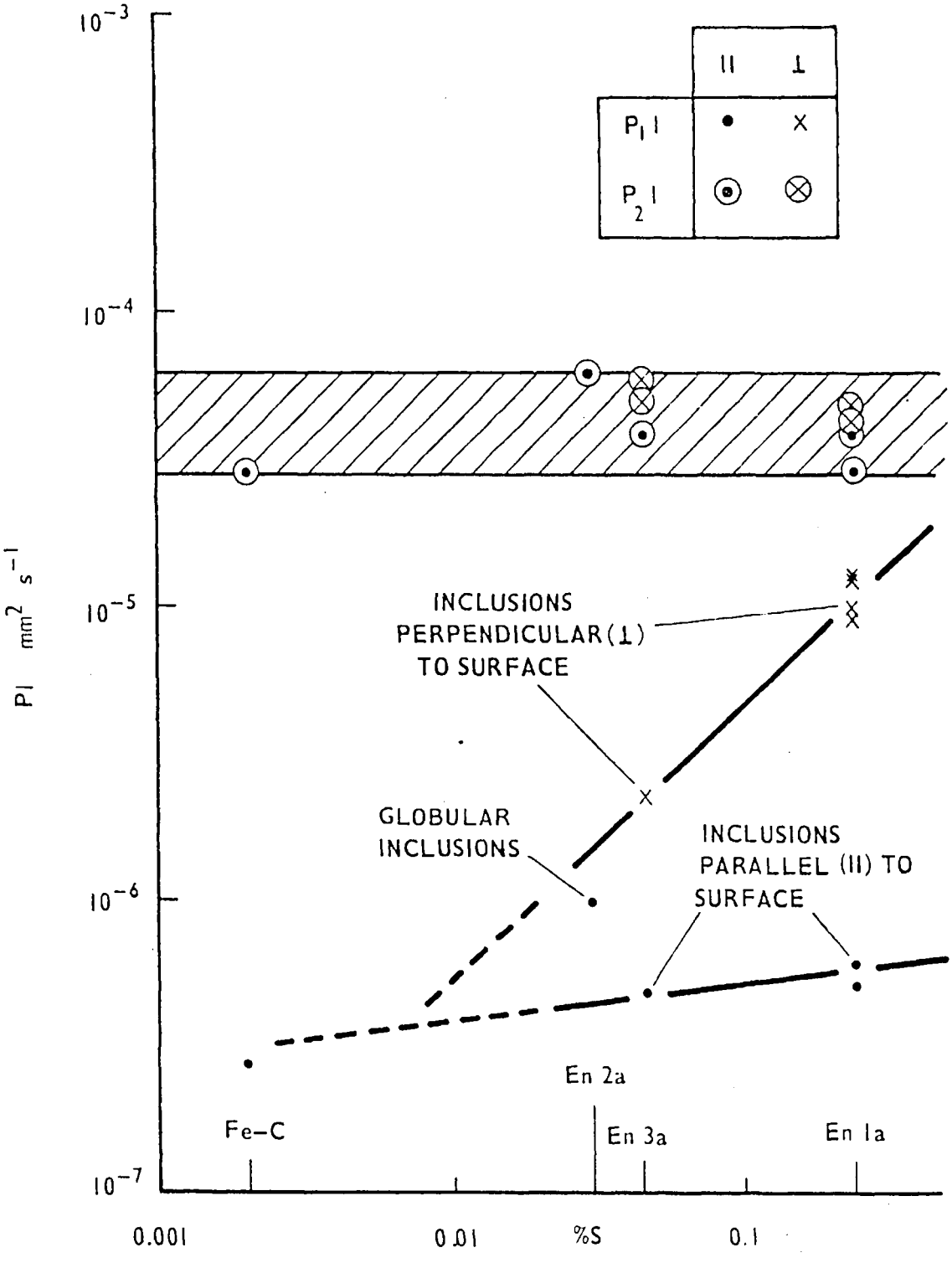


FIG. 7·8 NORMALISED STEADY STATE PERMEATION RATES $P_1 l$ (NO H_2S ADDED), $P_2 l$ (~ 10 ppm H_2S ADDED) FOR SPECIMENS CHARGED AT 20 μA mm^{-2} AT 2°C AS FUNCTION OF SULPHUR CONTENT OF ALLOY

(PUMPHREY, 1980)

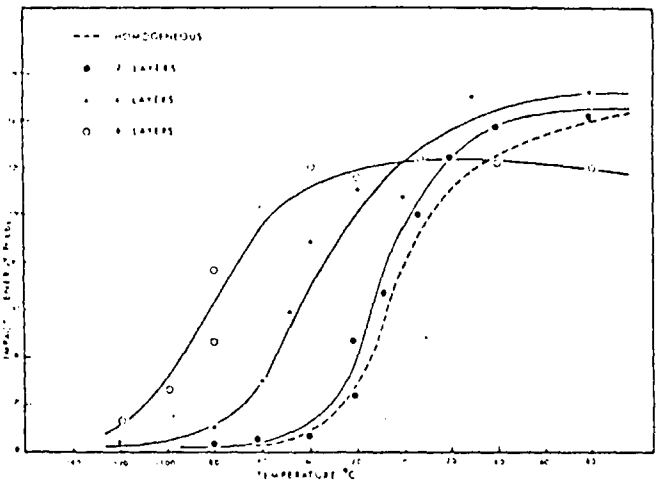


Fig. 7.9 – Energy-temperature curves for multiple laminates of the crack-divider type. Specimens were bonded with silver solder. (EMBURY et al 1967)

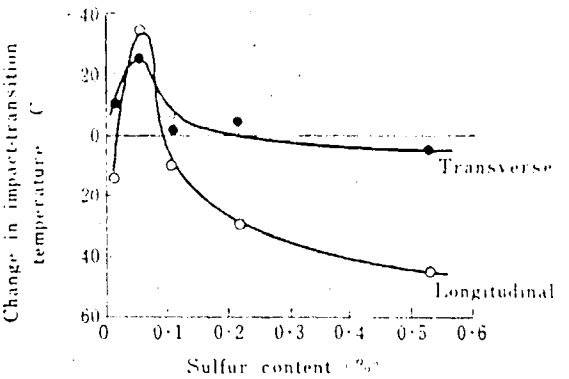


Fig.7.10 Effect of sulfur content on impact-transition temperature. (PICKERING, 1979)

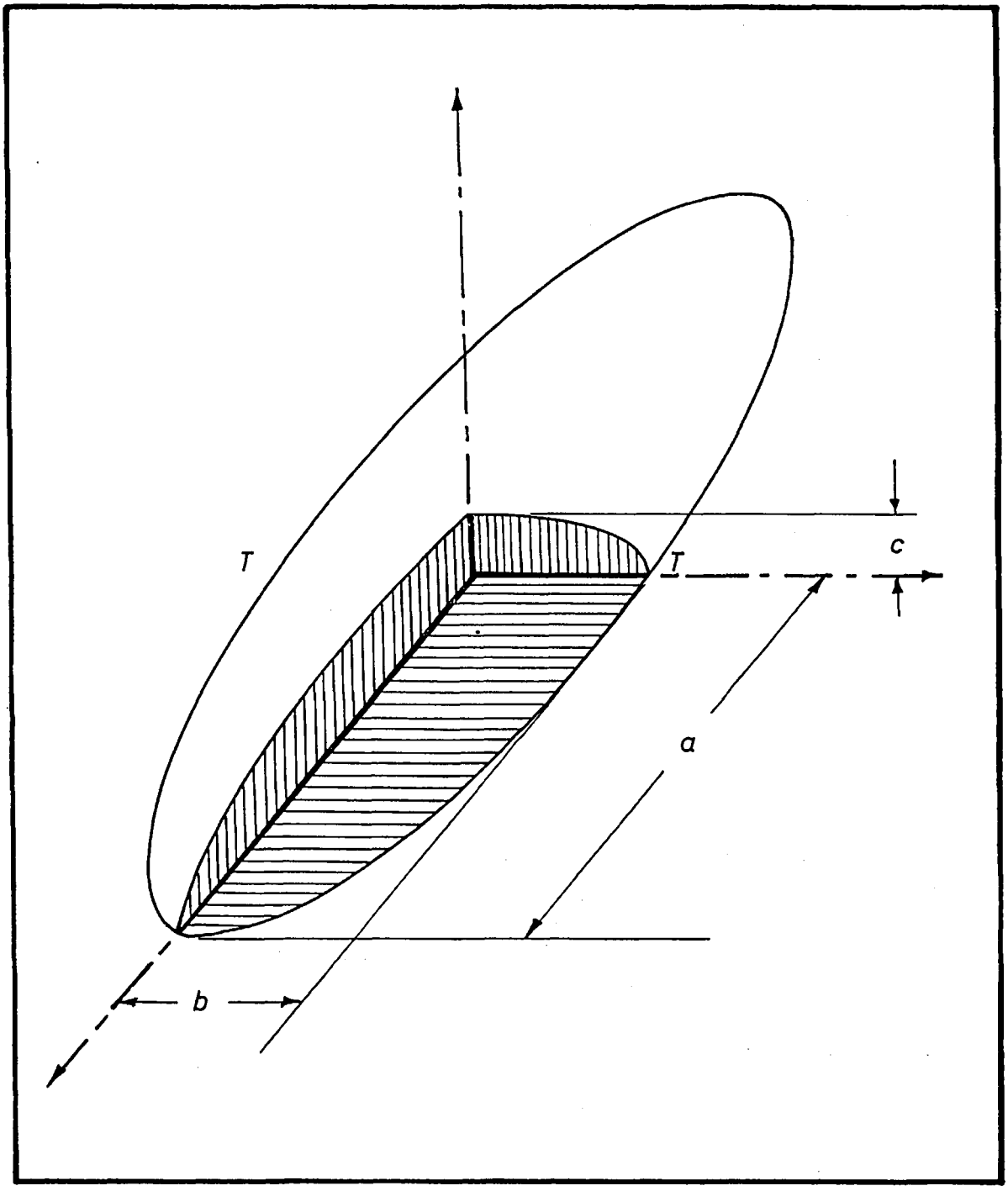


Fig. 7·11 Ellipsoidal inclusion

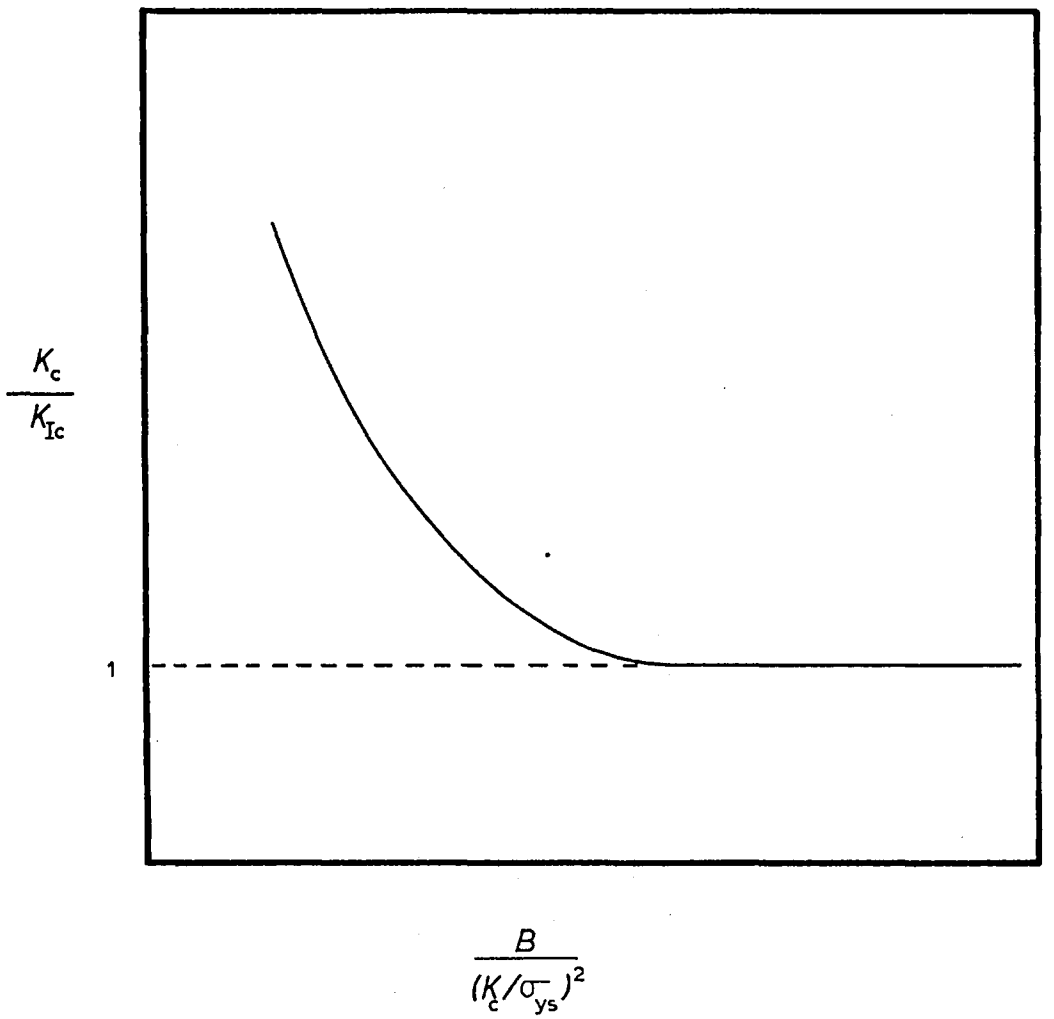


Fig. 7·12 Thickness dependence of K_c (fracture toughness)

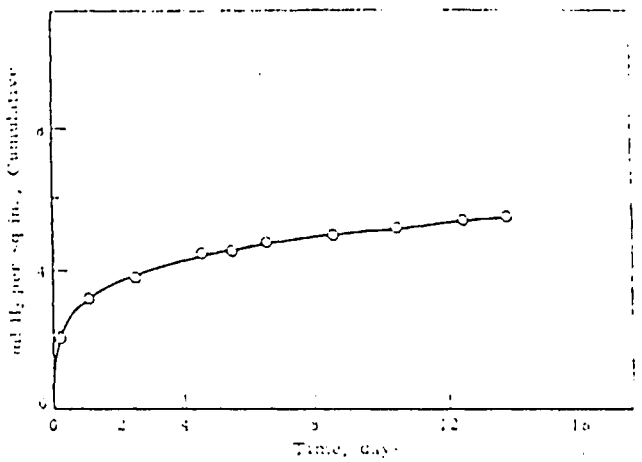


Fig.7.13 -Cumulative hydrogen transmission through steel in aqueous hydrogen sulfide solution. Conditions: Steel capsule, distilled water, one atmosphere hydrogen sulfide, 40 degrees C. (SKEI et al, 1953)

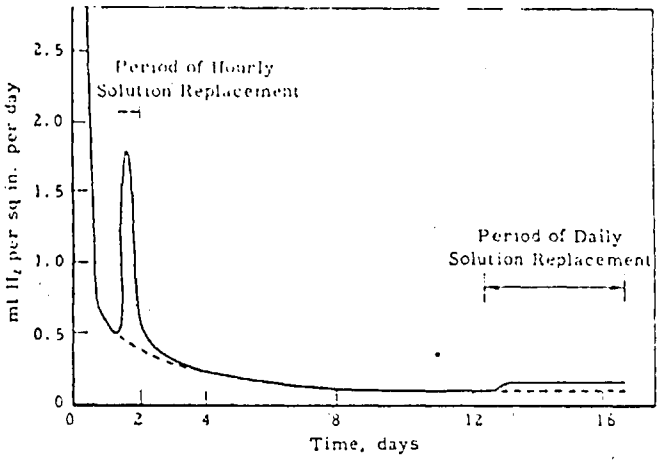


Fig.7.14 Effect of solution replacement on hydrogen transmission rate through steel in aqueous hydrogen sulfide solution. Dotted lines are reference for no solution replacement Conditions: Steel capsule, distilled water, one atmosphere hydrogen sulfide, 40 degrees C. Eight hourly replacements of solution in period indicated. Daily solution replacement on 13, 14, 15 and 16 days. (SKEI et al, 1953)

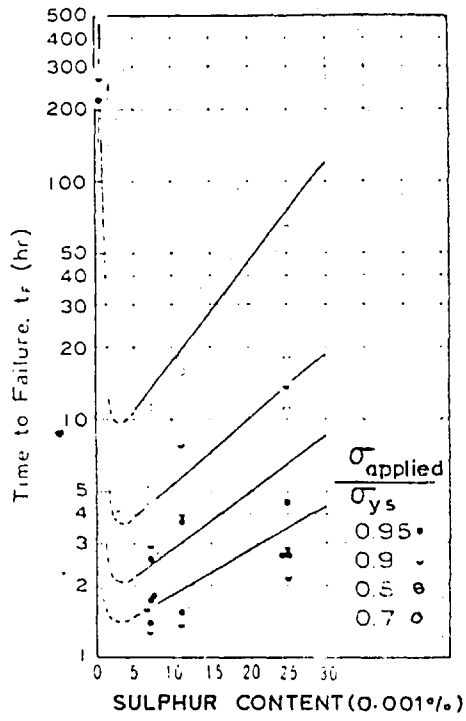


Fig.7.15 *Effect of sulphur content on time to failure in a constant load test under electrolytic charging* (IINO, 1979)

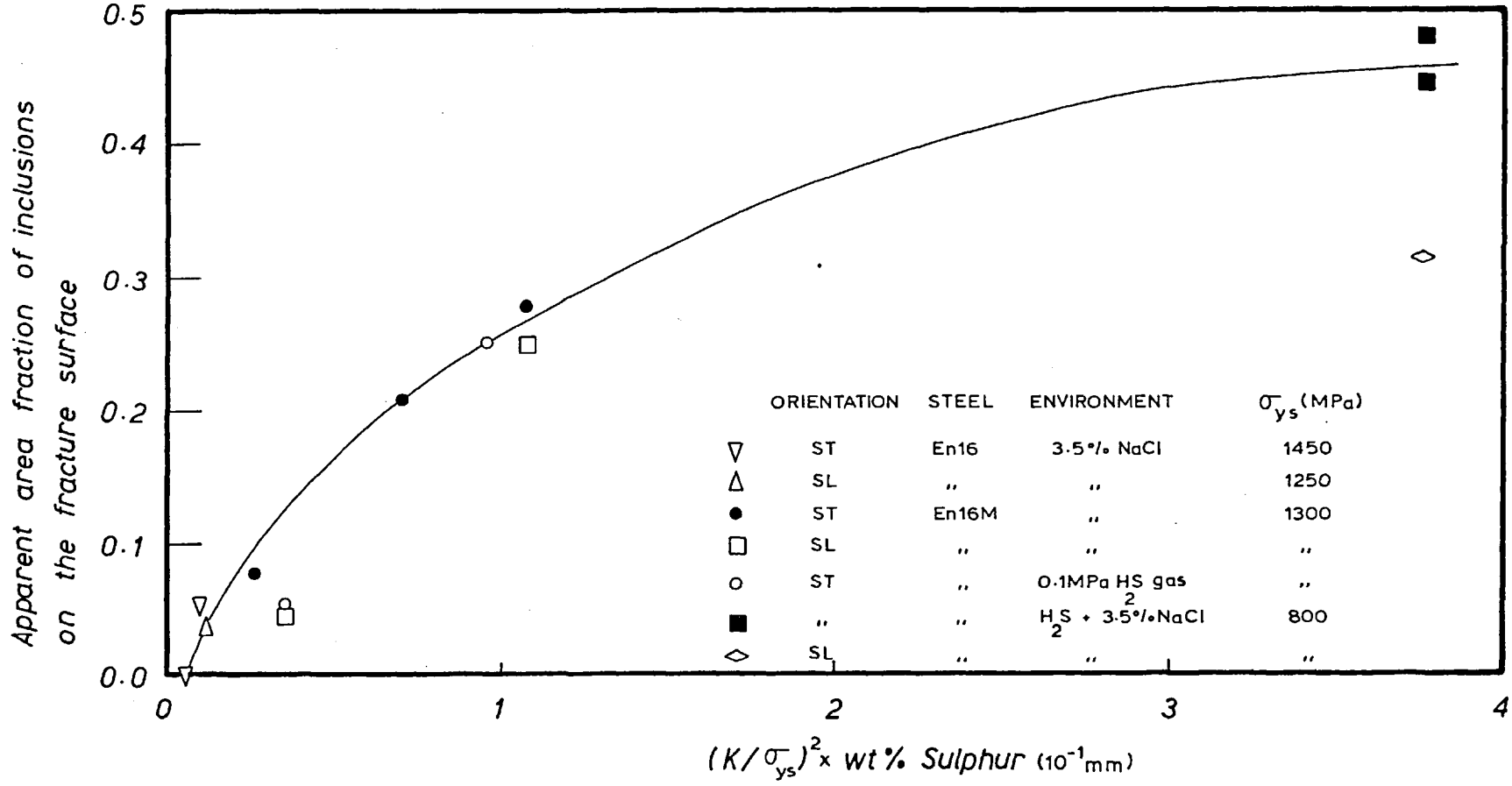


Fig. 7.16 Effect of plastic zone size and sulphur content on the apparent area fraction of inclusions seen on the fracture surfaces of the short transverse orientations.

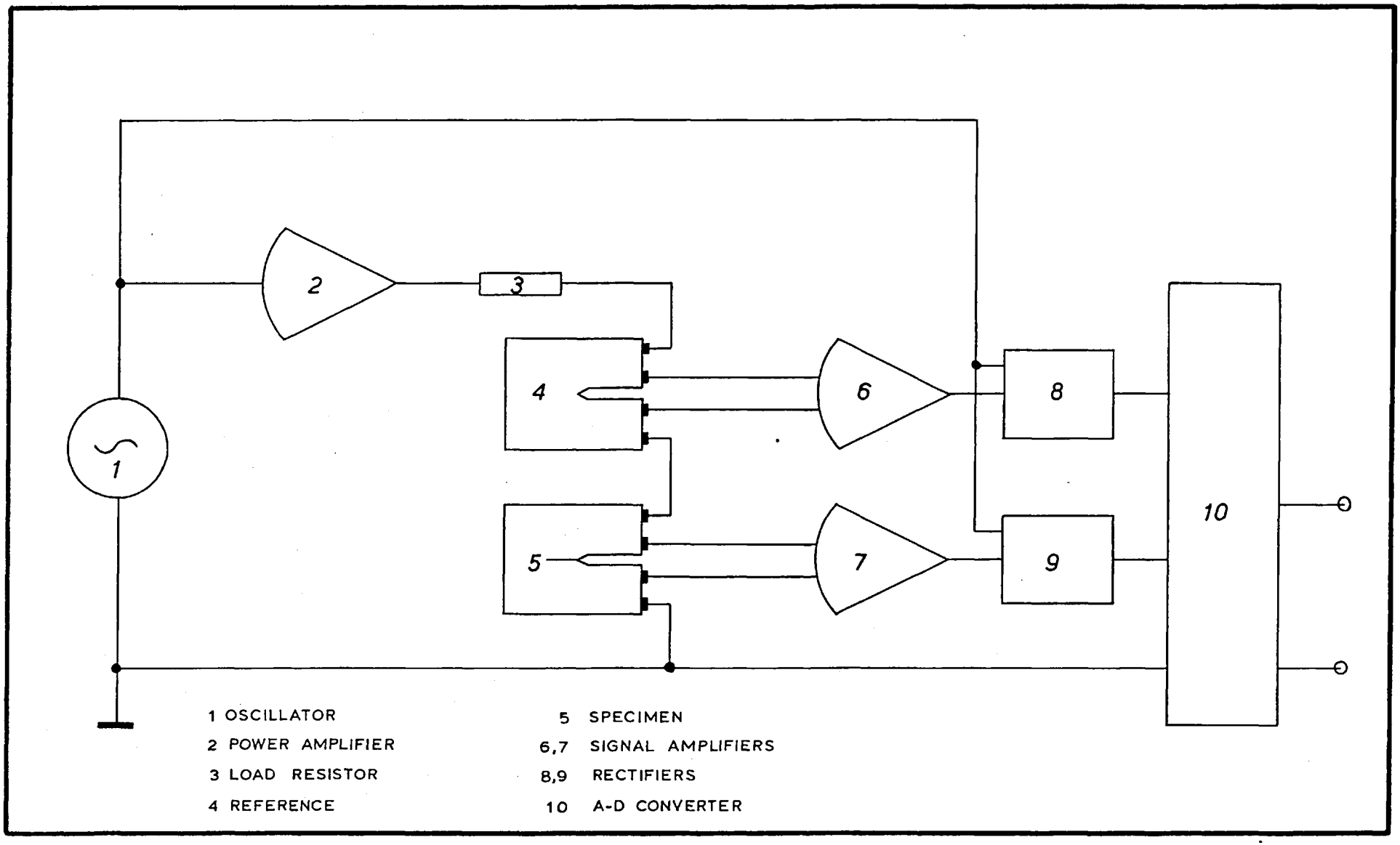


Fig. A1-1 Block diagram of the ACPD system.

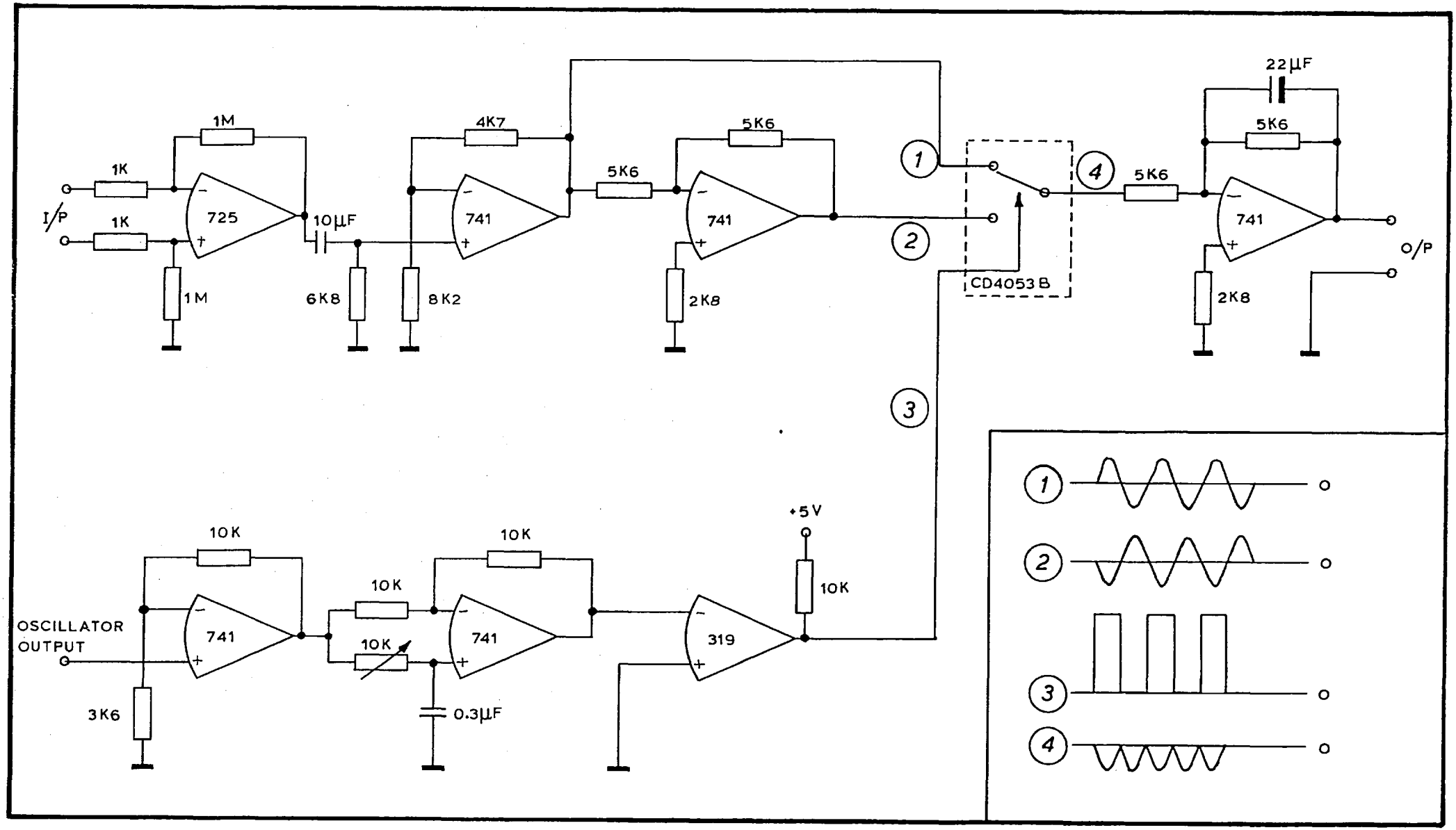


Fig. A1·2 Circuit for signal amplification and rectification

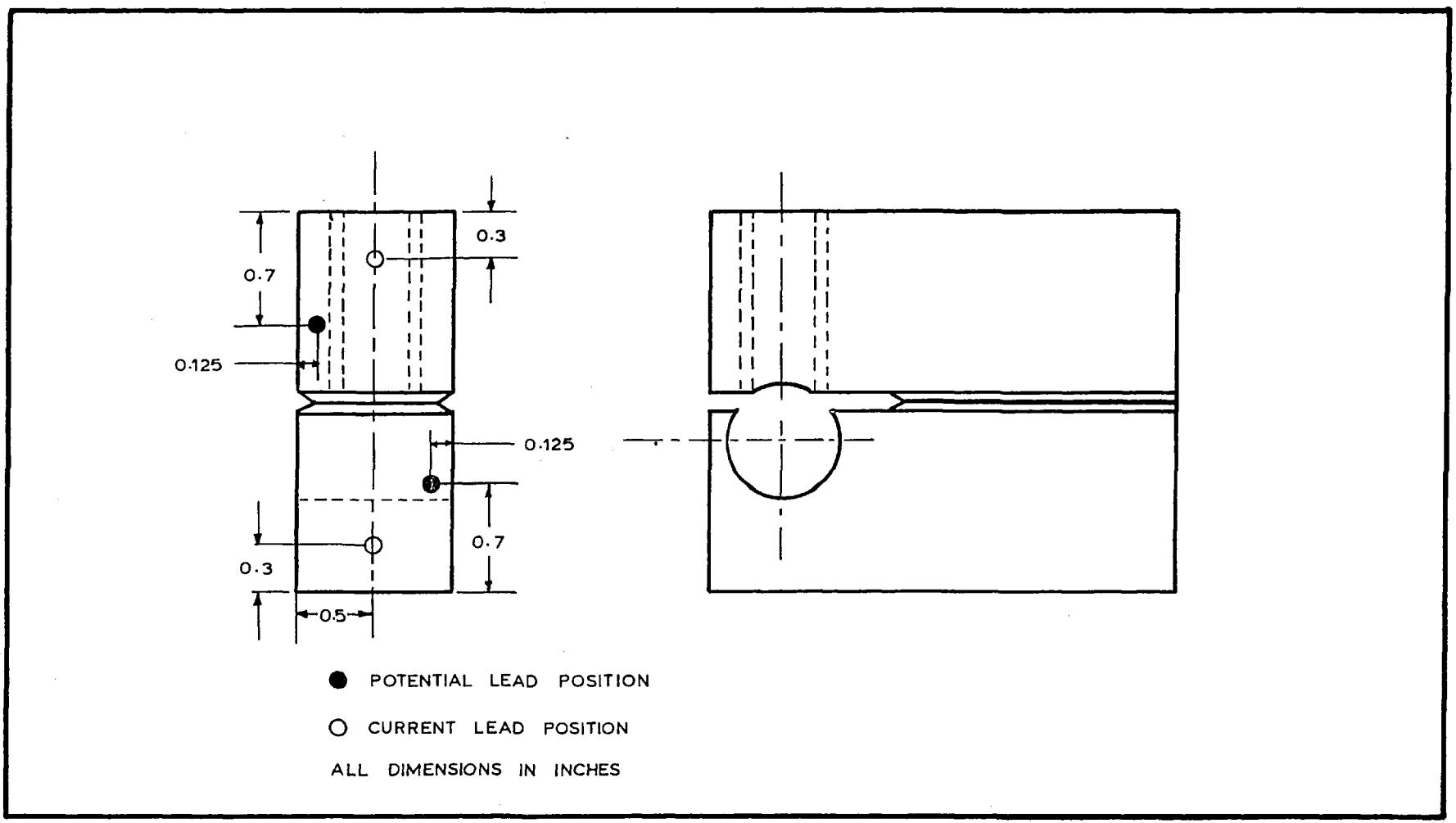


Fig. A1.3 Current and potential lead positions on WOL specimen

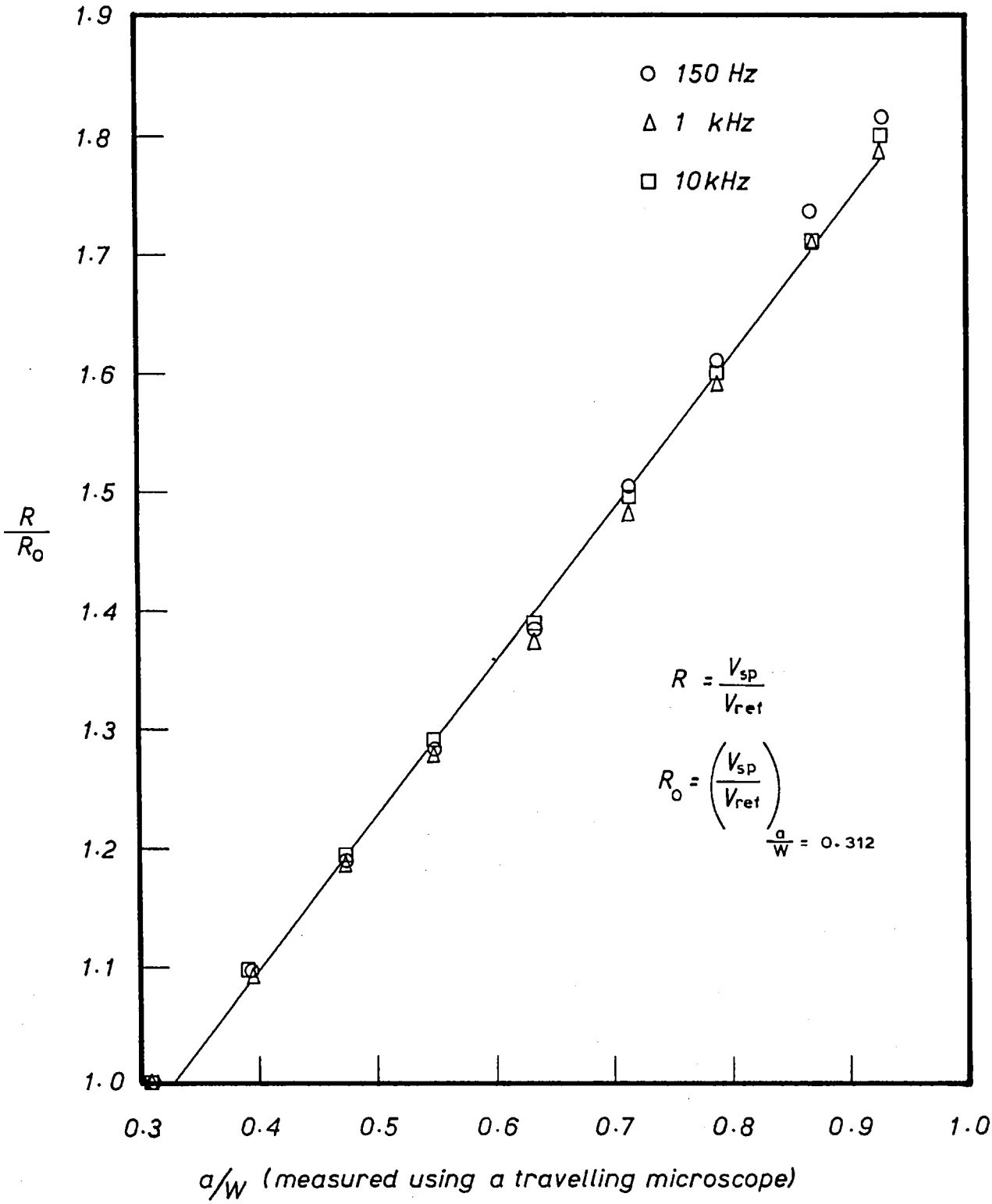


Fig. A1·4 ACPD calibration for a WOL specimen with a simulated crack.

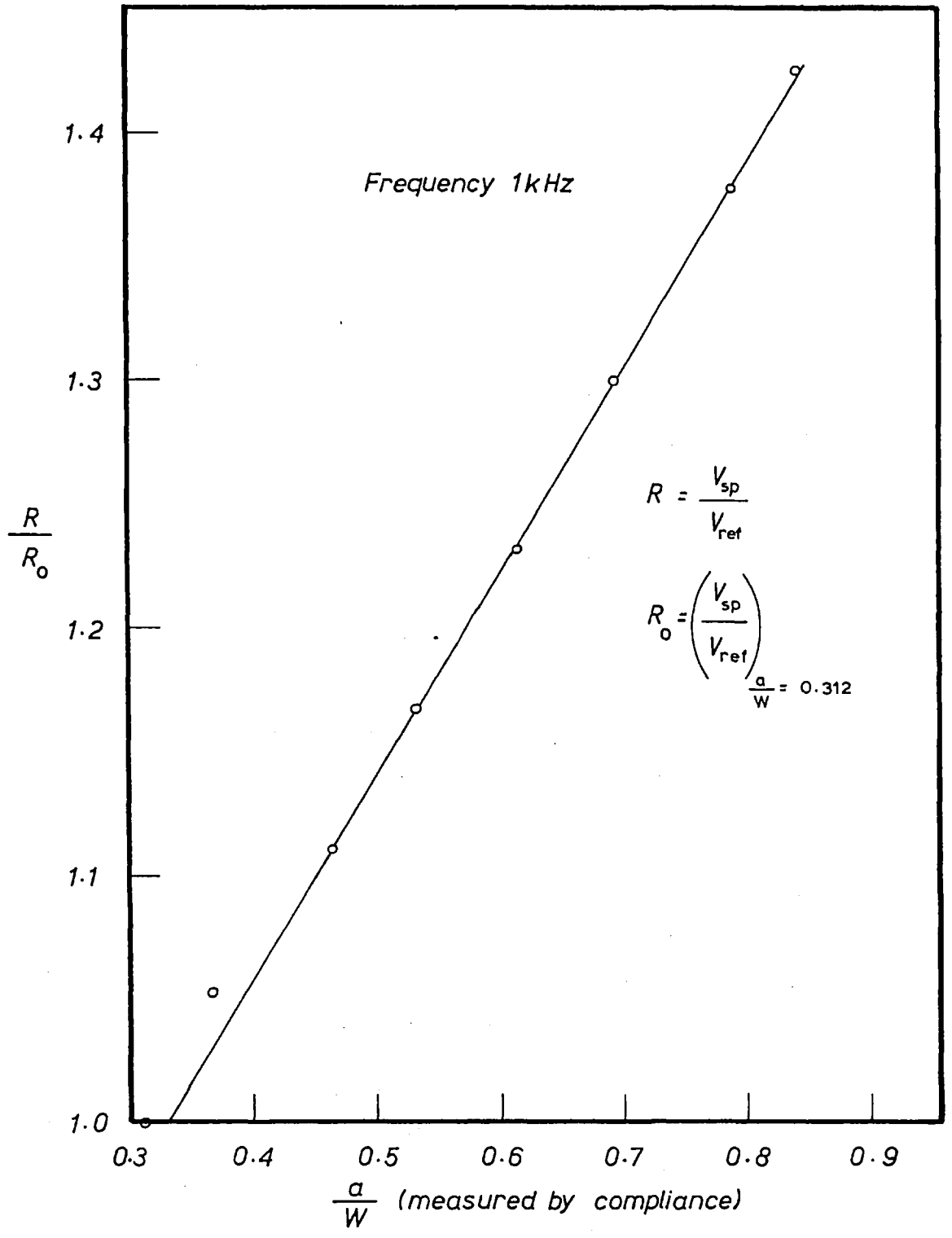


Fig. A1.5 ACPD calibration for a WOL specimen with a fatigue crack

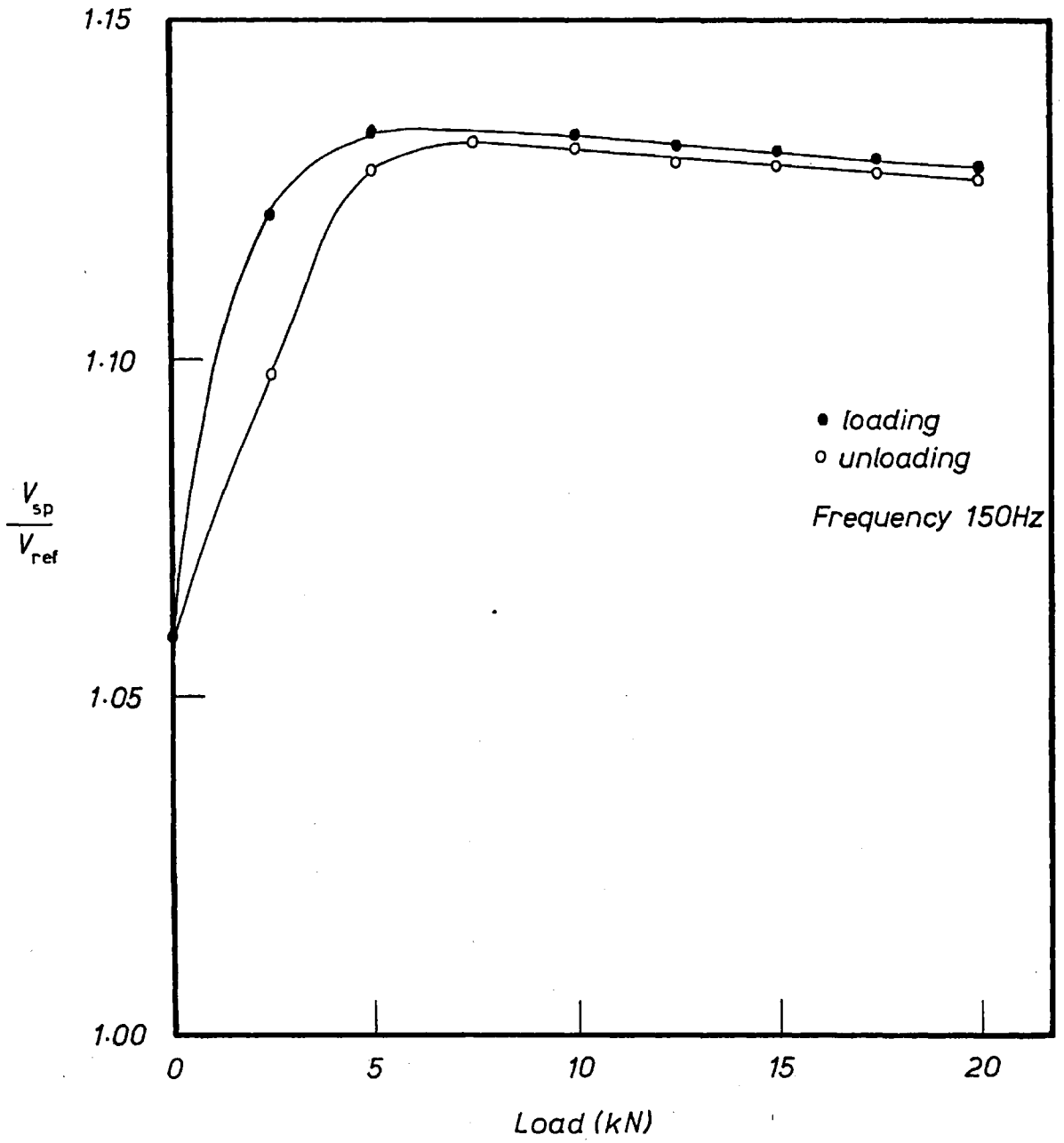


Fig. A1·6 Effect of load on the output from a fatigue cracked specimen.

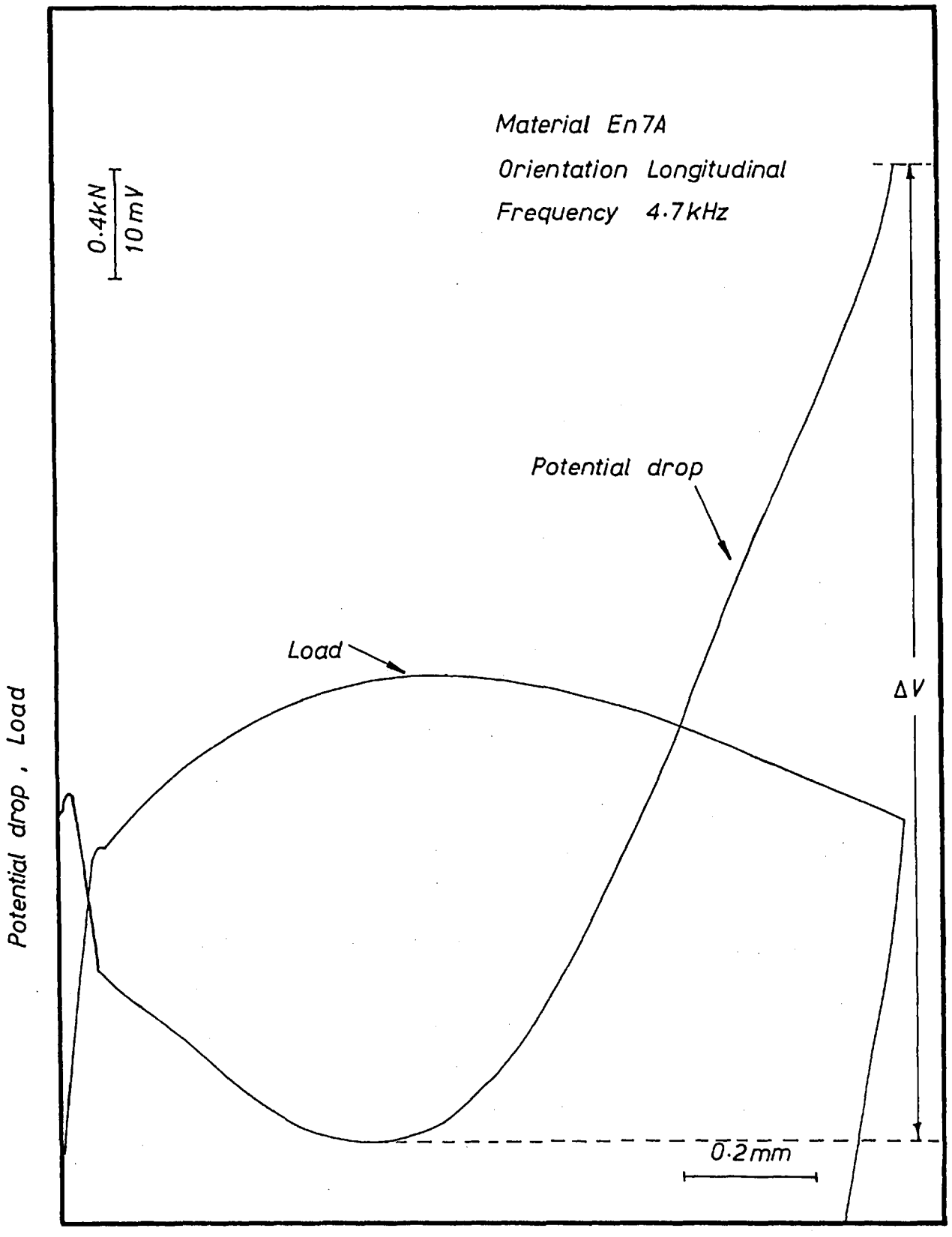


Fig. A1·7 Variation of PD and load with displacement during slow crack growth

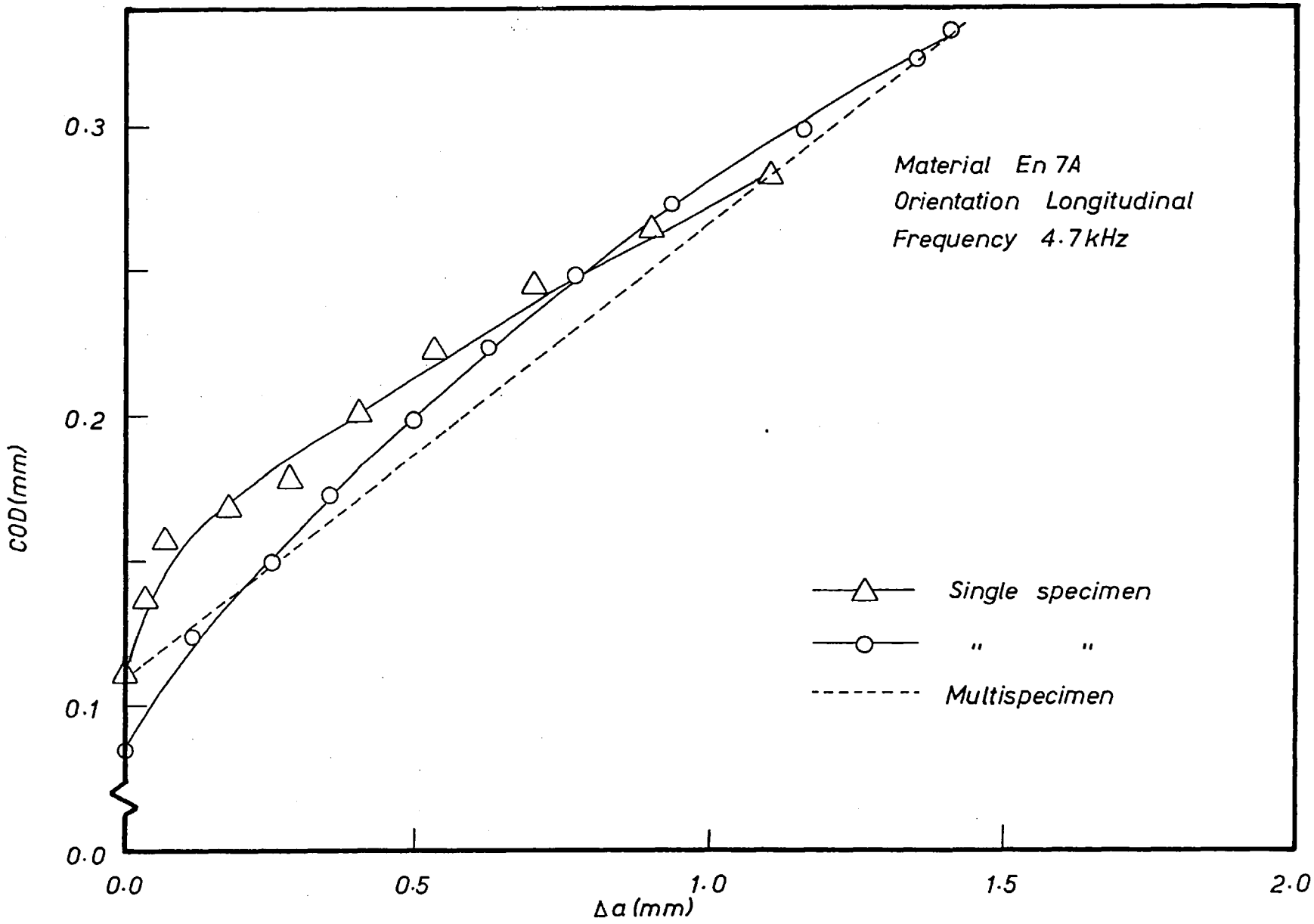


Fig. A1·8 Comparison of single specimen R curve obtained by ACPD with the multispecimen R curve

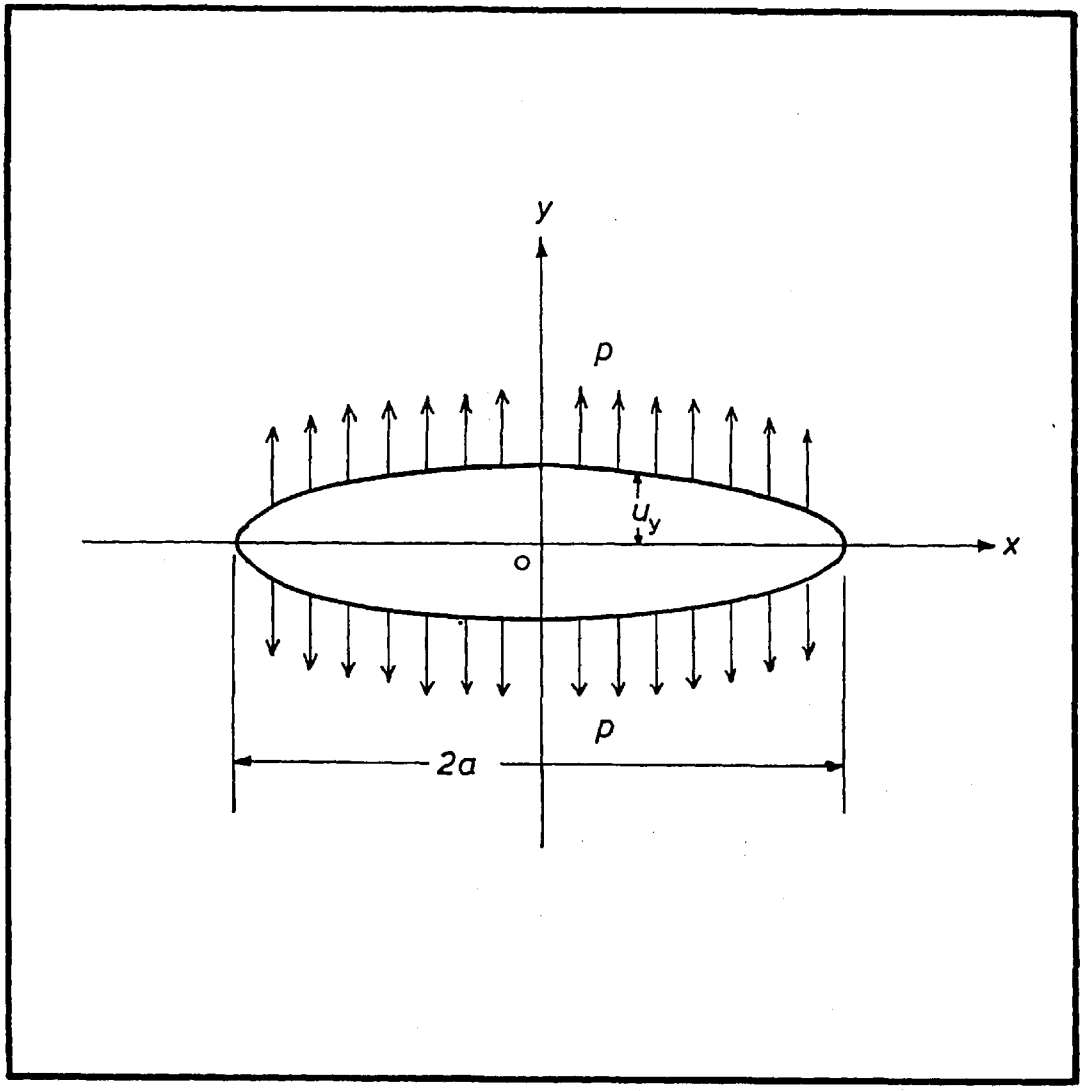


Fig A2·1 Mode I displacement of a Griffith crack under a uniform internal pressure 'p'